Effect of antecedent soil moisture on infiltration and preferential flow in texture contrast soils

By

Marcus Hardie.

BSc.(Hons), MSc.(App)

Submitted in fulfilment

of the requirements for the

Degree of Doctor of philosophy

School of Agricultural Science

The University of Tasmania (September 2011)

Statement of originality and copyright

This thesis does not contain material which has been accepted for a degree or diploma by the University or any other institution, except by way of background information and duly acknowledged in the thesis, and to the best of the candidate's knowledge and belief no material previously published or written by another person except where due acknowledgement is made in the text of the thesis, nor does the thesis contain any material that infringes copyright.

The research associated with this thesis abides by the international and Australian codes on human and animal experimentation, the guidelines by the Australian Government's Office of the Gene Technology Regulator and the rulings of the safety, Ethics and Institutional Biosafety Committees of the University.

Signed Marcus Hardie

This thesis may be made available for loan. Copying of any part of this thesis is prohibited for two years from the date this statement was signed; after that time limited copying is permitted in accordance with the *Copyright Act 1968*.

Abstract

Preferential flow has been shown to be both common and widespread in agricultural soils, however the processes and mechanisms responsible for preferential flow in texture contrast soils have not previously been investigated. Through a combination of dye tracer experiments, soil morphology, *in situ* soil moisture monitoring, infiltration studies, and soil water modelling, the effect of antecedent soil moisture on the occurrence, type and depth of preferential flow was investigated in a series of texture contrast soil profiles. Preferential flow was dominated by hydrophobicity induced finger flow in the A1 horizon and bypass flow through shrinkage cracks in the subsoil. Differences between sites in horizon thickness, chemical properties, presence / absence of an A2 horizon, and abundance of sand infills resulted in little variation in preferential flow. At low antecedent soil moisture, dye tracer infiltrated to 85 - 119 cm depth, infiltration bypassed up to 99 % of the soil matrix, and wetting front velocities were estimated up to 12 000 mm hr^{-1}. Perched water tables and subsurface lateral flow did not develop due to the abundance of subsoil shrinkage cracks. At high antecedent soil moisture dye tracer infiltrated to 24 – 40 cm depth. While water repellence had been overcome or leached from the A1 horizon, infiltration of new water was impeded by difficulty displacing existing soil water further down the soil profile. This resulted in wetting front instability and lateral flow through the A1 horizon rather than within the A2 horizon or along the upper surface of the B horizon as reported in the literature. Occurrence of preferential flow was not related to rainfall intensity or rainfall magnitude. Rather, preferential flow was significantly more likely to occur when antecedent soil moisture was below approximately 50 - 60 % PAWC. Water repellence had a profound effect on the development of preferential flow, however the relationship between water repellence and antecedent soil moisture was not straightforward. Potential water repellence varied seasonally in relation to rainfall history in which water repellence was not re-established after rainfall unless input of new hydrophobic substances occurred. Ability to model and predict the frequency and magnitude of preferential flow was limited by poor model performance, attributed to parameter uncertainty and inability to simulate water repellence and lateral flow. Results indicate that in agricultural landscapes which contain texture contrast soils, shallow groundwater and waterways may be at risk of contamination by preferential transport of agrochemicals at low antecedent soil moisture.

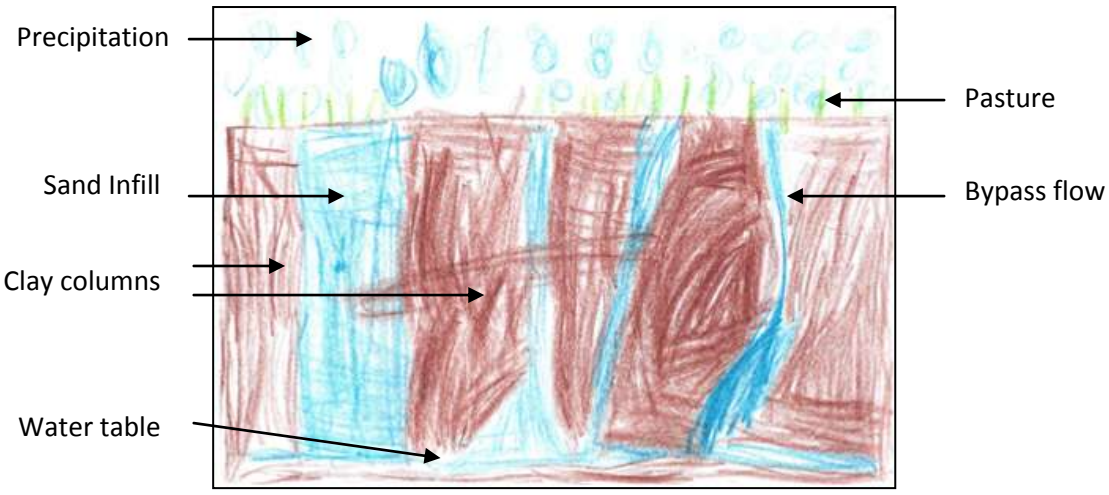

Figure i Depiction of my thesis topic by my son Jacob Hardie aged 5 years old. Figure demonstrates preferential flow through sand infills and bypass flow to a watertable.

Acknowledgements

There are many people I wish to thank and acknowledge. It would not have been possible to conduct or complete my PhD without your support and input. Firstly I wish to acknowledge Rob Clarke, Shaun Lisson and the many people in DPIPWE including Kim Evens, Greg Pinkard, Peter Voller and Declan McDonald who made possible my secondment to TIAR, and generously allowed me the time and space to conduct my studies.

I am indebted to Bill Cotching and Ted Lefroy for providing funding through the Landscape Logic project. I hope and trust I have delivered on your expectations. I am genuinely indebted to you guys for putting your trust in me, it would not have been possible to have conducted this work without your support.

I wish to acknowledge and thank my supervisory team, Shan Lisson, Bill Cotching and Richard Doyle. Thanks heaps guys, I know I caused you guys a fair deal or stress and torment over the last few years, all that I can say is that I am grateful, you all made an amazing contribution to this thesis in so many different ways.

I also wish to thank my poor long suffering family, having someone doing a PhD in a family is a strain on everyone especially my poor long suffering wife. I hope I didn't make life too difficult for you all. Boys you will now get your father back, sorry for my absences and grumpiness over the last 4 years.

I wish to thank the many people who assisted me with field work. Firstly I have to thank Kathrin Mattern who made such an amazing contribution to my PhD, you were a great friend and support, I am indebted to you and hope to see you back here in Tassie. I also wish to thank Marek Matuszek (the animal) for all that digging, sorry for dropping the shade tent on your head. Sam Rees thanks heaps mate, you were great support and really enjoyed spending time in the field with you, I hope you submit soon. Thanks also to a number of people who helped in the field or lab, Jorge De Carvalho Martins, Suresh Panta and Garth Oliver.

I am deeply indebted to Brent Clothier and his team, Markus Deurer and Steve Green who allowed me come over to their island and pester them for a week about my PhD. I sincerely thank you guys for your time, patience and most of all inspiration and insights. It was great working with you, I look forward to working with you again. Thanks also for technical support and advice from Hamish Cresswell, the crucially critical Greg Holtz, and Freeman Cook.

To Jane, Sally and everyone at TIAR thanks again.

Publications arising from this thesis

Hardie, M., Cotching, W.E., Doyle, R. and Lisson, S., (in press) Influence of climate, soil water and leaching on seasonal variations in potential water repellence. Hydrological Processes.

Hardie, M., Doyle, R., Cotching, W., Mattern, K., Lisson, S. (in press) Temporal variation in the hydraulic conductivity of a series of texture-contrast soils resulting from changes in antecedent soil moisture. Hydrological Processes.

Hardie, M., Cotching, W., Doyle, R., Holz, G., Lisson, S. (2011) Effect of antecedent soil moisture on preferential flow in a texture contrast soil. *Journal of Hydrology.* 398 (3-4) 191-201.

Hardie, M., Doyle, R., Cotching, W., Lisson, S. (2010) Development of preferential flow below a soil moisture threshold. World Congress of Soil Science Conference, Brisbane, Australia. Poster and short manuscript.

Hardie, M., Cotching, W., Doyle, R., Lisson, S. (2010) Effect of leaching on hydrophobicity and infiltration into a texture contrast soil. World Congress of Soil Science Conference, Brisbane, Australia. Poster and short manuscript.

Hardie, M., Doyle, R., Cotching, W., Lisson, S. (2009) Effect of antecedent soil moisture on preferential flow in a texture contrast soil. Current Activities in Tasmanian Soil Science Workshop, Launceston, Tasmania. Extended Abstract & Presentation.

Hardie, M., Doyle, R., Cotching, W., Lisson, S. (2008) Preferential flow in a texture contrast soil. ASSI Biannual Conference, Palmerston North, New Zealand. Extended Abstract & Presentation.

Contents

List of Figures

List of tables

1.0 Introduction

This chapter outlines the background to the development of the thesis, provides an overview of preferential flow, the hydrology of texture contrast soils, and details how preliminary dye tracer experiments shaped the focus and scope of the present study. The primary research question is posed in light of the emerging hydropedology paradigm, and the thesis structure and research questions are presented.

1.1 Development of the research concept

The author's interest in the hydrology of texture contrast soils has resulted from over 10 years research and extension experience with the management of these soils including; irrigation efficiency (Hardie *et al.* 2000); tunnel erosion (Hardie 2009; Hardie *et al.* 2007), salinity (Hocking *et al.* 2005; Lisson *et al.* 2005), and wastewater reuse (Lisson *et al.* 2005). Over this period, a number of personal observations and anecdotal evidence have suggested the hydrology of texture contrast soils are considerably more complex than the simple conceptual models of subsurface lateral flow resulting from impeded infiltration into the subsoil as proposed by Whipkey and Kirkby (1978), Cox and McFarlane (1995) and Eastham *et al.* (2000). Growing awareness of the complexity of flow processes in texture contrast soils led to concerns that current best practice guidelines for irrigation and agrochemical use may be contributing to production losses and environmental harm. Further research is required to improve understanding of water movement in these morphologically complex soils.

1.2 Preferential flow and environmental risk

Since the 1970's a considerable body of literature has demonstrated that preferential flow in soil is both common and widespread (Flury *et al.* 1994), resulting in either an enhanced or reduced capacity of the soil to buffer and filter potential contaminants (Clothier *et al.* 2008). Preferential flow consists of a number of different processes, operating at different scales, that result in rapid, deep movement of water and solutes via pathways that bypass a large portion of the soil matrix (Gerke *et al.* 2010; Hendrickx and Flury 2001). Improved understanding of the processes responsible for the occurrence of preferential flow in agricultural landscapes is important for:

I. Predicting the risk of agrochemical mobilisation to shallow groundwater and waterways (Gerke *et al.* 2010; Jarvis 2007).

II. Improving irrigation water use efficiency by minimising leaching beneath the root zone (Cullum 2009).
III. Improving crop emergence and growth by increasing rainfall and irrigation efficiency and reducing spatial variation in root zone wetting patterns (Garg *et al.* 2009).
IV. Salinity management, as preferential flow decreases leaching effectiveness and increases deep drainage to groundwater (Hamed *et al.* 2008).

Numerous studies in Europe and America have demonstrated the importance of preferential flow on agrochemical mobilisation (Jarvis *et al.* 2007; McCoy *et al.* 1994; Simunek *et al.* 2003). However in Australia, little is known about the importance of preferential flow processes in Australian soils despite its existence being commonly reported or observed.

1.3 Texture contrast soils

Texture contrast or 'duplex' are defined according to Northcote (1979) as having a profile form in which the texture of the subsoil is at least one and a half texture groups finer than the surface soil, with clear to sharp horizon boundaries. Texture contrast or duplex soils are estimated to occupy 17.0 % of the Australian landmass or 2.33 million km^2 (Isbell *et al.* 1997). They are considered important for agricultural production, as they occupy around 80 % of agricultural regions in southern Australia (Chittleborough *et al.* 1994). In contrast to uniform and gradational soils, the boundary between the A and B horizons separates soil material with very different chemical and physical properties. Tennant *et al.* (1992) argues that the principal soil attribute which has the greatest influence on the behaviour of the texture contrast soils is the low permeability of the B2 horizons. Unlike other soil types, duplex soils contain an abrupt reduction in hydraulic conductivity between the topsoil and the subsoil, which has been attributed to the formation of seasonal perched watertables and subsurface lateral flow in locations with sufficient slope (Cox and McFarlane 1995; Eastham *et al.* 2000; Ticehurst 2004).

The majority of the Australian research on the hydrology of texture contrast soils has focused on the development of perched watertables and subsurface lateral flow rather than preferential flow *per se* (Cox *et al.* 2002; Eastham *et al.* 2000; Fleming and Cox 1998; Stevens *et al.* 1999; Ticehurst 2004). However few of these studies have specifically investigated the effects of preferential flow on soil hydrology or solute mobilisation in texture contrast soils. Given the widespread use of texture contrast soils for agricultural production (Chittleborough *et al.* 1994).

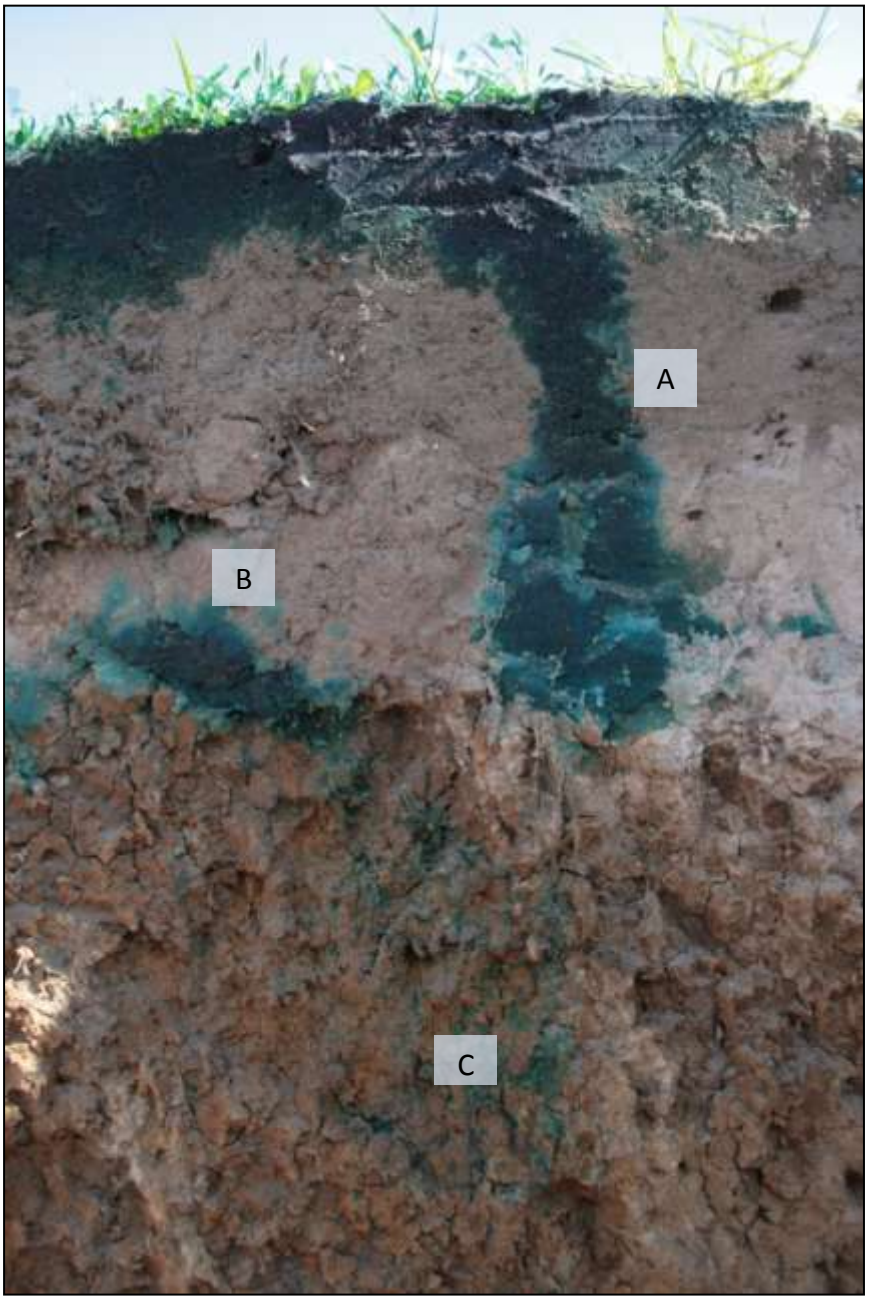

Figure 1.3-1 Preliminary dye tracer experiment, October 2007, demonstrated (a) finger flow in the A1 horizon, (b) ponding of dye tracer at the A / B horizon boundary (c) macropore flow through shrinkage cracks and root channels in the B21 horizon.

Evidence that preferential flow in texture contrast soils may result in off-site transport of environmental contaminants to waterways (Stevens *et al.* 1999) led to funding being sought from the Commonwealth Environmental Research Facilities (CERF) 'Landscape Logic' project, to investigate contaminant pathways and processes in texture contrast soils.

1.4 Preliminary experiments

A preliminary dye tracer experiment in October 2007 at the University of Tasmania Farm demonstrated infiltration into a dry texture contrast soil was considerably more complex than had been anticipated. Infiltration at low antecedent soil moisture resulted from a combination of preferential flow processes including: finger flow in the A1 horizon; funnel flow and ponding at the A / B horizon boundary; macropore flow through shrinkage cracks and root holes in the B21 horizon; and funnel flow through sand infills (Figure 1.3-1). The presence of hydrophobicity induced finger flow in the A1 horizon and bypass flow through shrinkage cracks in the B horizons suggested that infiltration was likely to differ when soil was at high antecedent soil moisture, yet the influence of antecedent soil moisture on structure and preferential flow remained unknown.

The preliminary dye tracer experiment demonstrated further opportunity to improve understanding of preferential flow processes in texture contrast soils at the University of Tasmania Farm.

1.5 Hydropedology

Study of water movement in soil has traditionally been conducted by three separate fields of science; pedology, soil physics and hydrology (Lin 2003). Typically, pedologists have focused on field soil profiles (pedons) as observed in the landscape, soil physicists have emphasized theoretical studies and laboratory investigations using small soil samples, and hydrologists have investigated landscape or watershed-scale processes (Lin 2003).

Recent emergence of 'hydropedology' as a research discipline offers the opportunity to integrate these three field of science into a single multiscale approach in which *pedology is* integrated with hydrology to *"enhance the holistic study of soil–water interactions and landscape–soil-hydrology relationships across space and time*" (Lin *et al.* 2008), (Figure 1.5-1).

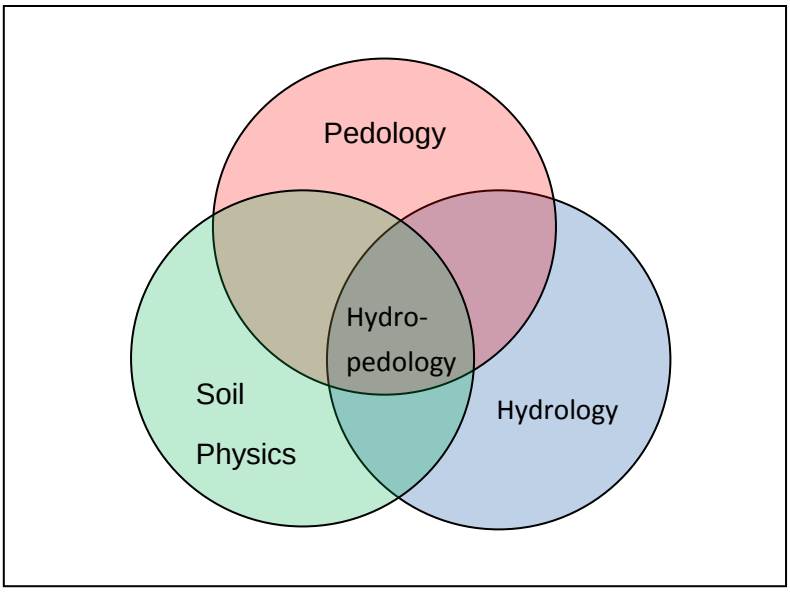

Figure 1.5-1 Conceptual representation of hydropedology concept, adapted from Lin (2003).

1.6 Thesis structure

The objective of the thesis is to investigate the effect of antecedent soil moisture on the dynamics of infiltration and preferential flow in texture contrast soils. By following the integrated hydropedology approach, pedological investigations have been coupled with physical measurements of water movement and soil water modelling, at the pore to pedon scale, to better understand the influence of soil morphology and antecedent soil moisture, on water and solute movement in a series of texture contrast soils.

Chapter 2 presents a detailed review of the literature on: preferential flow, texture contrast soils, and preferential flow modelling.

Chapter 3 investigates the morphology of texture contrast soils at the University of Tasmania Farm, from which the influence of soil properties on water movement is inferred.

Chapter 4 quantifies the effect of antecedent soil moisture content on infiltration and preferential flow using a series of dye tracer experiments.

Chapter 5 describes how high frequency soil moisture monitoring was used to investigate the relative influence of soil and climatic factors on the occurrence or triggering of preferential flow events following rainfall.

Chapter 6 examines the effect of antecedent soil moisture on soil porosity and hydraulic conductivity using *in situ* tension infiltrometers, intact soil cores, and the soil shrinkage characteristic curve.

Chapter 7 examines the importance of water repellence on flow instability using a combination of field monitoring, laboratory leaching experiments, *in situ* infiltration, and Hele-Shaw tank experiments.

Chapter 8 evaluates the effects of parameterisation approach, and the ability of single porosity and a dual permeability models, to simulate infiltration and soil water redistribution into a texture contrast soil.

1.7 Research questions

The principal research question investigated in this thesis is;

What effect does antecedent soil moisture content have on preferential flow and infiltration into a series of texture contrast soil profiles ?

Secondary research questions investigated in this thesis include:

RQ 1: Do differences in soil morphology, chemical and physical properties influence the depth of infiltration and soil water redistribution processes in four different texture contrast soils ?

RQ2: What effect does antecedent soil moisture have on the occurrence, form and depth of preferential flow in texture contrast soils ?

RQ3: Is the occurrence of preferential flow more closely related to antecedent soil moisture content, or rainfall attributes ?

RQ4 What effect does the occurrence of preferential flow have on the velocity of the wetting front, rainfall effectiveness and infiltration uniformity ?

RQ5: What effect does antecedent soil moisture have on *in situ* hydraulic conductivity and soil porosity?

RQ6: What effect does soil moisture have on subsoil porosity and density ?

RQ7: To what extent is water repellence influenced by seasonal variation in soil moisture, rainfall, and other climate factors ?

RQ8: What effect does water repellence, air / water entrapment, antecedent soil moisture, and wetting history, have on flow instability during infiltration ?

RQ9: What effect does parameterisation approach have on soil hydraulic parameters ?

RQ10: To what extent are soil water models able to reproduce infiltration of the dye tracer and changes in soil moisture following rainfall, as demonstrated in previous experiments ?

2.0 Literature Review

2.1 Preferential and non-uniform Flow

Hendrickx and Flury (Hendrickx and Flury 2001) defined preferential flow as constituting all phenomena where water and solutes move along certain pathways, while bypassing a fraction of the porous matrix, resulting in water and solutes moving to far greater depths, much faster, than predicted by the Richards equation for uniform flow. An alternative approach is provided by Gerke (2006) who explains that water movement in soils can be either uniform or non-uniform (preferential flow). Uniform flow described by the Richards' equation, leads to stable wetting fronts, which move downwards through the soil as a relatively homogeneous front parallel to the infiltrating surface. While in non-uniform flow, Richards' equation is invalid, wetting fronts develop spatial irregularities, infiltrating water does not equilibrate with the resident soil water, and infiltration penetrates rapidly to depth through a small portion of the soil volume.

Several different phenomena have been grouped under the common name of 'preferential flow', however it is important to consider that the mechanisms responsible for the different forms of preferential flow differ, and that each occur at distinct spatial scales (Hendrickx and Flury 2001; Nieber 2000) ranging from soil pores up to the field or catchment scale (Gerke *et al.* 2010). Gerke (2006) describes three classes of preferential flow;

- Macropore flow: preferential flow in continuous root channels, earthworm burrows, fissures, or cracks within well structured soils.
- Unstable flow or fingering: instabilities in the wetting front develop due to water repellence, or air entrapment.
- Funnel flow or heterogeneity-driven flow: textural or lithographic boundaries result in lateral redirection or funnelling of infiltration via pathways of least resistance, bypassing the less permeable zones. In the case of texture contrast soils, subsurface lateral flow is considered to be a hillslope or catchment scale manifestation of funnel flow.

Other forms of preferential flow have been described, including depression focused recharge and oscillatory flow (Nieber 2000). These forms of preferential flow are not discussed as they are not considered relevant to texture contrast soils, or occur at scales beyond those investigated in this thesis.

2.1.1 Preferential flow and environmental risk

Preferential flow has been found to be both common and widespread (Flury *et al.* 1994), resulting in either enhanced, or reduced capacity of the soil to buffer and filter potential contaminants (Clothier *et al.* 2008). Consequences of preferential flow include; (i) recharge of the groundwater before the soil reaches field capacity (Hamed *et al.* 2008; Kordel *et al.* 2008) (ii) reduced and uneven crop development resulting from water moving below the root zone and uneven wetting patterns in the root zone (Cullum 2009; Garg *et al.* 2009) (iii) mobilisation of fertiliser and pesticides to shallow ground water (Gerke *et al.* 2010; Jarvis 2007; Kordel *et al.* 2008) (iii) lateral movement of fertilizer and nutrients towards waterways (Cox *et al.* 2002; Stevens *et al.* 1999; White *et al.* 2000) (iv) greater salinity due to reduced leaching effectiveness and increased deep drainage to groundwater (Hamed *et al.* 2008).

In the past three decades considerable research has sought to quantify the risk posed by preferential flow on movement of pesticides to shallow groundwater (Flury 1996; Kladivko *et al.* 2001; Köhne *et al.* 2006a; Shipitalo and Edwards 1996). While macropores usually only represent a small part of the soil volume (0.1 – 5.0 %) their effect on the rate of water and solute movement can be substantial (Cox *et al.* 2000). For example, Watson and Luxmoore (1986) found that under ponding, 73 % of flow occurred through macropores larger than 0.1 cm diameter, and that 96 % of the water flux was transmitted through only 0.32 % of the soil volume. The disproportional effect of preferential flow on solute mobility is important, as leaching of as little as 0.1 % of an applied pesticide may result in contaminant concentrations in shallow groundwater which exceed the EU drinking water standard (<0.1 µg litre^{-1}) (Jarvis 2007). Preferential flow in soil represents a risk to the environment as agrichemicals moving in macropores have less residence time to adsorb to soil particles due to the faster flow rates. This results in the facilitation of agrichemicals transport through the soil even when it contains a significant amount of clay and sorption capacity (Cox *et al.* 2000).

Preferential flow has also been linked to off-site movement of nutrients from agricultural areas to groundwater and waterways. However the effect of preferential flow on mobilisation differs between nutrients. De Jonge *et al.* (2004) and Schelde *et al.* (2006) demonstrated that up to 75 % of leached phosphorous may be transported through macropores while adsorbed to mobile colloidal particles. However preferential flow of mobile solutes like nitrate is often curtailed by their isolation in the soil matrix (Clothier *et al.* 2008; Cote *et al.* 2000; Jarvis 2007). Preferential flow and transport may also compromise or boost a host of other ecosystem services such as gas regulation, waste treatment, provision of refugia for flora and fauna, and the damping of responses to environmental fluctuations (Clothier *et al.* 2008; Costanza *et al.* 1997).

Little is known about the quantitative significance of macropore flow on contamination of water resources at the larger catchment scale (Jarvis 2007). Drewry *et al.* (2006) reports there have been relatively few studies of nitrogen and phosphorous export to waterways in Australia, particularly in the valuable farming region of south eastern Australia. Studies such as Chittleborough *et al.* (1992; 1994), Cox *et al.* (2000; 2002; 2001), Fleming and Cox (1998; 2001), White *et al.* (2000; 1998), White and Kookana (1998), and Stevens *et al.* (1999) have demonstrated environmentally significant levels of nutrient mobilisation via subsurface lateral flow in texture contrast soils. However little is known about the importance of preferential flow on agrochemical mobilisation in other agricultural soils in Australia.

2.1.2 Effect of antecedent moisture on soil water movement and preferential flow

The effect of antecedent moisture content on uniform flow is a well documented aspect of soil physics, described by the $\theta(\psi)$ and $K(\psi)$ relationships in which unsaturated flow rates increase with increasing water content, or as matric potential approaches zero. This response is due to wetter soils having more continuous and thicker water films, and thus less convoluted flow paths than drier soils (Hillel 1998).

Researchers are however in disagreement about the extent to which antecedent soil moisture influences preferential flow in soils (Merdun *et al.* 2008). The effects of initial soil moisture content are complex, especially for soils that become water repellent when dry, or where the soil structure is influenced by moisture content (i.e. swell / shrink clay soils). In the absence of such complications, wetter soils tend to generate more macropore flow than dryer soils, due to reduced lateral losses into the soil matrix (Beven and Germann 1982; Greve *et al.* 2010; Jarvis 2007). Shipitalo and Edwards (1996) found the relative contribution of macropores to chemical transport and water movement appeared to be greatest when the soil was dry and decreased as the soil became wetter.

Merdun *et al.* (2008) also reported that preferential flow was more evident when soil was initially dry compared to two wetter treatments. However Granovsky *et al.* (1994) found that the degree of preferential flow increased with antecedent soil moisture. Additionally Jaynes *et al.* (2001) and Kung *et al.* (2000) reported that during irrigation events, pesticide transport increased due to larger pores becoming hydraulically active as the soil became progressively wetter.

Review of the literature indicates the influence of antecedent soil moisture on preferential flow is complex and may differ between soil types and forms of preferential flow. Presented below is a review of the literature which details current understanding of the process governing preferential flow in soil, with emphasis on the effect of antecedent soil moisture on flow processes.

2.1.3 Macropore flow

Preferential flow is highly dependent on macroporosity which is influenced by soil structure and management practices such as tillage and compaction (Germann and Beven 1981; Langner *et al.* 1999; Luxmoore 1981). Macropores consist of large, continuous, structural pores which constitute preferred flow pathways for infiltrating water. At the macroscopic scale, the presence of macropores results in large increases in unsaturated hydraulic conductivity across a small soil water pressure head range close to saturation (Jarvis 1998).

Definitions as to what constitutes a macropore vary. Luxmoore (1981) designated three classes of pores; macropore (>1000 µm), mesopore (10 - 1000 µm) and micropore (<10 µm), where micropore class corresponds to the soil matrix. Beven and Germann (1982) and Langner *et al.* (1999) however argued that macroporosity should be related to process differences between small and large pores rather than arbitrarily pore size classes. Functional definitions of macroporosity also need to consider pore structure in relation to continuity and connectivity (McDonnell 1990). Kutílek (2004) considered that macropores exist when the pore size is too great to support the formation of capillary menisci across the pore, and the shape of air–water interface across the pore is planar, consequently they reported macropores exist at equivalent pore radii greater than 1000 –1500 µm. From a functional perspective Jarvis (2007) reported that considerable evidence indicates that macropore flow and solute transport occurs in pores larger than about 300 – 500 µm diameter or at water entry pressures of –1.0 to –0.6 kPa. Kutílek (2004) also considered that a definition of macroporosity should include their mode of formation and persistence or stability over time.

Many of the manifestations of macropore flow have their genesis at the soil surface. Whether or not there is a film of surface free-water at positive pressure head is critical to determining how uniformly the infiltrating wetting front will enter the soil. If ponding occurs, free water can move rapidly across the surface to find local orifices, cracks or macropores down which water moves preferentially (Clothier *et al.* 2008). Consequently the occurrence of macropore flow is strongly influenced by rainfall attributes and properties of the soil surface including; antecedent moisture content, roughness, crusting, and water repellence (Jarvis 2007; Struthers *et al.* 2007).

Triggering of macropore flow has been attributed to; rainfall magnitude (Cheng *et al.* 2007; McGrath *et al.* 2010), rainfall duration (Heppell *et al.* 2002), rainfall intensity (Beven and Germann 1982; Lin and Zhou 2008; McGrath *et al.* 2008), and storm rainfall distribution (McGrath *et al.* 2008; McGrath *et al.* 2010). At the hillslope scale, threshold relationships between rainfall magnitude and subsurface lateral flow are considered to be a common property of hillslope drainage, (Lehmann *et al.* 2007; Mosley ; 1979; Tromp-Van Meerveld and McDonnell 2006b; Uchida *et al.* 2004; Weiler *et al.* 2005).

At the pore scale, macropore flow is generated when the water pressure locally increases to near saturation at some point on the interface with the surrounding soil matrix. Water entry into the pore occurs when the water entry potential of the pore is exceeded, however this does not necessarily require the soil to be saturated (McCoy *et al.* 1994). Water flow in soil pores is driven by the momentum balance between the governing forces of gravity, capillarity, viscous forces due to friction with the solid surfaces and within the fluid itself, and inertial forces. These forces operate on water in pores of all sizes, so that in this fundamental respect, the flow of water in a macropore does not differ from flow in any other pore. However in macropores, gravity dominates the driving force, as capillary pressure potential gradients are minimal (Jarvis 2007). Macropore flow is sustained when the vertical flux in the macropore is larger than losses into the matrix via lateral infiltration (Beven and Germann 1982; Greve *et al.* 2010). Water movement in macropores is often impeded by pore 'necks', discontinuous pathways, air entrapment, and the presence of 'dead-end' or otherwise isolated pores (Bouma and Dekker 1978). As water content increases capillary 'bridging' across the narrowest sections of variable-width fissures occurs resulting in intermittent or 'pulse flow' (Jarvis 2007). Lateral infiltration of water into the soil matrix may also be severely restricted by organic and inorganic linings which restrict lateral mass transfer, enhancing non-equilibrium water flow and solute transport (Jarvis 2007).

Macropores may conduct considerable amounts of water without being saturated, in which unsaturated laminar flow occurs as discrete 'rivulets' or film flow along the sides of the macropores (Beven and Germann 1982; Nimmo 2010). Free surface films differ hydraulically from the capillary bundle concept typically used to describe flow in cylindrical macropores such as the Darcy-Buckingham law, Richards' equation, and Woodings solution for infiltration from a ponded ring. Thin film or rivulet flow occurs at smaller pressure potentials than would be nominally required to generate flow according to the Laplace equation, as the air-water interface is not constrained by the capillary potential of the solid material (Nimmo 2010).

From a functional perspective it cannot be expected that all macropores in a soil will participate in flow (Beven and Germann 1982), even when driven by surface ponding or saturation. For example Mori *et al.* (1999a) found that only 10 – 50 % of the total macroporosity conducted water during 'saturated' flow through intact cores.

Although the physical mechanisms of water flow in macropores are complex, it is clear that the assumptions underlying Darcy's law are not always met (Jarvis 2007), as flow may occur in partly filled macropores (Cey and Rudolph 2009) and flow in large macropores may be turbulent (Logsdon 1995; Mori *et al.* 1999a). Furthermore, macropores represent a form of heterogeneity in the soil as the physical, chemical and biological microenvironment of macropores contrasts strongly with the bulk soil, particularly when macropores are lined by organic or inorganic coatings (Jarvis 2007).

2.1.4 Effect of antecedent soil moisture on macropore flow

Antecedent soil moisture influences flow in macropores by affecting (i) the pressure potential difference between the soil matrix and the water-entry pressure required to initiate flow (Jarvis 2007) and, (ii) the rate of lateral diffusion of infiltrating water into the soil matrix (Greve *et al.* 2010).

Higher antecedent soil moisture has been shown to increase the depth to which macropore flow penetrates (Greve *et al.* 2010) as well as increasing total percolate volume (McCoy *et al.* 1994). Higher moisture content in the soil matrix reduces the matrix potential gradient between the macropore wall and the surrounding soil, consequently less lateral flow occurs between the macropore and the soil matrix enabling deeper water penetration within the macropore (Beven and Germann 1982; McCoy *et al.* 1994). McCoy *et al.* (1994) also reported greater total percolate at high antecedent soil moisture due to an increased number of flow pathways conducting water.

Water movement through shrinkage cracks differs to that of other macropores (stable biopores). The appearance and disappearance of cracking planes is strongly related to soil moisture content (McCoy *et al.* 1994), in which maximum aperture is attained when soils are very dry (Greco 2002). The occurrence and extent of preferential flow in shrinkage cracks is influenced by antecedent moisture content of the soil matrix and rate of swelling in response to lateral diffusion of infiltrating water. In dry periods, the volume of cracks can be substantial, especially near the soil surface. As soil moisture tends to increase with depth, crack volume, width and connectivity also decrease with depth.

The hydraulic conductivity of soils containing shrinkage cracks cannot be characterized by a single value, rather hydraulic conductivity is inversely related to the soil moisture content (Jarvis 2007). For example, Lin *et al.* (1998) demonstrated that steady-state infiltration in a series of shrink-swell soils (Vertosols) varied from 360 mm hr^{-1} at 10 % soil moisture to 7.2 mm hr^{-1} at 45 % moisture content.

2.1.5 Finger flow (unstable or non uniform flow)

Unstable flow (finger flow) has been reported in both hydrophilic (wettable) and hydrophobic (non-wettable) soil, in unstructured sandy soils, and structured loams and clay soils, and under both rainfall and irrigation (Wang *et al.* 1998b). Jury *et al.* (2003) considered unstable flow differs from other forms of preferential flow in that it is a fluid phenomenon, resulting from small scale variation in water repellence and soil moisture content (Bachmann *et al.* 2007; Howell *et al.* 2006; Ritsema and Dekker 1994), rather than resulting from physical heterogeneity of the soil structure. During unstable flow, instability develops in the initial planar or sharp wetting front causing the wetting front to break up into preferential wetting columns, called fingers. Unstable flow (finger flow) has been attributed to a wide range of factors including;

- Vertical infiltration from a fine to a coarse textured soil layer, known as the 'Haines jump' (Baker and Hillel 1990; Glass *et al.* 1988; Hill and Parlange 1972; Nieber 1996).
- Infiltration into hydrophobic (water repellent) soil (Carrillo *et al.* 2000a; Dekker and Ritsema 1996a; Nguyen *et al.* 1999; Ritsema and Dekker 2000; Ritsema *et al.* 1998a; Ritsema *et al.* 2005; Wang *et al.* 2000b).
- Soil air compression during infiltration (Wang *et al.* 1998a; Wang *et al.* 1997; Wang *et al.* 1998c).
- Unsaturated infiltration under low application rates (Selker *et al.* 1992b; Wang *et al.* 1998b; Yao and Hendrickx 1996).
- Water application below the water entry potential (WEP, h_{we}) or critical depth of ponding (Wang *et al.* 1998b; Wang *et al.* 2004; Wang *et al.* 2000a).

The majority of research on unstable flow or finger flow has focused on its occurrence in water repellent soils. Water repellency (hydrophobicity) describes a situation during which the cohesive forces between water molecules are stronger than the adhesive forces between the water molecules and the soil particles. These forces cause water to ball up on the soil surface (Lemmnitz *et al.* 2008).

Water repellence is thought to affect approximately 5 million hectares in Australia (Blackwell 2000). Water repellence has been associated with increased erosion, poor seedling establishment, uneven crop growth, reduced irrigation efficiency and accelerated leaching of agrochemicals via finger flow (Blackwell 2000; Ritsema and Dekker 1994; 2000). Soil water repellency is caused by organic compounds derived from living or decomposing organisms, which form water repellent coatings on mineral or aggregate surfaces or as interstitial matter (Doerr *et al.* 2000; Rodriguez-Alleres *et al.* 2007). The compounds responsible for water repellence in soil have been divided into two main groups; (i) aliphatic hydrocarbons, which include insoluble, non polar carbon chains, and (ii) amphiphilic polar substances which have a hydrophilic end (i.e. fatty acids and waxes). The source of these compounds includes: vegetation (McGhie and Posner 1980), decomposing vegetation (McGhie and Posner 1981), roots (Dekker and Ritsema 1996b), bacteria (Schaumann *et al.* 2007), and fungi (Chan 1992). Hydrophobicity may also be induced by fire (Doerr *et al.* 1998; Fox *et al.* 2007; Howell *et al.* 2006; Sheridan *et al.* 2007) or irrigation with waste water (Wallach *et al.* 2005; Wallach and Graber 2007).

Development of unstable flow in hydrophobic soil results from; capillary hysteresis, the existence of a water-entry threshold, and a positive matric potential gradient behind the wetting front (Jury *et al.* 2003; Wang *et al.* 2004). Water cannot readily enter a water repellent soil due to the presence of a positive water entry potential at the soil surface which prevents infiltration until either, the water entry potential is exceeded by the depth of ponding (Wang *et al.* 2004) or the water repellence breaks down over time. The water-entry potential is the minimum matric potential head at the wetting front interface required to allow fluid to enter the dry portion of the soil (Jury *et al.* 2003). Once the water pressure head reaches the water entry value, water is able to penetrate into the soil. The depth of penetration becomes slightly greater at one point along the front due to increased soil moisture or localised variations in water repellence (Bachmann *et al.* 2007; Howell *et al.* 2006; Ritsema and Dekker 1994). This shifts water pressure distribution downward above that location, as a result, regions surrounding the matrix begin to supply the zone above the finger, by lateral flow through the distribution zone (Jury *et al.* 2003; Ritsema *et al.* 1993). Subsequently the water pressure in the surrounding matrix decreases, and the pressure at the wetting front drops below the water entry potential, thereby stopping downward flow in the matrix. Drainage of the soil profile then proceeds exclusively through the propagating fingers, in which downward movement is governed by the rate of loss of water from the soil matrix (Jury *et al.* 2003). Fingers remain narrow as they propagate through the soil due to hysteresis in the soil water characteristic (Jury *et al.* 2003), which prevents fingers dispersing (widening) by lateral diffusion (Glass *et al.* 1989) until such time that the water repellence in the adjacent soil has broken down as demonstrated by the water drop penetration test (WDPT).

2.1.6 Effect of antecedent soil moisture on finger flow in hydrophobic soil

Hydrophobicity (water repellency) is not a static soil property but is known to follow short-term or seasonal variations. Hydrophobicity is generally found to be most extreme when soils are dry, declining and eventually disappearing as soil becomes wet (Doerr and Thomas 2000; Ritsema and Dekker 1994). Many authors have reported an inverse relationship between soil moisture and water repellency (Dekker and Ritsema 1996b; 2000; King 1981; Wessolek *et al.* 2008) in which a 'critical soil moisture' threshold demarcates the soil moisture content at which soil changes from being non-wettable to wettable (Dekker and Ritsema 1994; Ritsema and Dekker 1994). Infiltration into soil below the critical water content usually results in breakdown of the wetting front and development of finger flow. While infiltration into soil above the critical water content usually results in uniform flow (Dekker and Ritsema 2000; Ritsema and Dekker 1994). However the soil moisture - water repellency relationship has proven to be more complex than previously thought (Doerr *et al.* 2007; Doerr *et al.* 2000). Bachmann *et al.* (2007) argues that the concept of a critical soil water content is too rigid and may not be correct for most field soils as the relationship between soil water content and water repellence has been shown to be hysteretic depending on wetting history (Doerr and Thomas 2000).

In addition to soil moisture content, water repellence has been demonstrated to be strongly affected by a range of environmental and analytical factors including; ambient temperature (King 1981), drying temperature (Dekker *et al.* 1998), ambient humidity (Doerr *et al.* 2002) and wetting and drying history of samples (Doerr and Thomas 2000). Seasonal variation in water repellence has been reported by Crockford *et al.* (1991), Doerr and Thomas (2000), Keizer *et al.* (2007; 2008) Leighton-Boyce *et al.* (2005), and Lemmnitz *et al.* (2008). Of the few studies conducted in agricultural soils, Keizer *et al.* (2007) found that variation in the severity of water repellence under potato - maize rotation could only partly be explained by moisture content at the time of sampling. However other factors such as microbes and roots also contributed to temporal patterns of water repellence. In Western Australia, Roper (2005) found that constant soil moisture (-10 kPa) in the laboratory and frequent irrigation in the field, decreased water repellence (MED) by increasing the population of wax degrading bacteria (*Rhodococcus* spp. and *Mycobacterium* spp.). Doerr and Thomas (2000) found that following wetting, a previously hydrophobic forest soil from Portugal remained hydrophilic when dried below the critical moisture content. Furthermore water repellancy did not return, even when samples were dried to near the air dried moisture content and allowed to equilibrate for several weeks. They postulated that for at least some soils the relationship between soil moisture and water repellence is hysteretic, and that water repellence is not re-established after seasonal rainfall, unless input of new hydrophobic substances occurs.

Few studies have investigated the effect of antecedent soil moisture on infiltration and water movement in hydrophobic soil. Bauters (2000a) found the initial moisture content influenced both the degree of water repellence and the formation of fingers, although the effect of antecedent water content on wetting front instability was not entirely clear (De Rooij 2000). Ritsema *et al.* (1998b) concluded that antecedent water content influenced whether perturbations at the wetting front either propagated or dissipated. In a repacked hydrophobic soil Wang *et al.* (2003) found antecedent soil moisture finger width increased from 4.5 cm in dry soil, to 17 cm when soil was very wet. Taumer *et al.* (2006) found occurrence of preferential flow was closely related to initial moisture content of the topsoil and short intensive rainfall events were more likely to trigger finger flow than long steady rain which tended to moisten the soil more uniformly.

The effect of water repellence on infiltration has been investigated by comparing infiltration of ethanol or surfactants to that of water, in which ethanol is considered to be a completely wetting liquid (Watson and Letey 1970). Lamparter *et al.* (2006) found infiltration of water was reduced by a factor of 3 – 170 compared to ethanol due to water repellence reducing the local connectivity of water flow paths, and Jarvis *et al.* (2008) reported water repellence reduced infiltration of water by approximately 15 times that of ethanol, due to water repellence preventing infiltration through structural pores. Leighton-Boyce *et al.* (2007) demonstrated that infiltration of water with non-ionic surfactant infiltrated to a depth of 42 mm with discontinuous wetting to 108 mm. However water repellence resulted in the water only infiltrating to an average depth of 6 mm with discontinuous wetting to 11 mm.

2.1.7 Funnel flow

The term 'funnel flow' was coined to describe the change in flow direction caused by textural discontinuity between inclined soil layers (Ju and Kung 1993). Kung (1990b) proposed that interbedding, textural and structural discontinuities and inclined bedding planes function like the walls of a funnel to concentrate initially unsaturated flow into irregularly spaced saturated flow columns. Funnel flow may also occur along an inclined boundary between a fine sand and a coarser layer provided there is a macroscopic Haines' jump between the two soil layers, and water application is less than a certain critical rate (Kung 1993).

Funnel flow has been shown to increase the potential for water borne contaminants to bypass the bulk of the soil matrix, due to flow becoming more congregated, faster and less subject to degradation and adsorption than flow through the remainder of the soil (Kung 1990b).

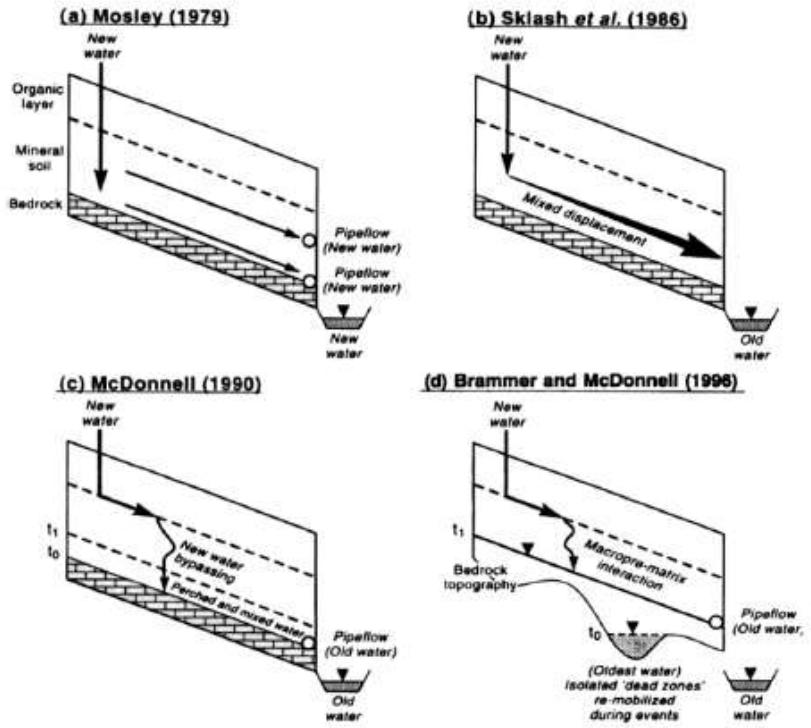

Figure 2.1-1 Changing conceptual understanding of subsurface flow in the Maimai catchment, New Zealand (McGlynn et al. 2002). (a) Mosley (1979); (b) Sklash et al. (1986); (d) McDonnell (1990); (e) Brammer (1996).

Unlike finger flow, occurrence of funnel flow depends on water application rates and layer configuration, and is independent of initial moisture content of the soil profile (Kung 1993).

2.1.8 Subsurface lateral flow (SLF)

Subsurface lateral flow refers to a range of processes in which infiltrating water accumulates and moves laterally downslope, usually due to the presence of one or more less permeable layers in the soil. Subsurface lateral flow is known by a range of terms including throughflow, subsurface storm flow, subsurface runoff, and interflow (Gregory *et al.* 1992; Lehman and Ahuja 1985; Ticehurst 2004).

Subsurface lateral flow in hillslopes may occur as saturated, unsaturated or as macropore flow (Anderson and Burt 1977; Ritsema *et al.* 1996; Weyman 1973) in a range of soil types, including; uniform soils (McCord and Stephens 1987), layered soils (Ritsema *et al.* 1996; Ticehurst 2004) and sands (Jackson and Cundy 1992; McCord and Stephens 1987).

Understanding of the processes responsible for the development of perched watertables and subsurface lateral flow in catchments with shallow bedrock is considerably more advanced than understanding of similar phenomenon in texture contrast soils. Early conceptual models such as those by Weyman (1973) and Whipkey and Kirkby (1978) which considered that saturation and subsurface lateral flow was induced by infiltration in excess of the hydraulic conductivity of an impeding layer (Figure 2.1-2).

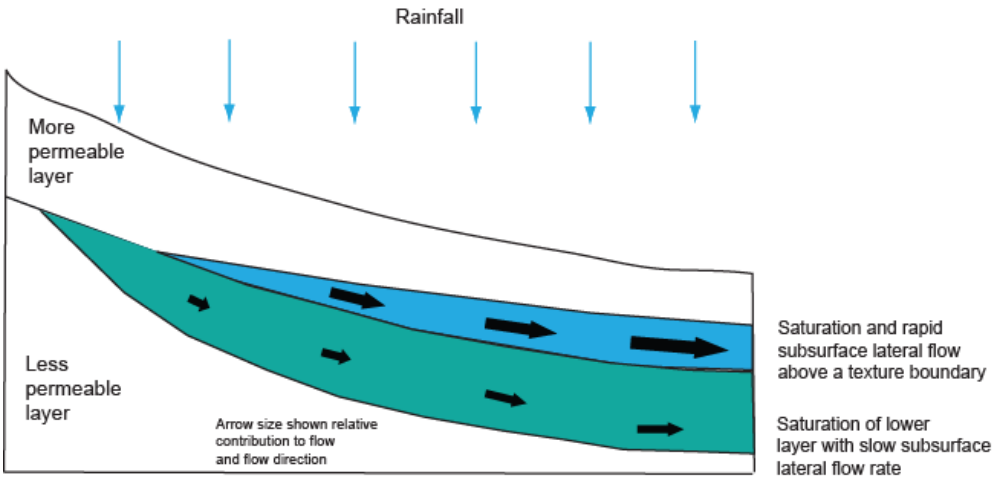

Figure 2.1-2 Simple conceptual model of subsurface flow in a texture-contrast soil (adapted from Whipkey and Kirkby 1978).

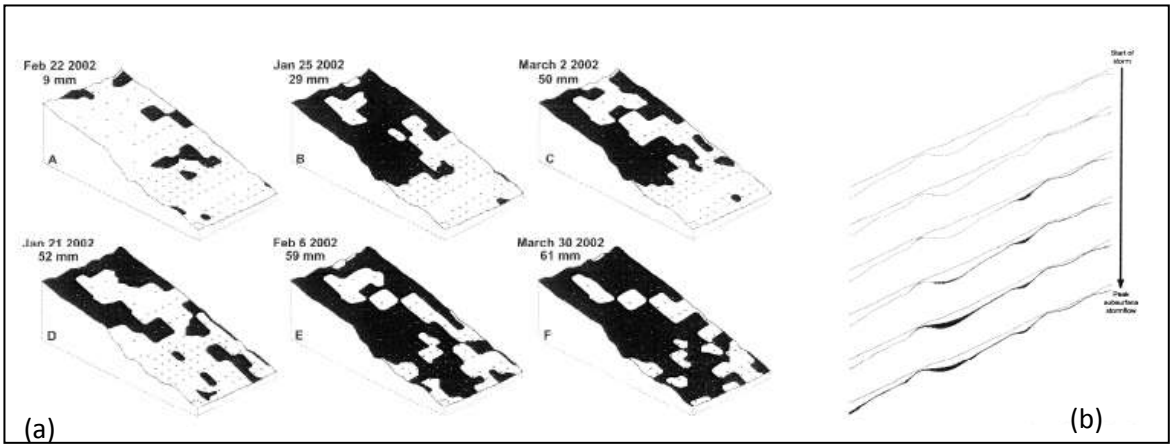

Figure 2.1-3 Spill and fill conceptual model of subsurface lateral flow: (a) sequential development of subsoil saturation at the soil-bedrock interface as precipitation increased. (b) Schematic representation of the fill and spill process (shaded areas represent areas of subsurface saturation) (Tromp-Van Meerveld and McDonnell 2006b).

However of studies in the Maimai catchment in New Zealand over a 30 year period have showed that subsurface flow occurred as a two-component system, in which macropore flow occurs via vertical cracks resulting in rapid saturation of the profile base ahead of a slower moving wetting front in the soil matrix. Perched watertables were short lived due to lateral flow through an interconnected macropore network at the soil-bedrock interface (McDonnell 1990; McDonnell *et al.* 1991; McGlynn *et al.* 2002). Further investigations by McDonnell *et al.* (1998) revealed significant bedrock surface control on subsurface flow timing and tracer breakthrough. Brammer (1996) and McDonnell *et al.* (1998) also demonstrated that small depressions and micro-topographic relief in the bedrock surface determined the pathway of mobile subsurface water flow and tracer breakthrough during events at the hillslope scale (Figure 2.1-1).

Tromp-Van Meerveld and McDonnell (2006a; b) demonstrated that the threshold dependant nature of subsurface lateral flows observed by Uchida *et al.* (2004) could be explained by the filling and spilling of bedrock depressions, in which saturated depressions become more connected as antecedent soil moisture increased (Figure 2.1-3). Tsuboyama *et al.* (1994) and Sidle *et al.* (2001) also demonstrated that macropore networks self-organise into larger preferential flow systems which expand upslope as antecedent soil moisture increased during storm events.

The extent to which conceptual models of subsurface lateral flow in catchments with shallow bedrock apply to subsurface lateral flows in texture contrast soils depends on the extent to which preferential flow in the A1 horizon is able to bypass the soil matrix and deliver rainfall to the impeding B horizon, and the extent to which the upper surface of the B horizon behaves like impermeable bedrock. Specifically the spatial variability in the hydraulic conductivity of the B horizon, reported by Cox and McFarlane (1995), and Hatton *et al.* (2002), and the extent to which soil moisture influences the hydraulic conductivity of the upper B horizon through the development of shrinkage cracks as postulated by Silberstein *et al.* (1999) and observed by Smettem *et al*. (1991).

2.2 Australian research on preferential flow (excluding lateral flow)

Review of the literature reveals that with the exception of research on subsurface lateral flow (presented above), little research has been conducted on preferential flow in Australian soils. Whilst the occurrence of preferential flow has been noted in many soil water studies, a SCOPUS literature search using the terms ‘macropore flow’ or ‘preferential flow’ in the title and ‘Australia’ in any field, identified only 16 manuscripts published between 2000 and 2010 (other papers have been identified using different search criteria).

A brief overview of the Australian literature on preferential flow (other than subsurface lateral flow) is presented. Blackwell (2000) reviewed the risks associated with preferential flow and pesticide leaching in Australian water repellent soils. He concluded that practices such as water harvesting increased risk of preferential flow, while claying and use of artificial surfactants reduced repellence and the risk of pesticide leaching. Thwaites *et al.* (2006) found that in order to prevent preferential flow and runoff on a water repellent sand, application of treated municipal sewage had to be conducted when soil was above a critical soil water content. Ritsema published three papers on preferential flow in hydrophobic soils in the Australian Journal of Soil Science (Ritsema and Dekker 1996; 2005; Ritsema *et al.* 2005) however none of these studies were conducted in Australia or with Australian soils. The effects of hydrophobicity on catchment process was investigated by Burch *et al.* (1989) who determined water repellence increased the proportion of runoff to rainfall by 5 % to 15 %.

The effect of rainfall on the occurrence of preferential flow and pesticide leaching has been investigated by McGrath *et al.* (2007; 2008; 2009; 2010), McLay *et al.* (1991) and Struthers *et al.* (2007). McGrath *et al.* (2007) found rainfall variability within a storm can have a significant impact on the amount of chemical transported by surface runoff and preferential flow, McGrath *et al.* (2010) reported that significant pesticide transport occurred by preferential flow when storm events exceeded a threshold rainfall magnitude of 19 mm. McGrath *et al.* (2009) also developed a preferential flow leaching index to asses climatic influence on the risk of pesticide leaching.

Stagnitti *et al.* (1999) investigated leaching of nitrate, chloride and phosphorous from large undisturbed soil cores. They found fifty percent of the applied nitrate was rapidly transported by preferential flow through macropores, while the phosphate was strongly adsorbed and not available for leaching via preferential flow. In contrast Cox *et al.* (2000) found high phosphorous mobility in macroporous soils within a range of soils from the Adelaide Hills, South Australia.

Using labelled 15N urea, Pakro and Dillon (1995) found that within a day of urine application up to 40 % of the applied urinary-N was leached below a depth of 150 mm as a result of macropore flow in an irrigated paddock, and up to 24 % in a non-irrigated paddock. Cote *et al*. (2001; 2000) found intermittent leaching increased mobilisation of bromide in large intact cores containing macropores, and that dispersivity increased with stronger soil structure and the presence of preferential flow paths, such as worm channels. Sarmah *et al.* (2000) found herbicide distribution in soil was attributed to preferential flow processes, which were greatest when rainfall occurred immediately following herbicide application.

Greve *et al.* (2010) found that lateral infiltration of water from the macropores into the soil matrix was important, especially at low antecedent soil moisture, and that preferential flow and deep drainage still occurred after the soil surface had been completely sealed by swelling of vertic clays.

Holland *et al.* (2007) found raised beds in a texture contrast soil in south-western Victoria had a better connected pore network than the conventionally cultivated soil, allowing faster solute flow and higher risk of pesticides and solute leaching via preferential flow at soil moisture contents close to saturation.

A recent review of soil water model development in Australia by Ranatunga *et al.* (2008) did not identify the use or development of preferential flow models in Australia. Extensive review of the literature and correspondence with Jika Simunek and Nick Jarvis (authors of HYDRUS and MACRO soil water models) were able to identify only three manuscripts in which preferential flow models had been applied to Australian soils. Bourgault Du Coudray et al. (1997) used the dual permeability model MACRO (Jarvis 1994) to investigated the degree of chloride leaching from a de-watered saline soil profile in the non-irrigated wheat belt region of south-western Australia. Stagnitti (1999) developed a mathematical model to predict preferential transport of bacteria following land application of effluent. The model accounted for preferential flow, microbial growth and decay, diffusion, dispersion, advection and adsorption. Verburg *et al.* (1996) accounted for macropore flow in SWIMv2 by adding an extra macropore function to the Brooks - Corey (1964) function to describe the sharp increase in conductivity due to macropores near saturation. Kramers *et al.* (2005) was the first to simulate the effects of water repellency in an Australian soil, (the laboratory analysis and modelling was conducted in the Netherlands). They developed a finger flow module (SWFING) for the soil water model SWAP (van Dam *et al.* 1997) to investigate the effects of clay spreading on the water balance components and plant stress, of a severely water repellent soil in South Australia.

Review of the Australian literature on preferential flow demonstrates that with the exception of the studies on subsurface lateral flow in the Adelaide hills (Chittleborough *et al.* 1992; Cox *et al.* 2002; Cox and Pitman 2001; Fleming and Cox 1998; Naidu *et al.* 1993; Stevens *et al.* 1999) and the series of studies which related triggering of preferential flow to rainfall attributes (McGrath *et al.* 2007; 2008; 2009; McGrath *et al.* 2010; Struthers *et al.* 2007), Australian researchers have made relatively little contribution to the international literature on preferential flow.

2.3 Texture contrast soils

2.3.1 Description and classification

The term 'texture contrast soil' has not been explicitly defined in a formal soil classification system. The term 'texture contrast' was first used in the Great Soil Group (Stephens 1953) and Handbook of Australian Soils (Stace et al. 1968) in reference to the solonetz, solodized solenetz and the soloths, which all have a marked texture contrast between the upper and lower horizons. Northcote (1979) was the first to coin the term 'duplex' soils. He formally recognized the uniqueness of the texture contrast soils by assigning them a unique primary profile form in '*A Factual Key for the Recognition of Australian Soils*'. The duplex profile form is described on the basis of morphology, as having a subsoil (B horizon) which is at least one and a half texture groups finer than the surface soil (A Horizon), and horizon boundaries which are clear to sharp. In the Australian Soil Classification (Isbell 2002) the 'texture contrast soils' include three soil orders, the Sodosols, Chromosols, and Kurosols, which have a strong textural contrast between the A horizons and B horizons. The difference between the three soil orders is based on sodicity and pH trend with depth. For the purpose of this thesis, texture contrast soils are defined according to Northcote (1979) as having a profile form in which the texture of the subsoil is at least one and a half texture groups finer than the surface soil, with clear to sharp horizon boundaries.

Although the term 'duplex' has only been used in Australia, soils with contrasting texture between soil horizons are found in other parts of the world (Chittleborough 1992). In 'Soil Taxonomy' (Soil Survey Staff 2006) soils showing characteristics most like those of the duplex soils are classified with the formative element 'pale' meaning to show excessive development. This includes 15 Great Groups in 3 Orders, the Mollisols, Ultisols and Alfisols.

Soils are classified into Pale-Great Groups if they posses either an argillic horizon, or a clay distribution profile that remains relatively constant for a depth of at least 1.5 meters, or an argillic horizon in which the upper 20 cm of which shows a clay increase of at least 20 %. Chittleborough (1992) however notes that this definition would however exclude many Australian duplex soils which have a sharp textural break between the A and B horizons. In the FAO-UNESCO World Soil Map (FAO-UNESCO 1987) duplex soils are accommodated in a range of classes, principally the Solonetz and Luvisol units (Chittleborough 1992). Approximate soil groups to the three texture contrast orders in the Australian Soil Classification are presented in Table 2.3-1 (Isbell 2002).

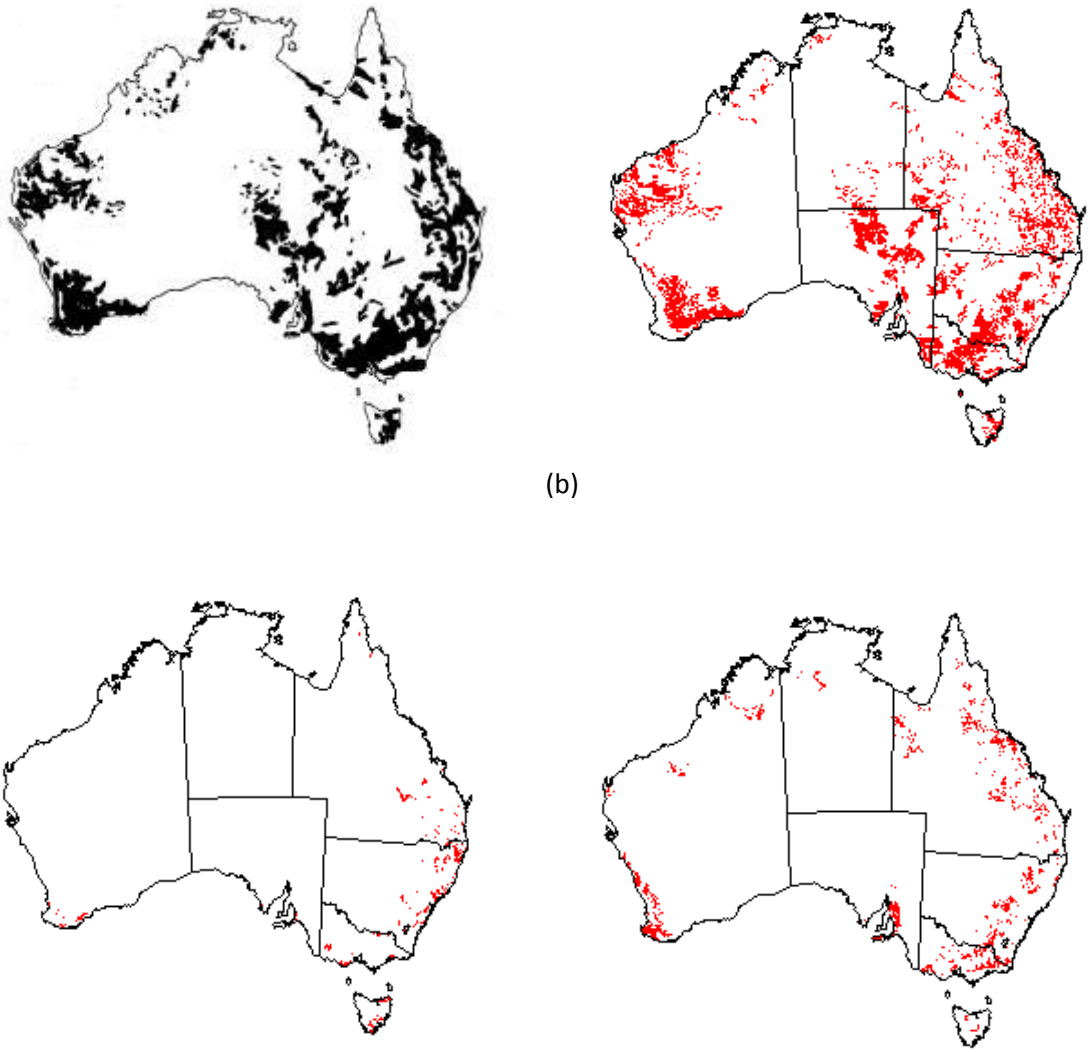

Figure 2.3-1 Distribution of (a) duplex soils (Chittleborough 1992), (b) Sodosols (Isbell 2002), (c) Kurosols (Isbell 2002), (d) Chromosols (Isbell 2002).

Table 2.3-1 Approximate correlation to other soil classification systems for the three orders of texture contrast soils described by Isbell (2002).

Order	Great Soil Group	Factual Key	Soil Taxonomy
Sodosols	Solodized solonetz and solodic, some soloths and red-brown earths, desert loams	Many duplex (D) soils	Alfisols, Aridisols
Chromosols	Non-calcic brown soils, some red-brown earths and a range of podzolic soils	Many forms of duplex (D) soils	Alfisols, some Aridisols
Kurosols	Many podzolic soils and soloths	Many strongly acid duplex soils	Ultisols, Alfisols

Estimates of the extent and distribution of texture contrast soils differ between soil classification systems. Based on the '*Factual Key for the Recognition of Australian Soils'* (Northcote 1979), Chittleborough (1992) estimated that the duplex soils cover approximately 20 % of the Australian land mass (Figure 2.3-1a). Using the Australian Soil Classification, Isbell *et al.* (1997) estimated that that texture contrast soils account for 17.0 % of the Australian landmass or 2.33 million km^2. Differences between estimates result from methodology, rather than extent. Texture contrast soils are important for agricultural production. According to Chittleborough *et al.* (1994) texture contrast soils occur on around 80 % of agricultural regions in southern Australia, and around 60 % of the agricultural regions of south-western Western Australia (Tennant *et al.* 1992).

2.3.2 Texture contrast, and sodic soils in Tasmania.

Based on Northcote (1962) map at 1 : 2 000,000 scale, and other small-scale soil maps, Doyle and Habraken (1993) estimated that at least 23 %, but possibly as much as 28 % of the land area of Tasmania is occupied by sodic soils. However reassessment based on the Australian Soil Classification (Isbell 2002), and the dominant Soil Orders of Tasmania Map (DPIWE 2004), Cotching *et al.* (2009) estimated that soil orders with texture contrast profiles, (Sodosols, Kurosols and Chromosols) occupy approximately 16.5 % of the Tasmanian landmass. Differences between estimates result from differences in classification and definition of what constitutes a texture contrast soil, and together with differences in reinterpretation and modelling of past soil surveys.

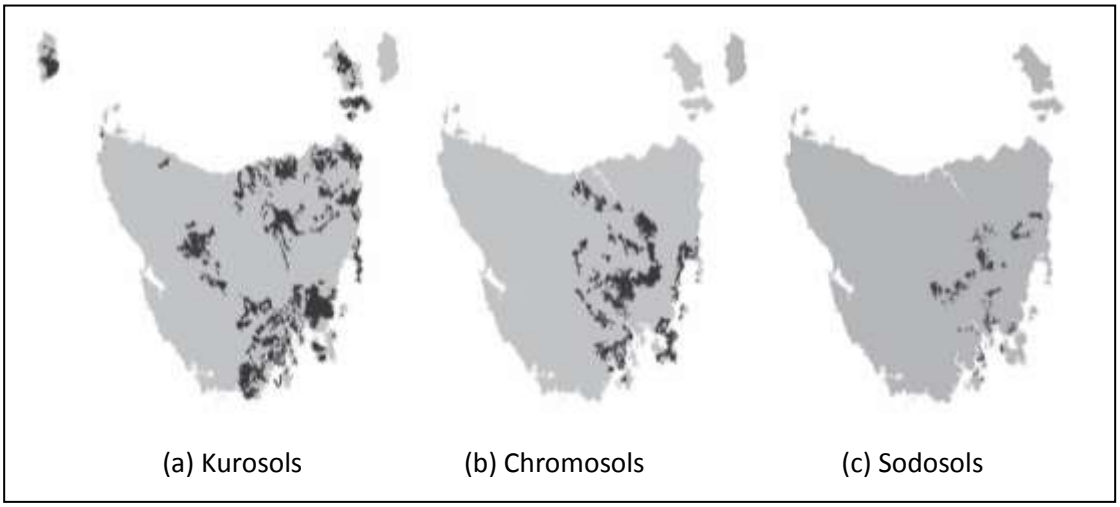

Figure 2.3-2 Distribution of texture contrast Soil orders in Tasmania (Cotching *et al.* 2009).

Table 2.3-2 Extent of texture contrast Soil Orders and landuse in Tasmania (Cotching *et al.* 2009).

	Total Area		Landuse (ha)							
Soil order	(ha)	(%)	Cropping	Perennial Hort.	Irrigated	Grazing		Forestry	Conservation	Urban
						Dryland	Natural			
Chromosol	348741	5.3	2527	487	390	110017	131365	64061	32553	7340
Kurosol	668870	9.6	14943	1571	4321	183610	129122	126553	159044	14741
Sodosol	108290	1.6	4115	327	11	73136	20070	4279	4957	1395

In Tasmania, the nature and characteristic of duplex soils varies enormously between geological units as well as over small distances within individual geological units (Osok and Doyle 2004). Sodosols occur in areas with annual rainfall less than 800 mm, primarily in the Launceston Tertiary Basin, the Derwent, Coal, Jordan, and Huon River Valleys, and on Flinders Island (Cotching *et al.* 2009). Sodosols have developed from a range of geological parent materials including; Permian Mudstones, Triassic sandstones, Jurassic dolerite, and recently formed Tertiary and Quaternary sediments (Doyle and Habraken 1993). Sodosols occupy 1.6 % of Tasmania, they are predominantly used for grazing, both on modified pastures and natural vegetation, however significant areas are also used for cropping (1600 ha, Table 2.3-2). Chromosols occupy 5.3 % of Tasmania (Table 2.3-2, Table 2.3-2), they occur in eastern and south-eastern regions in areas with less than 800 mm average annual rainfall. Kurosols occupy 9.8 % of Tasmania, they are predominantly used for grazing on both modified pastures and natural vegetation, with significant areas used for conservation and forestry (Table 2.3-2). After Ferrosols the Kurosols are the second most extensively used soil order for cropping in Tasmania (15 000 ha) (Cotching *et al.* 2009).

2.3.3 Texture contrast (duplex) soils of the Lower Coal Valley and University Farm

The occurrence, morphology and genesis of texture contrast soils in the Coal Valley and University Farm have been investigated by Holz (1993) and Beattie (1995). Beattie (1995) described the occurrence of three different classes of duplex soil (i) duplex soils of acid reaction trend formed in Tertiary clays (ii) other duplex soils of acid trend, and (iii) duplex soils of alkaline trend. The class (i) and (ii) soils are described as non-saline, strongly acidic and sodic, with high levels of exchangeable Al in the upper subsoil horizons and exchangeable sodium percentage (ESP) greater than 6.0. The subsoils are moderately to highly dispersive and internal drainage is extremely slow (Beattie 1995). Beattie (1995) described the occurrence of acid sodic duplex soils in the Lower Coal Valley as 'anomalous' as they have acid trend through the profile but otherwise lack evidence of strong leaching. Interestingly Beattie (1995) cites evidence of subsurface lateral flow in wet conditions, soil pits became "*water filled by lateral drainage (about 2°slope) through the sandy topsoils*". Holz (1993) inferred the majority of texture contrast soil in the Lower Coal Valley had formed in pebbly or stony debris-flow above an abrupt lithologic discontinuity to clast free tertiary clays. Holz (1993) noted the occurrence of sand infills in the B horizon of some duplex soils. He interpreted their formation as having occurred in a previous periglacial environment when cold, windy and dry conditions caused soil cracking and freezing. These conditions were also conducive to aeolian activity resulting in sand filling exposed vertical planar voids.

2.3.4 Management difficulties with texture contrast soils

Duplex soils are associated with a range of management problems including; waterlogging, poor crop establishment, crusting, poor root penetration, desiccation, wind erosion, water erosion, salinity and poor nutritional status (Edwards 1992; Gardner *et al.* 1992; Morrell 1992; Simeoni *et al.* 2009; Tennant *et al.* 1992). Crop production on these soils is constrained by existing and potential soil degradation (Gardner *et al.* 1992). A number of studies have reported degraded structure associated with cropping on texture contrast soils (Cotching *et al.* 2001; Gardner *et al.* 1992; Murphy and Flewin 1993; Tisdall and Oades 1980).

Texture contrast soils are naturally very hard setting (Hubble *et al.* 1983) and suffer low infiltration rates and poor water holding capacity (Greacen 1981) which is accentuated where excessive cultivation has occurred (Gardner *et al.* 1992). The presence of massive, poorly drained subsoils results in regular seasonal waterlogging which has consequences of poor aeration for roots, nitrogen deficiency, and increased manganese levels where pH is low (Gardner *et al.* 1992).

Crop yields are reduced and the poorer root development predisposes the plants to water stress late in the season. Cresswell and Kirkegaard (1995) and Pankhurst et al. (2002) report that texture contrast soils with dense clay B horizons restrict root growth and water infiltration causing up to 80 % of crop roots to be confined within or closely beside macropores. Reduced root distribution limits access to otherwise available soil water and nutrients in the subsoil, resulting in reduced crop production and greater potential for the unused water and nutrients to leach to shallow groundwater.

Reduced crop yields on duplex soils have also been attributed to poor aeration resulting from the slow movement of soil water through the upper B horizon resulting in the development of a perched watertables above the B horizon (Bakker *et al.* 2005; Brouwer and Fitzpatrick 2002a; Cox *et al.* 1996; Cox and McFarlane 1995; Eastham *et al.* 2000). In landscapes with sufficient slope, perched watertables may be exacerbated by lateral movement of water on the upper surface of the B horizon leading to waterlogging and salinity in lower parts of the landscape (Cox and McFarlane 1995; Gardner *et al.* 1992; McFarlane and Williamson 2002).

A small number of studies have reported management difficulties resulting from water repellence in texture contrast soils. Gardner *et al.* (1992) attributed development of water repellence in duplex soils in south eastern Australia to loss of organic carbon by cultivation. Chittleborough *et al.* (1992) noted that overland flow on duplex soils in the Mt Lofty Ranges resulted from seasonal development of water repellence associated with oxidation of organic carbon.

Hall *et al.* (2010) investigated use of clay spreading and deep cultivation to overcome severe water repellence in duplex soils along the south coast of Western Australia, and Crabtree and Gilkes (1999) investigated the use of wetting agents to overcome severe water repellence in duplex soils in Western Australia.

Current management of texture contrast soils in Tasmania has resulted in a number of soil degradation issues including; gully and tunnel erosion (Hardie 2009; Hardie *et al.* 2007), poor drainage and droughtiness, short cultivation window, salinity (Lisson *et al.* 2005) loss of organic carbon and structural decline (Cotching *et al.* 2001; Doyle and Habraken 1993). Cotching *et al.* (2001) reported that increased cropping on Sodosols in northern Tasmania decreased aggregate stability, infiltration rate and drainage at field capacity. Cotching *et al.* (2001) cites the major challenges for cropping Sodosols and Kurosols in the midlands of Tasmania's are to maintain organic matter levels, minimise tillage, prevent mixing the A1 and A2 horizons, and improve surface drainage.

2.3.5 Water movement and preferential flow in Australian texture contrast soils

The hydrology of texture contrast soils has received considerable research attention in relation to the development of seasonal ponding above the B horizon and development of subsurface lateral flow. Studies of seasonal ponding and subsurface lateral flow in texture contrast soils are listed by State; in Western Australia; Gregory *et al.* (1992), Smith and Hebbert (1983), Turner *et al.* (1987), in South Australia; Chittleborough *et al.* (1992; 1994), Cox *et al.* (2002), Cox and Pitman (2001), Fleming and Cox (1998), Naidu *et al.* (1993), Stevens *et al.* (1999), in New South Wales; Ticehurst (2004), Ticehurst *et al.* (2003a; 2005; 2003b) and Victoria; Brouwer and Fitzpatrick (2002b). No published studies have been conducted on the hydrology of texture contrast soils in Tasmania.

Review of the Australian literature indicates that subsurface lateral flows are a relatively minor component (<10 %) of the hydrological budget under rainfed conditions (Ticehurst 2004). However little data is available to make similar assessment in irrigated landscapes despite the widespread occurrence of irrigated agriculture on texture-contrast soils. Studies in South Australia have demonstrated that subsurface lateral flow in texture contrast soils is an important pathway for off-site transport of environmental contaminants. Stevens *et al.* (1999) found that environmentally significant amounts of both dissolved and particulate phosphorus, nitrate and dissolved organic carbon moved as subsurface lateral flow and via macropores at the A / B boundary in texture-contrast soils in the Adelaide Hills.

Studies at the Flaxley Research Station showed that only 2 % of total phosphorus movement resulted from subsurface lateral flow (Fleming and Cox 1998; 2001). While in the Keynes catchment, nitrate losses were found to be up to 21 times higher in subsurface flow than in overland flow (Cox and Ashley 2000; Cox and Pitman 2001). Cox *et al*. (2002) explain that solute variability in subsurface lateral flow resulted from differences in the relative contribution to flow from macropores and the soil matrix. Leaney *et al.* (1993) found that between 80 – 90 % of subsurface lateral flow in a texture contrast soil in South Australia resulted from flow through macropore networks.

The importance of macropores on the development of subsurface lateral flow and solute movement in texture contrast soils is poorly understood. Smettem *et al*. (1991) found that soil macroporosity and bypass flow were responsible for preventing subsurface lateral flow at the A / B horizon boundary in a texture contrast soil near Mt Bold, South Australia. They found bypass flow through soil macropores in the B horizon resulted in field saturated hydraulic conductivities that were considerably higher than would be predicted from textural analysis. Consequently, the distinct textural boundary within the profile did not act as a throttle to vertical infiltration, resulting instead in subsurface lateral flow, along the soil / rock interface.

Brouwer and Fitzpatrick (2002b) also found that macroporosity resulting from root holes provided sufficient hydraulic connectivity to prevent the development of subsurface lateral flow on a series of texture-contrast soils in the Dundas Tablelands, Western Victoria. Cox *et al.* (2002) speculated that the presence of clay cutains and large fractures and macropores reported by Kirkby *et al.* (1997) indicate preferential vertical flow of water and colloidal material through the profile of texture contrast soils in South Australia. Ticehurst (2004) also noted that in the Billabong Creek catchment in southern New South Wales, the B2 horizon did not impede vertical drainage in some locations, presumably due to macropore flow through the upper B horizon.

The effect of antecedent moisture on preferential flow and subsurface lateral flow in texture-contrast soils has not been specifically studied. Antecedent soil moisture has been shown to increase subsurface lateral flow in catchments with shallow bedrock (Kim *et al.* 2005; Lowery *et al.* 1982; Scanlon *et al.* 2000) due to increased connectivity between depressions in the bedrock surface (Sidle *et al.* 2001; Tromp-Van Meerveld and McDonnell 2006b), and macropore segments (Sidle *et al.* 2001). However Silberstein *et al.* (1999) postulated that seasonal shrinkage of a duplex soil in the Ucarro catchment, Western Australia, resulted in relatively rapid drainage in early winter when the soil was dry, however as winter proceeded subsoil swelling of clays is thought to have closed the preferential flow paths which increased ponding and lateral flow.

2.4 Soil water modelling

Soil water models enable evaluation of soil water processes outside the range of management or climatic conditions able to be tested using traditional experimental studies. Modelling also enables issues of concern such as the risk of agrochemical leaching to groundwater, or the effect of preferential flow on irrigation efficiency to be investigated (Beulke *et al.* 2001; Jarvis 2007; Köhne *et al.* 2009b; Simunek and van Genuchten 2008). Soil water models are also a component of larger farming system models or are used in conjunction with management / crop / climate models to explore a wide range of production and environmental questions.

Accurate process based modelling of preferential flow and solute transport remains a major challenge in vadose zone hydrology (Simunek and van Genuchten 2008). Direct modelling of water and solute movement in macroporous soils is difficult due to the complex nature of preferential flow paths, non equilibrium processes governing soil water movement, and difficulty quantifying macropore networks.

Increasing evidence exists that variably saturated flow in many field soils is not consistent with the uniform flow patterns typically predicted by the Richards equation (Flury *et al.* 1994; Hendrickx and Flury 2001; Simunek and van Genuchten 2007). This is due to the presence of preferential flow, which unlike uniform flow predicted by Richards equation, results in irregular wetting of the soil profile as a consequence of water moving faster in certain parts of the soil profile than others (Simunek and van Genuchten 2007).

Beven (2002) argues that the uniqueness of a site is impossible to characterise in detail, particularly for subsurface flow pathways and macroporosity, and as such can never be realistically represented in physical models. However over the last two decades, a relatively large number of commercially available models have been developed that consider preferential flow, reviwed by Köhne *et al.* (2009a), Simunek *et al.* (2003), Simunek and van Genuchten (2007; 2008). These models range from relatively simplistic bi-modal dual-porosity models to complex dual-permeability, and multi-region models (Figure 2.4-1).

2.4.1 Single Porosity Models – Richards equation models

Variably saturated flow in soils is described according to the Richards (1931) equation which combines the Darcy-Buckingham equation for the fluid flux with a mass balance equation (Simunek and van Genuchten 2007).

The Richards equation assumes that soil is incompressible, non-hysteretic, with atmospheric gas pressure throughout, and that moisture moves in a single phase within the soil matrix only, and not via macropores or non-uniform processes (Gerke 2006; Ranatunga *et al.* 2008), (Figure 2.4-1a). In uniform soil, infiltration is driven by the soil water potential gradient, which results in the development of a level, uniform wetting front. Well known examples of Richards equation based models include; HYDRUS (Simunek *et al.* 1999a), SWIMv2 (Verburg *et al.* 1996), and SWAP (Kroes *et al.* 2000), (although some of these models now contain multiple pore domain functionality).

Solutions of the Richards equation require knowledge of the soil water characteristic which relates the pressure head h to the water content $\theta(h)$ and the unsaturated hydraulic conductivity, $K(h)$. These relationships are typically described using either the van Genuchten - Mualem (Mualem 1976; van Genuchten 1980) or the Brooks - Corey (1964) functions.

In macroporous soils, single pore domain models must be able to adequately represent flow in all pore sizes with a single hydraulic function, however the van Genuchten - Mualem equation is often not able to adequately reproduce the shape of measured functions near saturation (Greco 2002). Difficulty also exists with the van Genuchten function near saturation due to non linearity and model instability resulting from the large increase in the hydraulic conductivity in response to small changes in pressure head (Clothier and Smettem 1990; Larsbo *et al.* 2005). Other simplifying assumptions inherent with the use of single pore domain models include the assumption of laminar flow, rigidity of the solid phase (i.e. no shrinkage or swelling), and no air entrapment (Gerke 2006).

2.4.2 Dual porosity and dual permeability models

Non-equilibrium flow and transport in soil requires approaches which are convenient for mathematical description and computation. Presently the two region approach in which the porous medium consists of two interacting pore domains, one associated with the macropores, and the other the soil matrix, are the most popular and widely accessible approaches for simulating flow in macroporous soils. This is largely due to the commercialisation of dual porosity / permeability models, their straight forward formulation, limited parameter requirements and increasing development of inverse techniques and pedotransfer functions to simplify parameterisation (Leij and Toride 1998).

Dual porosity and dual permeability models assume that the porous media consists of two interacting regions, one associated with the inter-aggregate, macropore or fracture system, and one comprising micropores inside soil aggregates or the soil matrix.

Dual permeability models treat the persistence of the preferential flow domain as a continuum without identifying the actual geometry of the domain (Gerke *et al.* 2010). The actual size, form and number of macropores are not explicitly defined in the modelling. Instead the macropore characteristics are captured by the unsaturated soil hydraulic properties near saturation as described by the soil moisture retention function and mass transfer parameters that enable exchange between the micropore and macropore domains (Christiansen *et al.* 2004).

Due to the complex nature of water movement in macropores, simple quasi-physical approaches are often invoked to describe gravity-driven flow in macropores rather than the more complex Navier-Stokes law which describes the flow of viscous fluids (Jarvis 2007).

A range of approaches exist for simulating flow within the macropore domain including the use of; Poiseuille's equation (Ahuja and Hebson 1992) the Green and Ampt or Phillip infiltration model (Ahuja and Hebson 1992), the kinematic wave equation (Di Pietro *et al.* 2003) (Germann and Beven 1985; Jarvis 1994), and a modified form of the Richards equation (Simunek *et al.* 1999a). Hincapié and Germann (2009) describe water movement in macropores as a gravity driven wave, while Nimmo (2010) recently conceptualised preferential flow as laminar based film along the walls of pores, in which flow was simulated by combination of the Darcy-Buckingham law and the continuity equation. A range of approaches exist to describe the mass transfer between the micropore and macropore domains including pressure head gradient and structural effective diffusion pathlengths (Gerke *et al.* 2010; Gerke and Van Genuchten 1993b; Jarvis 1994; Simunek *et al.* 2003)

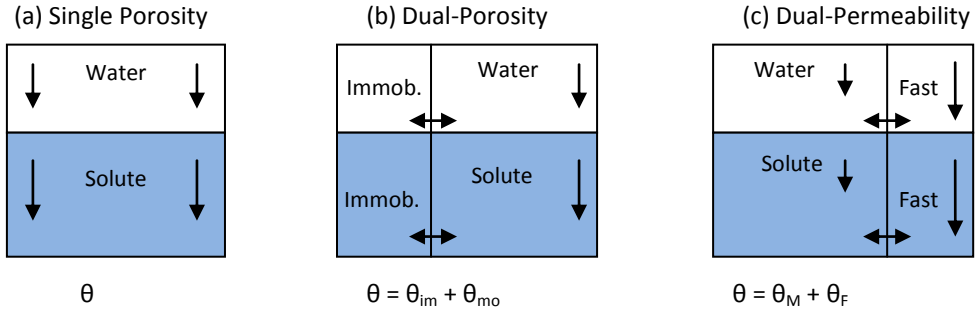

Figure 2.4-1 Conceptual representation of physical non-equilibrium models for water flow and solute transport, adapted from Simunek and van Genuchten (2008), (a) Uniform flow, θ water content, (b) Dual-Porosity, θ_{mo} and θ_{im} water content of the mobile and immobile flow regions, (c) Dual-Permeability, θ_M, and θ_F water content of the mobile flow regions of the matrix domain, and in the macropore (fracture) domain.

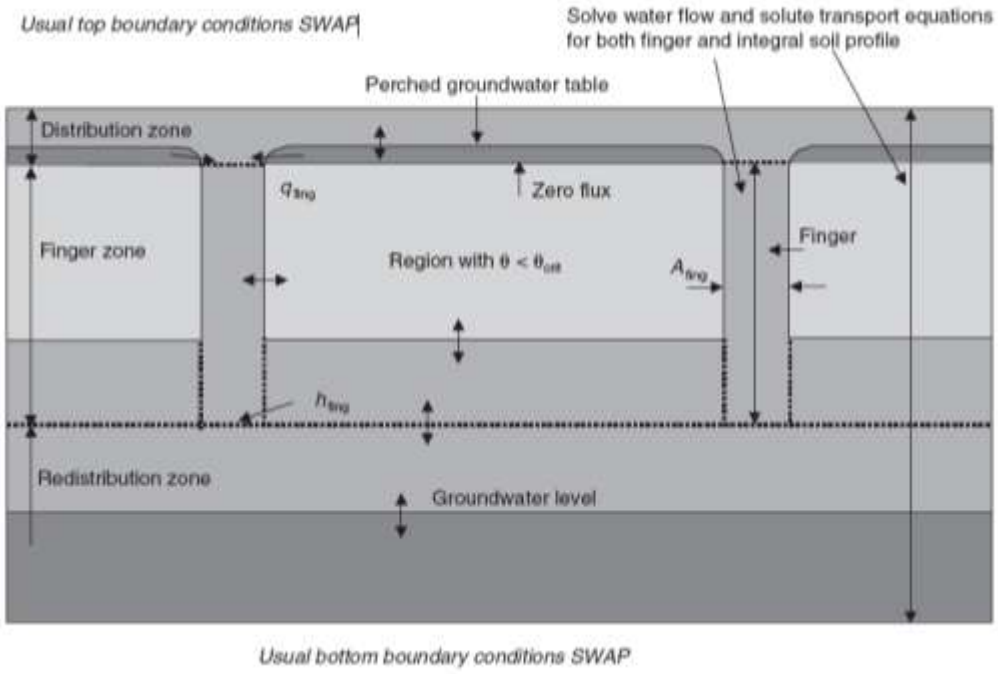

Figure 2.4-2 Schematic overview of finger flow concept in SWAP (Kramers *et al.* 2005).

2.4.3 Modelling water movement through shrinkage cracks

While the swelling of clay minerals at the scale of individual clay lamellae is relatively well understood, prediction of hydraulic properties of swelling soils is limited, as modelling requires coupled hydraulic and mechanical models capable of simulating both movement of solids and water (Gerke 2006; Haws *et al.* 2005; Tuller and Or 2003). Modelling water and solute movement in shrinkage cracks poses difficulties in terms of quantifying the variable pore size and connectivity, as well as simulating water movement in planner voids as opposed to cylindrical pores. While x-ray computed tomography (CT) have been successfully used to quantify pore networks at specific moisture contents (Mori *et al.* 1999b), ability to simulate water movement in shrink-swell soils has proven difficult, due to; the complexity of the pore networks, the exhaustive requirement for input data (van Dam *et al.* 2004), and unresolved difficulties with the simulation of changing pore geometries (Gerke *et al.* 2010).

Despite these difficulties, simplified crack flow routines have been incorporated into a number of existing dual porosity and dual permeability models including; MACRO (Jarvis 1994), VIMAC (Greco 2002), SWAP (van Dam *et al.* 1997), and the FRACTURE module (Novak *et al.* 2000; Novak *et al.* 2002) in HYDRUS (Simunek *et al.* 1999a). Rather than attempting to simulate water movement through individual pore networks, these models account for the additional porosity created by shrinkage by adding to the existing (stable) macropore domain. The shrinkage crack porosity at a specific antecedent soil moisture content is determined from the soil shrinkage characteristic curve (SSCC) which relates changes in bulk volume of the soil to water content (Cornelis *et al.* 2006; Greco 2002). Treatment of water movement within cracks differs substantially between models.

2.4.4 Simulating water movement in water repellent soil

The conventional Richards equation cannot predict the occurrence, solute transport, or final extent of finger flow unless both hysteresis and the water entry pressure are considered. Without these factors, capillary diffusion smooths out fingers at the moment of formation and water in the matrix between the fingers is able to move downward (Jury *et al.* 2003). Development of models capable of simulating finger flow has proved difficult (van Dam *et al.* 2004), as a sufficiently flexible conceptual model that describes the effect of moisture content and wetting history on water movement in water repellent soil is still missing (Bachmann *et al.* 2007). Modelling finger flow requires combining Richards' equation with a kinematic wave approach (Di Pietro *et al.* 2003; Selker *et al.* 1992a) or extensions of the Richards' equation (Gerke *et al.* 2010).

Ritsema *et al.* (2005) developed a finger flow module (SWFING) for the Soil-Water-Atmosphere-Plant (SWAP) model (van Dam *et al.* 1997) in which preferential flow paths (fingers) formed when infiltration occurred in soil below a critical water content (θ_{crit}) (King 1981; Ritsema and Dekker 1994), (Figure 2.4-2). Recently Bachmann *et al.* (2007) and Deurer and Bachmann (2007) developed a water-content and time-dependent Contact Angle (CA) model. Their approach represented an extension of the van Genuchten equation for the capillary pressure-saturation relationship, in which the van Genuchten α parameter is modified to account for the effect of the time-dependent contact angle on the hysteresis of the capillary pressure-saturation relationship.

2.4.5 Model parameterisation of single and multiple pore domain models

Single porosity models require knowledge of the θ(ψ) and K (ψ) relationships for each soil layer. The θ(ψ) relationship is usually described by either the van Genuchten (1980), or Brooks - Cory (1964), equations while the K (ψ) relationship is derived from the saturated hydraulic conductivity and the θ(ψ) relationship via Mualem (1976) or Burdine (1953) equations. Parameter values are typically solved using curve fitting software such as RETC (van Genuchten *et al.* 1991) in which analytical models are fitted to observed water retention data. Fitting is achieved by nonlinear least-squares optimization to estimate the unknown model parameters from observed data by finding a solution to the equation that maximizes the sum of squares, while minimizing the residual sum of squares, SSQ (van Genuchten *et al.* 1991).

Dual permeability and porosity models require parameterisation of both the micropore and macropore flow domains and mass transfer parameters that control flow between the two domains. The additional parameterisation requirement of dual porosity and permeability models has limited their widespread adoption and use. For example, the dual-permeability model of Gerke and van Genuchten (1993a) requires 16 parameters to describe water flow (Simunek *et al.* 2003) compared to 6 parameters required for the single porosity flow model in HYDRUS-2D.

Many soil parameters required by dual porosity and dual permeability models are either difficult or impossible to measure (Larsbo and Jarvis 2005; Simunek and van Genuchten 2008). To date, model developers have provided little guidance on the direct approaches for measurement of the macropore domain and mass transfer soil parameters in multiple porosity models (Simunek *et al.* 2003).

While independent direct measurement of soil parameters is always preferred (Logsdon 2002), a number of inverse techniques have been developed to estimate soil water parameters for both single and multiple porosity models. Use of inverse parameterization techniques is particularly attractive for parameterising dual porosity and dual permeability models due to the large number of difficult to measure or un-measurable parameters (Köhne *et al.* 2006b; Larsbo and Jarvis 2005).

Inverse modelling estimates the unknown parameters through minimization of the difference between observed and simulated flow variables, which are defined in an objective function. Minimization is achieved through an iterative solution of the transient flow equation (Hopmans *et al.* 2002).

Estimation of soil hydrological parameters by inverse techniques is relatively complex, involving use of mathematical methods to determine unknown causes based on observation of their effects (Hopmans *et al.* 2002). Inverse modelling approaches assume *a priori* that the applied process model and the selected hydraulic relationships are the exact description of the soil's physical behaviour, and therefore model error is negligible. This implies that deviations between simulations and observations are caused by randomly distributed measurement errors rather than model inadequacy. Inverse methods require three interrelated components (i) a controlled transient flow experiment for which boundary and initial conditions are specified (ii) a numerical model for simulating transient flow, and (iii) an optimisation algorithm.

Inverse modelling techniques have been used to determine soil and solute parameters for single porosity models from column experiments (Köhne *et al.* 2006b; Roulier and Jarvis 2003), evaporation experiments (Minasny and Field 2005; Romano and Santini 1999; Simunek *et al.* 1998d), and tension infiltrometers (Kodesova *et al.* 2010; Ramos *et al.* 2006; Simunek *et al.* 1998a; Simunek and van Genuchten 1997; Simunek *et al.* 1999b). Kodesova *et al.* (2010) used inverse solution of disk infiltrometers and Guelph permeameter data to derive hydraulic conductivity parameters for the dual permeability model in HYDRUS-2D/3D.

Interpreting the reliability of results from inverse solutions is not straight forward, as estimates of parameter accuracy and range of validity are not readily obtained (Durner *et al.* 1997). Difficulty with inverse parameter estimation of soil hydraulic functions may result from a ill-posed problem which cause the model to diverge (fail to find global minimum) or result in inaccurate or non unique parameter estimates (equifinality) (Hopmans *et al.* 2002). Despite the obvious appeal and potential application of inverse techniques to deriving 'field based' input parameters, Simunek *et al.* (2003) warns "*Very little is currently known about the possibilities and potential problems of applying inverse modelling techniques to preferential flow models*".

2.5 Conclusion

Since the 1970's a considerable body of literature has demonstrated that preferential flow is the "rule rather than the exception" (Bachmair *et al.* 2010), being both common and widespread (Flury *et al.* 1994). The term 'preferential flow' refers to a number of non-equilibrium flow processes which may act independently or together, including but not limited to; macropore flow in stable biopores (Beven and Germann 1980), funnel flow between different soil layers (Kung 1990a), finger flow in hydrophobic soils (Ritsema and Dekker 2000), and macropore flow in shrink-swell clays (Greco 2002).

Preferential flow has been demonstrated to result in rapid, deep leaching of pesticides and nutrients, resulting in contamination of ground water and surface waterways (Flury 1996; Kladivko *et al.* 2001; Köhne *et al.* 2006a; Oostindie and Bronswijk 1995; Shipitalo and Edwards 1996). Preferential flow results in uneven wetting of agricultural soils, resulting in uneven seedling germination and crop growth, reduced water use efficiency (Garg *et al.* 2009) and mobilisation of fertiliser and nutrients beneath the root zone (Jarvis 2007). Despite considerable progress over the last three decades, Gerke *et al.* (2010) states that "*many aspects of preferential flow are still not fully understood*".

Australian research on preferential flow is limited in scope and volume of publications. A number of studies have investigated the occurrence of perched watertables, subsurface lateral flow and nutrient mobilisation in texture contrast soils (Cox and Pitman 2001; Stevens *et al.* 1999). However, little is known of the other forms of preferential flow in texture contrast soils or preferential flow in other Australian soils. Additionally very few studies have sought to apply preferential flow models to Australian soils. Considering the importance of texture contrast soils for agricultural production in south eastern Australia (Chittleborough *et al.* 1994), and their inherent hydrological complexity further research is required to understand how antecedent soil moisture influences the occurrence, nature and extent of preferential flow in texture contrast soils.

Management and assessment of the risks posed by preferential flow requires the use of soil water models that specifically account for preferential flow and non equilibrium solute movement. However, the occurrence of preferential flow invalidates the assumptions inherent in the Richards equation and thus use of single pore domain models (Gerke 2006; Jarvis 2007). Of the range of preferential flow models which have been developed over the last 20 years, the dual porosity and dual permeability models have become the most widely accepted approaches for predicting agrochemical leaching in agricultural soils (Köhne *et al.* 2009a).

There has been considerable progress in understanding preferential flow processes, and development of inverse parameter estimation procedures over the last two decades. However significant challenges for accurately modelling preferential flow remain. These include: development of robust parameterisation techniques (Gerke 2006; Larsbo and Jarvis 2005), process understanding of film and rivulet flow (Gerke *et al.* 2010), spatial representation of hydrophobicity and microtopography (Bachmair *et al.* 2010), simulating finger flow in temporally variable hydrophobic soil (Bachmann *et al.* 2007), and representation of volume or structure change with soil moisture content and burrowing (Gerke 2006; Gerke *et al.* 2010).

Review of the literature demonstrates considerable opportunity to acquire deeper understanding of the processes by which water infiltrates hydrologically complex soils such as the texture contrast soils. Detailed investigation of the hydrology of texture contrast soils is expected to provide a number of valuable opportunities for further development of preferential flow capability in existing soil water models.

3.0 Site and Soil Profile Characterisation

3.1 Introduction

Initially it was expected that a number of sites would be established around Tasmania to investigate soil water processes in texture contrast soils. However the complexity of the infiltration processes revealed by the preliminary dye staining experiment at the University of Tasmania Farm (Figure 1.3-1) focused attention on infiltration processes at the pedon rather than the hillslope scale. As the methodology for the project developed, it became apparent that research would require considerable excavation and disturbance to field sites. This was considered unacceptable on privately owned, or commercially operated property. Consequently research activities were conducted solely at the University of Tasmania Farm. A reconnaissance soil survey was conducted of the University of Tasmania Farm in May 2007, based on prior mapping by Holz (1993). The survey identified the variety of texture contrast soils within the vicinity of the Far Dam and Radar paddocks broadly represented the typical range of texture contrasts soils found in Tasmania.

The University of Tasmania Farm comprises an area of 342 ha on the edge of Pitt Water, a RAMSAR listed wetland, approximately 12 km N-E of Hobart (42^{o}47'S, 147^{o}26'E) within the Coal River valley. Climatic data recorded at the Hobart Airport located 7.7 km S-E of the University Farm is presented in Table 3.1-1 (Bureau of Meteorology 2009). The climate of the Coal River valley is described as 'dry subhumid warm' (Gentilli 1972), with notable rainfall uniformity throughout the year.

Table 3.1-1 Climate data Hobart Airport, location 42.83 °S , 147.50 °E, 1958 – 2009.

	Jan	Feb	Mar	Apr	May	Jun	Jul	Aug	Sep	Oct	Nov	Dec	Annual
Mean Rainfall (mm)	41.0	36.6	36.6	43.2	34.5	32.1	43.9	46.4	40.7	47.0	43.3	53.6	498
Mean maximum temperature (°C)	22.5	22.3	20.7	18.1	15.2	12.9	12.4	13.4	15.3	17.3	18.9	20.6	17.5
Mean minimum temperature (°C)	12.0	12.0	10.7	8.7	6.6	4.6	4.1	4.6	6.0	7.5	9.1	10.7	8.0
Mean daily sunshine hours (hrs)	8.2	7.8	6.7	5.8	4.6	4.2	4.8	5.6	6.3	7.2	7.5	7.8	6.4

Figure 3.1-1 Location of soil physical investigations, at the University of Tasmania Farm, Cambridge, Tasmania.

Note bright green colour of the farm dam (south) suggests offsite movement of nutrients to waterways leading to algal growth.

Soils within the vicinity of the Radar and Far Dam paddocks (Figure 3.1-1). have been described by Holz (1993), as having a single grain, loamy sand A horizon and a thin conspicuously bleached A2 horizon, overlying a mottled yellowish brown (2.5YR5/6) medium clay, with a columnar structured B2 horizon. The vertical faces of the columns in the upper B2 horizon are stained by organic matter and carry a coating of sand washed down from the A horizon. Soils within the Radar unit are derived from distal deposits of an alluvial fan overlying Tertiary clay sediments, in which the sandy A horizon is predominantly derived from aeolian material (Holz 1993). The Radar soil unit was classified as Dy 5.41 (Northcote 1979), Soloth (Stace *et al.* 1968), Aquic Natrustalf (Soil Survey Staff 2006) and Mottled Eutrophic Brown Kurosol (Isbell 2002).

Following the reconnaissance survey, the Radar and Far Dam paddocks were selected for detailed study. Investigations were conducted to:

- Determine the extent and nature of spatial variation of soil properties using electromagnetic induction (EMI).
- Identify appropriate sites for detailed hydrological investigations.
- Determine differences in soil physical and chemical properties between field sites.
- Characterise differences in soil morphology between field sites.
- Infer infiltration and soil water redistribution processes based on soil morphology, and basic chemical and physical attributes.

Figure 3.1-2 Equipment used for EMI survey, Geonics EMI38, ad Garmin 12 Xl GPS

Figure 3.1-3 Equipment used in sample collection for calibration of EMI data, Far Dam paddock.

3.2 Methodology

3.2.1 Survey of soil variability (EMI38)

Electromagnetic induction (EMI) techniques are able to detect variations in electromagnetic response from differences in the ionic concentration of earthen materials. Factors influencing the apparent conductivity of earthen materials include (i) moisture content, (ii) amount and type of ions in the soil water, (iii) and amount and type of clays in the soil matrix. While EM devices are highly sensitive to changes in soil salinity, in non-saline soils, soil texture, moisture content, and cation exchange capacity also influence apparent conductivity (Doolittle *et al.* 1994). EMI techniques have been used to identify and map the depth to stratigraphic units such as hydraulically impeding layers (Doolittle *et al*. 1994) and infer the existence of subsurface lateral flow paths (Yoder *et al.* 2001).

The EMI surveys were conducted using a Geonics EMI38 in QP mode, and a handheld Garmin 12 XL GPS (accurate to 3-5 meters) (Figure 3.1-2). The surveys consisted of 467 readings of apparent conductivity (ECa) in both vertical and horizontal dipoles, 261 spot heights (elevation) measured from a nominal datum using a WILD NAK2 level. Calibration of apparent conductivity (EC_a) to soil moisture and soil salinity ($EC_{1:5}$) was conducted from 144 soil samples, from 21 locations in three series (U1 to U3) (Figure 3.3-1 and Figure 3.3-3). Details of the sampling depths are presented in Appendix 3.0. EC_a values were determined at the time of sampling from five EC_a readings within 2 meters of the sampling point prior to auguring (Figure 3.1-3).

Electrical conductivity was determined as a 1:5 extract using 20 g, <2 mm, air dried samples according to procedure 3A1 Rayment and Higginson (1992) using a calibrated HACH 9333100 meter. Gravimetric moisture content was determined according to method 2A1 Rayment and Higginson (1992). Apparent electrical conductivity (EC_a) was calibrated with soil moisture and $EC_{1:5}$ using average values for the whole soil profile and depth weighted values**.**

As EMI38 response varied with soil depth and device orientation, a depth weighting factor based on the depth response curves of Huth and Poulton (2007) was applied to the calibration data. (Appendix 3.1). Conductivity maps were produced using SURFER version 8, employing default kriging settings and a low level of contour smoothing**.**

3.2.2 Site location, profile description and classification

Sites for detailed pedological and soil physics investigations were determined following the EMI38 survey. Sites were selected to represent the range of texture contrast soils in Tasmania, especially in relation to the thickness of the A2 horizon and degree of sand infill development.

Sites A (lower slope), B (mid slope) and C (upper slope) were located within the Far Dam paddock. Site A was located adjacent to a pesticide degradation study (Doyle *et al.* 2008) in order to contribute to current knowledge of pesticide mobility in Tasmanian soils. The Far Dam paddock had been managed as long term native dominated by Velvet (*Poa rodwayi)* and Silver *(Poa labillardierei)* tussock grass with grazing by sheep. Site D was located in the Radar paddock, on soils derived from Tertiary sediments (Holz 1993). The Radar paddock has been managed for irrigated cropping two in every five years with pasture grown in other years (Figure 3.1-1).

Profile descriptions were conducted according to McDonald *et al*. (1990) in October 2007 following a prolonged period without rainfall. Pits were excavated using a 6 tonne excavator to approximately 1.5 meters depth. Soils were classified according to Australian Soil Classification (Isbell 2002), USDA - Keys to Taxonomy (Soil Survey Staff 2006), and FAO - Soils of the World (FAO-UNESCO 1987).

3.2.3 Soil chemistry

Chemical analysis was conducted on bulked 300 g samples, obtained at 10 cm depth intervals between 0 cm and 70 cm, and at a further two depth intervals between 70 cm and 130 cm depending on horizon depth (Table 3.2-1). An additional sample was obtained from the A2 horizon at sites A, B & C. Details of the sampling depth for chemical analysis is presented in Table 3.2-1.

Samples were analysed for the following attributes at CSBP laboratories (Bibra Lake, W.A.).

- EC, pH_{h20} & pH_{CaCl} – 1:5 soil : solution ratio stirred for 1 hour at 25°C. The extract was measured using a combination pH electrode calibrated against 0.01M KCL (Rayment and Higginson 1992).
- Organic Carbon – Walkley-Black approach, concentrated sulphuric acid & dichromate oxidation. The proportion of chromic ions was measured colorimetrically at 600 nm (Walkley and Black 1934).

Table 3.2-1 Sampling depth (cm) for chemical analysis.

Depth (cm)	Site A	Site B	Site C	Site D
0-10	✓	✓	✓	✓
10-20	✓	✓	✓	✓
20-30	✓	✓	✓	✓
30-40	✓	✓	✓	✓
40-50	✓	✓	✓	✓
60-70	✓	✓	✓	✓
70-80		✓		
80-90			✓	✓
90-100	✓	✓		
100-110				✓
110-120		✓		
120-130	✓		✓	✓
$A2_e$	12-14cm	15-17cm	16-18cm	

Table 3.2-2 Sampling depths (cm) for liquid limit, linear shrinkage and particle size analysis.

Horizon	Site A	Site B	Site C	Site D
A1	0-10 cm	0-10 cm	0-10cm	0-10 cm
$A2_e$	12-14 cm	15-17 cm	na	na
B21	20-30 cm	30-40 cm	20-30cm	20-30 cm
B22	60-70 cm	60-70 cm	60-70 cm	60-70 cm
B23	90-100 cm	90-100 cm	80-90 cm	100-110 cm

Table 3.2-3 Sampling depths (cm) for Emerson dispersion test.

Horizon	Site A	Site B	Site C	Site D
A1	5 cm	5 cm	5 cm	5 cm
$A2_e$	12 cm	16 cm		
B21	35 cm	25 cm	20 cm	15 & 30 cm
B22	63 cm	75 cm	45 cm	65 cm
B23	110 cm	110 cm	90 cm	105 cm
B24		135 cm		
Mixed A1/ B21			15 cm	

- Exchangeable Cations – Gilman and Sumpter method, with ethanol prewash and 0.1M $BaCl_2$ / 0.1M NH_4Cl extraction. Concentrations of Ca, Mg, Na, Al and K measured by ICP-AES (Rayment and Higginson 1992).
- Total Nitrogen – combustion at 950 ^oC in oxygen using Leco FP 428 Nitrogen Analyser.
- Total Phosphorous – digested in sulphuric acid with colorimetric determination at 880 nm (Allen and Jeffery 1990).
- Ammonium and Nitrate – 2M KCL 1:5 soil solution ratio. Ammonium was measured colorimetrically at 420 nm using indo-phenol blue reaction. Nitrate was measured colorimetrically at 520 nm using a Lachat Flow Injection Analyser (Searle 1984).
- Chloride – was determined colorimetrically with a Lachat Flow Injection Analyser following liberation of thiocyanate ion from mercuric thiocyanate (Rayment and Higginson 1992).

Total Exchangeable Bases (TEB) was calculated as the sum of exchangeable Ca^{2+}, Na^{+}, Mg^{2+} and K^{+}. Cation Exchange Capacity (CEC) was calculated as TEB plus exchangeable Al. Effective Cation Exchange Capacity (ECEC) was calculated as CEC plus exchangeable acidity. Base saturation was calculated as the TEB divided by ECEC. Exchangeable Sodium percent (ESP) was calculated as the percent exchangeable Na^{+} divided by TEB in which AL^{+3} was included as a cation due to subsoil acidity.

3.2.4 Water repellence

Water repellence was measured at 0 - 3 cm and 10 - 13 cm depths from the A1 horizon at each site. Samples were dried at 40 ^oC for 24 hours, passed through a 2 mm sieve to remove roots, and allowed to cool to room temperature.

The persistence of water repellence was determined by the Water Drop Penetration Time (WDPT) test in which the time taken for five 10 µg drops of distilled water to penetrate soil was determined (Doerr *et al.* 2007; Letey *et al.* 2000). Samples in which the drops had not penetrated the soil after 1 hour were covered to reduce evaporation (Caron *et al.* 2008). WDPT was classed according to Dekker *et al.* (2000).

The severity of water repellence was measured using the Molarity of Ethanol Droplet (MED) test, in which the molarity of ethanol solution at which three 10 µm drops penetrate the soil in 10 seconds was determined (Carter 2002). MED values were classed according to Watson and Letey (1970).

Figure 3.2-1 Apparatus for measuring liquid limit (a) Drop cone penetrometer (b) Casagrande device.

3.2.5 Soil physical properties

Sampling for physical analysis was conducted in October 2007. Bulked samples were obtained at 10 cm increments from the soil surface to 100 cm depth. Sampling details are presented in Table 3.2-2 and Table 3.2-3. Particle size was determined for key soil horizons by modified pipette procedure (Indorante *et al.* 1990) at CSBP laboratories, and classified according to the ISSS (McDonald *et al.* 1990). Liquid limit was determined on three samples from bulked soil which had been ground and sieved to < 500 µm (a 425 µm sieve was not available). Liquid limit was determined by either drop cone penetrometer (McBride 2008) (BS 1377: part 2: 1990) for sands, or the one point Casagrande method (McBride 2008) (ASTM D4318-98; BS 1377: part 2: 1990) for clays (Figure 3.2-1).

For the one point Casagrande method the liquid limit was calculated as;

$$w_L = w(N/25)^{0.12}$$

w_L = Upper plastic limit Index (reported to nearest whole number).

w = Moisture content at sampling.

N = Number of blows.

Linear shrinkage was determined from remoulded ground <500 µm soil, wet-up to the liquid limit, pressed into standard semi-cylindrical mould and dried to 105 ^{0}C for 24 hours. A minimum of two replicates were tested on all samples. If linear shrinkage differed by more than 5 mm (4 %) a third test was conducted. Linear shrinkage was classified according to Mills *et al.* (1980).

Subsoil dispersion was assessed using the Emerson dispersion test (Emerson 1991) in which three 2 - 5 mm diameter, air dried (40 ^{o}C for 24 hrs) aggregates were placed in at least 100 ml distilled water. Visual assessment of dispersion was conducted after 2 and 20 hours. Samples with slight to nil dispersion after 20 hours were remoulded at field capacity into a 5 mm ball and re-immersed in 100 ml distilled water. Classification was conducted after 20 hours immersion. The extent of dispersion was ranked from 0 (none) to 4.0 (severe) according to Emerson (2002). Further separation of non-dispersed classes (Classes 4- 7) was not conducted.

3.3 Results and Discussion

3.3.1 EMI survey

A significant (p<0.05) although poor correlation (R^2 = 0.59 to 0.67) existed between apparent electrical conductivity and mean electrical conductivity ($EC_{1:5}$) (Table 3.3-1, Appendix 3.2). The use of depth weighted values to normalize EC_a response with depth, did not improve the correlation between EC_a and $EC_{1:5}$. The low R squared values in Table 3.3-1 suggest that a weak but significant (p< 0.05) correlation exist between EC_a and $EC_{1:5}$ and EC_a and gravimetric soil moisture, however salinity and moisture content only partly explained the differences in apparent conductivity. Other factors such as depth to the B horizon are thought to have contributed to variation in EC_a at the site.

Table 3.3-1 Linear regression of apparent conductivity (EC_a) with soil salinity ($EC_{1:5}$) and soil moisture (θ %).

	Apparent Conductivity – Vertical Dipole (EC_a-V)			Apparent Conductivity – Horizontal Dipole (EC_a-H)		
	R^2	DF	Significance	R^2	DF	Significance.
Mean electrical conductivity ($EC_{1:5}$)	0.589	19	0.000	0.668	19	0.000
Mean gravimetric moisture content (%)	0.296	19	0.013	0.391	19	0.003
Depth weighted mean electrical conductivity ($EC_{1:5}$)	0.342	19	0.007	0.134	19	0.113
Depth weighted mean gravimetric moisture (%)	0.157	19	0.084	0.004	19	0.363

Variables that had a significant correlation (p< 0.05) with $EC_{1:5}$ were incorporated in a multiple linear regression using a stepwise, backwards elimination maximum likelihood procedure. The multiple linear regressions demonstrated that EC_a-V and EC_a-H were significantly (p<0.05) correlated to $EC_{1:5}$ when all other variables were excluded.

Variation in apparent conductivity (EC_a - V) and calibrated electric conductivity ($EC_{1:5}$-V) for the vertical dipole are presented for the Near Dam and Radar paddocks Figure 3.3-1, Figure 3.3-2, and Figure 3.3-3. Maps of apparent conductivity and electrical conductivity for the horizontal dipole are presented in Appendix 3.2.

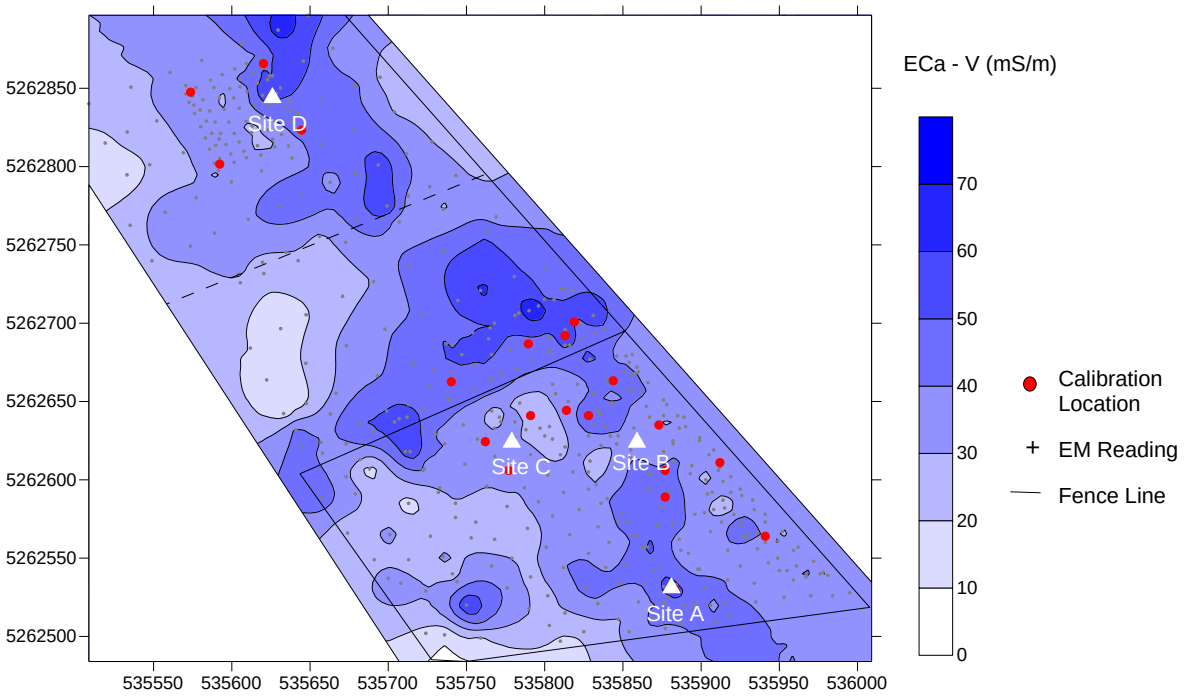

Figure 3.3-1 Apparent electrical conductivity – vertical dipole (ECa-V).

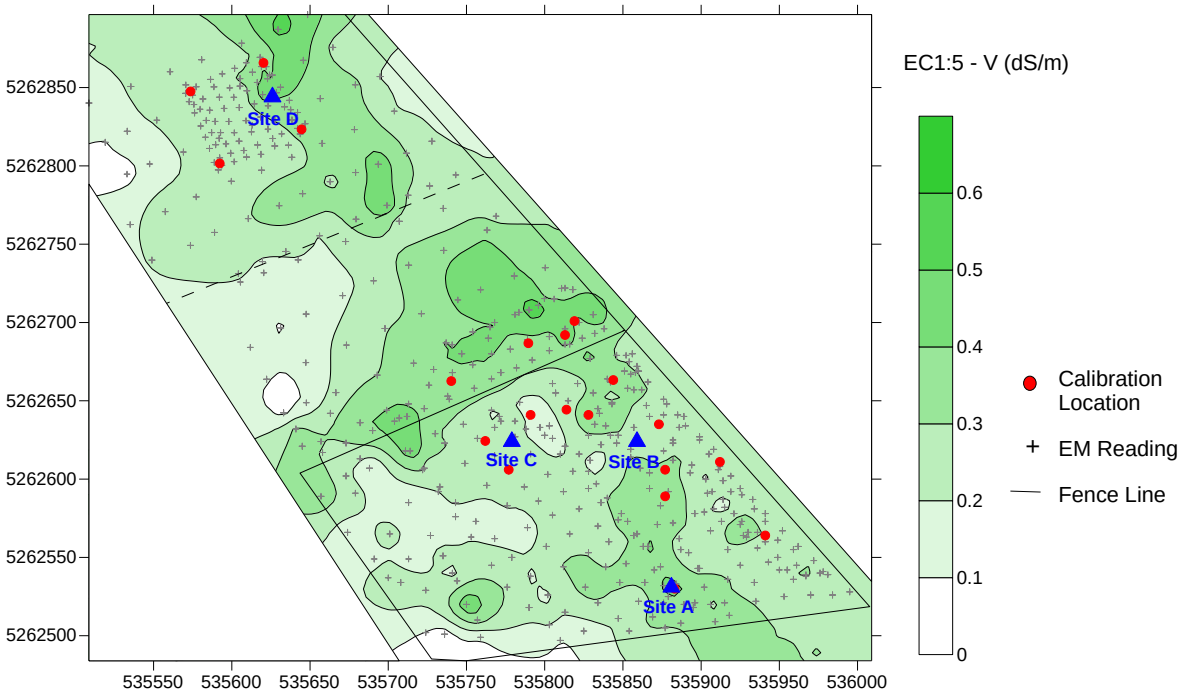

Figure 3.3-2 Calibrated electrical conductivity – vertical dipole (ECa-V).

Apparent conductivity varied considerably across the two paddocks (Figure 3.3-1 and Figure 3.3-3). Experience with EMI38 mapping in southern Tasmania has demonstrated that in most soils EC_a values greater than 100 m*S* m^{-1} indicate moderate soil salinisation, however poor calibration of EC_a with salinity and soil moisture suggested the variation in EC_a resulted from other factors including depth to the B horizon and clay content. Within the Far Dam paddock, higher apparent conductivity was associated with the elevated area adjacent the eastern fence line, in which clay subsoils were found to be closer to the soil surface. The higher apparent conductivity in the drainage line (south western corner of the paddock), was associated with salt accumulation from discharge of saline groundwater. In the Radar paddock, the area of low apparent conductivity along the western boundary of the mapped area was associated with deep, windblown sand deposits.

Differences in apparent conductivity between the two paddocks are thought to result from differences in pedological development resulting from different parent or basement material, rather than management history. Excavation of soil pits associated with field investigations between 2007 and 2009 were unable to provide further explanation of variations in apparent conductivity.

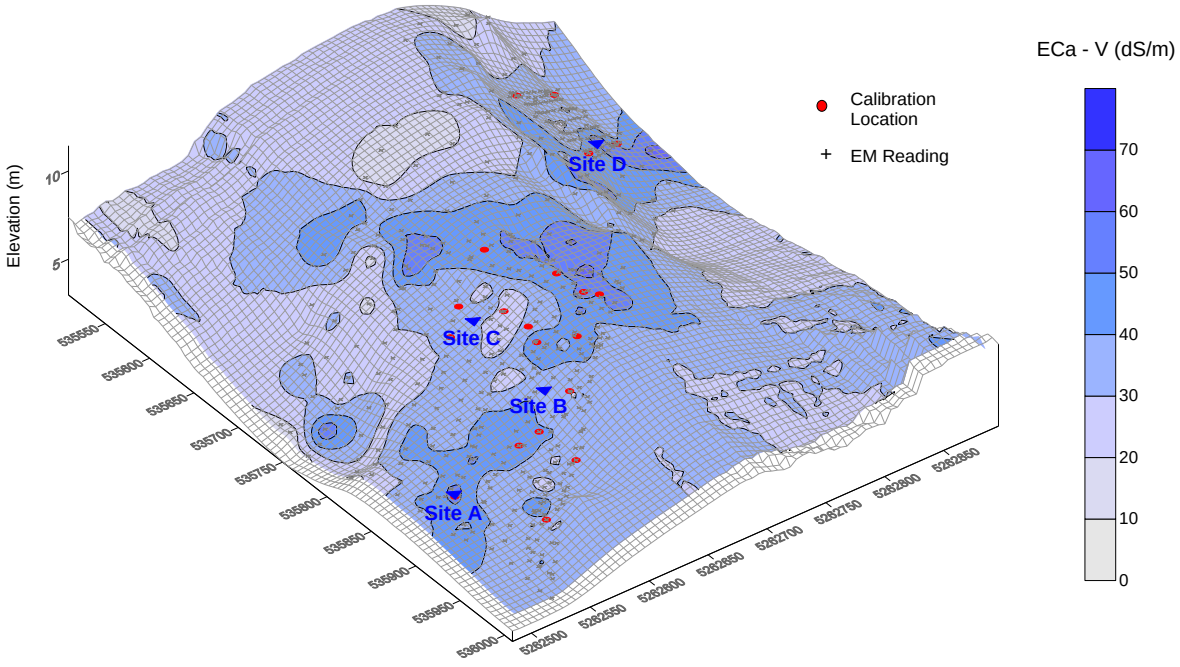

Figure 3.3-3 Apparent electrical conductivity – horizontal dipole draped over topographic wireframe (EC_a-H).

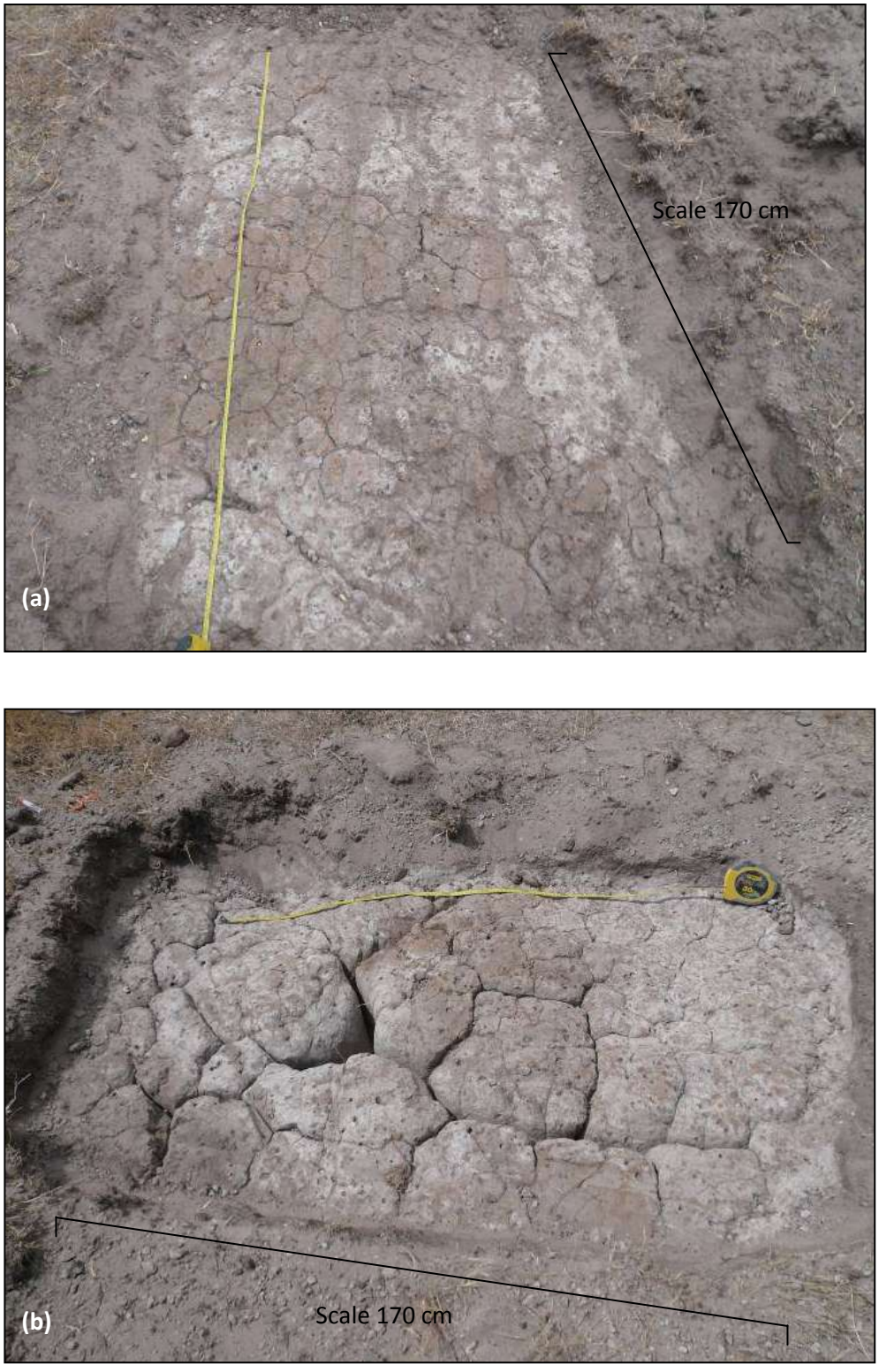

Figure 3.3-4 Site A, (a) A1 horizon removed by garden leaf blower, view is of $A2_e$ and $2B21_t$. Note linear scalping from tillage in upper $2B21_t$ horizon (dark colour) with white $A2_e$ in between tops of the $2B21_t$. Note length of excavation 2.0m. (b) Same site with A2 and sand infills removed. Note tops of very coarse columnar structure and cracks. Excavation was conducted at low antecedent soil moisture. Length of excavation was approximately 1.7 m.

3.3.2 Profile description and classification

Soil profile descriptions and classification are presented for each of the four field sites.

3.3.2.1 Site A, lower slope

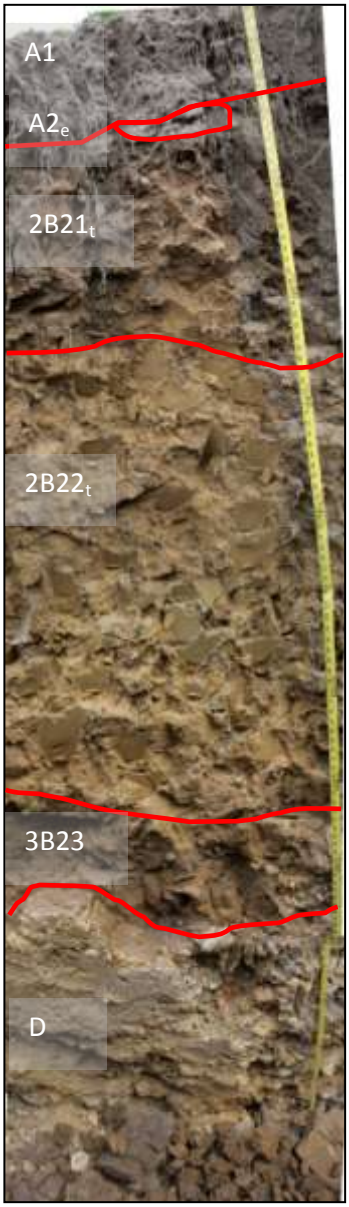

Figure 3.3-5 Site A soil profile.

A1: 0-13 cm, Dark grey (10YR 4/1 moist), loamy sand; weak 2-5 mm subangular-blocky structure; loose dry consistence; few coarse 2 - 5 mm pores (cockchafer beetle); abundant fine roots, broken boundary.

$A2_e$: 12-14 cm Discontinuous; light grey (10YR 7/1 dry); loamy sand; massive; loose to firm (dry); very few fine faint brown mottles; no cracks or pores; common fine roots; water repellent; sharp wavy boundary.

$2B21_t$: 15-33 cm, Yellowish-brown (10YR 5/6 moist); light clay; moderate coarse 50 -100 mm columnar structure breaking to 20-50 mm moderate to medium coarse angular blocky structure; strong consistence (dry); common distinct brown organic cutans; few, dispersed, rounded, fine-medium gravels; common fine shrinkage cracks; many fine roots along ped faces; few very fine pores; gradual smooth boundary.

$2B22_t$: 33 -85 cm; Olive yellow (2.5Y 6/6 moist); light clay; weak coarse 50 -100 mm angular blocky structure breaking to 20-50 mm angular blocky structure; firm consistence (moist), common fine faint light yellow brown mottles; few faint brown organic cutans; few distinct slickensides; few dispersed, rounded large 20 -200 mm Permian mudstone pebbles; no live roots, few medium pre-clearing roots; few very fine pores; few fine cracks; clear wavy boundary.

3B23: 85-100 cm; Grey (2.5Y 5/1 moist); light clay; weak angular blocky structure; firm (moist); abundant stratified rounded – subrounded medium 6-200 mm Permian mudstone gravel to cobbles: distinct orange sandy clasts; clear wavy boundary.

D: 100-130+ cm; Stratified gravels – stones of Permian mudstone.

Classification: Bleached Sodic, Natric, Brown, Sodosol (Isbell 2002), Mollic Natrustalf (Soil Survey Staff 2006), and Solodic Planosol (FAO-UNESCO 1987).

Figure 3.3-6 Site B (a) A1 horizon removed by a garden blower, view of $A2_e$ and 2B21 surface. (b) Detail of upper surface of the B21 horizon and $A2_e$ horizon. (c) Same location with $A2_e$ and sand infills removed by blower vac. Note tops of coarse columnar structure in the B horizon (d) Excavation to 65 cm depth showing pattern of sand infills. (e) View of $A2_e$ development and presence of sand infills every approximately 300 - 600 mm. Excavation was conducted at low antecedent soil moisture. Scale, each yellow or black section equals 5 cm.

3.3.2.2 Site B, middle slope

Figure 3.3-7 Site B soil profile

A1: 0-20 cm; Very dark grayish brown (10YR 3/2 moist); loamy sand; weak sub-angular blocky structure; loose consistence (dry); few medium pores (cockchafer beetle); many fine roots; water repellent; sharp smooth boundary.

$A2_e$: 20-30 cm; Brown (7.5YR 5/2 moist, 7.5YR 6/2 dry); loamy sand; massive structure; very firm (dry) to loose (moist) consistence; few distinct organan staining of root holes, very few angular dispersed fine 2 – 6 mm gravel quartz, suspected to be Permian drop stones; many fine roots; sharp –wavy boundary.

$2B21_t$: 30-51 cm; Dark yellowish brown (10YR 4/4 moist); light clay; moderate, very coarse 200-500 mm, columnar structure breaking to 50 – 100 mm sub angular blocky structure, sand infilling between ped faces to depth of approximately 65 - 70 cm; strong consistence (moist), common distinct clay cutans and brown organic cutans on ped faces and root holes; few subangular dispersed fine 2 – 6 mm gravel coarse fragments; few medium horizontal and vertical cracks; few very fine pores; few very fine roots (preferentially located between ped faces); diffuse smooth boundary.

$2B22_t$: 51-83 cm; Yellowish brown (10YR 5/6 moist); light clay; weak very coarse 200 – 500 mm columnar structure breaking to moderate coarse 50 – 100 mm angular blocky structure; strong consistence (moist); many medium prominent light olive brown mottles associated with organic faces; few common rounded dispersed fine 2-6 mm quartz gravel; cutans on root holes and ped few very fine pores; few fine roots; few fine cracks; gradual smooth boundary.

2B23: 83-115 cm; Grey (2.5Y 5/1 moist); light clay; weak 10-100 mm medium coarse to coarse angular blocky structure; strong consistence (moist); many medium distinct yellowish brown mottles; common distinct clay skins and organic cutans lining pores and cracks; faint fine slickensides; few cracks; no pores; no roots; gradual smooth boundary.

2B24: 115-150cm +; Olive grey (5Y 5/2 moist); sandy light clay; weak 10 – 50 mm medium to coarse angular blocky structure; very strong consistence (moist); common medium prominent red mottles; few-common, fine-medium, prominent yellowish brown mottles; organic cutans associated with pre-clearing roots.

Classification: Bleached Sodic, Natric, Brown, Kurosol (Isbell 2002), Mollic Natrustalf (Soil Survey Staff 2006), and Solodic Planosol (FAO-UNESCO 1987).

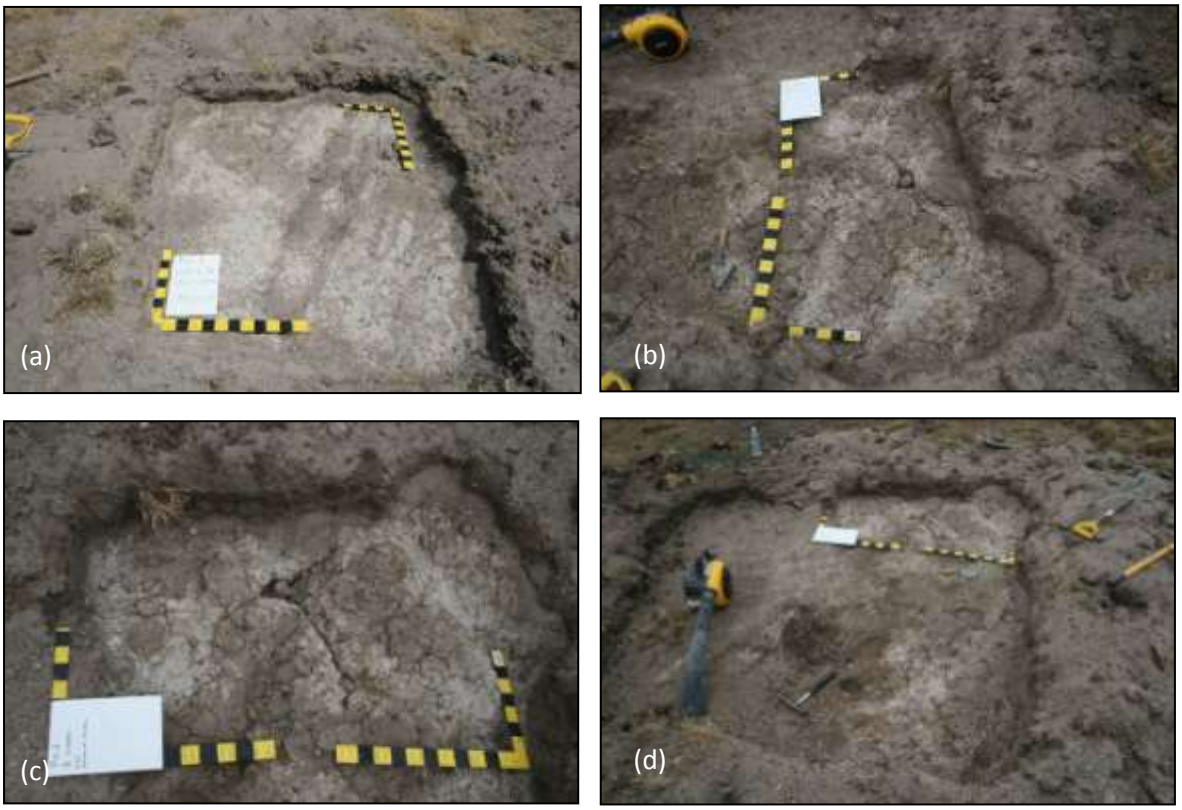

Figure 3.3-8 Site C: (a) A1 horizon removed by garden leaf blower, view of upper $A2_e$ and $2B21_t$ surface. Note linear tine marks in A2 layer and some scalping of B horizon. (b) Detail of upper B horizon and A2 horizon. (c) Detail of upper B horizon with A2 and sand infills removed by a garden leaf blower. (d) Upper surface of B horizon prior to infiltration from disk permeameters. Scale, each yellow or black section equals 5 cm.

3.3.2.3 Site C, upper slope.

Figure 3.3-9 Site C soil profile**.**

A_1: 0-16/18 cm; Dark greyish brown (10YR 3/2 moist, 10YR 5/2 dry); sandy loam; weak 2-5 mm subangular blocky structure; loose consistence (dry); many fine roots; water repellent; sharp smooth boundary.

$A2_e$: 16-18 cm; Discontinuous; light grey (10YR 6/2 moist, 10YR 7/1 dry); loamy sand; massive structure; very few fine distinct brown mottles at base of horizon; common fine roots; sharp wavy boundary.

$2B21_t$: 18-39 cm; Brown (10YR 5/3 moist); light clay; strong 50 – 100 mm coarse columnar structure; sand infilling between peds; very strong consistence (dry); many medium yellowish brown organic cutans with very few distinct black (manganese) mottles; many fine to very fine roots preferentially located between ped faces; few very fine pores; few fine vertical and horizontal cracks; diffuse smooth boundary.

$2B22_t$: 39-62 cm; Dark yellowish brown (10YR 4/6); light clay; weak – medium 10 – 50 mm coarse angular blocky structure; strong (moist); many fine medium prominent grey organic cutans; few slickensides; few fine cracks, few fine roots; few very fine pores; diffuse smooth boundary.

2B23t: 62- 95 cm; Strong brown (7.5YR 4/6); light clay; weak – medium 10 – 50 mm coarse angular blocky structure, strong moist); many fine - medium prominent light brown organic cutans, with very few consistence (medium prominent red mottles; few sub-rounded disperse 2- 6 mm coarse fragments; few fine cracks; diffuse smooth boundary.

2B24: 95-130cm; Grey (2.5Y 5/1); light clay; moderate medium coarse angular blocky structure; strong consistence (moist); many distinct large orange mottles; common rounded – sub-rounded, stratified, Permian mudstone, 6 – 200 mm coarse gravel – cobble, clear wavy boundary.

D: 130-160+cm; Common rounded stratified Permian mudstone 20 -200 mm coarse gravel – cobbles.

Classification: Bleached Sodic, Natric, Brown, Kurosol (Isbell 2002), Mollic Natrustalf (Soil Survey Staff 2006), and Solodic Planosol (FAO-UNESCO 1987).

Figure 3.3-10 Site D. (a) Surface of B horizon following removal of $A1_p$ horizon. Note linear cultivation marks. (b) Same site with $A2_e$ removed. (c) Pocket of deep A1 and A2 three meters distance from excavation in figure 3.12 a &b. (d) 'Picked' upper surface of B horizon for disk permeametery showing organic staining. Scale, each yellow or black section equals 5 cm.

3.3.2.4 Site D, cropped paddock

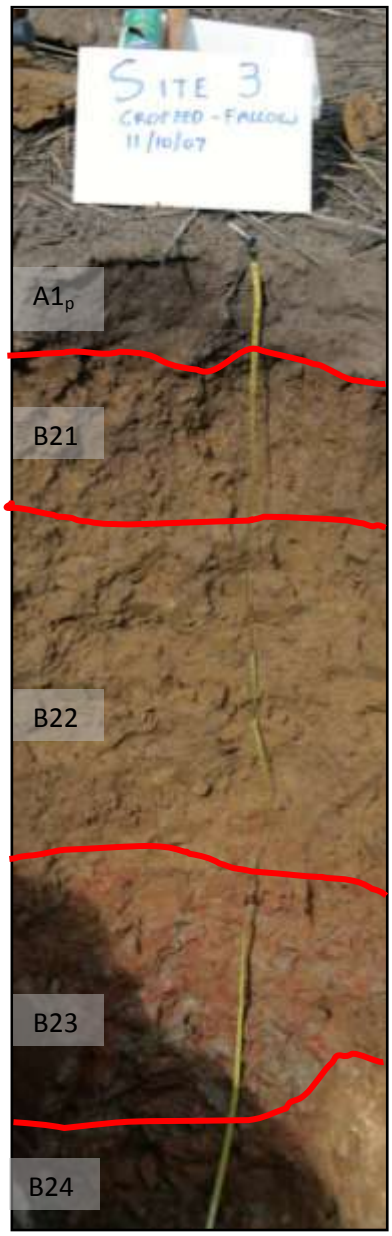

Figure 3.3-11 Site D soil profile

A1p: 0-14 cm; Black (5YR 2.5/1 moist); clay loam; weak 2-5 mm sub-angular blocky structure; loose consistence (dry); few very fine roots: water repellent and crusts when dry; sharp to wavy boundary.

$A2_e$: 14-20 cm Discontinuous; grey (10YR 5/1 dry); loamy sand; massive; firm consistence (dry); few dispersed angular medium gravelly charcoal fragments; few black distinct manganese mottles; common very fine pores; common fine roots; tends to occur in pockets possibly old tree hollows; sharp wavy boundary.

B21: 15-35 cm; Yellowish brown (10YR 5/8 moist); medium clay; medium coarse angular blocky structure; strong consistence (dry); many fine-medium faint brown mottles; many distinct brown organic cutans on ped faces and root channels; fine horizontal and vertical cracks; few very fine pores; many very fine roots; diffuse and smooth boundary.

B22: 35-82 cm; Yellowish brown (10YR 5/6 moist); light clay; weak 10 – 50 mm coarse angular blocky structure; few faint brown organic cutans on ped faces and roots; few very fine roots; few, very fine pores; diffuse irregular boundary.

B23: 82-120 cm; Gray (5YR 6/1 moist); silty clay; massive; firm (moist); many coarse prominent red mottles (Tertiary clay); large slickensides; few, medium (pre-clearing) roots; diffuse irregular boundary.

C: 120+ cm; Grey (5YR 6/1); Clay derived from deeply weathered Tertiary sediments (red-orange).

Classification: Mesotropic, Subnatric, Brown, Kurosol (Isbell 2002), Mollic Natrustalf (Soil Survey Staff 2006), and Solodic Planosol (FAO-UNESCO 1987).

For the remainder of this chapter and throughout the thesis, description of soil horizons for all sites have been simplified by removing horizon suffixes, for example the $2B21_t$ is simply referred to as B21 and $A2_e$ is referred to as A2.

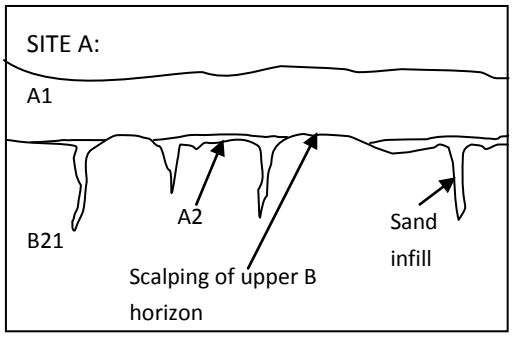

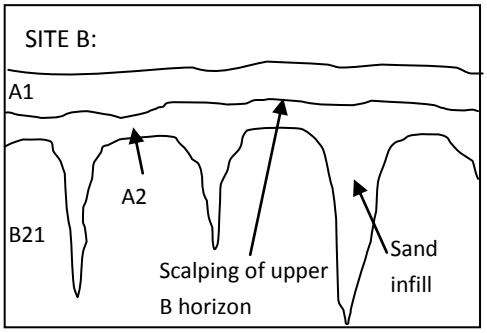

Site A: The A2 horizon is not laterally continuous. The A2 horizon may be up to 4 cm thick. Sand infills were <5 cm thick extending to approximately 40 cm depth.

Site B: The A2 horizon was continuous and extended up to 10 cm thick. Sand infills were common, spaced approximately 30-60 cm apart, width ranged from 1 to 10 cm, and extended to approximately 70 cm depth.

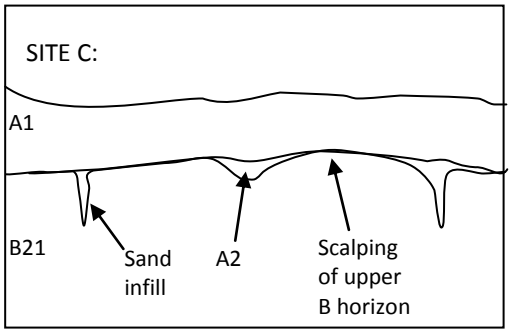

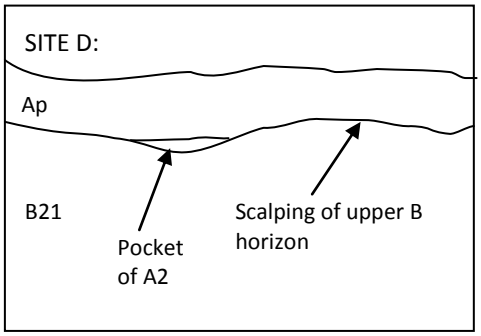

Site C: Little A2 development, where present the A2 was less than 2 cm thick. Few < 1 cm thick sand infills extended to approximately 40 cm depth.

Site D: Development of the A2 horizon was difficult to determine due to cultivation. The A2 existed as pockets usually <3 cm thick below the depth of cultivation. No sand infills were observed.

Figure 3.3-12 Conceptual diagram demonstrating differences in A2 horizon and sand infill development between the four field sites.

3.3.3 Hydropedology integration of soil morphology and water movement

3.3.3.1 A1 horizon

Textural differences suggest that infiltration and hydraulic conductivity of the A1 horizon is likely to be higher in the sandy loam to loamy sand topsoils at sites A, B and C compared to the clay loam A1p horizon at site D. However the effects of hydrophobicity on infiltration and soil water redistribution in the A1 horizons were largely unknown. Studies by Wang *et al.* (2000b) and Philip (1998) suggest that infiltration into hydrophobic soil is lower than would otherwise occur in similarly textured and structured hydrophilic soil.

3.3.3.2 A2 horizon and sand infills

The most prominent pedological difference between the four sites was the level of A2 horizon and sand infill development (Figure 3.3-13 and Figure 3.3-12). At site D the A2 horizon was not able to be recognised due to incorporation of the A1 and A2 horizons into an $A1_p$ horizon. However in isolated pockets the A2 horizon was retained below the depth of cultivation. Development of the A2 horizon at sites A and C were limited to small discontinuous, 1 - 4 cm thick pockets. The A2 horizon was thickest and most continuous at site B in the midslope of the Far Dam paddock, in which the thickness of the A2 horizon ranged from 1 cm to 10 cm. Based on soil texture, the A2 horizon would be predicted to have similar hydraulic conductivity to that of the A1 horizon, however the scarcity of visible macropores and firm to very firm consistence of the A2 horizon when dry indicated it would have had lower than expected infiltration.

Cementing in the A2 horizon was attributed to precipitation of amorphous silica. Chartres *et al.* (1990) found cementing in the A/E horizons of a texture contrast soil (Aeric Albaqualf) was due to silica bridging resulting from precipitation of amorphous silica between sand grains. Silica bridging in hard setting A / E horizons is thought to be similar to formation of subsurface duripan and fragipans horizons in which silica enriched bridges form at the contact points of skeletal grains (Norton 1994). As with fragipan formation, development of silica bridging and hardsetting in A / E horizons was expected to result in lower permeability of the A2 horizon compared to A1 horizon, despite their similar particle size. However unlike fragipans, silica bridging in A / E horizons is revisable at high antecedent soil moisture resulting in their characteristic low consistence when above field capacity.

1) Site D. Least development of cracking in subsoil. Upper B2 horizon had moderate blocky structure.

2) Site C. Weak development of cracking and sand infills. Upper B2 horizon had strong columnar structure.

3) Site A. Moderate development of cracking and sand infills in the B2 horizon. The upper B2 horizon had moderate columnar structure.

4) Site B. Extensive development of cracks and sand infills. Upper B2 had strong columnar structure.

Figure 3.3-13 Degree of cracking and sand infilling in the upper B horizon increases in order from site D to site C, to site A to site B. Upper B horizon revealed by removal of A1, A2 and sand infills using a garden leaf blower. Yellow and black bars indicate 5 cm increments, Image 3 length of excavation is 170 cm.

The extent of sand infill development also differed between sites. Figure 3.3-12 demonstrates a conceptualisation of the difference in A2 horizon and sand infill development between sites. No sand infills were identified at site D. At sites A and C, sand infills did not extend past 40 cm depth. At site B sand infills were numerous, up to 10 cm wide, spaced every 30 cm to 60 cm apart, and extended to approximately 70 cm depth (Figure 3.3-6 and Figure 3.3-14). Sand infills had similar texture, structure and consistence to the overlying A2 horizon. Presence of sand infills in clay subsoils would normally be expected to facilitate water movement into the subsoil, however when dry the sand infills contained few visible macropores and were 'cemented' presumably due to silica bridging (Norton 1994), whilst the clay subsoils contained numerous cracks and voids extending to 80 cm depth.

3.3.3.3 B Horizons

The variable surface relief of the B2 horizon (Figure 3.3-13) are thought to represent remnants of the drainage surface which existed during early stages of profile development (Tennant *et al.* 1992). At sites A, B and C the structure of the B horizon consisted of course, columnar or prismatic structure (depending on the degree of scalping associated with past cultivation) (Figure 3.3-14). At all sites, the clay columns broke along cleavage plains to angular blocky structure. At site D, the B horizon had moderate blocky structure, with a notable absence of the columnar structure and the prominent vertical cleavage plains observed at the other three sites. At all sites, roots and pores were very rare to absent within the clay columns indicated low intra-ped hydraulic conductivity and little capacity to transmit water within the soil matrix. The presence of shrinkage cracks in the B21 and B22 horizons when dry, indicates potential for preferential flow to bypass the soil matrix and enable rapid deep infiltration to between 85 cm (site A) and 115 cm depth (site B). The lower proportion of shrinkage cracks and cleavage plains at site D, indicates site D had lower potential for preferential flow in the B horizon compared to the other three sites. The presence of slickensides between 85 cm to 120 cm depth however indicates that further drying may extend the depth of crack development and preferential flow below the depth of cracking observed at the time of excavation (October 2007).

3.3.3.4 Ponding and subsurface lateral flow

The texture contrast between the A and B horizons would normally be expected to result in development of perched watertables and subsurface lateral flow along the A / B horizon boundary (Cox and McFarlane 1995; Eastham *et al.* 2000; Ticehurst *et al.* 2007).

Figure 3.3-14 Upper surface of B21 horizon at site B. A1 and A2 horizons have been removed by garden leaf blower and shovelling.

Pedological observations however indicate that when dry, the development of perched watertables and subsurface lateral flow at the A / B horizon boundary are unlikely to occur, evidence includes:

I. Sand infills at three of the four sites. Due to their coarse texture and hydrophilic nature the presence of sand infills are expected to facilitate water movement into the B horizon preventing development of ponding above the B2 horizons.
II. Organic cutans in the B21 and B22 horizons result from vertical translocation of organic carbon from the A horizon to depths of up to 100 cm in the B horizon. Their presence in the B horizon, provides evidence that deep vertical infiltration, presumably via preferential flow (Cox *et al.* 2002) is a key hydraulic process at all sites (although the presence of organans in the B2 horizons does not exclude the existence of lateral flow).
III. Shrinkage cracks in the B21 and B22 horizons. At low antecedent soil moisture the presence of shrinkage cracks creating continuous macropores which are likely to prevent water accumulating on the upper surface of the B21 horizon and facilitate bypass flow into the B2 horizons.
IV. The scarcity of visible macropores and cementation in the A2 horizon was predicted to reduce the hydraulic conductivity of the A2 horizon. Consequently ponding and development of lateral flow may occur at the A1 /A2 boundary rather than the A2 / B21 horizons as commonly cited in the literature (Cox and McFarlane 1995; Eastham *et al.* 2000; Ticehurst *et al.* 2007).

At high antecedent soil moisture ponding of water at the A / B boundary is predicted. Evidence for ponding in wet antecedent conditions includes;

I. Hydrophobicity in the A1 horizon. Breakdown in hydrophobicity at higher antecedent soil moisture is expected to result in reduced runoff and increase infiltration into the A horizon (Wang *et al.* 2003).
II. Presence of vertic clays in the B2 horizon. Increased moisture in the B horizon is expected to result in clay swelling, sealing shrinkage cracks, thus preventing bypass flow into the B horizon (Gupta *et al.* 2006).
III. Mottling in the lower A2 horizon. Where the A2 horizon formed in deeper pockets, faint brown mottles were noted. This mottling is thought to have resulted from ferrolysis in which repeated drying and wetting resulted in the decomposition of the clay lattice, resulting in the leaching of exchangeable cations (Brinkman 1970; Chittleborough 1992).

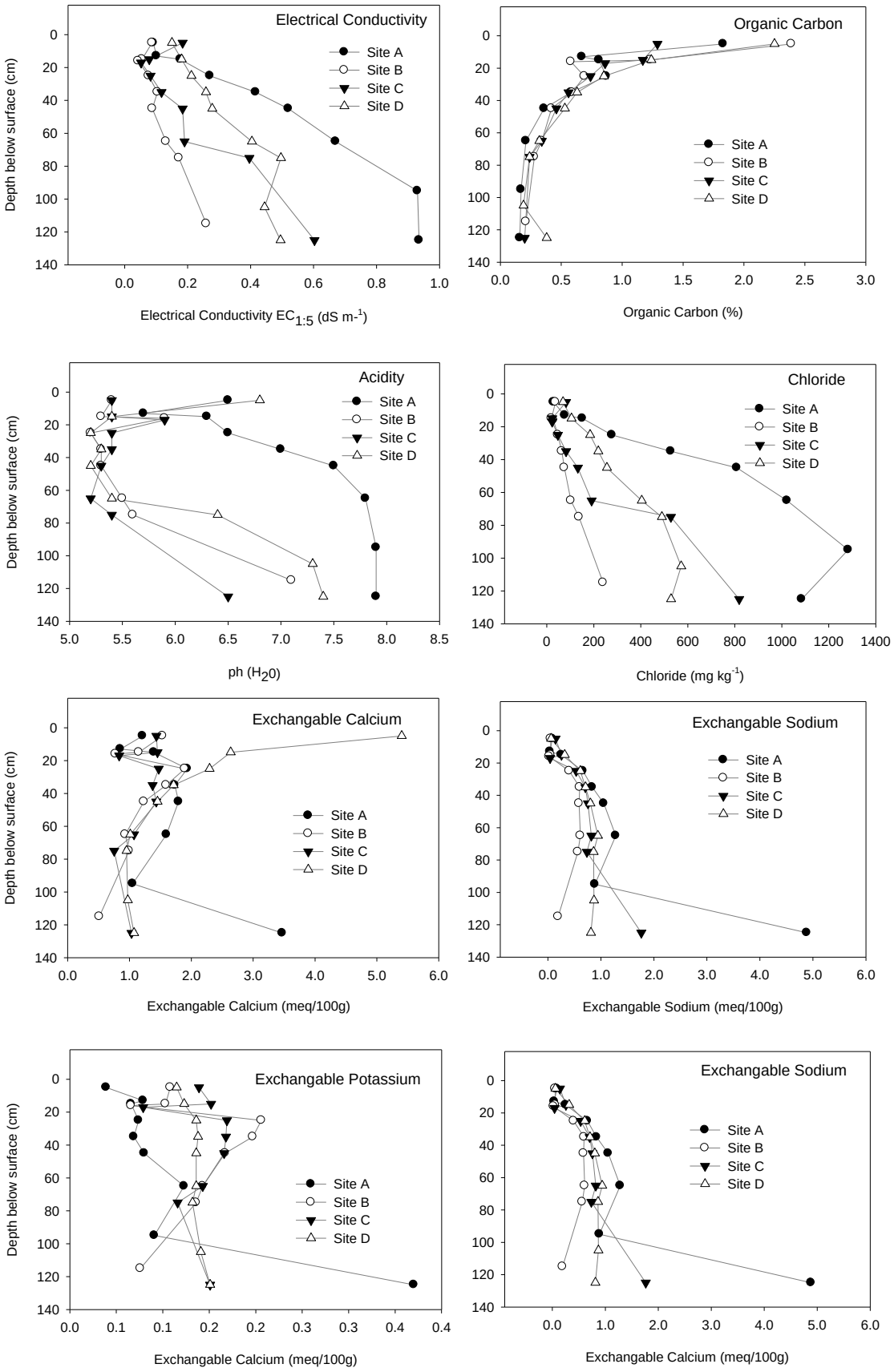

Figure 3.3-15 Results of chemical analysis: (a) Electrical conductivity. (b) Organic carbon. (c) Soil pH. (d) Chloride. (e) Exchangeable calcium. (f) Exchangeable sodium. (g) Exchangeable potassium. (h) Exchangeable magnesium.

Mottling of the lower A1 horizon suggests the upper B horizon is subjected to repeated cycles of wetting and drying presumably resulting from ponding of infiltration in depressions in the upper surface of the B21 horizon.

Whilst there is evidence of ponding on the upper surface of the B horizon when soils are at high antecedent soil moisture, the likelihood that ponding and subsurface lateral flow will develop may also be influenced by the depth, size and frequency of sand infills and the rate of water movement from the sand infills into the clay subsoil. In order for sufficient ponding to develop to generate lateral flow at the A / B horizon boundary the rate of infiltration through the A1 horizon would have to exceed the rate of water movement from the sand infills into the clay matrix.

3.3.4 Soil chemistry

Chemical properties in texture contrast soils often mirror the physical properties due to the historic influence of the texture contrast over movement of leachate (Tennant *et al.* 1992). Chemical analysis presented in Figure 3.3-15and Figure 3.3-16 demonstrates soils at site A have been subjected to less leaching than the other three sites, evidence includes; (i) higher electrical conductivity (Figure 3.3-15a), higher chloride content (Figure 3.3-15d) and higher exchangeable sodium percent throughout the B horizon (Figure 3.3-16i), (ii) less acidity below 10 cm compared to the other three sites (Figure 3.3-15c), (iii) absence of exchangeable acidity (Figure 3.3-16h), and a base saturation of 1.0 below 20 cm depth (Figure 3.3-16n). The accumulation of chloride (Figure 3.3-15 d) at 95 cm indicates that seasonal leaching extended to approximately 90 – 100 cm depth at site A. By comparison site B located 90 meters away had consistently lower electrical conductivity, lower chloride, lower base saturation, lower pH, and higher exchangeable acidity than site A, which indicated that subsoils at site B had undergone more leaching than the other three sites. It is postulated that the greater occurrence and depth of sand infills at site B may have facilitated leaching compared to the less prominent development of sand infills at the other sites.

Analysis of base saturation and exchangeable acidity (Figure 3.3-16 j & n) tentatively indicate the depth of annual wetting was between 20 cm to 30 cm at site A, 70 cm to 80 cm at site D, and 110 cm to 130 cm at sites B and C. However the trend in subsoil chloride (Figure 3.3-15d) did not demonstrate ‘bulging’ or accumulation at these depths which indicates that at site B and site C the seasonal depth of leaching may exceed 130 cm depth.

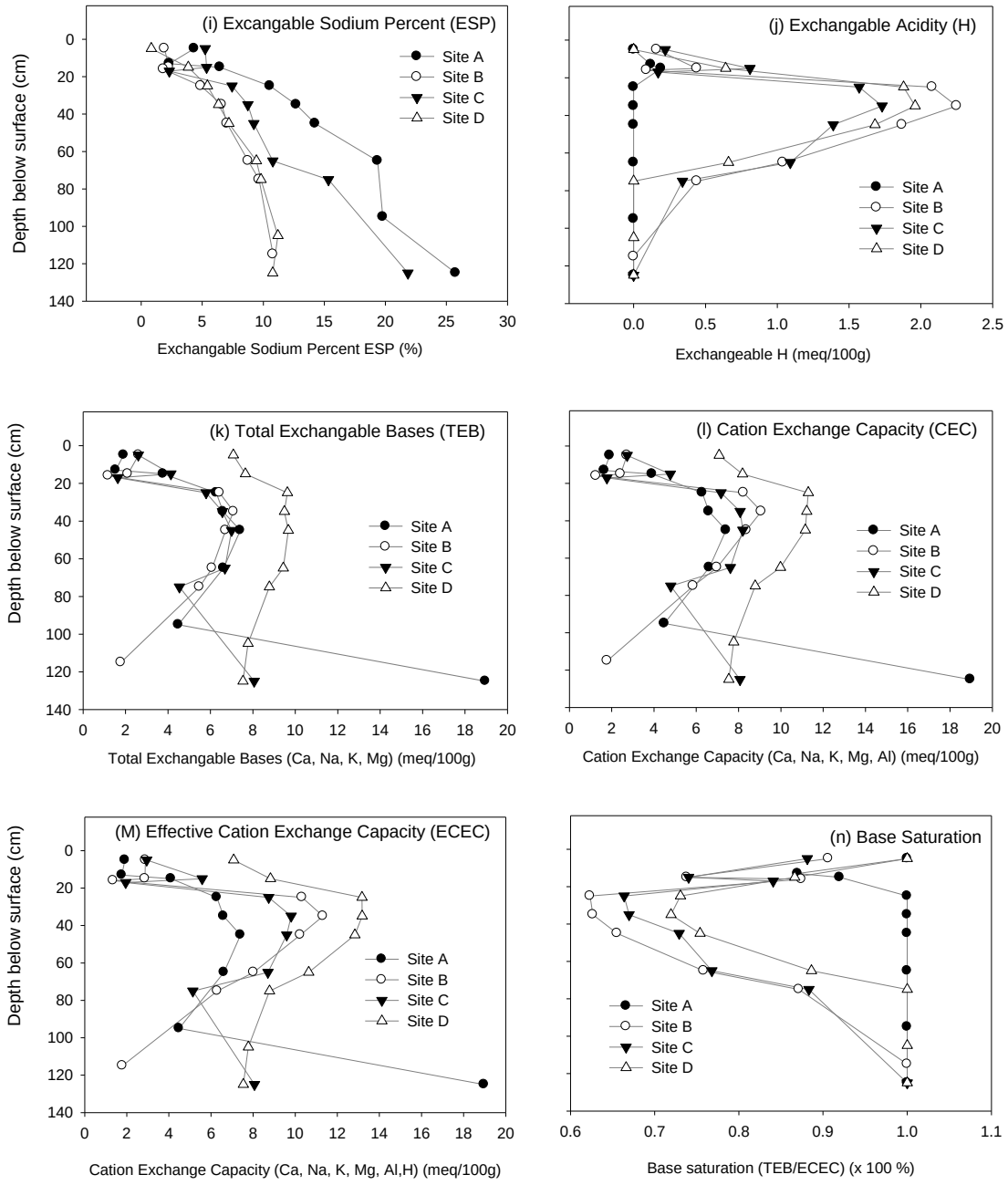

Figure 3.3-16 Results of chemical analysis continued. (i) Exchangeable sodium percent (ESP), (j) Exchangeable acidity, (k) Total exchangeable bases (TEB), (l) Cation exchange capacity (CEC), (m) Effective cation exchange capacity (ECEC), (n) Base saturation. Data is presented in Appendix 3.4.

Chemical analysis suggests the A2 horizons at sites A, B and C were more leached than the other soil horizons. Evidence includes: (i) lower ESP in the A2 compared to the A1 and B21 horizons; (ii) lower levels of organic carbon in the A2 compared to the A1 and B21 horizons at sites A and B; (iii) lower levels of electrical conductivity in the A2 compared to the A1 and B21 horizon at sites B and C; and (iv) presence of organic cutans in the B21 horizon, indicating vertical translocation of organic substances from the A horizon to the B horizon (Chapter 3.3.3).

3.3.5 Water repellence

The persistence and severity of water repellence varied between sites and sampling depths (Table 3.3-2). The persistence of water repellence at 0 - 3 cm depth was found to range from week (5 sec) at site D to severe (900 - 1200 sec) at site C, whilst the severity of water repellence indicated by the MED test ranged from very low or hydrophilic at site D to severe at sites A and C. The persistence and severity of water repellence tended to be higher at 10-13 cm than at the soil surface.

Table 3.3-2 Water repellence, samples collected April 2008 - Air dried ~20^{o}C 48hr

Site	Sample Depth (cm)	Gravimetric Soil Moisture (%)	MED			WDPT	
			Ethanol Molarity	Repellancy Class	Description	Penetration Time (sec)	Repellancy Class
A	0-3	1.0	2.5	9	Severe	420-480	High
	10-13	1.0	2.75 - 3.0	10	Severe	7200 - 9000	Extreme
B	0-3	0.9	1.75 - 2.0	8	Moderate	300	High
	10-13	0.9	4.5 - 5.0	12+	Very Severe	7200 - 9000	Extreme
	A2	0.3	0.5	4	Low	54	Weak
C	0-3	1.1	3.0 - 3.25	11	Severe	900-1200	Severe
	10-13	1.1	4.5 - 5.0	12+	Very Severe	12600-14400	Extreme
D	0-3	1.3	0	2	Very Low	5	Weak
	10-13	1.0	0.25	3	Low	15	Weak

3.3.6 Physical properties

3.3.6.1 Particle size analysis

The A1 horizon had considerable fine sand content, suggesting aeolian inputs at all four sites (Holz 1993). The particle size distribution of the A1 horizon at sites A, B and C was very similar. The coarse sand (200 – 2000 µm) content varied from 54.1 % to 58.9 % and fine sand content (20 – 200 µm) from 27.7 % to 30.8 % (Figure 3.3-17 and Table 3.3-3).

Table 3.3-3 Particle size analysis.

Site	Horizon	Depth	C.Sand 0.2 - 2.0 mm	Fine Sand 0.02 - 0.2 mm	Silt 0.002 - 0.02 mm	Clay < 0.002 mm	Total Sand 0.02 - 2.0 mm	Texture*
	A1	0-10	54.1	30.8	7.1	8.0	84.9	Loamy Sand
	A2	22-25	51.6	35.8	4.9	7.7	87.4	Loamy Sand
A	B21	20-30	28.1	29.5	2.0	40.4	57.6	Sandy Clay
	B22	60-70	22.8	24.8	5.9	46.4	47.7	Clay
	B23	90-100	27.9	24.3	6.8	40.9	52.3	Clay
	A1	0-10	58.9	27.7	5.1	8.2	86.7	Loamy Sand
	A2	20 -25	54.4	32.0	8.8	4.8	86.4	Loamy Sand
B	B21	30-40	25.8	25.6	4.8	43.8	51.4	Clay
	B22	60-70	42.4	18.7	3.9	35.0	61.1	Sandy Clay
	B23	90-100	31.0	30.5	2.9	35.6	61.5	Sandy Clay
	A1	0-10	54.5	30.0	5.2	10.3	84.6	Loamy Sand
	A2	27-30	54.8	30.2	6.0	8.9	85.1	Loamy Sand
C	B21	20-30	32.3	25.6	4.9	37.2	57.9	Clay
	B22	60-70	30.1	25.8	4.8	39.3	55.9	Clay
	B23	80-90	34.3	29.1	1.9	34.7	63.4	Sandy Clay
	A1p	0-10	40.5	33.3	9.1	17.1	73.8	Sandy Clay Loam
	B21	20-30	15.6	26.2	5.9	52.3	41.8	Clay
D	B22	60-70	18.2	23.0	9.0	49.8	41.2	Clay
	B23	100-110	13.6	19.8	12.6	54.0	33.4	Clay

*Based on particle size ISSS classification as presented in McDonald *et al.* (1990).

The A1 horizon at site D, had less coarse sand and higher silt and clay content than the other three sites. The elevated clay and silt content in the A1 horizon at site D is thought to have resulted from either (i) incorporation of the A2 into the A1 horizon as a result of cropping activities, or (ii) down slope movement and incorporation of weathered Tertiary clay sediments. The relationship between clay percent and sand percent is presented in Figure 3.3-17 for each site and horizon.

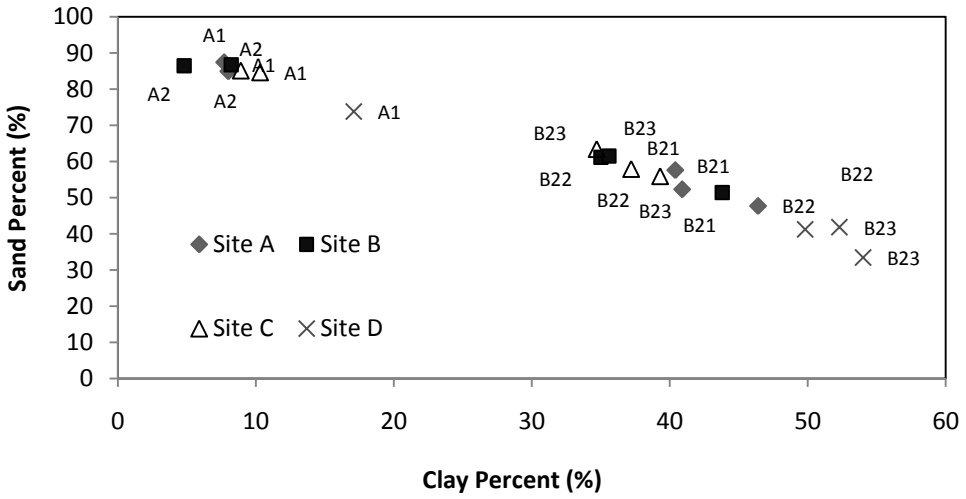

Figure 3.3-17 Particle size analysis, sand vs clay percent.

3.3.6.2 Liquid limit and linear shrinkage

Figure 3.3-19 and Table 3.3-5 demonstrate that subsoils at all sites have the potential to undergo volume change in response to changes soil moisture status. Linear shrinkage varied from 6.4 % in the B21 horizon at site D, to 17.4 % in the B22 horizon at site C. Linear shrinkage at sites B and D were generally lower than the other two sites. Variation between sites and horizons was related to particle size. A significant (p = 0.005, df = 11, R^2 = 0.557) relationship existed between clay content and linear shrinkage. However no significant relationship existed between clay content and liquid limit (p=0.32, df = 11, R^2 = 0.312) (Figure 3.3-18).

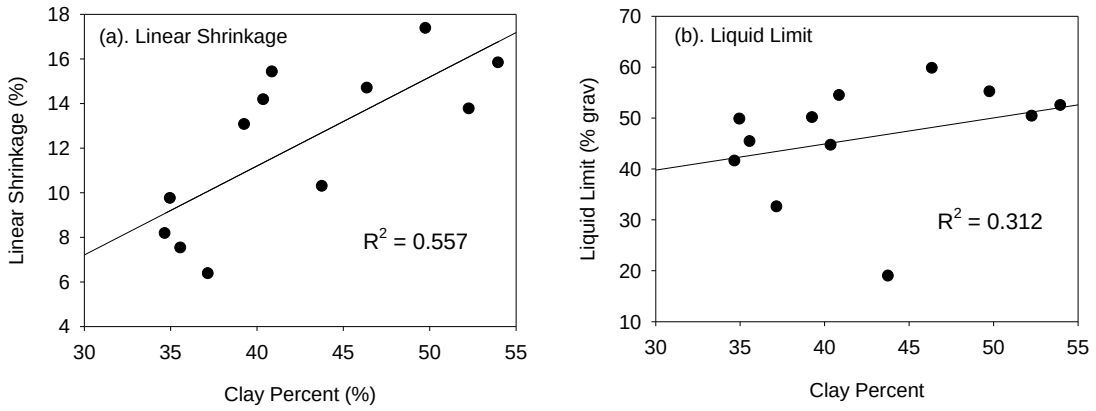

Figure 3.3-18 Relationship between clay content (%) and (a) Linear shrinkage, (b) Liquid limit. Note R^2 values are for linear regression.

Table 3.3-4 Emerson dispersion test.

Site	Depth (cm)	Horizon	Air Dried Aggregate		Remoulded	Emerson Class
			Observation after 2 hrs	Observation after 20 hrs	Observation after 20 hrs	
Site A	5	A1	None 0	None 0	Slight 1.0	4-7
	12	A2e	None 0	None 0	Slight 1.0	4-7
	35	B21	Slight 1.0	Slight 2.0	na	2
	63	B22	Slight 1.0	Moderate 3.0	na	2
	110	D	Slight 1.0	Severe 4.0	na	1
Site B	5	A1	None 0	None 0	None 0	4-7
	16	A2e	None 0	None 0	None 0	4-7
	25	B21	None 0	None 0	Severe 4.0	3a
	75	B22	Moderate 2.0	Severe 4.0	na	1
	110	B23	Moderate 3.0	Severe 4.0	na	1
	135	B24	Moderate 3.0	Severe 4.0	na	1
Site C	15	Mixed A1/B21	None 0	None 0	Moderate 2	3b
	20	B21	Slight 1.0	Slight 1.0	Moderate 2	3b
	45	B22	Slight 1.0	Moderate 2.0	Severe –Mod.3.5	3a
	90	B23	Severe 3.5	Severe 4.0	na	1
Site D	5	A1	None 0	None 0	Slight 0	4-7
	15	B21	None 0	None 0	None 0	4-7
	30	B21	None 0	None 0	Moderate 3.0	3b
	65	B22	None 0	None 0	Severe 4.0	3a
	105	B23	Slight 1	Severe 3.5	na	1

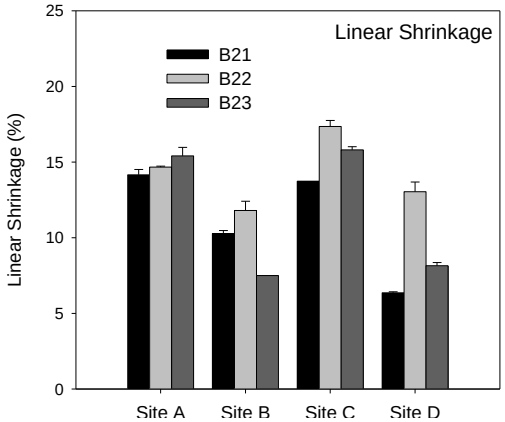

Table 3.3-5 Classification of linear shrinkage according to Mills *et al.* (1980).

Horizon	Site A	Site B	Site C	Site D
B21	Marginal	Non-critical	Marginal	Non-critical
B22	Marginal	Non-critical	Critical	Marginal
B23	Marginal	Non-critical	Marginal	Non-critical

Figure 3.3-19 Linear Shrinkage. Note shrinkage was not observed in A1 and A2 horizons at any site. Error represents ±1 SD. Results for liquid limit are presented in Appendix 3.3.

Vertic properties in the subsoil of texture contrast soils have been reported by Chittleborough *et al.* (1984) who observed that the shrink swell potential of subsoils increased with the degree of texture contrast in a soil chronosequence. In contrast to the study by Chittleborough *et al.* (1984), data from the four field sites revealed that linear shrinkage increased with decreasing degree of texture contrast, (change in clay content between the A1 and B21 horizons, Table 3.3-3). Site B had the greatest degree of texture contrast, and the lowest linear shrinkage, whilst site C had the highest linear shrinkage and lowest degree of texture contrast.

3.3.6.3 Dispersion

Subsoils at all sites were dispersive (Emerson classes 1, 2 or 3) (Table 3.3-4). Differences in dispersive behaviour existed between sites, generally the degree of dispersion increased with depth, whilst the highest dispersion was observed at site B. The presence of exchangeable aluminium did not appear to prevent dispersion, notably site B had both the highest levels of exchangeable aluminium and lowest (most dispersive) Emerson class. Propensity to disperse in the field may also be ameliorated by the high level of salts (EC), chloride and exchangeable magnesium (Figure 3.3-16).

3.4 Conclusion

EMI mapping and soil excavations demonstrated considerable variation in soil properties over short distances within the Radar and Far dam paddocks. It was expected that EMI mapping would assist with understanding subsoil variability, however calibration indicated that salinity and moisture content only partly explained differences in EC, and that other factors, (suspected to be depth to the B horizon) contributed to variation in the apparent conductivity.

Despite three of the four sites having identical soil classification (Bleached Sodic, Natric, Brown, Kurosols), considerable differences existed between the three sites with respect to subsoil structure, degree of subsoil crack development, extent of A2 horizon development, and depth and frequency of sand infills. At all sites, the A1 horizon appeared to have formed from aeolian sand (Holz 1993). Chemically sites A, B and C were very similar, the A1 horizons were all acid (pH_{H20} 5.7 to 6.5), weak to potentially dispersive (ESP 1.9 to 5.4) with low CEC (1.65 to 4.78). Differences in chemical attributes at site D were attributed to addition of material derived from weathering of Tertiary sediments, and / or cropping activities including cultivation mixing the A1 and A2 horizons.

Beattie (1995) describes the existence of acid, sodic, texture contrast soils within the vicinity of the four field sites as being 'anomalous' as they demonstrate little evidence of leaching, however existence of sodic, texture contrast soils with acid trend in the subsoil is relatively common. Of the texture contrast soil profiles examined by Northcote and Skene (1972) 46 % had ESP greater than 15 or more in the subsoil, and 22 % had acid subsoils.

Water repellancy was reported in the A1 horizon at all sites. In dry conditions water repellence was expected to result in reduced infiltration and increased runoff than would otherwise be expected for a hydrophilic soil with similar texture (Wang *et al.* 2000b). In dry soil conditions hydrophobicity is expected to result in the development of unstable wetting fronts and 'fingering' (Ritsema *et al.* 1998b).

The scarcity of visible macropores in the A2 horizon was expected to result in lower hydraulic conductivity than the overlying A1 horizon, despite the similar particle size of the two horizons. The presence of silica bridging and precipitation of amorphous silica (Norton 1994) at low antecedent soil moisture is expected to reduce the hydraulic conductivity of the A2 horizon, however this has not been quantified in texture contrast soils. The A2 horizon generally had lower potassium, organic carbon, EC, ESP and CEC than either the A1 or the B21 horizons due to higher rates of elluviation.

Field morphological observations were unable to determine if elluviation of the A2 horizon resulted from dominance of lateral flow or vertical infiltration, however the presence of organic coatings in the B21 and B22 horizons indicated vertical water movement to be a key process at the site. The B2 horizons consisted of vertic, dispersive, light to medium clays, and sandy clays. Low antecedent soil moisture at the time of observation revealed the presence of shrinkage cracks within and between the clay columns. At the time of observation, shrinkage cracks had developed from the upper surface of the B21 to a depth between 82 cm to 115 cm. Presence of slickensides between 62 cm and 120 cm depth indicate that development of shrinkage cracks may extend beyond the depth of observation. At low antecedent soil moisture, shrinkage cracks would enable rapid water movement from the base of the A1 / A2 horizons to at least 85 cm depth at all sites. Water movement from the shrinkage cracks into the soil matrix (mass transfer) would however be severely restricted by the lack of visible pores within the clay matrix. Preferential flow in the A and B horizons may result in transport of low electrolyte water into the subsoil resulting in dispersion of the clay matrix.

The effect of sand infills on infiltration and soil moisture redistribution in the B horizon is difficult to infer. Based on texture alone, the presence of sand infills within the clay subsoil would be expected to facilitate infiltration through the B horizon. However the presence of silica cementation and lack of visible macropores in the A2 horizon and sand infills suggest that infiltration through the sand infills will be restricted. At low antecedent soil moisture it is expected infiltration through shrinkage cracks in the B2 horizons is expected to be greater than flow through sand infills. At high antecedent moisture content when shrinkage cracks have closed, sand infills may assist infiltration into the subsoil, albeit at slower rates than would otherwise be expected in dry antecedent soil moisture conditions due to clay swelling and lack of visible porosity in the B2 horizons.

Differences in the structure of the B2 horizons, thickness of the A2 horizon and degree of sand infill development were considerable between the four sites. Physical and chemical data suggests that site B had higher rates of leaching than the other three sites. Site B also had the lowest linear shrinkage, and the highest level of dispersion of the four sites. By comparison site A, located 94 m away at the bottom of the slope, had the least evidence of leaching. Physical evidence included minimal A2 development, higher subsoil acidity, higher chloride, and higher base saturation than the other three sites. Chloride and EC trend with depth cautiously indicate the current annual depth of wetting at site A to be around 90 - 100 cm, compared to at least 130 cm at site B.

Soil morphology and chemical data indicate that development of perched watertables and subsurface lateral flow along the A / B horizon boundary is unlikely, especially at low antecedent soil moisture. These findings are supported by Smettem *et al*. (1991) who found that soil macroporosity and bypass flow were responsible for preventing subsurface lateral flow at the A / B horizon boundary of a texture contrast soil near Mt Bold, South Australia. They found bypass flow through soil macropores in the B horizon resulted in field saturated hydraulic conductivities that were considerably higher than would be predicted from textural analysis. Consequently, the distinct textural boundary within the profile did not act as a throttle to vertical infiltration, resulting instead in infiltration to the soil / rock interface rather than lateral flow along the boundary between the A and B horizons. Brower and Fitzpatrick (2002) also found that macroporosity resulting from root holes which pre-dated land clearance, provided sufficient hydraulic connectivity to prevent the development of subsurface lateral flow on a series of texture-contrast soils in the Dundas Tablelands, Western Victoria. In soil with high antecedent moisture, subsurface lateral flow at the A / B boundary is only likely to occur if the infiltration rate through the A1 horizon exceeds the flow rate of water from the sand infills into the clay matrix.

3.5 Key Points

- Soils are classified as Kurosols or Sodosols.
- Factors other than soil salinity and soil moisture were responsible for variation in apparent conductivity.
- Soil excavations and EMI mapping demonstrated that soils at the Far Dam and Radar paddocks are highly variable.
- Variation in soil morphology between sites is most apparent in the development and extent of the A2 horizon and sand infills. Minor differences with respect to structure, colour, and depth of organic cutans also exist between sites.
- Soil chemical attributes vary between sites, particularly; electrical conductivity, acidity, chloride, exchangeable magnesium, exchangeable sodium percent, exchangeable acidity, effective cation exchange capacity and base saturation.
- At all sites, the A1 horizon consisted of aeolian sand to clay loam which was hydrophobic when dry.
- Subsoils consisted of vertic, columnar to massive blocky structure, dispersive clay to sandy clay.
- The A2 horizon consisted of hydrophilic, cemented (silica bridging) loamy sand.
- In dry antecedent soil moisture conditions preferential flow is expected to occur in the A1 horizon as a result of hydrophobicity, and bypass flow in the subsoil via shrinkage cracks.
- In moist or wet conditions, subsurface lateral flow may occur, although absence of visible macropores in the A2 horizon suggest lateral flow may occur in the lower A1 horizon rather than the A2 horizon.
- When dry, the sand infills are not expected to contribute greatly to flow through the subsoil as cracks existed between and within the clay columns. In wet soil conditions, sand infills are expected to facilitate infiltration into the B horizon.
- Site B was inferred to have undergone the most leaching, while site A was inferred to have undergone the least leaching.
- Preferential flow is not predicted in wet conditions as hydrophobicity is expected to have been overcome, and subsoil clays are expected to have swelled closing shrinkage cracks.
- Development of subsurface lateral flow is not expected in dry conditions due to the presence of shrinkage cracks in the B horizons.

4.0 Dye Staining Experiments

4.1 Introduction

In chapter three differences in infiltration and soil water movement between the four sites was inferred from soil chemical and physical data, and soil morphology. Presence of water repellence in the A1 horizon, and shrinkage cracks and slickensides in the subsoil indicated that infiltration and soil water redistribution were likely to be influenced by antecedent soil moisture content. In this chapter, a series of dye staining experiments will explore the effect of antecedent soil moisture and soil morphology on infiltration and soil water redistribution. Understanding the extent to which antecedent soil moisture influences preferential flow and soil water movement is important for development and use of soil water models (Merdun *et al.* 2008) and assessment of the risks posed by preferential flow to off-site movement of agrichemicals (Jarvis 2007).

Dye tracers have been extensively used to characterise preferential flow paths in soils, and examine the interaction between soil morphology and water movement (Flury *et al.* 1994; Weiler and Fluhler 2004). Dye tracers enable visualisation of flow pathways, and quantification of areas of the soil that are active in flow from those which are not (Mooney and Nipattasuk 2003; Morris and Mooney 2004). Dye tracers provide insights into pore scale phenomena, such as macropore–matrix interaction, as well as delineating the extent of flow in the bulk soil (Cey and Rudolph 2009). Coupled with image processing and digital analysis, dye tracing techniques enable rapid determination of semi-quantitative measures of preferential flow (Forrer *et al.* 2000).

A number of dye tracers have been used to stain soil profiles, of these Brilliant Blue FCF (C.I. Food Blue 42090) has become the most popular as it provides the best combination of mobility, high visibility and low toxicity (Flury et al. 1994). Use of dye tracers is limited by the adsorption of dyes to soil particles, which cause the dye to move at a slower velocity than the water in which it is dissolved (Lipsius and Mooney 2006; Mon and Flury 2005). In general soils with high clay content and low organic carbon tend to absorb more dye than other soils (German-Heins and Flury 2000; Kasteel et al. 2002; Ketelsen and Meyer-Windel 1999). Brilliant Blue FCF dye is known to undergo adsorption (German-Heins and Flury 2000) with a retardation factor of 1.2 relative to an iodide tracer (Flury and Fluhler 1995). Consequently Brilliant Blue is considered a conservative tracer in the sense that the actual movement of water would be greater than that represented by the dye staining (Cey and Rudolph 2009). Potential limitations associated with the use of dye tracers have been reviewed by Allaire et al. (2009), Flury and Fluhler (1995), Flury and Wai (2003).

Figure 4.1-1 Establishment of soil water treatments: (a) Rainout shelter located at site D. (b) Irrigation supplied by 100 drippers in a 3 x 3 meter area. Water application was controlled by battery powered timers, supplied from two 44 gallon reservoirs. (c) Sprinklers at sites A, B and C were connected to S.E. irrigation scheme adjacent a stock drinking trough. (d) Sprinkler set up at site C, note shade cloth as a permeable wind fence and EnviroSCAN probe.

4.2 Methodology

4.2.1 Establishment of antecedent soil moisture treatments

Two contrasting antecedent soil moisture contents were established at each of the four field sites (Table 4.2-1, Figure 4.1-1). At sites A and C, the dry treatment was established following a prolonged period without substantial rainfall, while at sites B and D, a rainout shelter was constructed to enhance drying of the soil profile. The wet treatments were established at sites A, B and C by applying 20 to 30 mm irrigation with sprinklers four times a week, for a period of 45 days. Irrigation was supplied in excess of the infiltration capacity of the soil such that runoff occurred with each irrigation event. At site D, irrigation was supplied by drippers operating six times a week for a period of four months. Soil moisture content prior to dye tracer application was determined from gravimetric analysis of hand augured samples at sites A, B and C in the dry treatments. In the wet treatment at all sites, and site D in the dry treatment, volumetric soil moisture content was determined by a continuously logging capacitance probe, (EnviroSCAN Solo - Sentek Environmental Technologies).

Table 4.2-1 Volumetric soil moisture content at each site prior to dye tracer application

Disturbed samples m^3m^{-3}				*In situ* EnviroSCAN probe m^3m^{-3}					
Depth Interval (m)	Dry Treatment			Sensor Depth (m)	Wet Treatment				Dry Treatment
	Site A	Site B	Site C		Site A	Site B	Site C	Site D	Site D
0.0 - 0.1	2.6	1.7	5.0	0.1	36.6	34.3	32.4	31.6	4.56
0.1 -0.2	15.2	6.2	6.6	0.2	43.4	28.0	37.2	46.0	27.75
0.2 - 0.3	23.1	10.7	24.0	0.3	47.8	35.8	44.8	49.6	30.86
0.3 - 0.4	24.7	17.4	22.4	0.4	49.9	44.1	43.1	51.4	35.33
0.4 - 0.5	30.5	15.5	21.8	0.5	50.2	42.4	44.4	52.0	36.15
0.5 - 0.6	35.5	15.3	19.8						
0.6 - 0.7	33.9	22.5	22.8	0.7	55.3	45.7	43.5	51.7	43.75
0.7 - 0.8	32.3	18.9	22.5						
0.8 - 0.9	30.1	23.3	18.9	0.9	51.2	45.9	52.4	52.9	48.36
0.9 - 1.0		26.0	26.9	1.1	50.5	51.3	56.9	53.7	

4.2.2 Dye tracer application

At sites A, B and C, dye tracer solution was applied to the dry treatments with a Morin rotating-disk rainfall simulator (Morin *et al.* 1967) with a Fulljet H30 spray nozzle, 10^o disk aperture, operating at 75 kPa, rotation speed of 23 rpm, to unbound plots (Figure 4.2-1b). However, due to irreparable breakdown of the rainfall simulator, dye tracer application in the wet treatments, and the dry treatment at site D were conducted using a hand held sprayer, with an Albuz Atr 80 nozzle, operated at a constant 240 kPa to bound plots inserted 2-3 cm into the soil (Figure 4.2-1 a & c).

Figure 4.2-1 Dye application techniques: (a) Spray chamber used with hand held sprayer, note EnviroSCAN probe and localised ponding, (b) Rotating disk rainfall simulator used for dye application in the dry treatments at site A, B and C, (c) Hand held pressure sprayer used in all wet treatments, and the dry treatment at site D, (d) Calibration of the rainfall simulator.

Dry treatments received 25 mm dye solution containing 4 g L^{-1} Brilliant Blue, while the wet treatments received 25 mm dye solution containing 8 g L^{-1} Brilliant Blue (previous experiments with 4 g L^{-1} Brilliant Blue were difficult to detect in wet soil, site C wet treatment 20 mm). Calibration of the rainfall simulator is presented in Appendix 4.0. Initial application rate of the dye tracer averaged 17 mm hr^{-1}, however once ponding in shallow depressions occurred, the application rate was lowered to prevent runoff and maintain the depth of ponding at less than 5 mm. Average application rates are presented in Table 4.2-2. The 25 mm application amount was selected to represent a 'typical' irrigation event from a travelling irrigator. Rainfall intensity-frequency-duration (IFD) analysis was conducted by the Bureau of Meteorology (2007) in order that the dye application events could be related to rainfall events within the vicinity of the University of Tasmania Farm. Table 4.2-2 indicates that dye application in the dry treatments had IFD return periods of 2 - 10 years, and 1 - 5 years in the wet treatment.

Table 4.2-2 Dye tracer application rate, duration and (IFD) return period.

	Site A		Site B		Site C		Site D	
	Dry	Wet	Dry	Wet	Dry	Wet	Dry	Wet
Average application rate (mm hr^{-1})	10.3	4.1	20.6	10.0	10.1	11. 5	12.5	5.9
Application duration (minutes)	146	363	73	150	148	131	120	256
IFD return period (yrs)	2 - 5	1 - 2	10	2-5	2-5	2-5	5	1-2

4.2.3 Excavation of dye stained soil and image capture

Dye stained areas were excavated approximately 48 hours after dye application, following a similar procedure to Ghodrati and Jury (1990) and Bachmair *et al.* (2010). Half the dye stained area was excavated in five vertical slices 10 cm apart, and the other half, excavated in a series of horizontal slices in which depth increments were determined by the maximum depth of dye infiltration. Horizontal and vertical excavations could not be conducted on the same day due to the time required for excavation. Shadows and variations in colour cast were prevented by diffusing sunlight using a portable white nylon tent which spanned the excavated area (Figure 4.2-2). Images of dye stained soil were captured using a Cannon 400D EOS digital camera, using the lossless CCD format (Persson 2005), under both natural light (diffuse) and artificial lighting provided by four 500 watt halogen lights. A Kodak colour chart, grey scale and large set square or adjustable square metal frame were placed on each soil profile as a reference for image correction.

Figure 4.2-2 (a) Use of excavator to expose dye stained soil. Photographing (b) horizontal and (c) vertical exposures, site A. Note use of portable lighting, tripod, set squares, colour chart and white shade tent to prevent shadows. (d) Holding down the shade tent with the excavator in a 35 knot wind.

Images were converted from the CCD image format to 8 bit / channel PSD format in Photoshop software. As excavation was conducted approximately 48 hours after dye infiltration commenced, dye patterns result from a combination of both infiltration and redistribution processes.

4.2.4 Image correction and analysis

Radial distortion was corrected following the procedure by Reis (2007) in which the relationship between focal length and image correction was determined by photographing graph paper at a range of focal lengths (Figure 4.2-3). Keystone distortion was manually corrected by adjusting image dimensions until the reference set squares or metal frame matched a generated parallel grid (Appendix 4.1). Following correction pixel size averaged 0.22 mm^2.

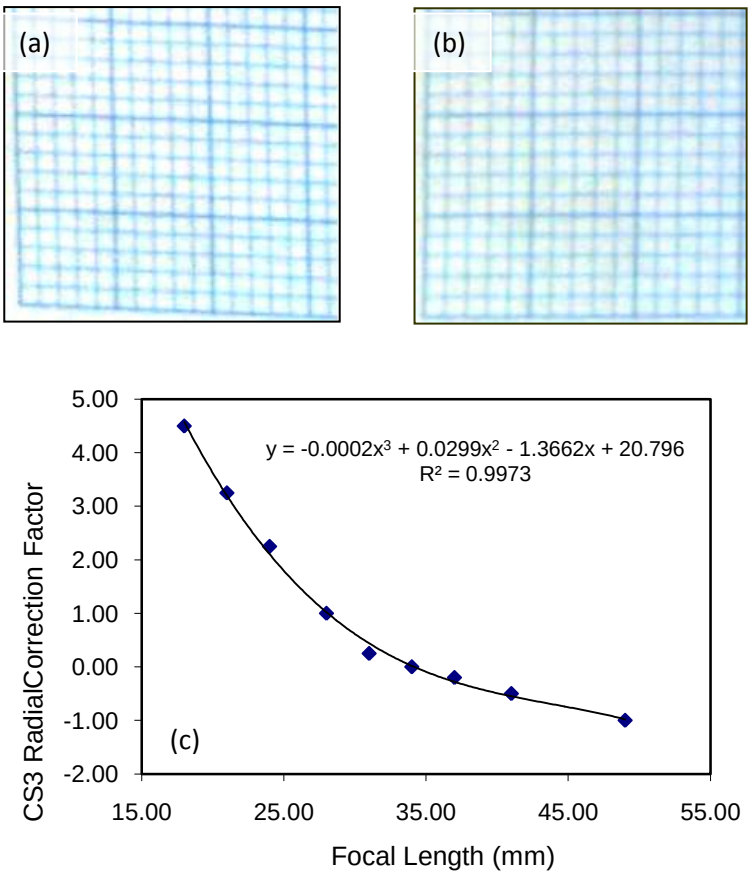

Figure 4.2-3 Correction for barrel distortion for Canon EOS400D camera. (a) Example of radial distortion at 18 mm focal length, note curvature in bottom left. (b) Same image corrected by applying +4.5 correction factor in Photoshop CS3. (c) Relationship between focal length and radial distortion correction factor.

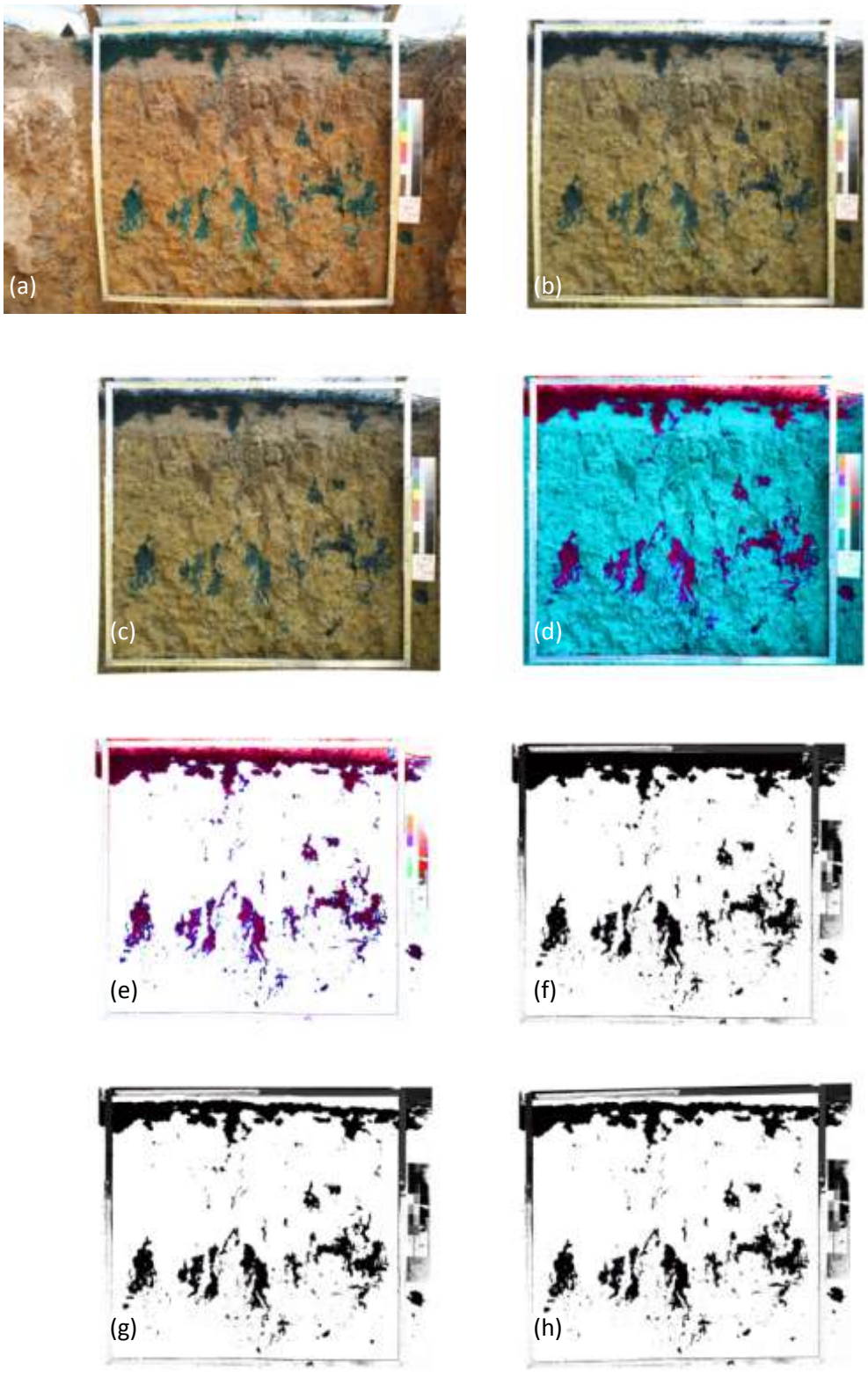

Figure 4.2-4 Image correction procedure: (a) Original image, (b) Cropped, corrected for white balance, (c) Corrected for radial and keystone distortion, (d) Hue aberation 140, saturation 100 %, (e) Unstained soil removed, (f) Converted to black and white, (g) Surface soil separated from background, (h) Image tilted to correct for site slope ready for conversion to binary format (Animation Appendix 8.1.1). Scale of metal frame 1.0 x 1.0 m.

Quantitative procedures have been developed to determine dye concentration from digital images (Forrer *et al.* 2000), however in mottled soils with multiple background colours, each background colour requires its own calibration (Bogner *et al.* 2008). Consequently analysis of dye stained soil was limited to binary images representing dye presence or absence. Dye stained pixels were separated from unstained pixels by setting the hue and saturation sliders in the Photoshop CS3 software to 140 % and 100 %. Unstained pixels were removed and the coloured flow paths underexposed to generate a black and white image. These images were imported into Image J software (Abramoff *et al.* 2004) and converted to binary format using default settings in which dye stained pixels (black) were assigned a value of 255, and unstained pixels (white) a value of zero. Images were corrected to account for site slope in order that the proportion of dye stained pixels was reported on a 'depth below surface' basis (Figure 4.2-4). Analysis of the proportion of dye stained soil was performed on all vertical binary images at 1 cm depth increments. Digital animation of the image correction process is presented on the CD Rom (Appendix 8.1.1).

4.2.5 Determination of infiltration uniformity

Infiltration uniformity (degree of variation in infiltration depth) was determined by calculating Christensen's coefficient of uniformity (Christiansen 1942) using binary vertical images of dye stained soil in which the cumulative depth of dye stained soil was determined at 0.5 mm intervals (pixel width). Rooting depth was determined by *in situ* soil moisture monitoring Appendix 4.2.

4.3 Results and Discussion

4.3.1 Dye tracer infiltration – site A

Dye staining analysis - Site A – Dry treatment

In the dry treatment, the maximum depth of dye tracer infiltration ranged from 77 cm (slice 3) to 94 cm (slice 4) (Figure 4.3-1). Vertical dye staining patterns showed similar characteristics in all four slices (Figure 4.3-1). Near the soil surface (0-4 cm depth) the dye tracer penetrated across the entire width of the analysis area (Figure 4.3-2, Figure 4.3-1). Ritsema *et al.* (1993) describe this uniformly infiltrated area as a distribution zone in which water flows laterally towards preferential flow paths or fingers. Vertical excavation demonstrated that the wetting front started to break down and form fingers at approximately 4 cm depth (Figure 4.3-1) resulting in the average proportion of dye stained soil decreasing from 81 % at 2 cm depth in the upper A1 horizon, to 20 % at 13 cm depth, in the lower A1 horizon (Figure 4.3-2). The width of the fingers ranged from 2 to 12 cm. Finger location was not related to the location of macropores or root pathways. In slices 1, 2 and 4, accumulation of dye on the upper surface of the B21 horizon was noted (Figure 4.3-1), however horizontal excavations demonstrated the proportion of dye stained soil was lower on the upper surface of the B21 horizon (19.3 % at 13 cm depth) than in the lower A1 horizon (26 % at 10 cm depth), (Figure 4.3-3), which suggests the textural discontinuity between the A and B horizons resulted in minimal if any ponding on the upper surface of the B21 horizon.

Dye staining in the B21 horizon (18-35 cm depth) occurred as thin films (<1 cm wide) or rivulets which flowed down the inside walls of large shrinkage cracks or ped faces (Figure 4.3-1). The proportion of dye stained soil within the B21 horizon was less than 2 % in all vertical excavations (at approximately 20 cm depth), and only 0.3 % in the horizontal excavations at 20 – 22 cm depth (Figure 4.3-3). This analysis demonstrates that infiltration bypassed as much as 99.7 % of the soil matrix in the B21 horizon. Unstained shrinkage cracks were common in all vertical slices (Figure 4.3-1) as only cracks which were hydrologically connected to the base of a finger actually participated in flow.

In the B22 and B23 horizons (35 – 95 cm), dye staining consisted of vertically oriented ‘patches’ within thin void spaces (Figure 4.3-1). Dye staining patterns in the horizontal excavations at 53 - 55 cm and 70 - 73 cm depth (Figure 4.3-4) revealed that in the lower B2 horizons, the dye tracer accumulated in terminal shrinkage cracks which spread laterally into small voids or cleavage cracks. Dye infiltration terminated at approximately 95 cm depth, beneath which shrinkage cracks and cleavage plains were not observed, and gravels of Permian mudstone were encountered (not dye stained) (Figure 4.3-4).

Site A - Vertical excavation - Dry treatment

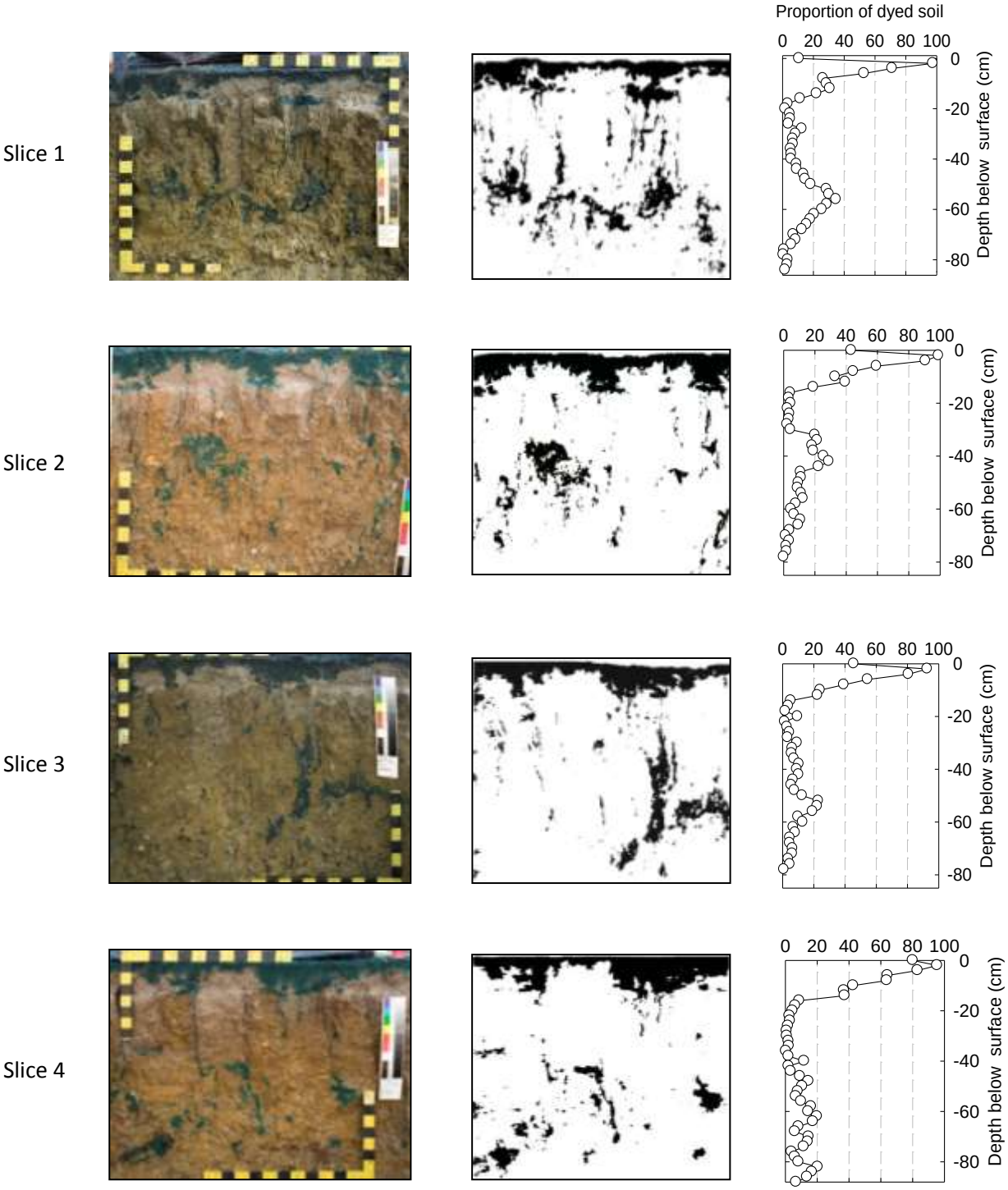

Figure 4.3-1 Site A, dry treatment, dye tracer infiltration. First column - vertical excavation showing dye staining. Second column - binary image of dye stained soil. Third column – proportion of dye stained soil with depth.

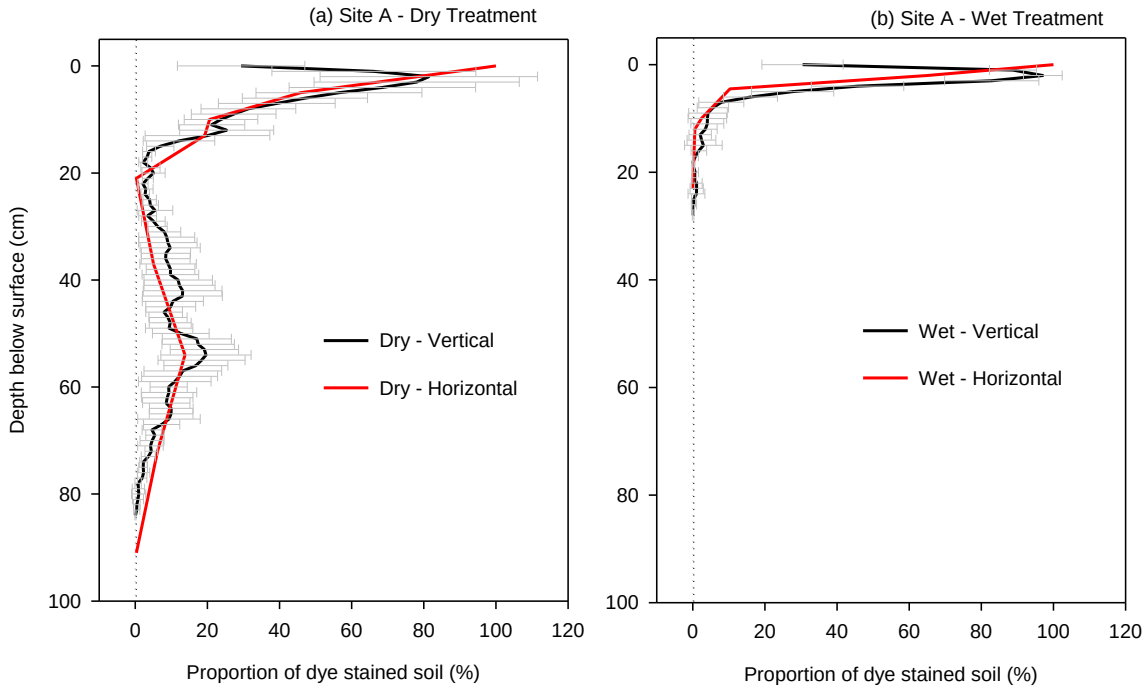

Figure 4.3-2 Site A, effect of antecedent soil moisture on the proportion of dye stained soil in vertical (1 cm increments) and horizontal excavations (a) dry treatment, (b) wet treatment. Error bars represent ±1 SD for the vertical excavations.

Dye staining analysis, site A – Wet treatment

In the wet treatment, the dye tracer infiltrated to a maximum depth ranging from 11 cm to 28 cm (Figure 4.3-5). In all five slices, the soil was uniformly stained to approximately 4 cm depth. Horizontal excavations revealed the proportion of dye stained soil fell from 65 % at 2 cm depth to 10 % at 5 cm depth, indicating that the wetting front broke down at approximately 4 -5 cm depth (Figure 4.3-6). Vertical dye staining patterns indicate the wetting front developed perturbations in slices 1 and 2, while in slices 3, 4 and 5 breakdown of the wetting front appeared to have developed into 'true' fingering (Figure 4.3-5). In slices 1, 2, and 5, patches of dye stained soil appear to be disconnected from other areas of dye stained soil. Further excavation revealed these apparent disconnections resulted from flow paths behind the excavated soil face.

Site A - Horizontal excavation - Dry treatment

5 cm depth

45.9 % stained

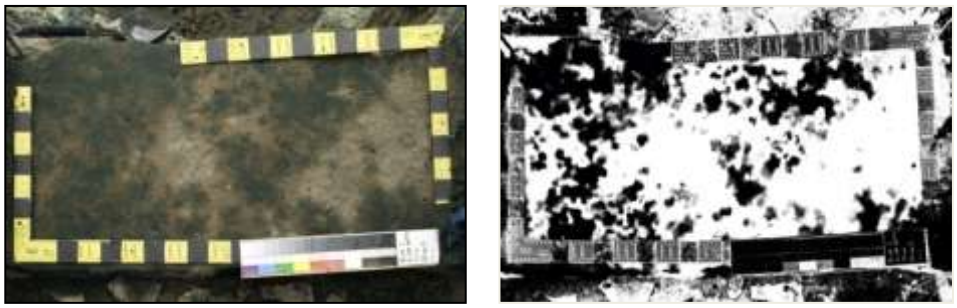

10 cm depth

26 % stained

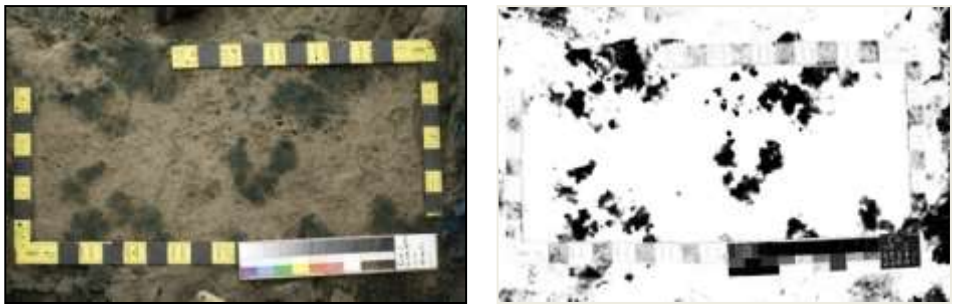

13 cm depth

(Surface B21)

19.3 % stained

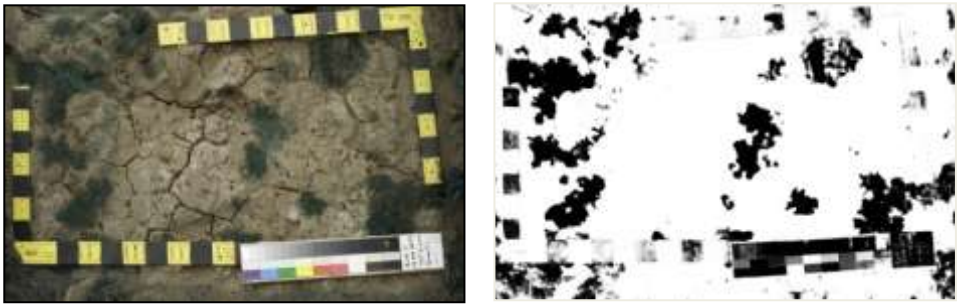

20-22 cm depth

0.33 % stained

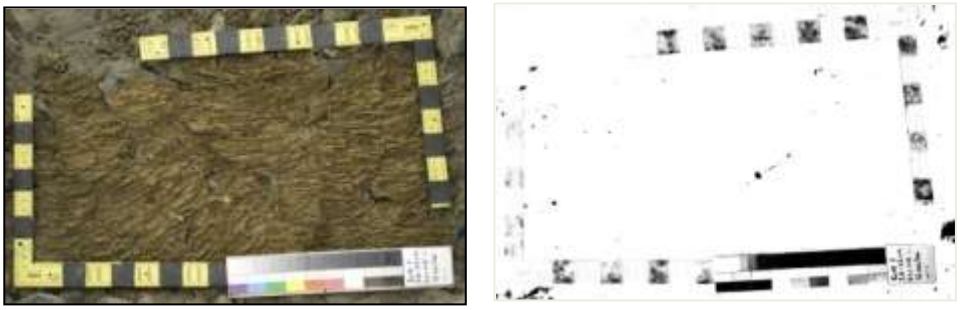

Figure 4.3-3 Site A, dry treatment. Horizontal excavation at 5 cm - 22 cm depth. First column - excavation depth and % of dye stained soil. Second column- dye stained soil. Third column - binary image of dye staining.

35 -40 cm depth

5.1 % stained

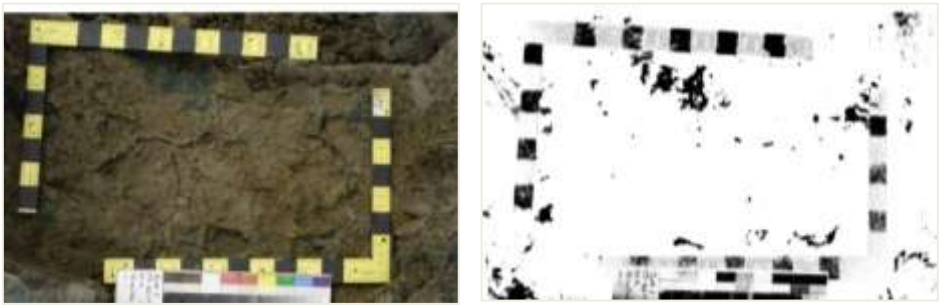

53 - 55 cm depth

13.8 % stained

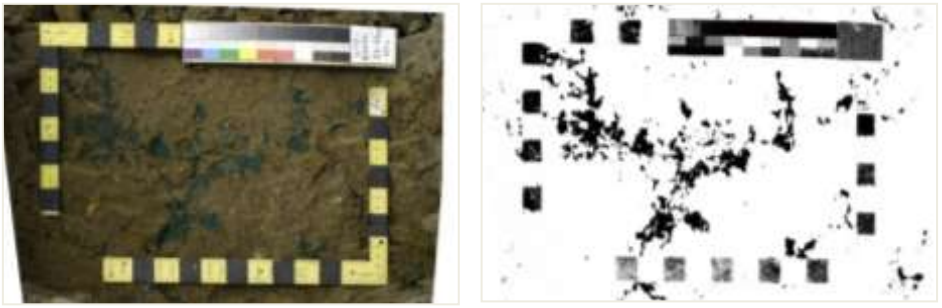

70-73 cm depth

6.2 % stained

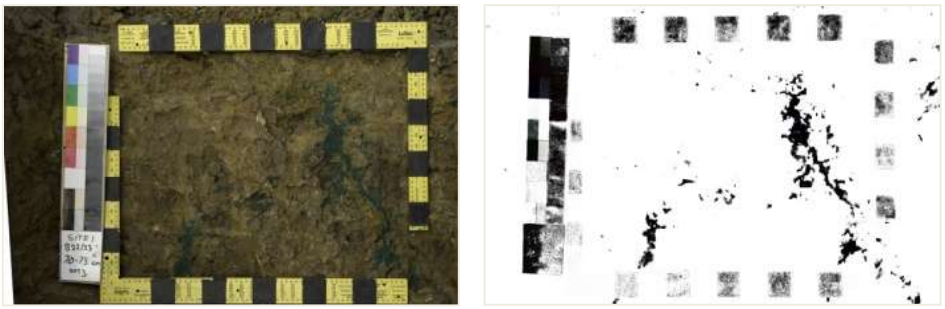

90-92 cm depth

0.35 % stained

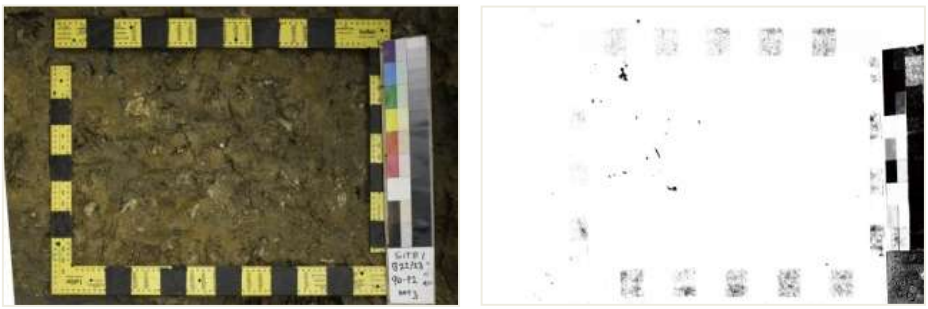

Figure 4.3-4 Site A, dry treatment. Horizontal excavation at 35 cm - 92 cm depth. First column - excavation depth and % of dye stained soil. Second column- dye stained soil. Third column - binary image of dye staining.

Site A - Vertical excavation - Wet treatment

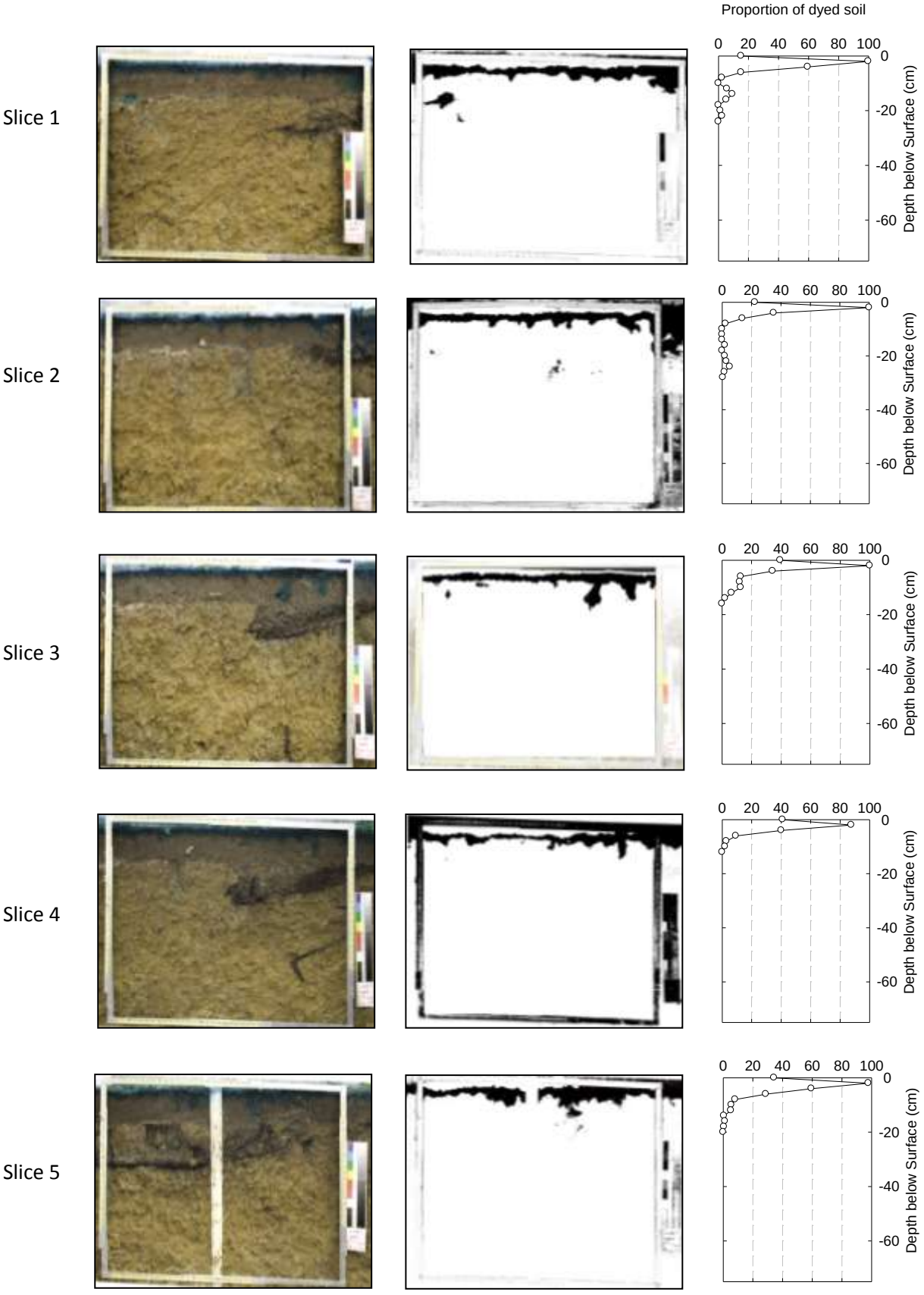

Figure 4.3-5 Site A, wet treatment, vertical excavation. First column – vertical excavation displaying dye staining. Second column - binary image of dye stained soil. Third column – proportion of dye stained soil with depth.

2cm depth

65% dye stained

5 cm depth

10 % dye stained

10 cm depth

2.4 % dye stained

12 depth

0.6 % dye stained

22 – 24 cm

0.003 % dye stained

60 cm depth

0.0001 % dye stained

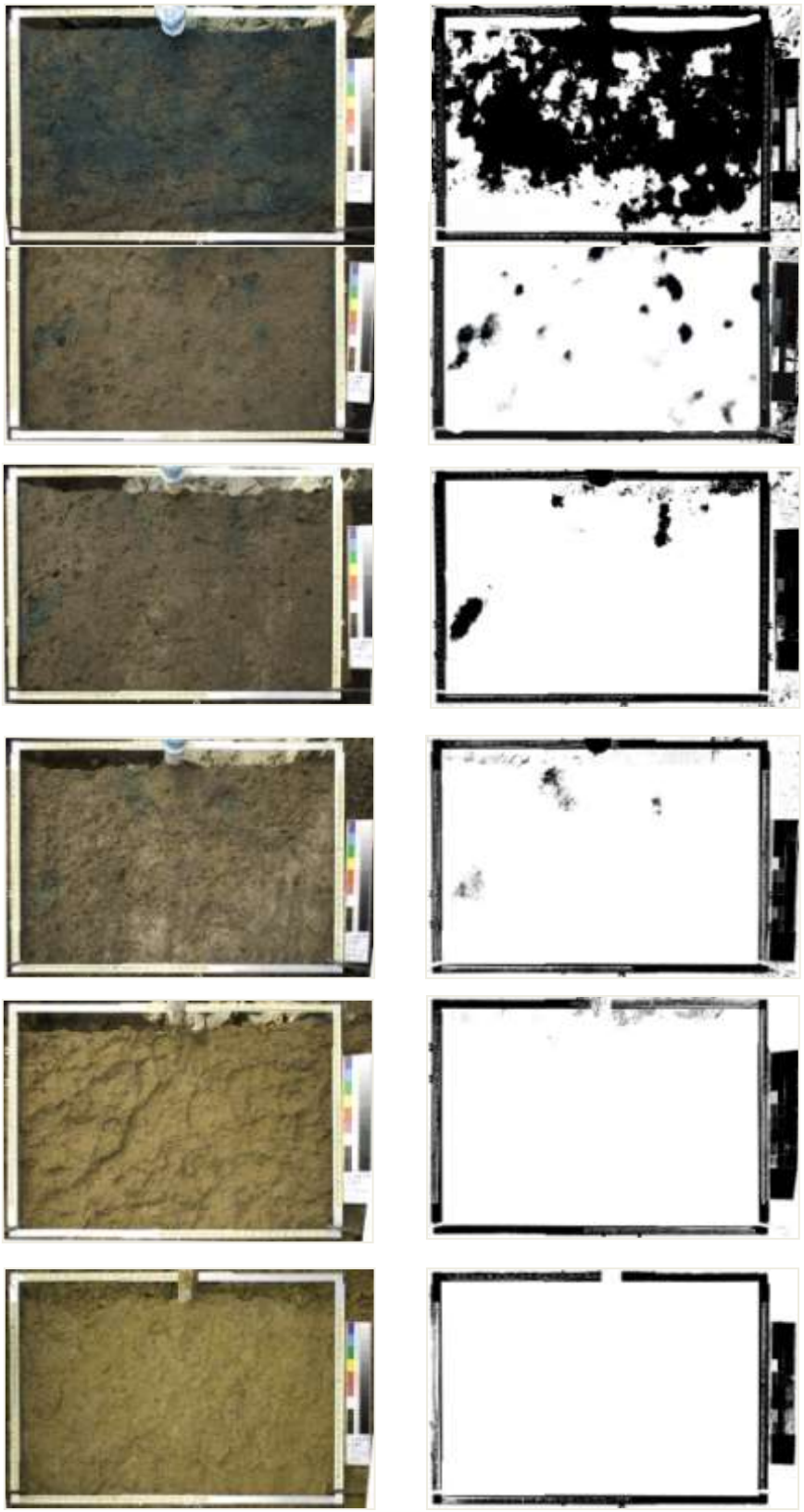

Figure 4.3-6 Site A, wet treatment. Horizontal excavation at 2 cm - 60 cm depth. First column - excavation depth and % of dye stained soil. Second column- dye stained soil. Third column - binary image of dye staining**.**

Site B - Vertical excavation - Dry treatment

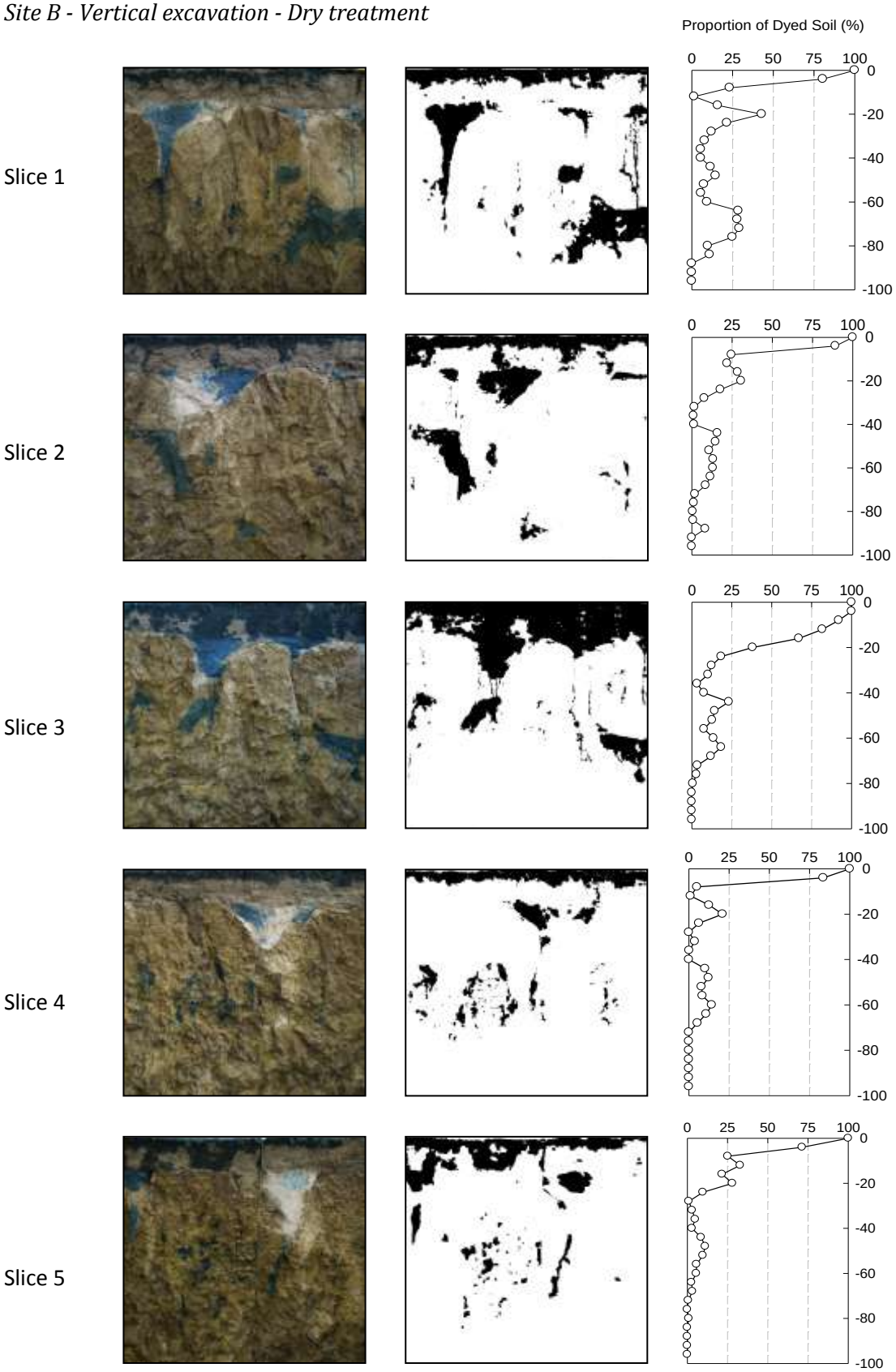

Figure 4.3-7 Site B, dry treatment. Dye tracer infiltration. First column – vertical excavation showing dye staining. Second column - binary image of dye stained soil. Third column – proportion of dye stained soil with depth.

4.3.2 Dye tracer infiltration – site B

Dye staining analysis, site B– Dry treatment.

In the dry treatment, dye tracer infiltrated to depths ranging from 74 cm (slice 4) to 90 cm (slice 2) (Figure 4.3-7). Similar to site A, the upper A1 horizon was uniformly stained to approximately 4 cm depth (Figure 4.3-7), while horizontal excavations indicated that the wetting front broke down to form fingers between 2 cm and 5 cm depth. At 5 cm depth, infiltration was restricted to fingers and isolated large macropores created by red headed cockschafer beetles (*Adoryphorus couloni*). The proportion of dye stained soil increased by 4.3 % between the middle of the A1 horizon (5 cm) and the lower A1 horizon (10 cm), which indicated hydraulic conductivity decreased to 5 - 10 cm within the A1 horizon (Figure 4.3-8).

The presence of a thick A2 horizon and sand infills resulted in minor differences in the dye staining patterns at site B compared to the other sites. At site B, the proportion of dye stained soil in the upper A2 horizon (30.6 % at 16 cm depth) was considerably greater than the lower A1 Horizon (11.4 % at 10 cm depth). This suggested that vertical infiltration from the A1 into the A2 horizon was impeded by the lower hydraulic conductivity of the A2 horizon. The proportion of dye stained soil decreased between the lower A2 horizon (30.8 % at 20 cm depth) and the upper B21 horizon (12.4 % at 20 - 25 cm depth) which indicated that the upper B21 horizon did not impede vertical infiltration (Figure 4.3-3). Dye staining in the sand infills appeared discontinuous (vertical and horizontal excavations), which suggested that infiltration in the sand infills was not entirely top down, rather that water moved into the sand infills from multiple locations in the B2 horizons (Figure 4.3-7, slices 2 and 4, and, Figure 4.3-10).

Dye staining patterns between 20 cm and 60 cm in the B21 and upper B22 horizons (slices 1, 2, and 3) (Figure 4.3-8 and Figure 4.3-10) consisted of thin rivulets or film flow. Horizontal excavation at 30 cm depth revealed only 1.3 % of the soil participated in flow (most of which was within the sand infill), and that not all shrinkage cracks participated in flow. In the B22 and B23 horizons, large dye stained ‘patches’ occurred between 45 cm and 95 cm depth (Figure 4.3-7). These patches were generally larger and more regularly shaped than those observed at site A (Figure 4.3-1). Horizontal excavation at 50 cm depth also revealed the presence of ‘lattice’ like dye staining patterns (Figure 4.3-10), resulting from the dye tracer spreading laterally as saturated flow through an interconnected network of inter-pedal shrinkage cracks at the base of terminal shrinkage cracks. Infiltration of the dye tracer into the clay columns (matrix) via cleavage plains or the soil matrix was minimal (upper right - Figure 4.3-10, 50 cm depth) (Digital animation of sequential dye infiltration is presented on the CD Rom, Appendix 8.1.2 and 8.1.3).

Site B - Horizontal excavation - Dry treatment

2 cm depth

57.5 % stained

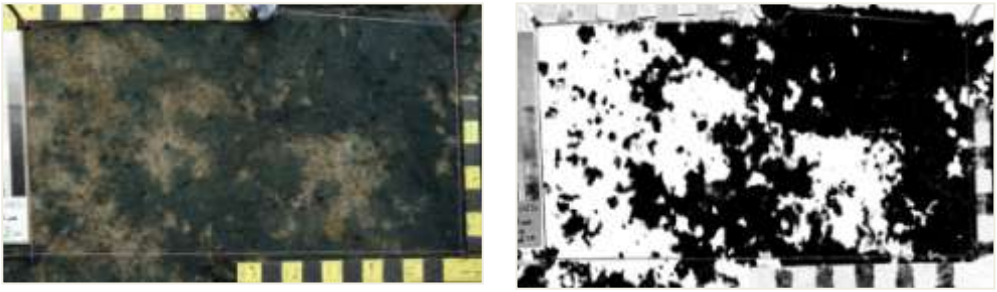

5 cm depth

7.1 % stained

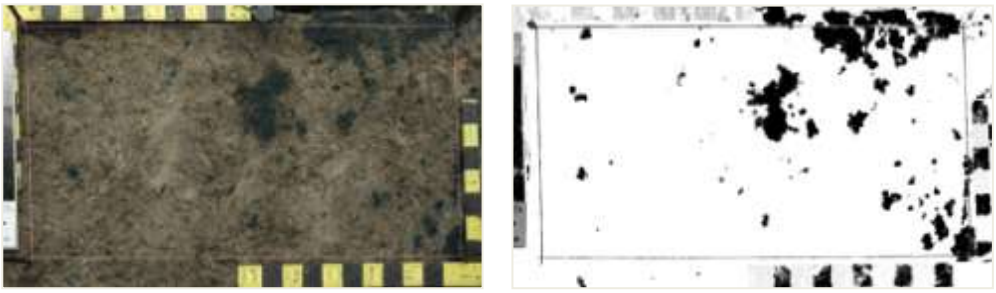

10 cm depth

11.4 % stained

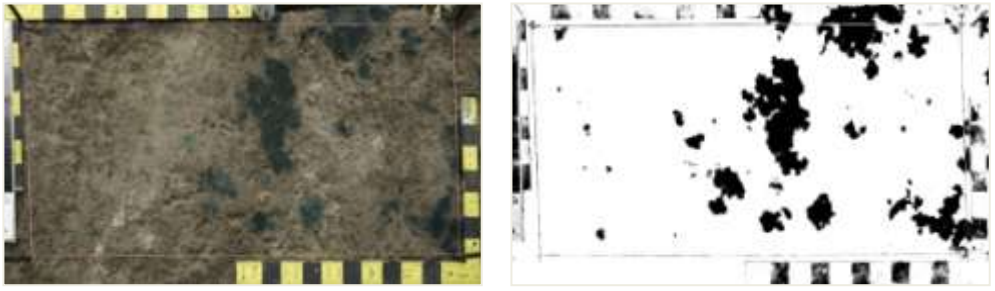

16 cm depth

30.6 % stained

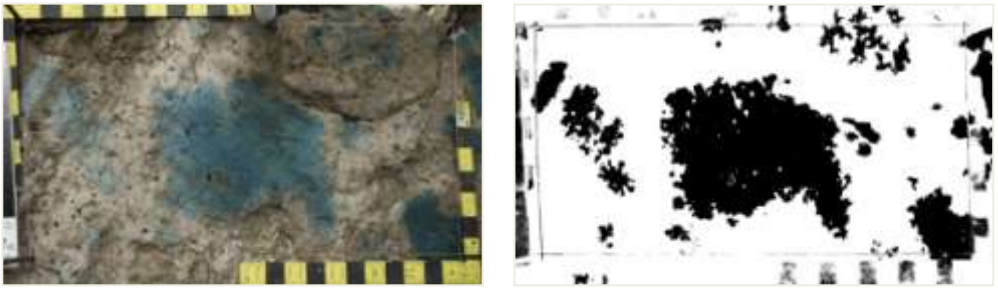

20 cm depth

30.8 % stained

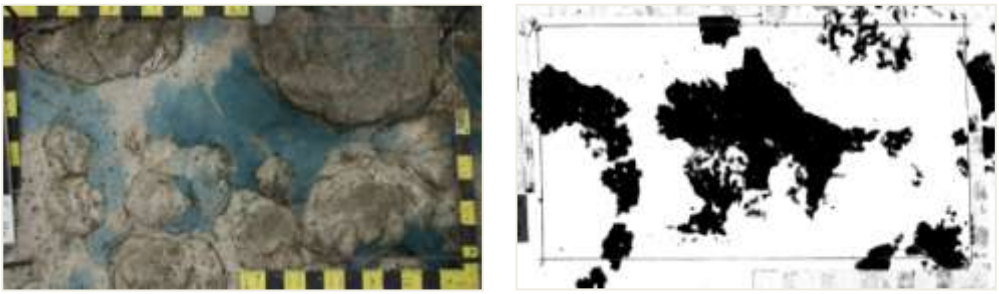

Figure 4.3-8 Site B, dry treatment. Horizontal excavation 2 cm - 20 cm depth. First column - excavation depth and % of dye stained soil. Second column- dye stained soil. Third column - binary image of dye staining (Animation Appendix 8.1.2 and 8.1.3).

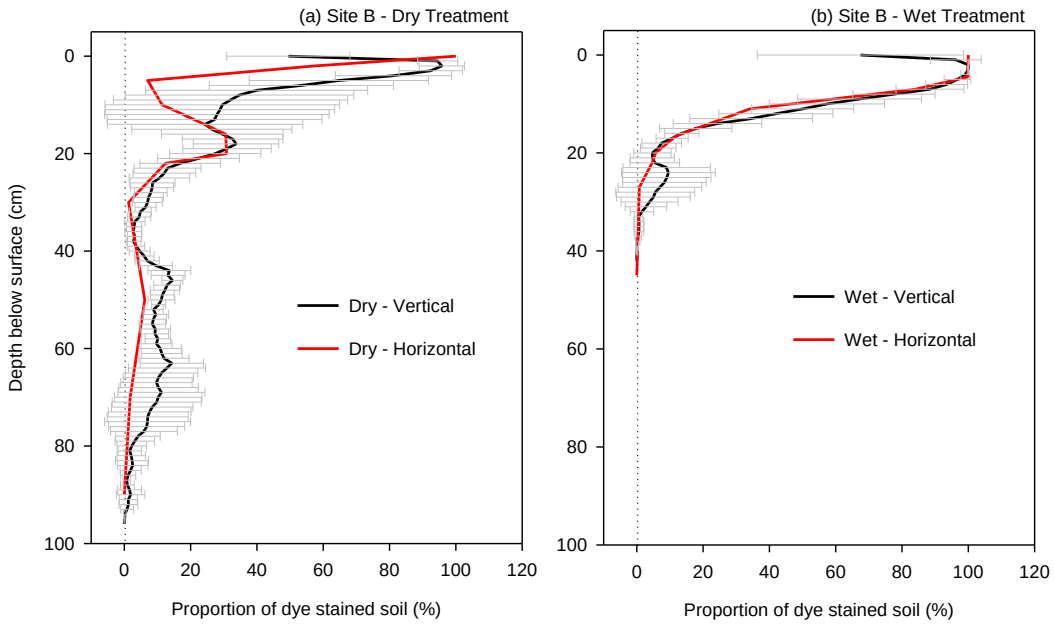

Figure 4.3-9 Site B, effect of antecedent soil moisture on the proportion of dye stained soil in both vertical excavations (1 cm increments) and horizontal excavations (a) dry treatment, (b) wet treatment. Error bars represent ±1 SD for the vertical excavations.

Dye staining analysis, site B– Wet treatment

In the wet treatment, the dye tracer infiltrated to a maximum depth between 18 cm (slice 3) and 38 cm depth (slice 5) (Figure 4.3-12). Deeper infiltration in slice 5 resulted from flow within a sand infill, while slices 1 and 3 demonstrated deeper infiltration due to infiltration into the A2 horizon. Horizontal excavation revealed the wetting front had broken into large fingers or perturbations at approximately 10 - 12 cm depth. These fingers or perturbations extended to the upper surface of the A2 horizon at 15 - 18 cm depth. Lack of dye accumulation or spreading at the A1 / A2 boundary indicated that at high antecedent soil moisture, the A2 horizon did not restrict vertical infiltration as had been observed in the dry treatment. Excavation at 30 cm depth revealed that infiltration terminated at or before the upper surface of the B horizon. The absence of dye accumulation or lateral dye movement at the A2 / B21 boundary indicated that neither ponding nor subsurface lateral flow occurred along the upper surface of the B horizon in the wet treatment. Few differences existed between the vertically excavated dye patterns at site B (Figure 4.3-12) and site A (Figure 4.3-5). However, uniform infiltration through the A1 horizon at site B was deeper (approximately 10 cm) than at site A (approximately 4 cm).

Site B - Horizontal excavation - Dry treatment

20 -25 cm depth

12.4 % stained

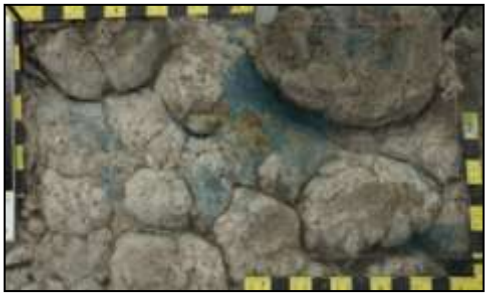

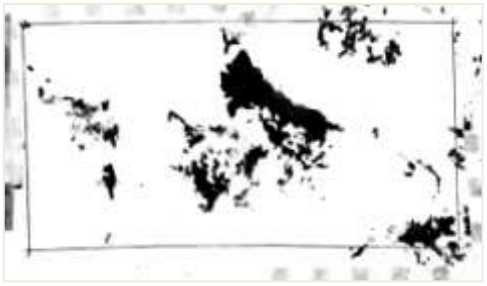

30 cm depth

1.3 % stained

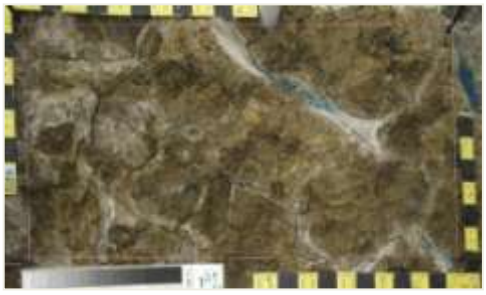

50 cm depth

6.2 % stained

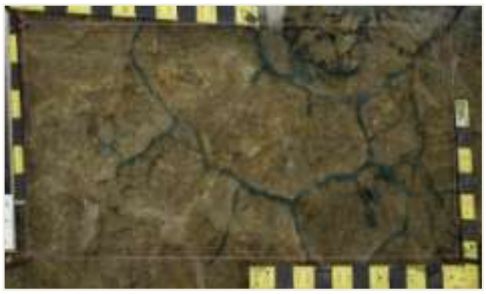

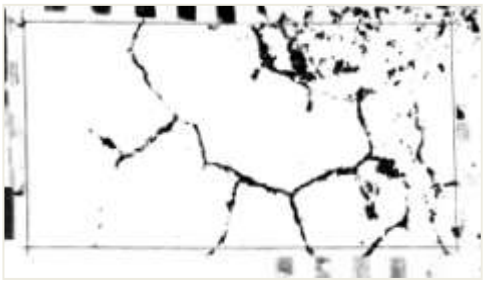

70 cm depth

1.8 % stained

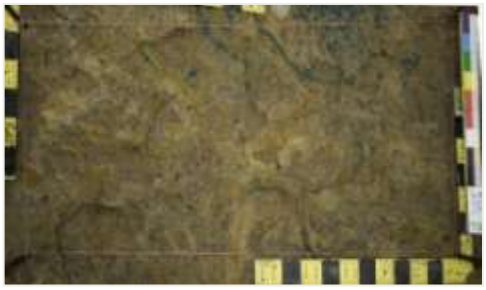

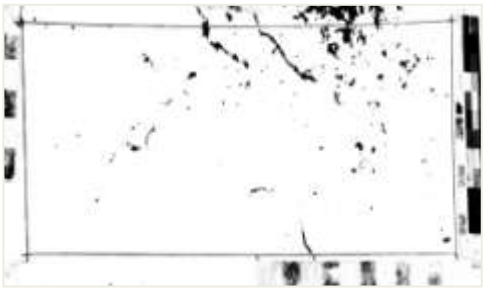

90 cm depth

0.03 % stained

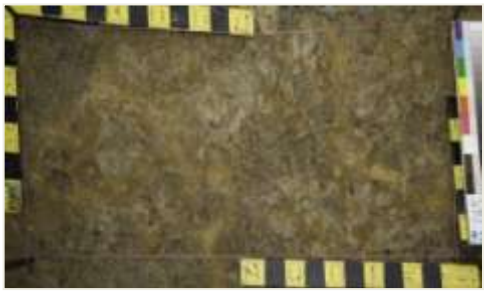

Figure 4.3-10 Site B, dry treatment. Horizontal excavation 20 cm - 90 cm depth. First column - excavation depth and % of dye stained soil. Second column- dye stained soil. Third column - binary image of dye staining (Animation Appendix 8.1.2 and 8.1.3.

The presence of sand infills (SI) at site B confounded analysis of the proportion of dye stained soil with depth. As such, the proportion of dye stained soil and the fate of the applied dye was determined on a soil horizon basis (Figure 4.3-11). In the wet treatment, 57.6 % (SD 4.9 %) of the A1 horizon participated in flow compared to 49.3 % (SD 17.0 %) in the dry treatment, differences between the soil moisture treatments were not significant. In the dry treatment, inability to wet up the A1 horizon resulted from hydrophobicity induced finger flow. Whilst in the wet treatment, inability to wet-up the A1 horizon was thought to have resulted from difficulty displacing existing water from soil pores, and / or reduced hydraulic conductivity of the B2 horizons resulting from clay swelling and closure of shrinkage cracks.

Figure 4.3-11 a demonstrates the A2 and sand infills had significantly (p<0.05) higher participation in flow than the B21 horizon, however this does not imply the sand infills were more effective at transferring infiltration into the subsoil than bypass flow through shrinkage cracks, as rivulet flow did not infiltrate laterally into the soil matrix, and thus may have carried a greater flow volume than flow in the sand infills. In the dry treatment, the proportion of infiltrated dye tracer retained by each horizon did not decrease sequentially with depth as a significantly (p<0.05) higher proportion of the dye tracer was retained in B22 horizon than the B21 horizon.

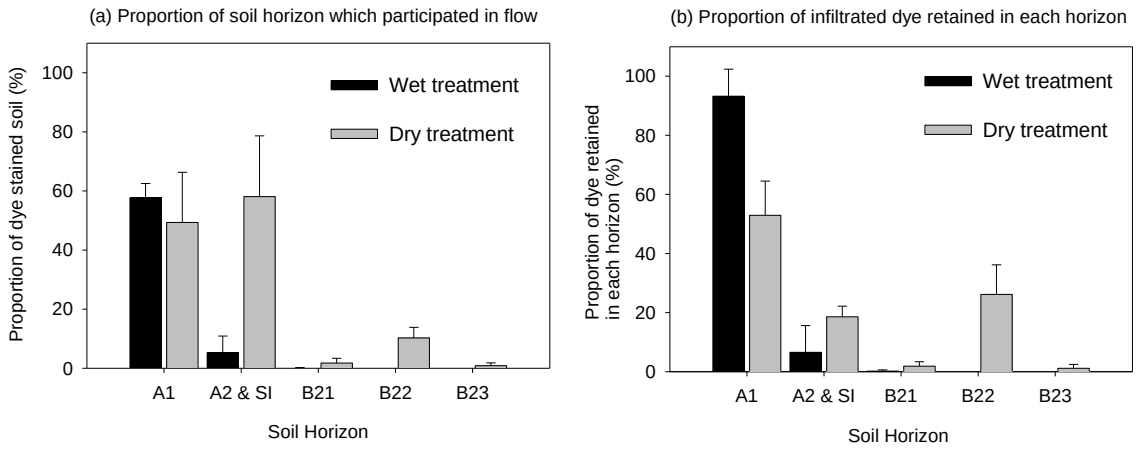

Figure 4.3-11 Effect of antecedent moisture content on the proportion of dye stained soil by horizon. (a) Proportion of dye stained soil, i.e. the proportion of soil which participated in flow. (b) Proportion of infiltrated dye tracer retained in each horizon (sum 100%). Note A2&SI refer to combined A2 horizon and sand infills. Error bars represent ± 1 SD.

Site B - Vertical excavation - Wet treatment.

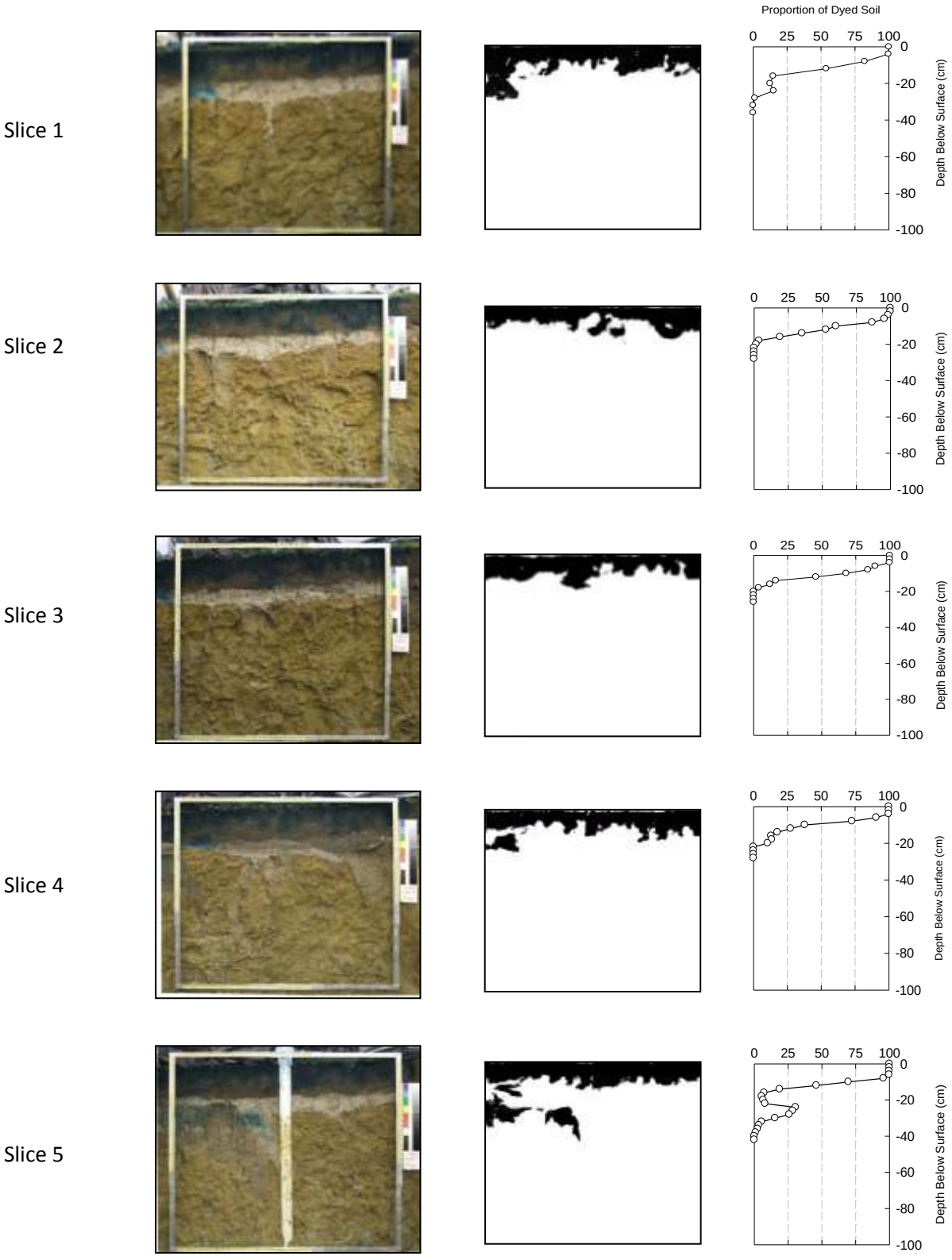

Figure 4.3-12 Site B, wet treatment, vertical excavation. First column – vertical excavation showing dye staining. Second column - binary image of dye stained soil. Third column – proportion of dye stained soil with depth.

Site B - Horizontal excavation - Wet treatment.

4-5 cm depth

99.8 % stained

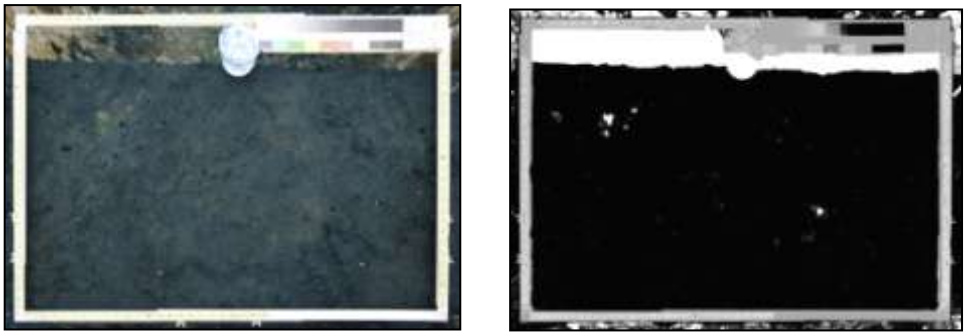

7 cm depth

84.1 % stained

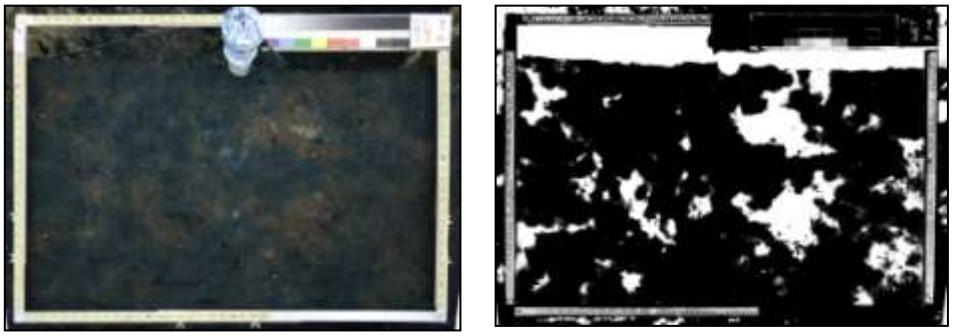

10-12 cm depth

34.1 % stained

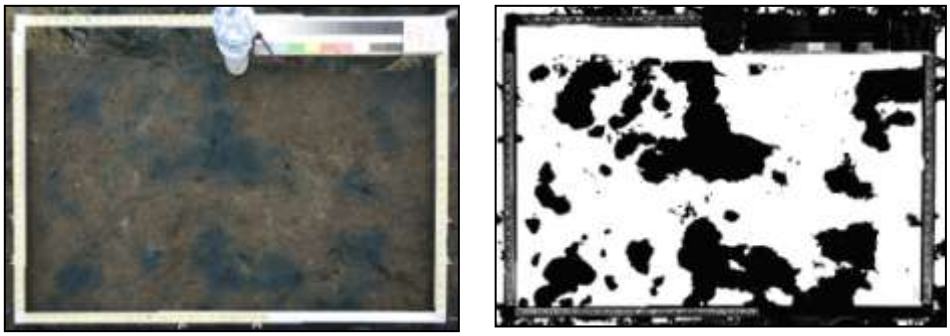

15-18 cm depth

Upper A2 horizon

11.9 % stained

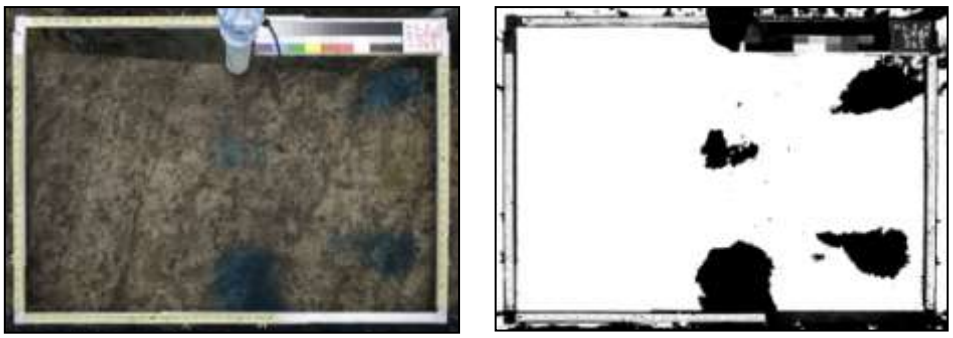

Figure 4.3-13 Site B. Wet treatment. Horizontal excavation 4 cm - 18 cm depth. First column - excavation depth and % of dye stained soil. Second column- dye stained soil. Third column - binary image of dye staining.

Site B - Horizontal excavation - Wet treatment.

18 – 22 cm depth

5.7 % stained

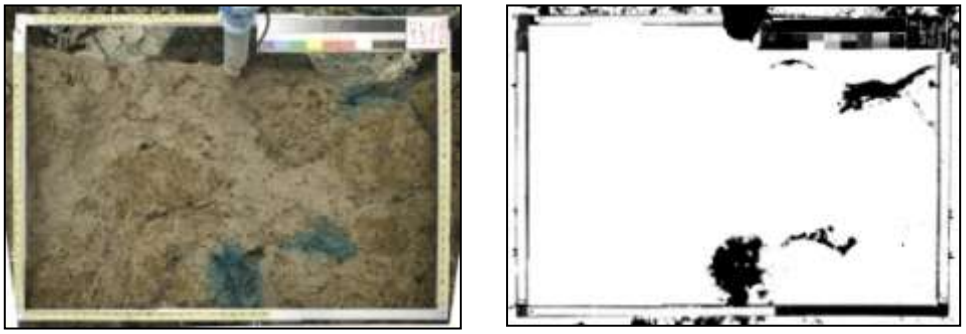

18-25 cm depth

A2 removed

4.7 % stained

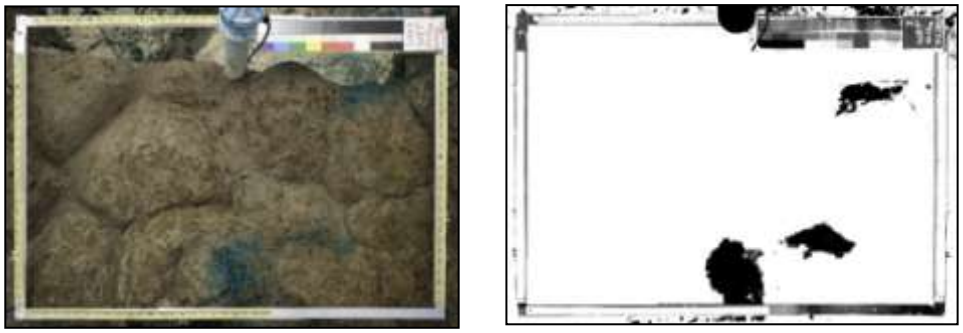

25-30 cm depth

0.8 % stained

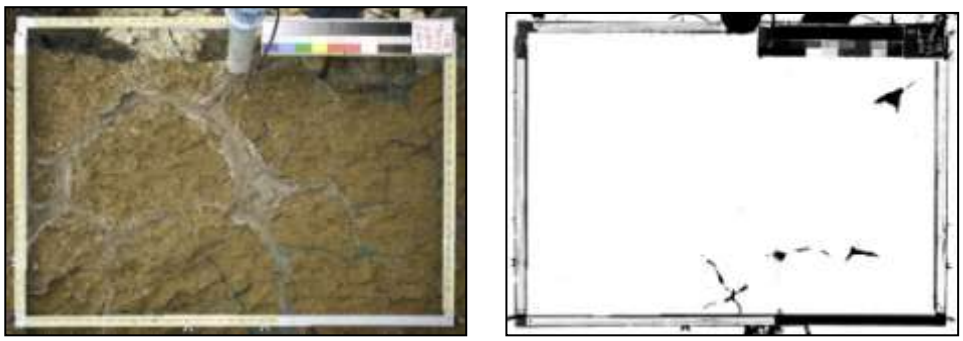

45 cm depth

0.001 % stained

Figure 4.3-14 Site B. Wet treatment. Horizontal excavation 18cm - 45 cm depth. First column - excavation depth and % of dye stained soil. Second column- dye stained soil. Third column - binary image of dye staining.

4.3.3 Dye tracer infiltration – site C

Dye staining analysis, site C– Dry treatment.

In the dry treatment, dye staining patterns at site C were similar to site A, due to the minimal development of the A2 horizon and sand infills at both sites (Figure 4.3-15). Uniform dye staining in the upper A1 horizon extended to 3 - 4 cm depth at site C (Figure 4.3-15), compared to 4 - 5 cm depth at sites A and B. Unlike the other three sites, finger flow was not apparent in the vertically excavated soil profiles at site C. Consequently flow between 0 - 4 cm depth appeared 'disconnected' from dye staining further down the soil profile (Figure 4.3-15). Horizontal excavation (Figure 4.3-17) demonstrated that relatively few large (5 -7 cm diameter) soil water fingers existed at 5 – 6 cm depth resulting in only 14 % of the lower A1 horizon having participated in flow. The absence of dye staining at the A / B boundary (12 – 15 cm) indicated that dye tracer did not accumulate on the upper B horizon, and that the B2 horizons did not impede vertical infiltration at low antecedent soil moisture.

The proportion of dye stained soil within the B21 was less than 0.2 % (Figure 4.3-16). Excavation at 14 - 15 cm depth revealed numerous cockchafer beetle burrows in the upper surface of the B horizon, however these were not associated with dye staining and thus not involved in infiltration. Dye staining patterns at 14 - 15 cm were similar to site A (13 cm depth) in which finger flow from the A horizon spread laterally (5 - 8 cm) across the surface of the B horizon until it encountered a shrinkage crack. Infiltration through the B21 and B22 via shrinkage cracks resulted in infiltration through only 2.2 % (50 cm depth) to 0.4 % (52 - 55 cm depth) of the soil.

In the B22 and B23 horizons dye staining appeared as many, small, vertically oriented patches (Figure 4.3-15), similar to those observed at site A. At 65 cm and 83 - 85 cm depth (Figure 4.3-18), horizontally oriented dye staining patterns indicate lateral spreading of dye through cleavage plains, (observed at 53-55 cm depth at site A), and filling of connected vertically oriented shrinkage cracks, as observed at 50 cm depth at site B. Compared to sites A and B, lateral spreading and filling of void spaces occurred at greater depths (65 - 85 cm) at site C than the other sites (50 - 75 cm). The number of small complex dye staining patterns in Figure 4.3-15 and Figure 4.3-18 suggest that infiltration through the B2 horizons at site C were more obstructed and convoluted than the other three sites.

Site C - Vertical excavation - Dry treatment

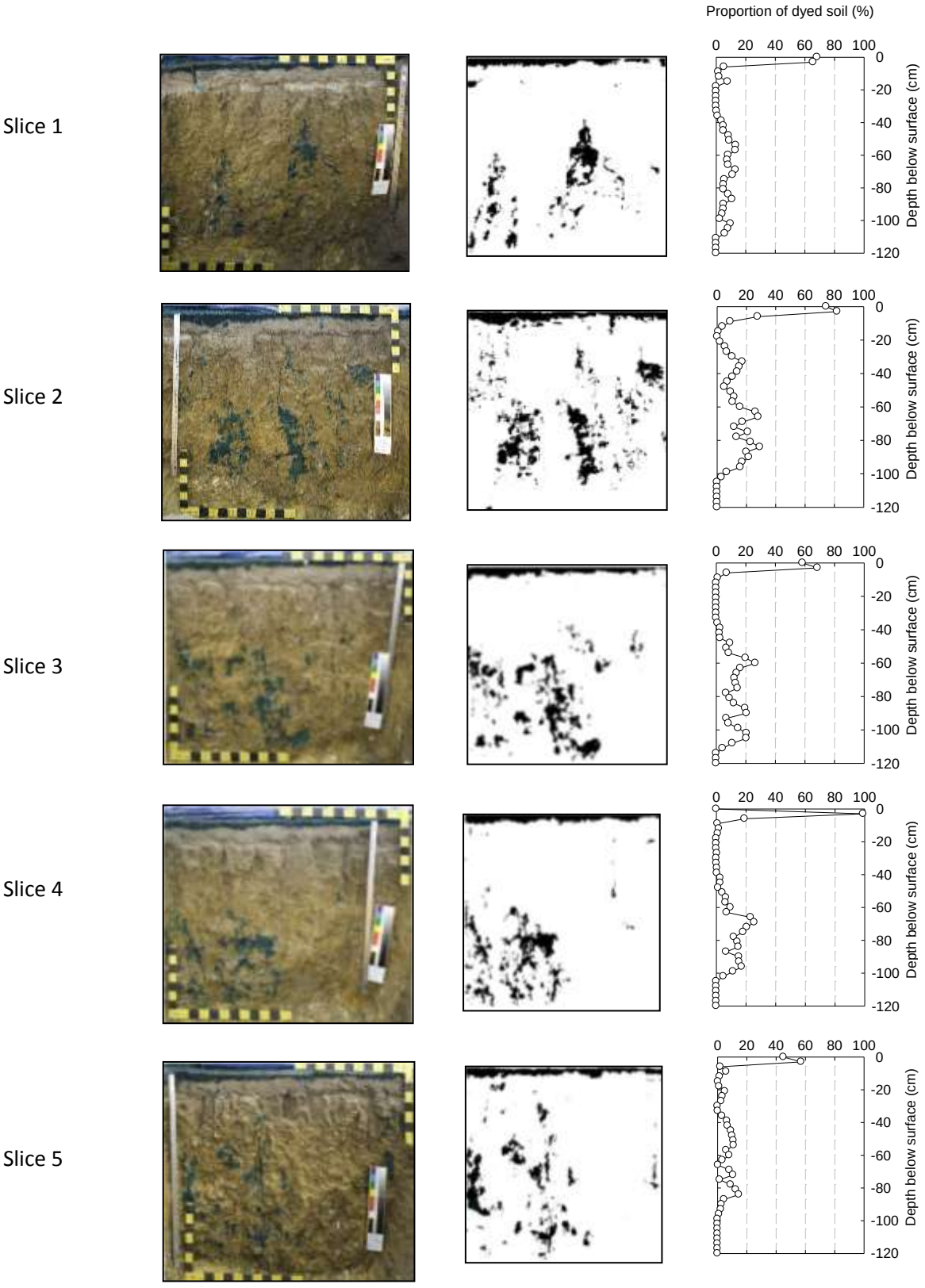

Figure 4.3-15 Site C, dry treatment, dye tracer infiltration. First column – vertical excavation showing dye staining. Second column - binary image of dye stained soil. Third column – proportion of dye stained soil with depth.

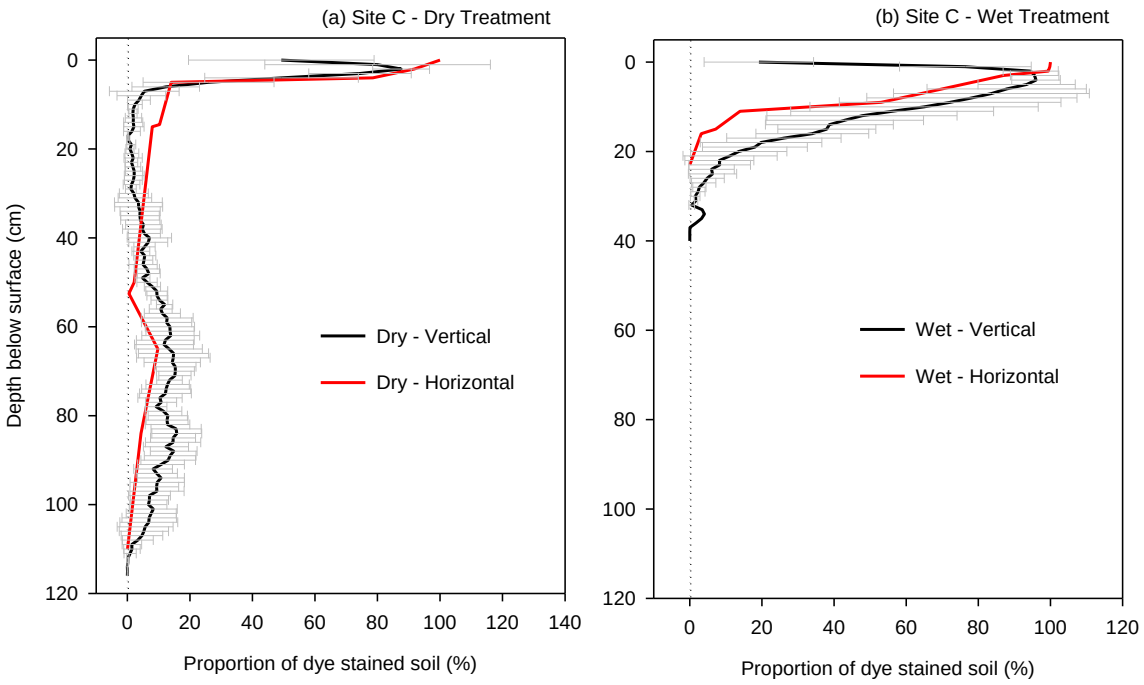

Figure 4.3-16 Site C, effect of antecedent soil moisture on the proportion of dye stained soil in both vertical excavations (1cm increments) and horizontal excavations (a) dry treatment, (b) wet treatment. Error bars represent ±1 SD for the vertical excavations.

4.3.3.1 Dye staining analysis, site C– Wet treatment

Difficulty was encountered with the establishment of the wet treatment at site C. Despite the site receiving 20 - 30 mm irrigation up to 4 times a week for a period of 4 weeks, patches of dry (hydrophobic) soil were present in the A1 horizon (particularly slice 1) (Figure 4.3-19). Inconsistent moisture content in the A horizon, did not appear to effect results as vertically excavated dye infiltration patterns were similar to the other sites. In the wet treatment, dye infiltrated to between 21 cm and 36 cm depth (Figure 4.3-19). The depth of uniform infiltration was deeper (5 - 9 cm) than the dry treatment (3 - 4 cm). Dye staining in sand infills (15 - 25 cm depth), was noted in slices 2 and 4 (Figure 4.3-19). Excavation at 22 - 25 cm depth (Figure 4.3-21) revealed the dye tracer did not enter the B horizon, presumably due to the absence of macropores, clay swelling, and absence of sand infills.

Site C - Horizontal excavation - Dry treatment

2 cm depth

92 % stained

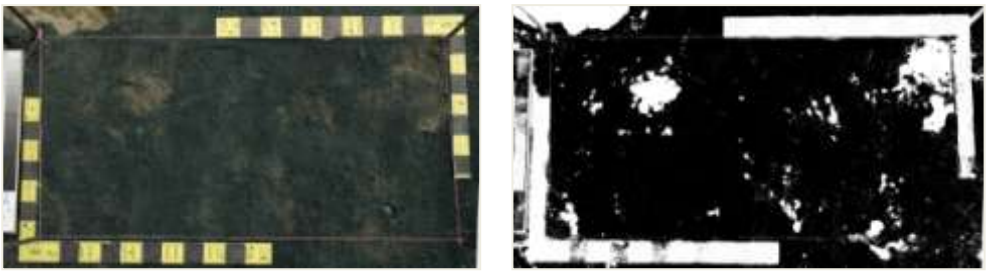

4 cm depth

79 % stained

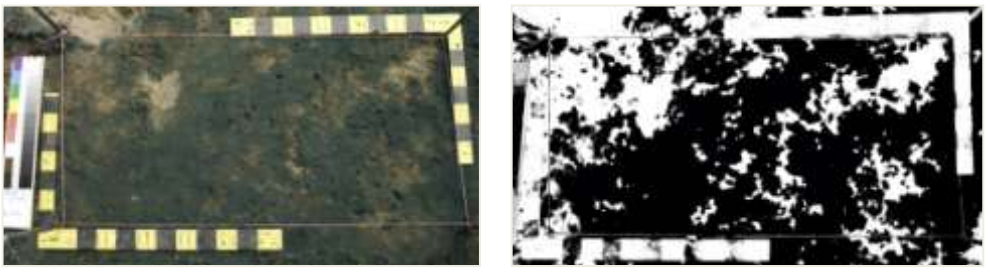

5-6 cm depth

14 % stained

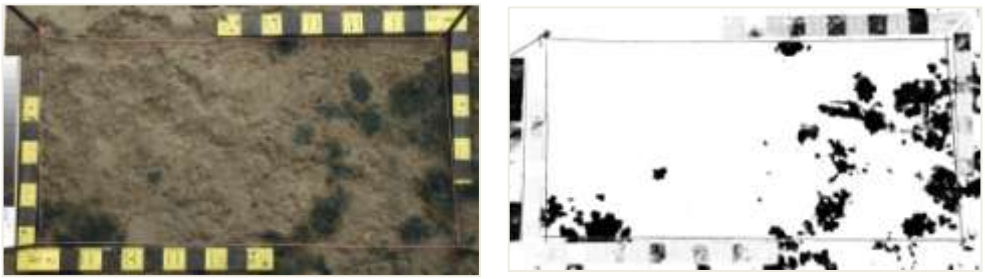

14-15 cm depth

10 % stained

30-35 cm depth

0.4 % stained

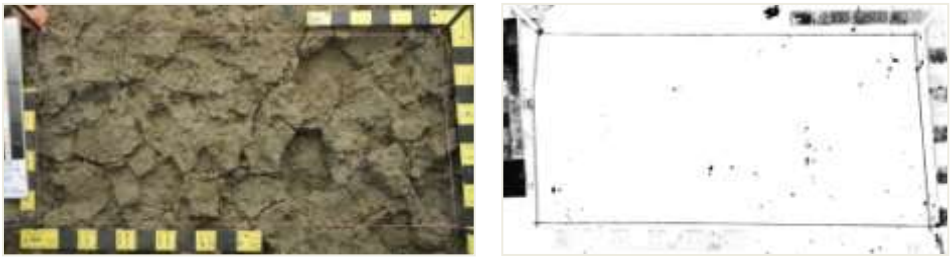

Figure 4.3-17 Site C, dry treatment. Horizontal excavation 2cm - 50 cm depth. First column - excavation depth and % of dye stained soil. Second column- dye stained soil. Third column - binary image of dye staining.

Site C - Horizontal excavation - Dry treatment

50 cm depth

2.2 % stained

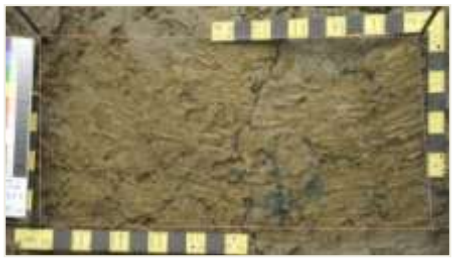

65 cm depth

9.7 % stained

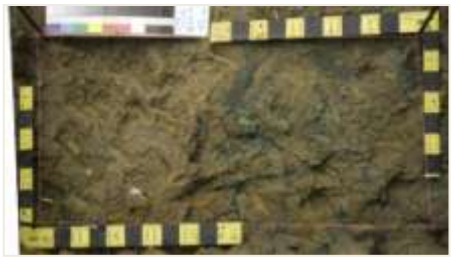

83-85 cm depth

4.3 % stained

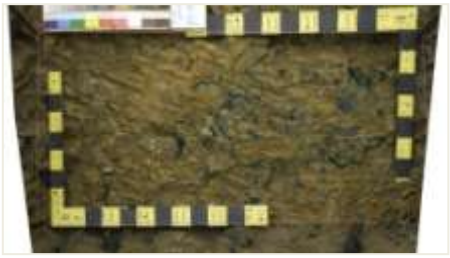

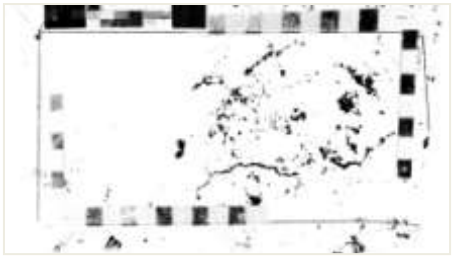

110 cm depth

0.02 % stained

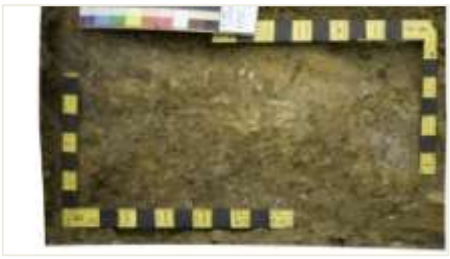

Figure 4.3-18 Site C, dry treatment. Horizontal excavation 55 cm - 110 cm depth. First column - excavation depth and % of dye stained soil. Second column- dye stained soil. Third column - binary image of dye staining.

Site C - Vertical excavation - Wet treatment

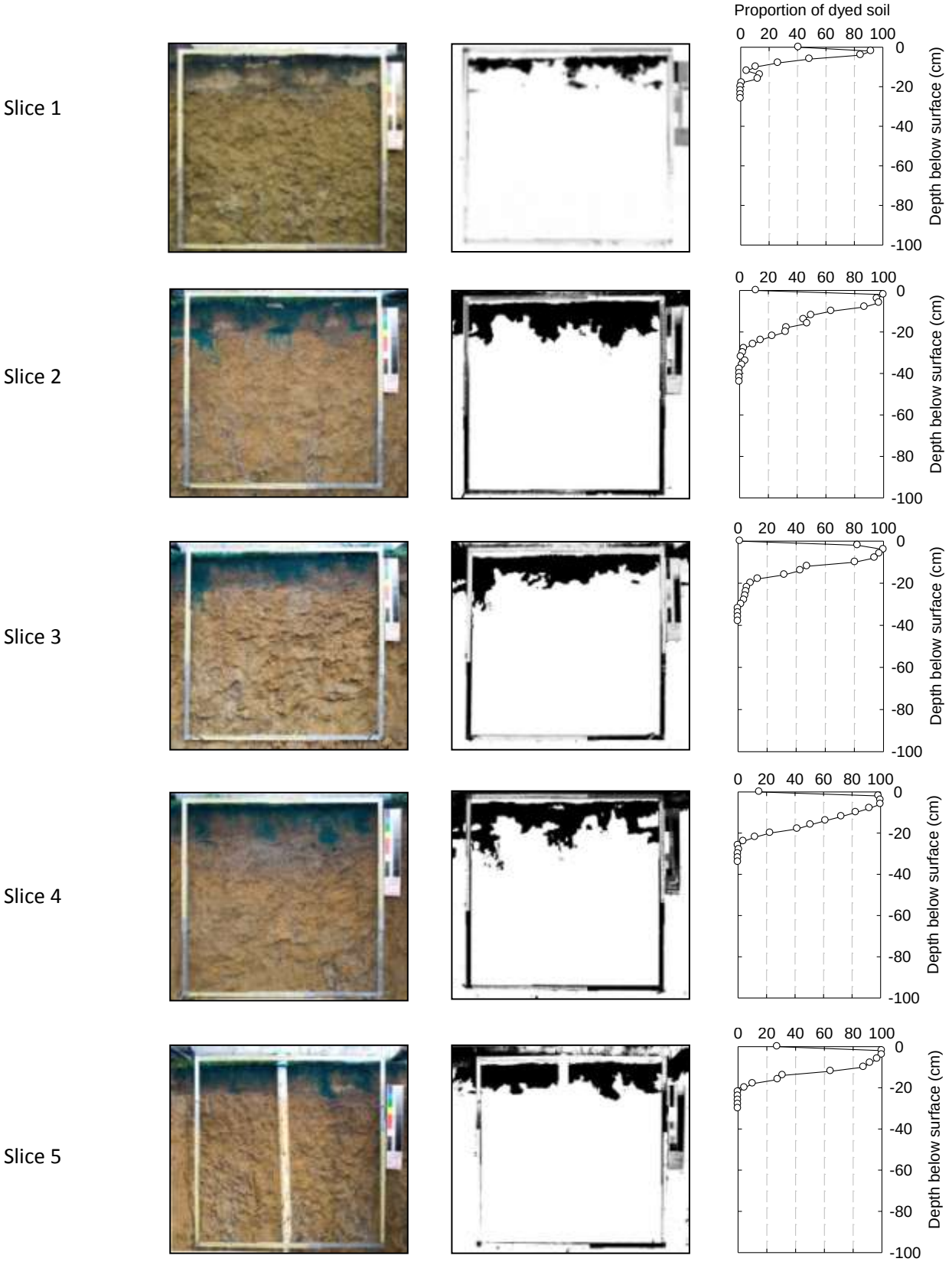

Figure 4.3-19 Site C, wet treatment, vertical excavation. First column – vertical excavation showing dye staining. Second column - binary image of dye stained soil. Third column – proportion of dye stained soil with depth.

1 cm depth

99.9 % stained

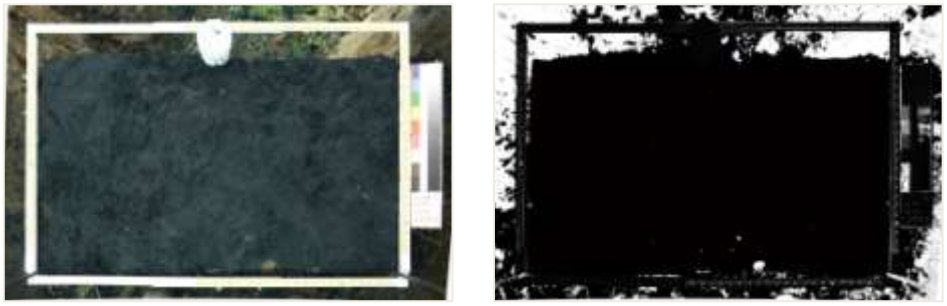

2 cm depth

99.4 % stained

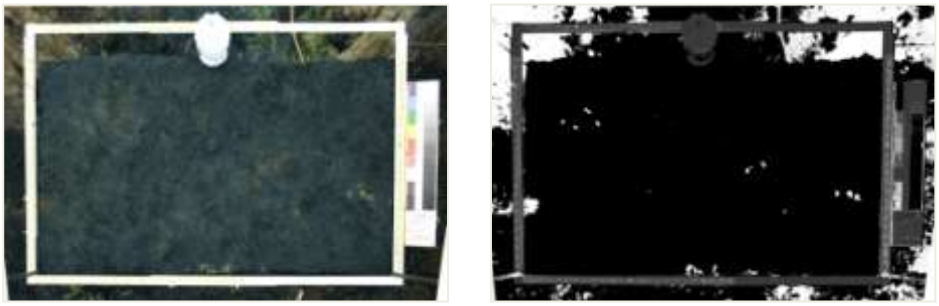

5 cm depth

87 % stained

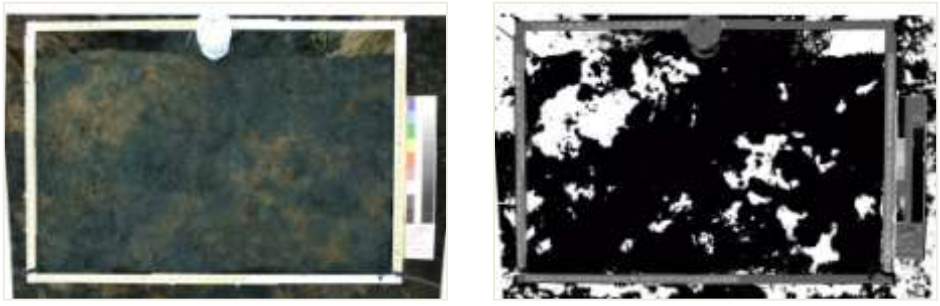

9 cm depth

53 % stained

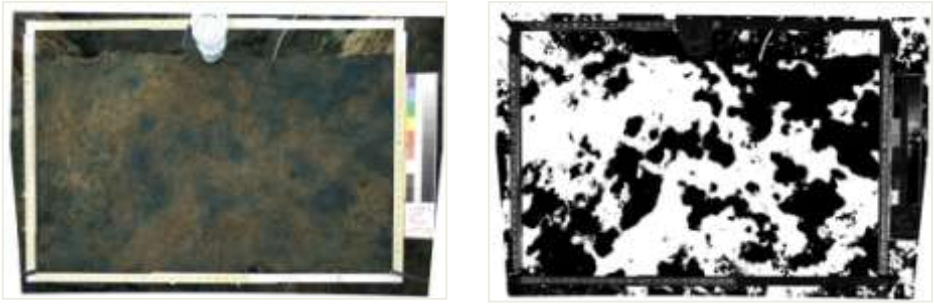

Figure 4.3-20 Site C, wet treatment. Horizontal excavation 1 cm - 9 cm depth. First column - excavation depth and % of dye stained soil. Second column- dye stained soil. Third column - binary image of dye staining.

11 cm depth

14% stained

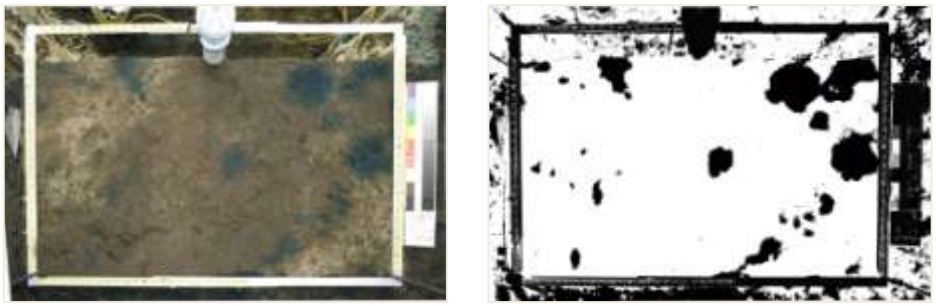

15 cm depth

7.2 % stained

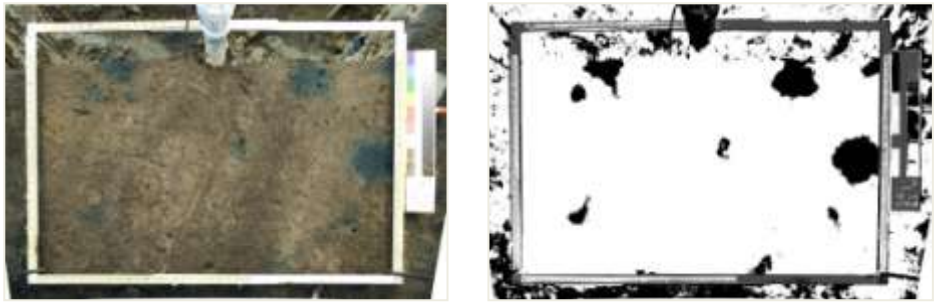

15-17 cm depth

A2 upper surface

3.2 % stained

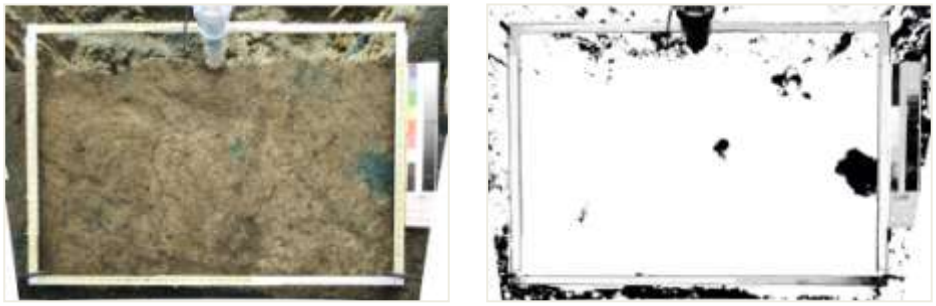

22-25 cm depth

0.02 % stained

Figure 4.3-21 Site C, wet treatment. Horizontal excavation 11 cm - 25 cm depth. First column - excavation depth and % of dye stained soil. Second column- dye stained soil. Third column - binary image of dye staining.

4.3.4 Dye tracer infiltration – site D

Dye staining analysis, site D– Dry treatment

Cultivation and cropping influenced infiltration in the A1 horizon at site D. Horizontal excavation between 2 cm and 7 cm depth demonstrated the dye tracer infiltrated along the line of weakness created by direct drilling wheat (*Triticum aestivum*) (Figure 4.3-24). Dye infiltration along drill lines may have been assisted by a reduction in surface crusts, and creation of voids along the rip lines. Water repellence of the surface soil may have also acted to funnel runoff into the line of weakness created by direct drilling. Vertical excavation displayed similar dye staining patterns to those observed at sites A and C (Figure 4.3-23). The depth of uniform dye staining or zone of distribution (Ritsema *et al.* 1993) was approximately 3 - 4 cm, below which, the wetting front broke down to form soil water fingers. Horizontal excavation at 11 -12 cm revealed 'spotty' dye patterns, which are usually typical of finger flow, however at site D, it is thought that these patterns may have resulted from funnelling of infiltration through the void spaces created by direct drilling and or root growth.

Both horizontal and vertical excavations found no evidence of dye accumulation on the surface of the B horizon. In the B21 horizon, the proportion of dye stained soil ranged from 3.3 % (vertical excavation, Figure 4.3-23) to 1.3 % (horizontal excavation 32 – 35 cm depth, Figure 4.3-25), which indicated that infiltration bypassed 97 % to 99 % of the soil matrix. Similar to sites A and C, vertical dye patterns in the B21 horizon consisted of thin rivulets with few large dye stained areas or dye staining in sand infills. Despite the presence of prior-crop roots throughout the B21, there was no association between roots and dye patterns in the B21 horizon. Dye staining was noted around old decaying roots below 65 cm depth, which presumably originated from the pre-clearing vegetation. Below approximately 40 cm depth, the presence of many small vertically oriented patches of dye staining suggest that flow through the B22 and B23 horizons was highly convoluted due to the subangular blocky structure at the site.

4.3.4.1 Dye staining analysis, site D– Wet treatment

In the wet treatment, the maximum depth of infiltration ranged from 14 cm (slice 5) to 24 cm (slice 3) (Figure 4.3-26). Horizontal excavation indicated that dye had infiltrated to approximately 30 cm depth (Figure 4.3-23) within a deep (52 cm) pocket of A2 horizon. 'True' fingers are not thought to have formed at site D, as dye staining at 11 - 13 cm and 15 - 17 cm depth, were not 'spotty' as observed at other sites (Figure 4.3-27). There was no evidence of dye accumulation on the surface of the B horizon in any of the vertical or horizontal excavations.

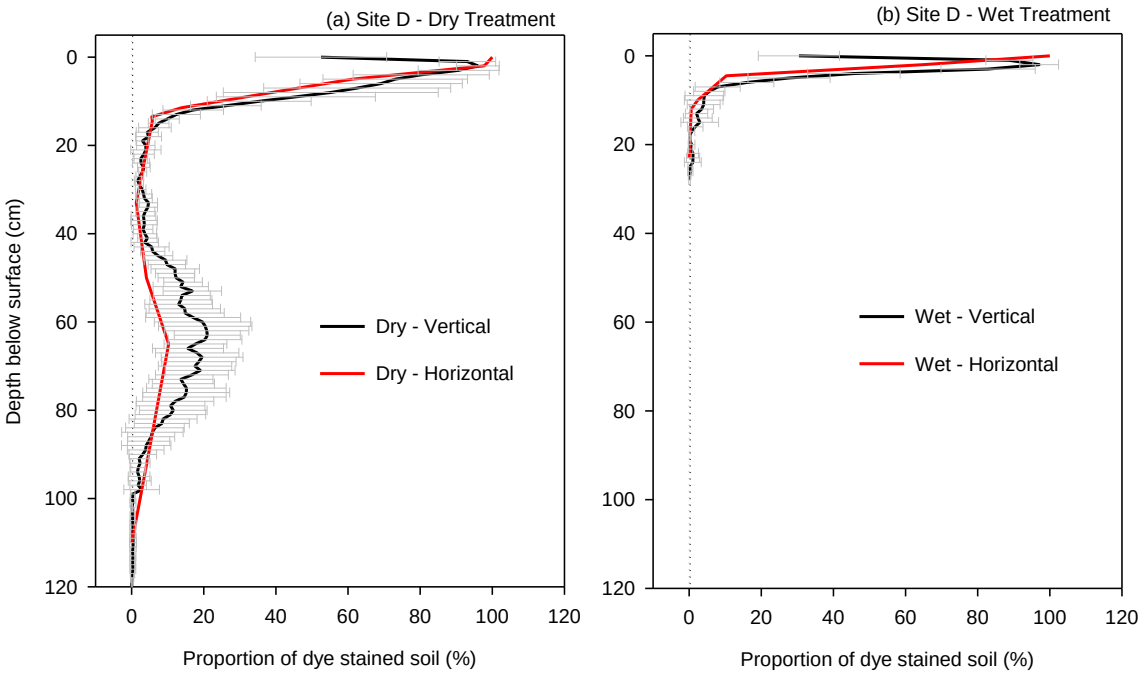

Figure 4.3-22 Site D, effect of antecedent soil moisture on the proportion of dye stained soil in both vertical excavations (1cm increments) and horizontal excavations (a) dry treatment, (b) wet treatment. Error bars represent ±1 SD for the vertical excavations.

4.3.4.2 Site D - Vertical excavation - Dry treatment

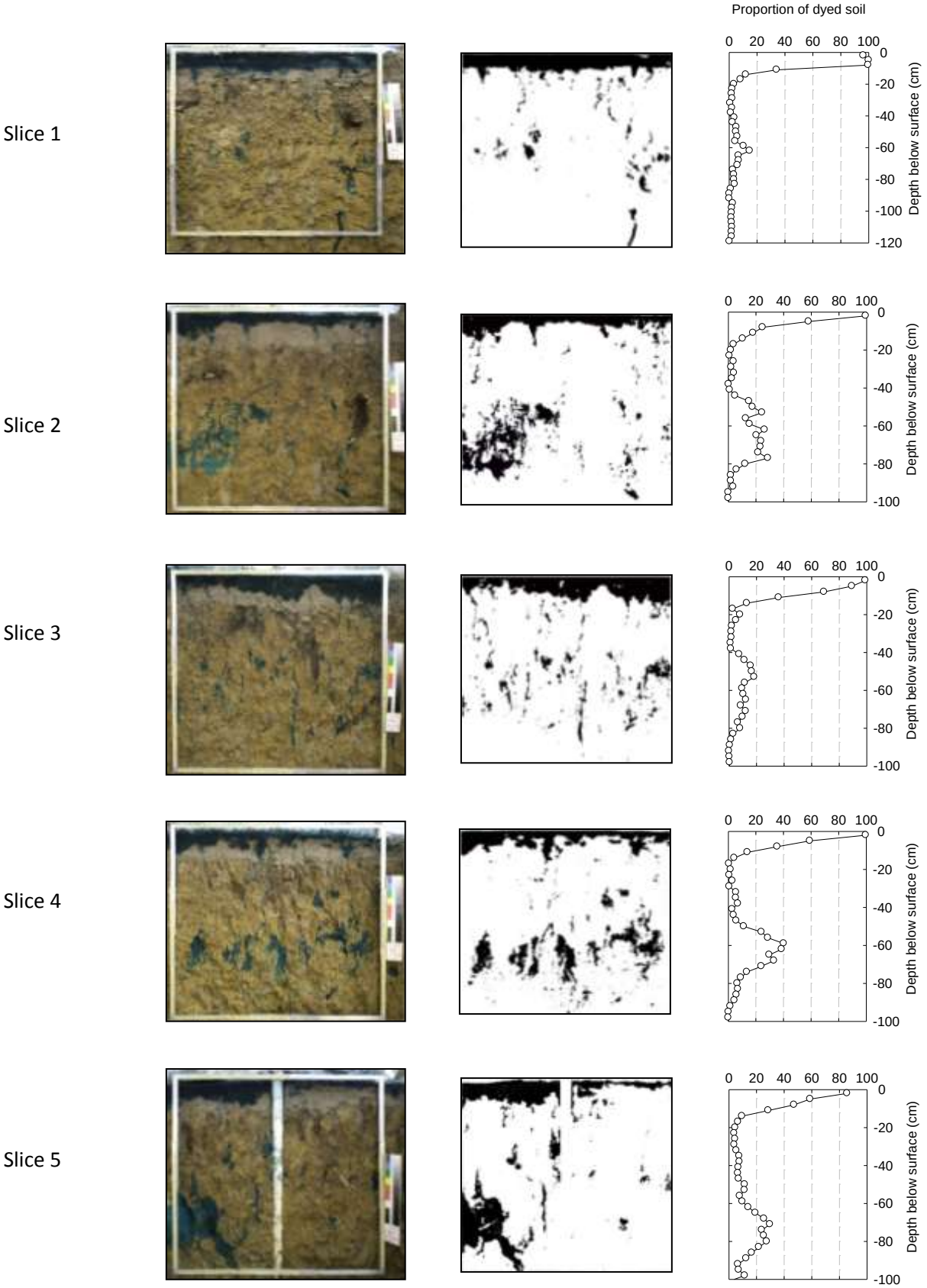

Figure 4.3-23 Site D, dry treatment, vertical excavation. First column – vertical excavation showing dye staining, digitally corrected for radial and keystone distortion. Second column - binary image of dye stained soil. Third column – proportion of dye stained soil with depth.

Site D - Horizontal excavation - Dry treatment

2 cm depth

97.8 % stained

5 cm depth

61 % stained

7-8 cm depth

43 % stained

11-12 cm depth

14 % stained

13 – 14 cm depth

5.6 % stained

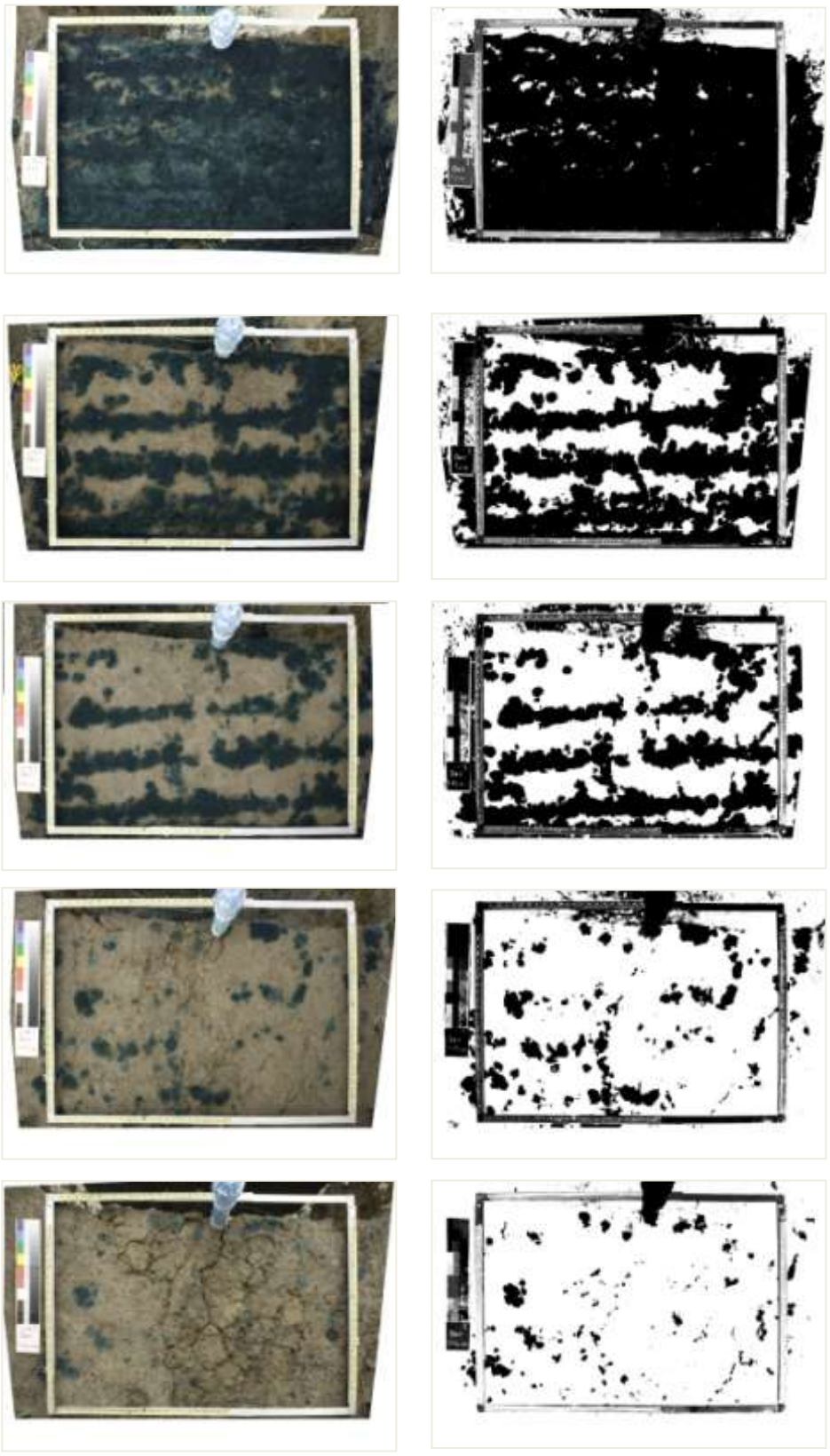

Figure 4.3-24 Site D, dry treatment. Horizontal excavation 2 cm - 14 cm depth. First column - excavation depth and % of dye stained soil. Second column- dye stained soil. Third column - binary image of dye staining.

14 -17 cm depth

5.8 % stained

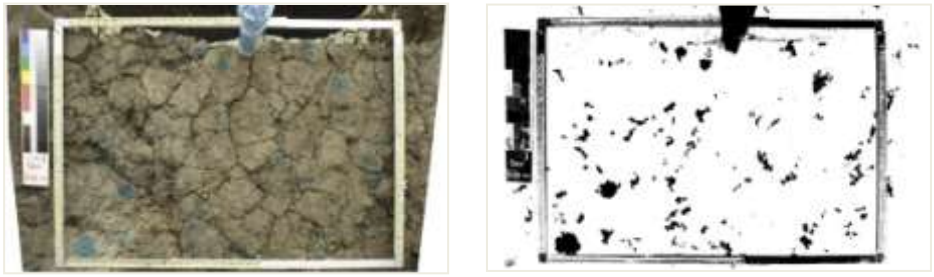

32 – 35 cm depth

1.3 % stained

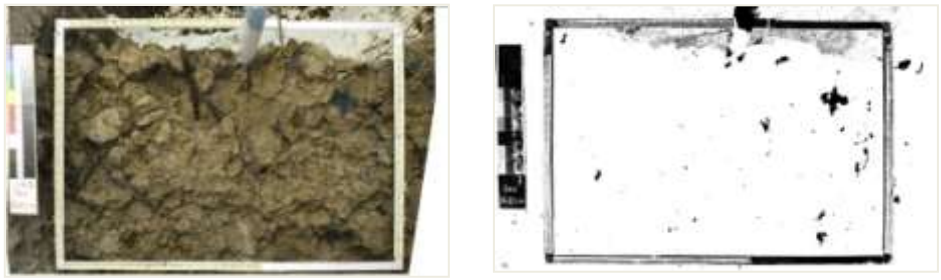

50 cm depth

4.1 % stained

65 cm depth

10.3 % stained

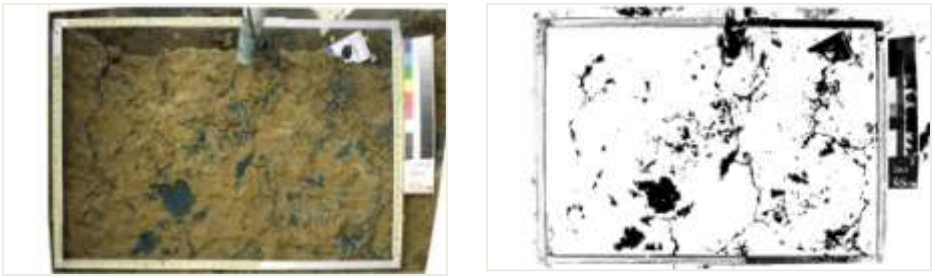

90 cm depth

4.7 % stained

110 cm depth

0.05 % stained

Figure 4.3-25 Site D, dry treatment. Horizontal excavation 14 cm - 110 cm depth. First column - excavation depth and % stained soil. Second column- dye stained soil. Third column - binary image of dye staining.

Site D - Vertical excavation - Wet treatment

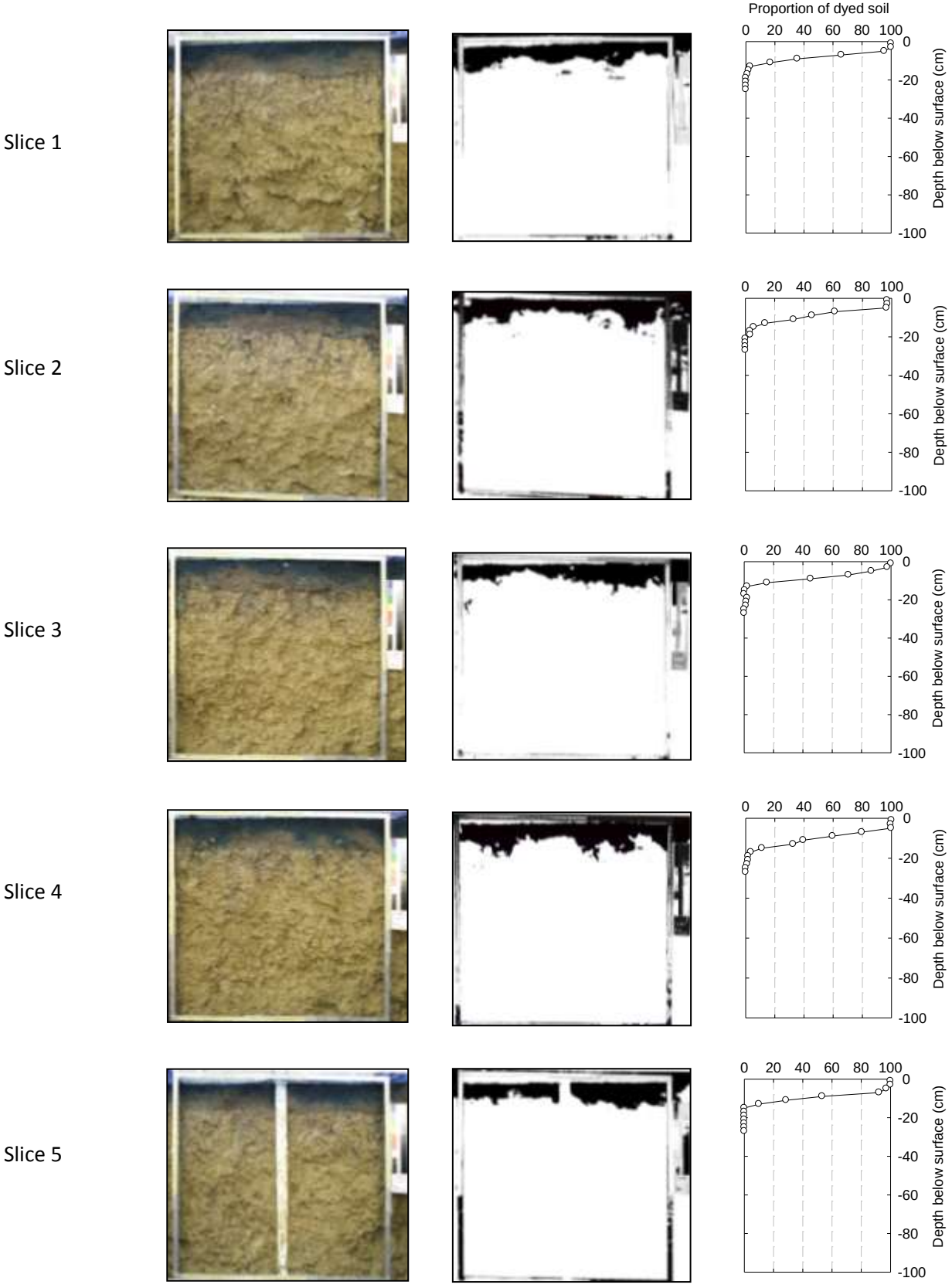

Figure 4.3-26 Site D, wet treatment, vertical excavation. First column – vertical excavation showing dye staining, digitally corrected for radial and keystone distortion. Second column - binary image of dye stained soil. Third column – proportion of dye stained soil with depth.

3-4 cm depth

99.2 % stained

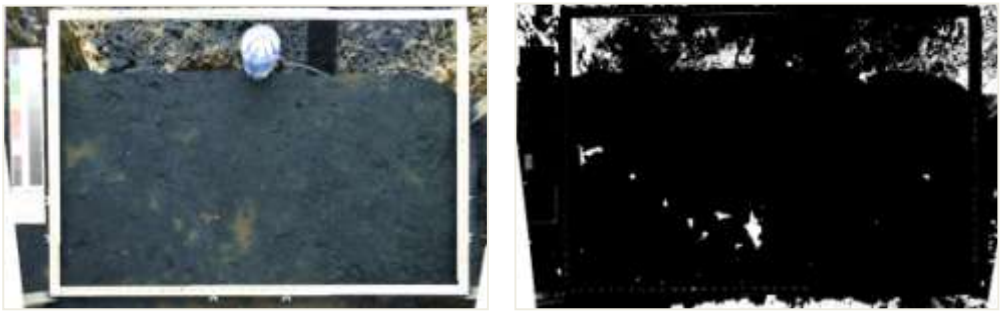

7-8 cm depth

92.9 % stained

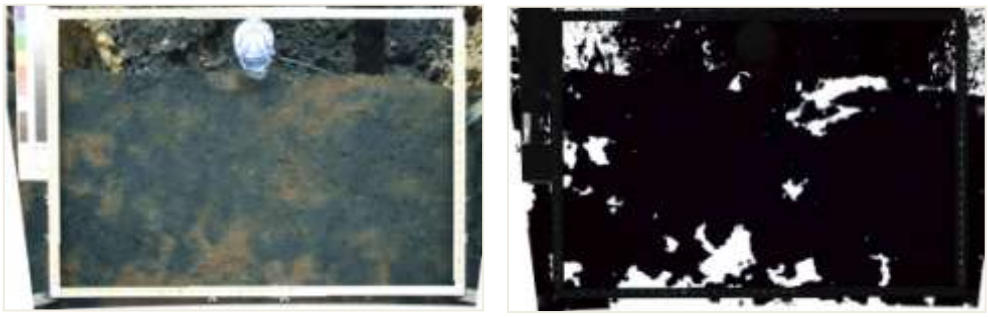

11-13 cm depth

49.3 % stained

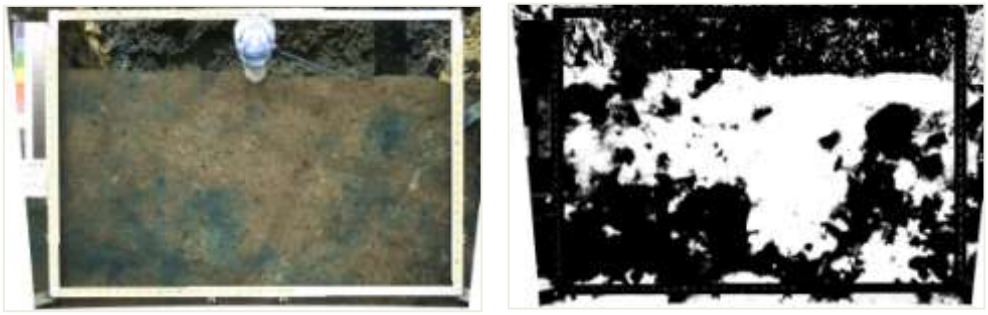

15–17 cm depth

18.1 % stained

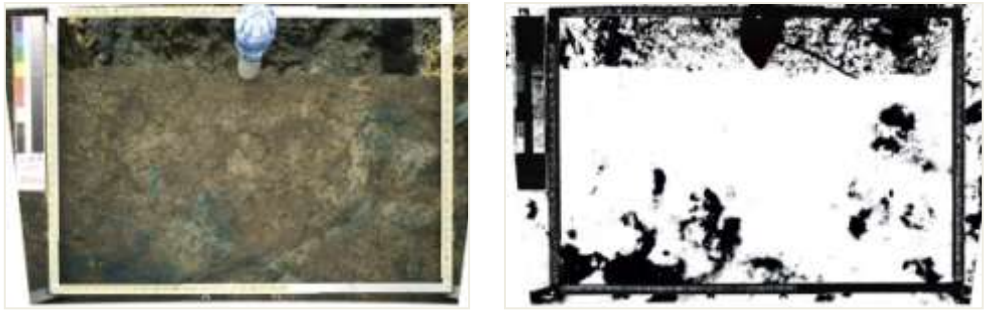

Figure 4.3-27 Site D, wet treatment. Horizontal excavation 3 cm - 17 cm depth. First column - excavation depth and % stained soil. Second column- dye stained soil. Third column - binary image of dye staining.

17 – 19 cm depth

5.8 % stained

30 cm depth

0.66 % stained

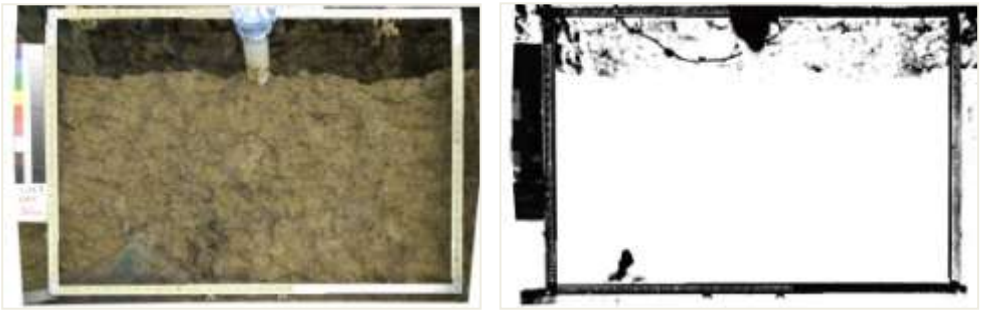

50 cm depth

0.002 % stained

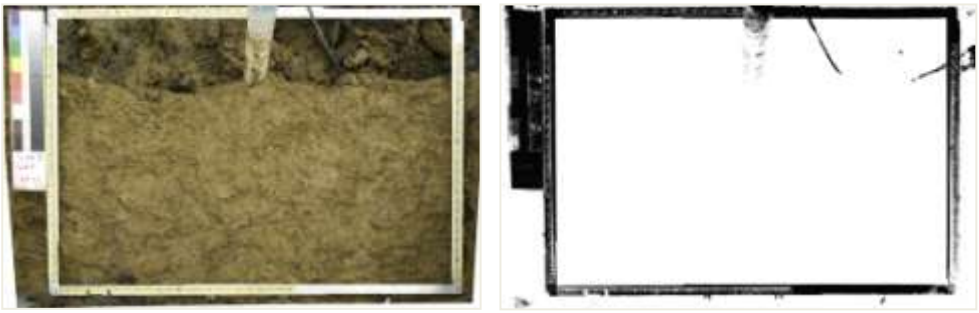

Figure 4.3-28 Site D, wet treatment. Horizontal excavation 17 cm - 50 cm depth. First column - excavation depth and % stained soil. Second column- dye stained soil. Third column - binary image of dye staining.

4.3.5 Comparison of dye distribution between sites

With the exception of flow within the A2 horizon and sand infills at site B, differences in particle size, soil morphology and chemical attributes between the four sites had little influence on the depth and proportion of dye stained soil (Figure 4.3-29). In the dry treatment, notable differences in the proportion of dye stained soil existed between sites. At site C at 10 - 20 cm depth, absence of dye staining in the lower A1 horizon resulted from excavation exposing few soil water fingers. At site B at 15-30 cm depth, the high proportion of dye stained soil resulted from flow through a large sand infill. The highest proportion of dye stained soil occurred between 63 cm (site B and D) and 70 cm at site C, and the maximum depth of dye staining ranged from 85 cm at site A, to 118 cm at site C (Figure 4.3-29). Differences in the maximum depth of dye staining in the dry treatment corresponded to predictions of seasonal leaching based on trend in depth of EC, pH and Cl^- which indicated site A had been subjected to less leaching, than site B (Chapter 3.3.4).

In the wet treatment, the maximum extent of dye infiltration (> 0.1 %) ranged from 24 cm (site D) to 39 cm (site B) (vertical excavations). Between 0 cm and 20 cm depth, the proportion of dye stained soil was lower at site A than the other sites (similar to the dry treatment) resulting from shallower breakdown of the wetting front. At sites B and C the dye tracer was able to infiltrate below 20 cm depth via sand infills.

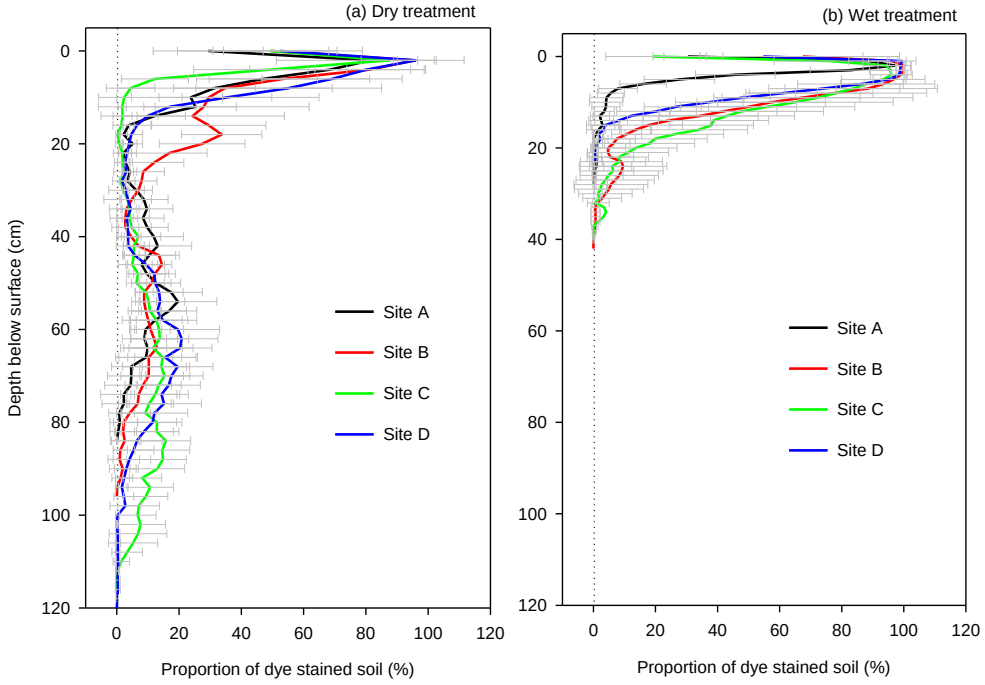

Figure 4.3-29 Effect of antecedent soil moisture on the proportion of dye stained soil with depth (a). Dry treatment (b) Wet treatment. Analysis conducted on 2cm interval, error bars represent ±1 SD.

Dry: 5cm depth: 7.1 % Stained

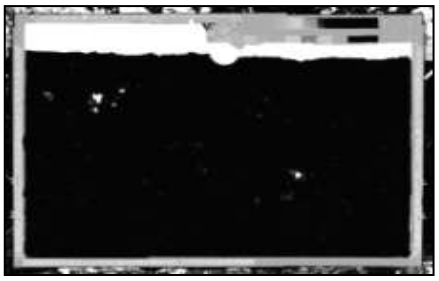

Wet: 5cm depth: 99.8 % Stained

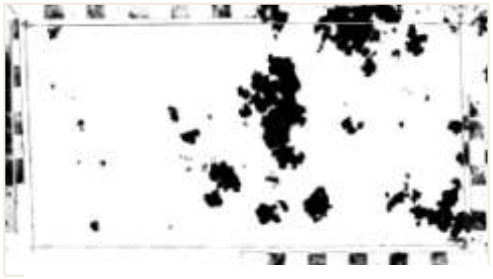

Dry: 10 cm depth: 11.4 % Stained

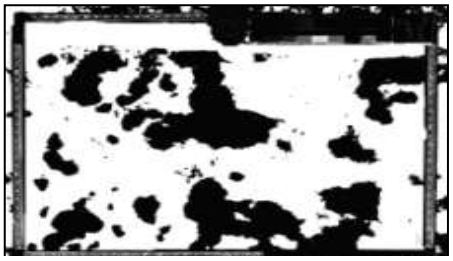

Wet: 10 cm depth: 34.1 % Stained

Figure 4.3-30 Site B, effect of antecedent soil moisture on the development of finger flow as indicated by reduced proportion of dye stained soil (horizontal excavations). Black areas represent dye tracer.

4.3.6 Interpretation of flow processes

4.3.6.1 Infiltration process in the A1 horizon

Within the A1 horizon, antecedent moisture influenced the depth of uniform flow, and proportion of soil participating in flow (Figure 4.3-29). The depth at which uniform flow (indicated by complete dye staining) broke into fingers (Figure 4.3-31) or permutations was deeper in the wet treatments than the dry treatments. Consequently a greater proportion of the A1 horizon participated in flow at high antecedent soil moisture than in the dry treatments. For example, site B - wet treatment, the proportion of dye stained soil at 5 cm depth was 99.8 % compared to 7.1 % in the dry treatment, (Figure 4.3-30). Dye patterns indicate the wetting front became unstable and irregular at both high and low antecedent soil moisture. The degree to which the wetting front broke down or developed perturbations in the wet treatment differed between sites. However at all sites, fingers were larger and more uniform in the wet treatment than the dry treatment. Ritsema *et al*. (1998b) also found that in comparison to drier sites, infiltration into 'wet' hydrophobic soils resulted in deeper infiltration, and deeper development of perturbed wetting fronts, which did not grow into 'true' fingers. Ritsema *et al.* (1998b) attribute the development of perturbations in wetting fronts to wetter places within the soil, leading to slightly deeper wetting fronts in some places than others. Wang *et al.* (2003) also demonstrated that the width of fingers in a Hele-Shaw tank ranged from 4.5 cm to 17 cm depending on antecedent soil moisture. Further investigation and discussion of the effects of hydrophobicity on the breakdown of wetting fronts and development of finger flow are presented in Chapter 7.

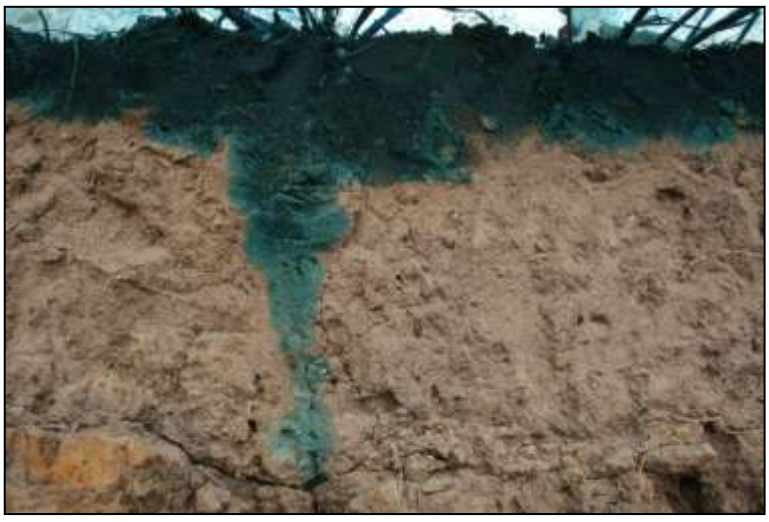

Figure 4.3-31 Example of fingering at site D.

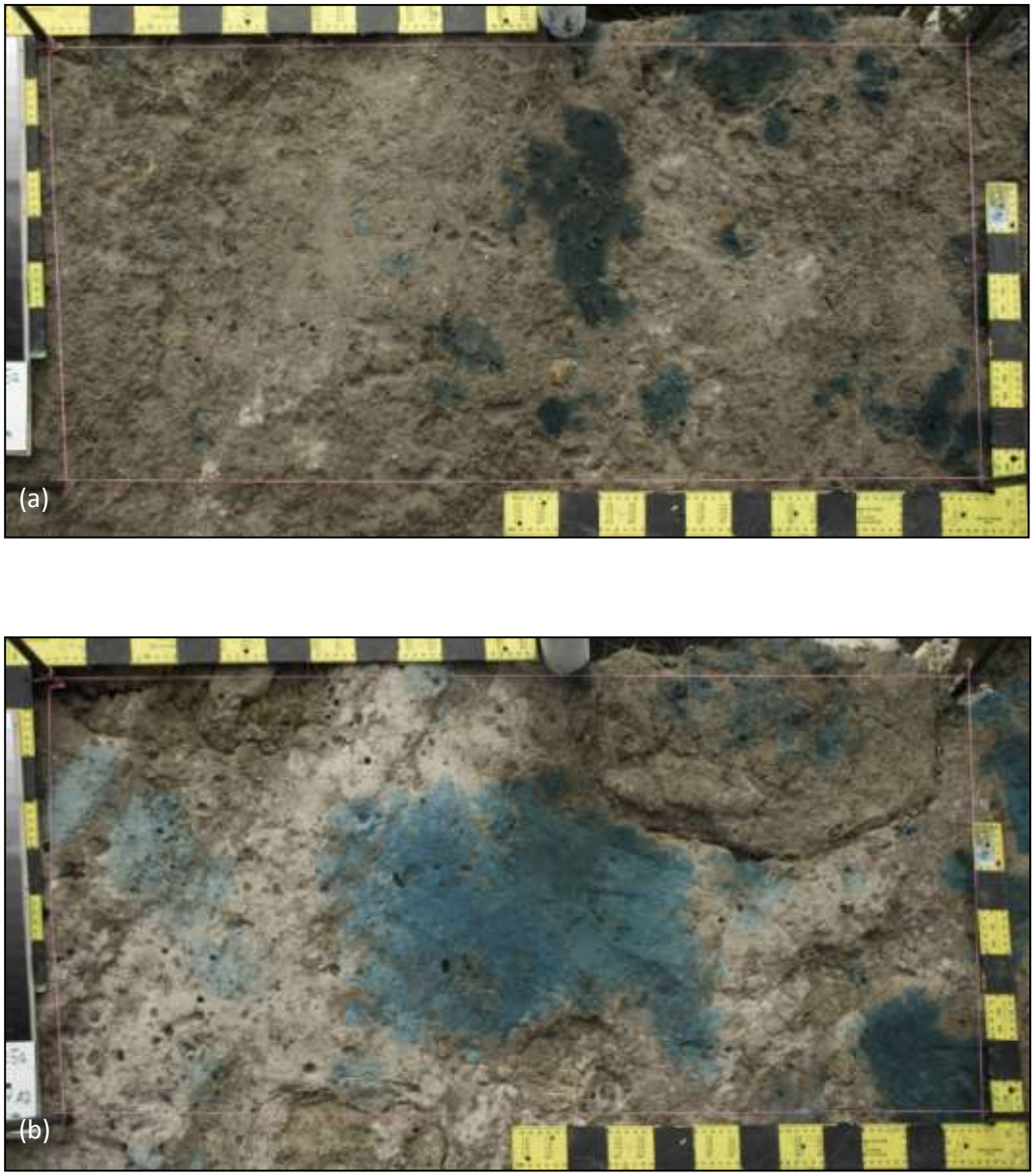

Figure 4.3-32 Lateral spreading of the dye tracer on the upper surface of the A2 horizon, site B, dry treatment. (a) 10 cm depth, lower A1 horizon - 11.4 % stained. (b) 30.6 % stained in the upper A2 horizon at 16 cm depth.

4.3.6.2 Infiltration processes in the A2 horizon and sand infills

A2 horizon development and presence of sand infills varied between sites, ranging from site D with effectively no A2 development or sand infills to site B in which the A2 horizon was approximately 7 - 10 cm thick and sand infills were up to 10 cm wide, and 70 cm deep (Chapter 3.3.3). At low antecedent soil moisture, infiltration and redistribution resulted from a combination of funnel flow and sorptive flow, without dye having entered the surrounding clay columns (Figure 4.3-33). The discontinuous nature of flow in the sand infills and A2 horizon (Figure 4.3-33 b), and colour gradients highlighted by manipulation of hue and saturation (Figure 4.3-34) suggest that flow within the A2 and sand infills was a result of capillary processes or 'sorptive' flow which diminished dye colour (concentration) away from the dye source. This diminishing of colour away from the source was not observed in any other soil horizon.

Horizontal excavation at site B revealed the proportion of dye stained soil increased from 11.4 % in the lower A1 horizon to 30.6 % in the upper A2 horizon (Figure 4.3-32). This suggests the A2 horizon impeded vertical infiltration of the dye tracer from the A1 horizon resulting in lateral spreading of the dye tracer across the upper surface of the A2 horizon. This finding is supported by soil morphology investigations which found the A2 and sand infills had few visible macropores and very few roots, compared to the A1 horizon which had many visible macropores and many fine roots (Chapter 3.3.3).

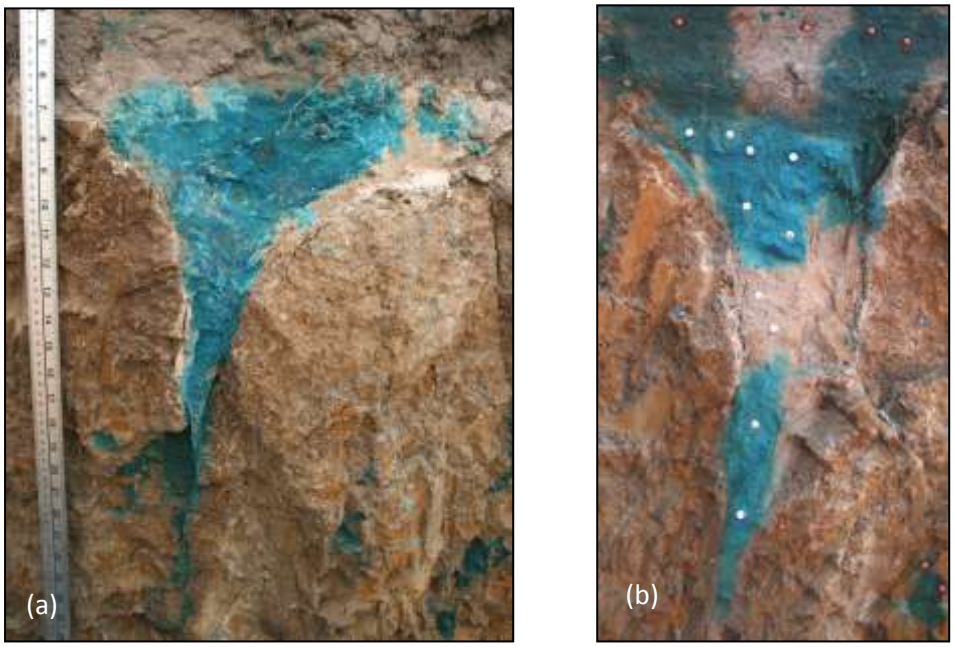

Figure 4.3-33 Funnel flow in the A2 horizon and sand infills, site B dry treatment, (a) continuous Funnel flow in sand infill, (b) Apparent discontinuous flow in sand infill.

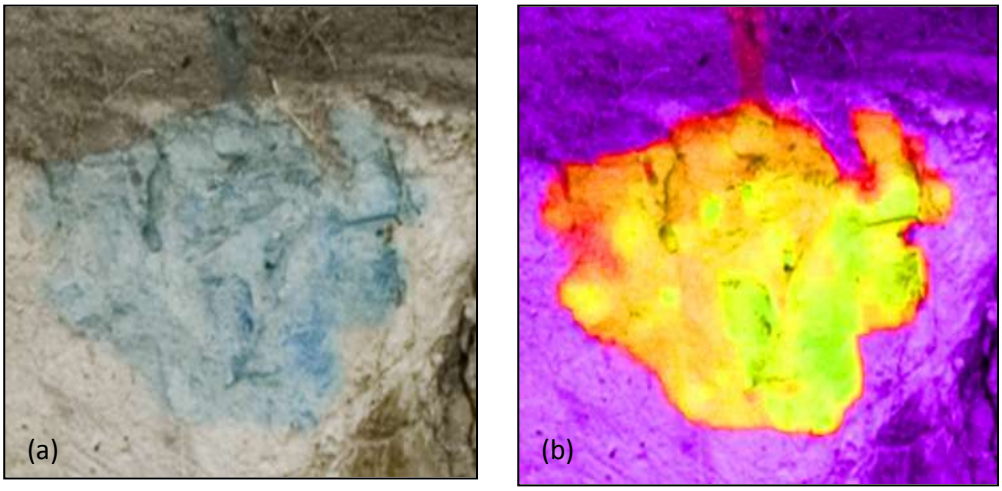

Figure 4.3-34 Effect of capillary or sorptive flow in the A2 horizon and sand infills demonstration diminished colour intensity away from the dye tracer origin (a) original image, (b) Hue and saturation aberration.

In the wet treatment (site B) the A2 did not appear to impede vertical infiltration of the dye tracer, The proportion of dye stained soil in the lower A1 horizon was higher (34.1 %) than the upper A2 horizon (11.9 %) (Figure 4.3-35). This suggests that either the hydraulic conductivity of the A2 horizon was similar to the A1 horizon in the wet treatment. During excavation and soil morphology investigations (Chapter 3.3.3) the A2 horizon was noted to be weakly cemented with very firm consistence when dry. However when moist, the cementation in the A2 was not apparent, consistence was loose, and the soil underwent a transition from plastic to liquid behaviour with minimal disturbance (discussed Chapter6.3.5). This change in the behaviour of the A2 horizon is thought to result from the precipitation of soluble amorphous silica within the micropores and mesopores of the A2 horizon during drying (Chartres *et al.* 1990; Norton 1994). The effect of antecedent soil moisture on the hydraulic conductivity of the A2 horizon has been investigated further in Chapter 6.3.5.

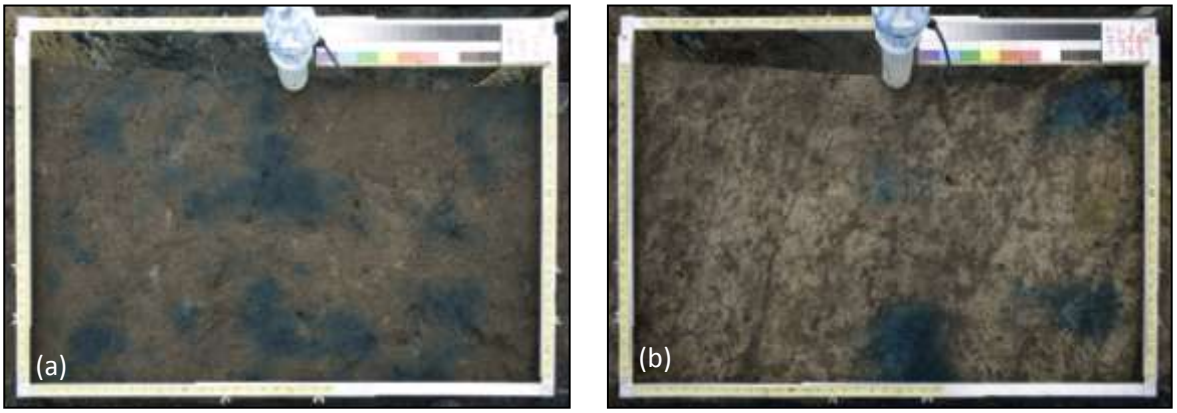

Figure 4.3-35 Lack of dye spreading on upper surface of A2 horizon in the wet treatment, site B. (a) 10-12 cm depth 34.1 % stained in the lower A1 horizon. (b) 15-18 cm depth, 11.9 % stained in the upper A2 horizon.

4.3.6.3 Infiltration process in the B21 horizon

Differences in subsoil structure resulted in minor differences in dye staining patterns and the proportion of dye stained soil in the B21 horizon. In the dry treatments, horizontal analysis revealed that infiltration through shrinkage cracks bypassed 98.7 % (sites B and D) to 99.6 % (site C) of the soil matrix (Figure 4.3-36 and Figure 4.3-37). Infiltration occurred as thin (2-3 mm wide) film flow or rivulets which flowed down the sides of the clay columns or walls of shrinkage cracks (Figure 4.3-39). Infiltration from the rivulets into the soil matrix was negligible.

Figure 4.3-36 Site A, dry treatment. Horizontal excavation revealed that bypass flow occurred in only 0.33 % of the B21 horizon.

Figure 4.3-37 Lack of dye staining in upper B21 and sand infills at site B- wet treatment 0.8 % dye stained.

Note closure of shrinkage cracks, and lack of dye staining in sand infills.

Not all shrinkage cracks participated in flow, only shrinkage cracks which were hydrologically connected to either the base of a finger or an area of dye ponding on the upper B horizon were able to participate in flow (Figure 4.3-38).

Similar film like flow has been described by Cresswell *et al.* (2008), Tokunaga and Wan (1997) and Cey and Rudolph (2009). Tokunaga and Wan (1997) found that film flow was an important mechanism contributing to fast flow in unsaturated fractures and macropores, especially in soils with low-permeability soil matrix such as the clay columns in vertic texture contrast soils. Flow through partly filled macropores or non-saturated flow in macropores invalidates the use of flow prediction models based on capillary tube models or the Laplace equation which assume that pores are completely filled with either air or water depending on soil water potential. These models typically under predict the contribution to flow from macropores, as flow in larger macropores is only invoked when they become completely water filled (Cey and Rudolph 2009). Infiltration of the dye tracer into the B21 horizon via macropores created by ants was also noted at site B and C, however this flow mechanism was relatively unimportant (Figure 4.3-40).

Figure 4.3-38 Site B, dry treatment. Presence of unstained shrinkage cracks (indicated by arrows) in the B21 horizon indicates that not all shrinkage cracks participated in flow.

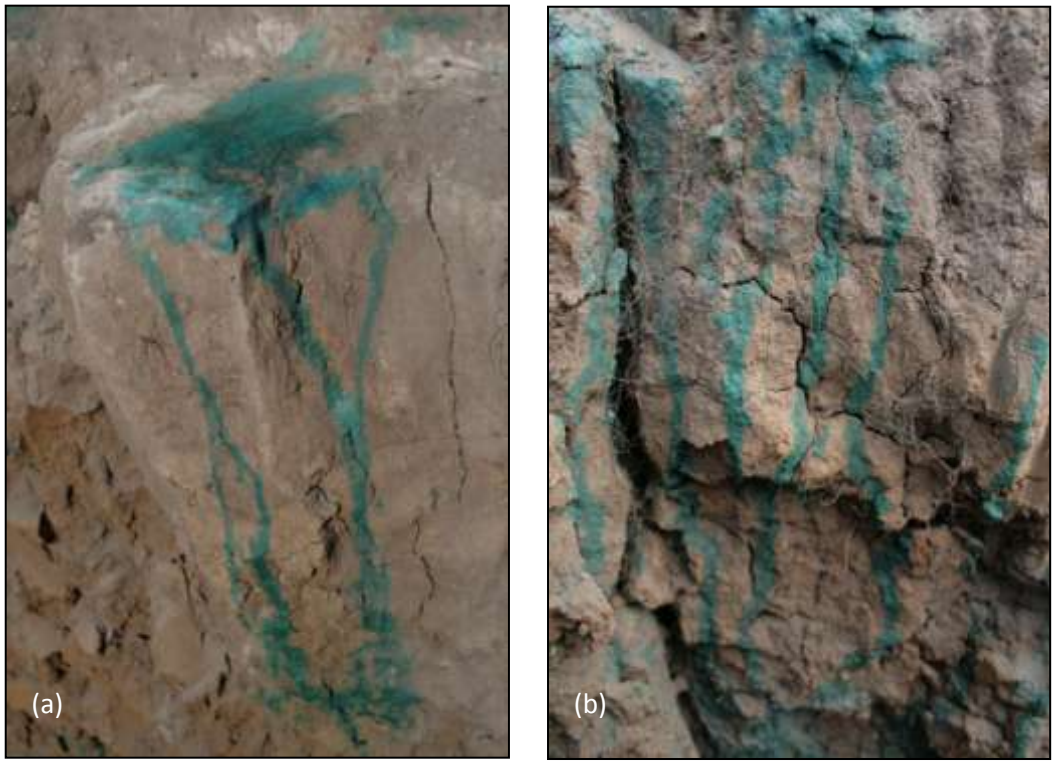

Figure 4.3-39 Site B, dry treatment. (a) Ponding on upper surface of clay column and rivulet flow down side of the column face. (b) Thin film flow or rivulet flow on the side of soil columns site A, dry treatment.

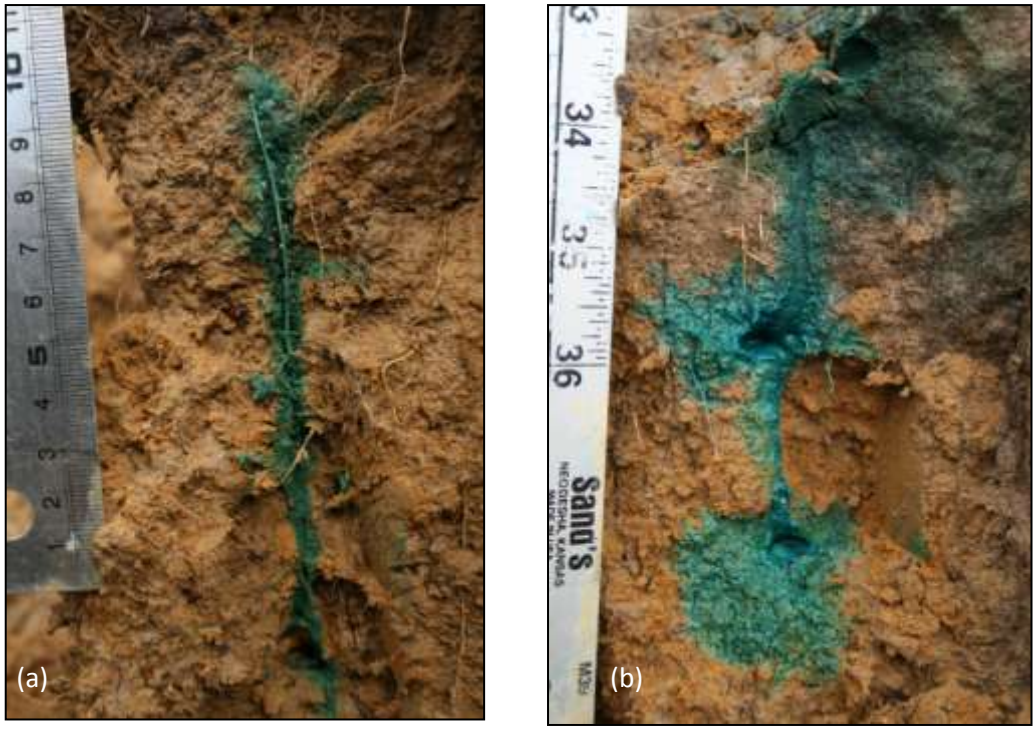

Figure 4.3-40 Infiltration into the B21 horizon via macropores created by ants:(a) site B, (B) site C. Note root growth through ant burrow.

4.3.6.4 Infiltration process in the in the B22 and B23 horizons

In dry antecedent conditions, flow in the B22 and B23 horizons principally resulted from rivulet flow or film flow accumulating in terminal shrinkage cracks, and backfilling void spaces, a process described as 'filling from the bottom up'. The extent and nature of dye staining patterns depended on the size, shape and orientation of the shrinkage cracks. At site B, the shrinkage cracks formed large vertical, continuous voids around the clay columns. Rivulet flow from the B21 horizon resulted in back filling of pore spaces, which resulted in large vertically oriented dye staining patterns (Figure 4.3-41) or lattice like horizontal patterns (Figure 4.3-42 b). In Figure 4.3-41 back filling of a large void by rivulet flow resulted in dye staining patterns with a horizontal upper surface representing the height to which the void had been filled when infiltration ceased. Internal catchment and backfilling of bypass flow in dead-end pores has been described by Bootlink and Bouma (1991) and Cey and Rudolph (2009), and conceptualized in the shrinkage crack infiltration model VIMAC (Greco 2002) and soil water model SWAP (van Dam *et al.* 2004).

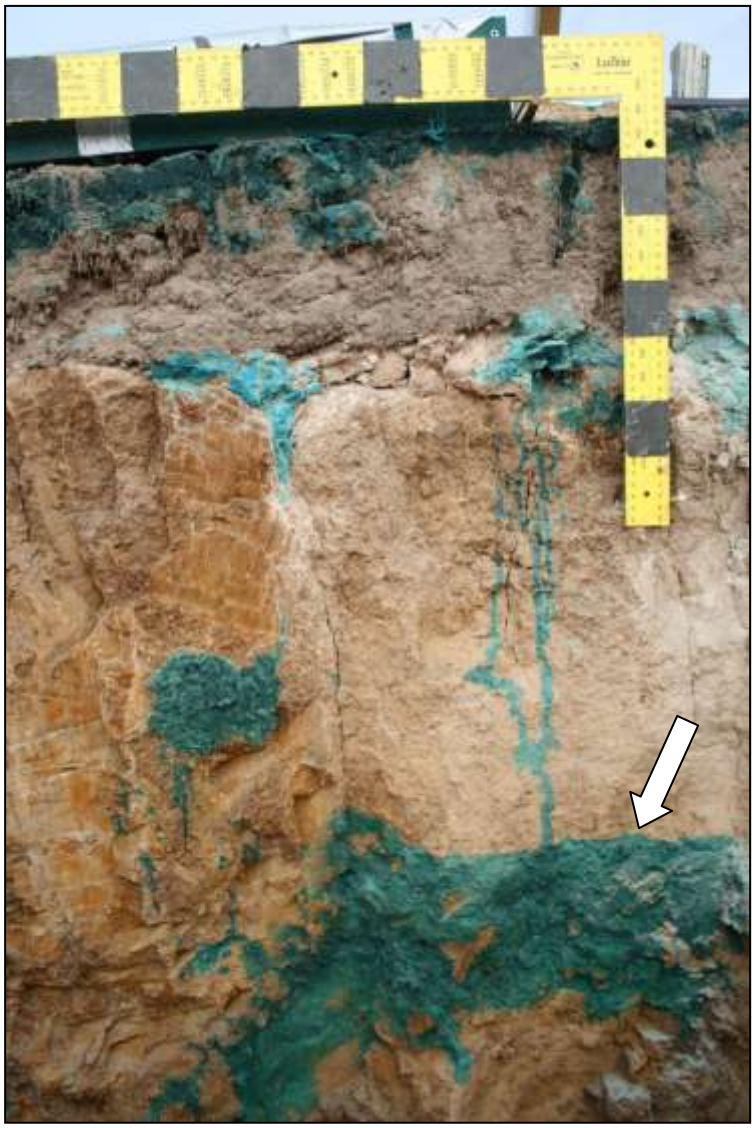

Figure 4.3-41 Preferential flow in the B2 horizon at low antecedent soil moisture content. Rivulets flow on the side of soil columns (within shrinkage cracks) terminated in the B22 horizon resulting in 'bottom-up' filling of the void space. Notice the upper surface of the large dye stained area is level with the horizon indicating the depth of filling.

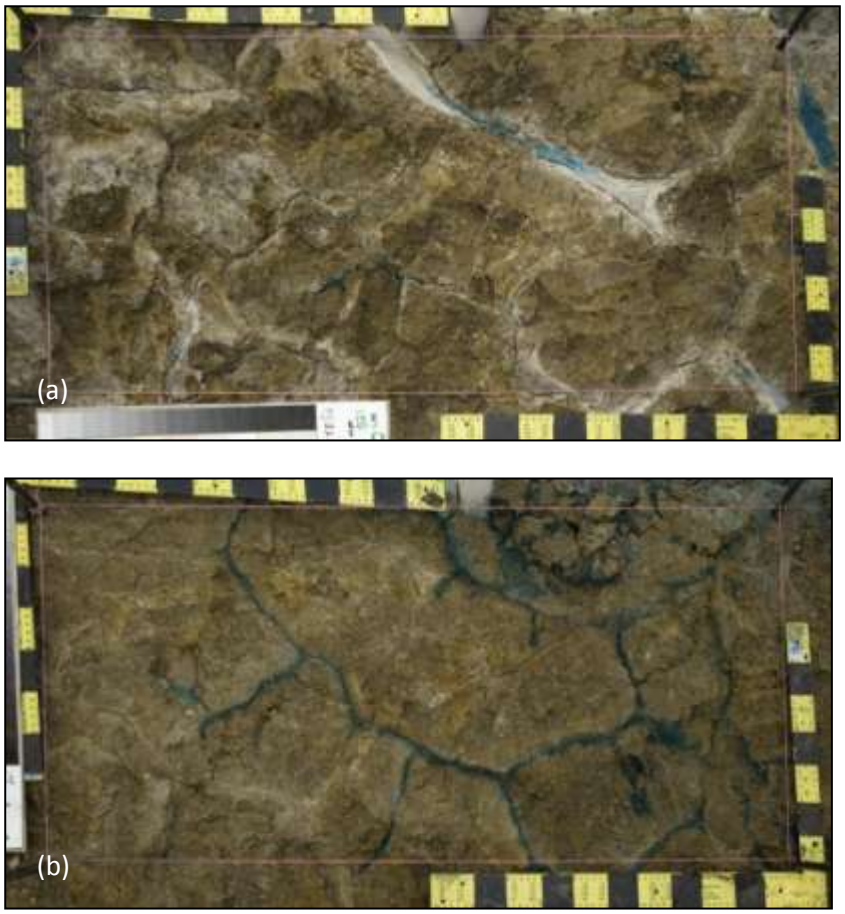

Figure 4.3-42 Horizontal excavation at site B, dry treatment. Change in dye staining pattern at (a) 30 cm depth – 1.6 % dye stained, to (b) 50 cm depth 6.9 % dye stained. Increased dye staining at 50 cm depth resulted from backfilling of void spaces around clay columns which did not extend to 30 cm depth.

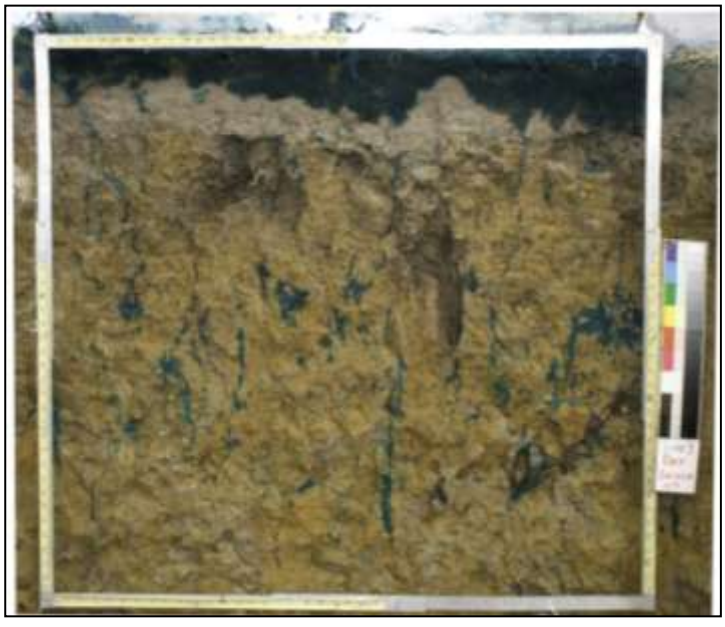

Figure 4.3-43 Vertical dye staining patterns at site D, dry treatment.

At sites A, C and D, dye staining patterns did not demonstrate the horizontal upper surface evident at site B. Rather dye staining in the B22 and B23 horizons appeared as irregularly shaped patches indicating that void spaces were smaller than at site B. The weaker sub-angular blocky structure at site D resulted in a larger number of considerably smaller dye stained patches (Figure 4.3-43) than those observed at the other sites. Horizontal excavation revealed the sub-angular blocky structure also resulted in horizontally oriented patches of dye stained soil where the dye tracer had infiltrated along horizontal cleavage plains (Figure 4.3-44) (also noted at site A).

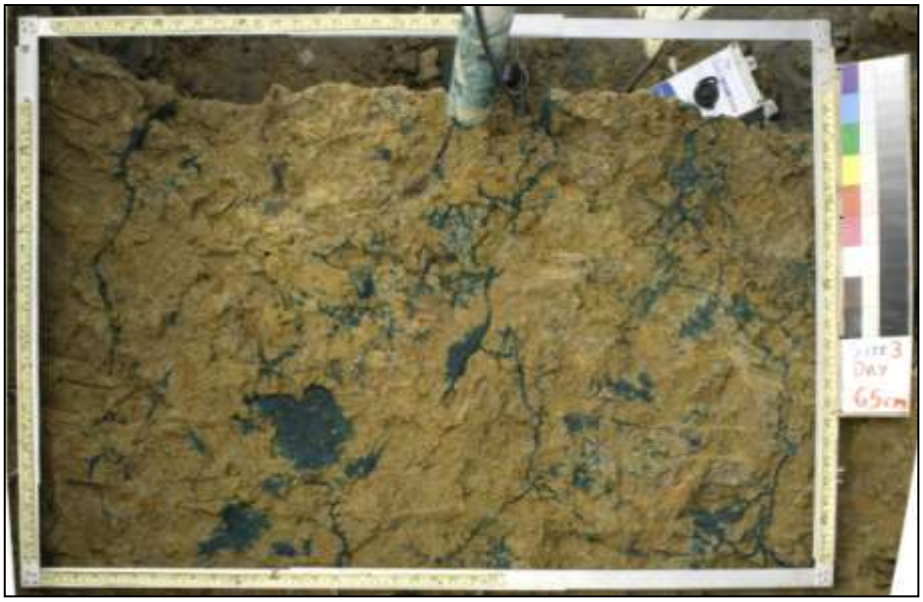

Figure 4.3-44 Horizontal dye staining patterns at site D (dry treatment) resulting from sub-angular blocky structure in the B horizon.

At site B and D, dye staining was observed within decomposing root channels at depths between 65 cm and 95 cm depth (Figure 4.3-45). Given the degree of decomposition, depth and absence of deep rooted vegetation post clearing and settlement, it is thought these roots result from the native vegetation (trees) prior to clearing. Due to their relative scarcity (2-3 roots in 4 sites), these decayed roots are not considered to be an important pathway for infiltration.

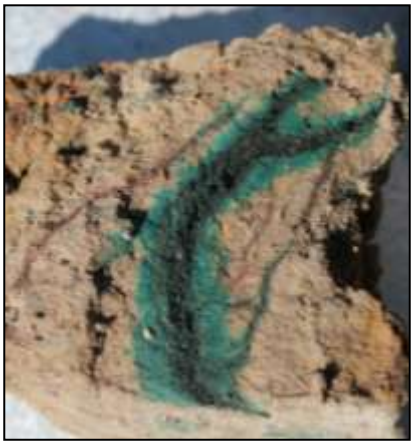

Figure 4.3-45 Dye staining along pre-clearing root holes, site B.

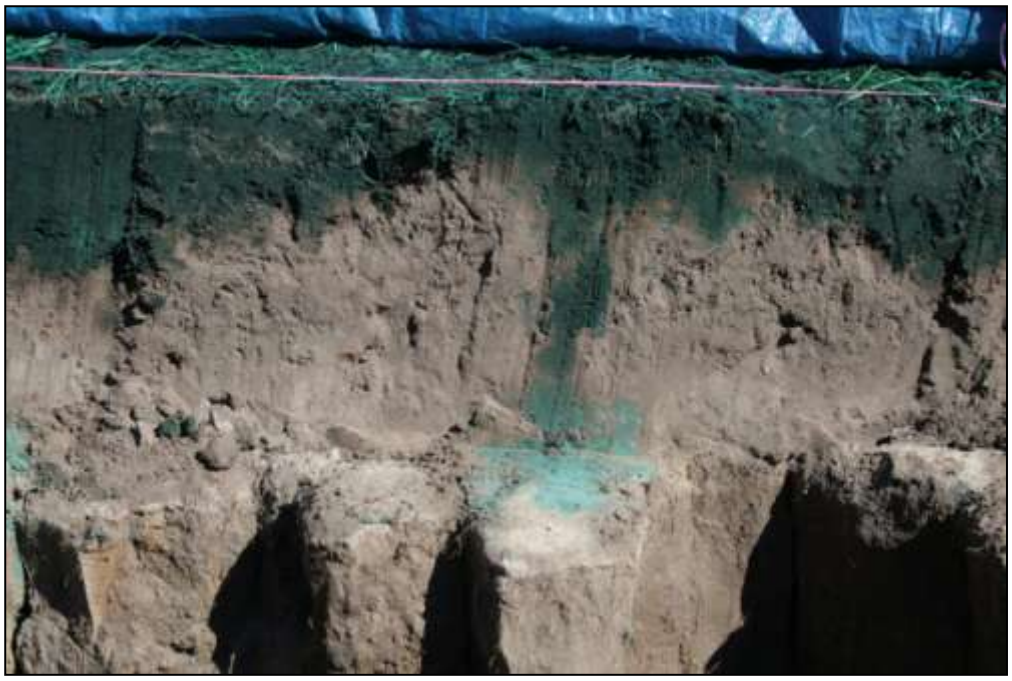

Figure 4.3-46 Site B, dry treatment. Finger flow leading to ponding and lateral flow on the upper surface of the B21 horizon.

Figure 4.3-47 Site D, dry treatment. No evidence of dye ponding or lateral flow between the A and B horizons.

4.3.6.5 Ponding and subsurface lateral flow at the A / B boundary

In the dry treatment, development of subsurface lateral flow was largely prevented by the abundance of intra-ped and inter-ped shrinkage cracks. These cracks allowed the dye tracer to spill down the sides of the clay columns or within the shrinkage cracks (Figure 4.3-39), rather than accumulate to any great extent on the upper surface of the B horizon. The extent of ponding and lateral flow varied between sites depending on the distance between cracks and sand infills. Spacing between shrinkage cracks in the upper B21 horizon ranged from approximately every 7 cm at site B (Figure 4.3-46) to 1 - 4 cm at site D (Figure 4.3-47). Lack of ponding and subsurface lateral flow due to the presence of subsoil shrinkage cracks and macropores has also been reported by Smettem *et al.* (1991) and Brower and Fitzpatrick (2002b) who found that preferential flow through shrinkage cracks and root holes, prevented the development of seasonal perched watertables and subsurface lateral flow in a series of texture-contrast soils.

In the wet treatment, the reduced hydraulic conductivity in the B2 horizons was expected to result in ponding and accumulation of the dye tracer at the A / B boundary as reported by studies such as Eastham *et al.* (2000), Cox and McFarlane (1995) and Whipkey and Kirkby (1978). However in the wet treatment, ponding and lateral flow did not occur at the A / B boundary. The absence of dye accumulation at the A / B horizon boundary was attributed to difficulty displacing existing soil water further down the soil profile. Prolonged wetting is thought to caused the clay subsoils to swell which reduced their hydraulic conductivity and impeded vertical infiltration of the dye tracer which then moving laterally through the A1 horizon rather than along the upper surface of the B21 horizon as reported by Cox and McFarlane (1995), Ticehurst (2004), and Ticehurst *et al.* (2007).

Evidence for lateral flow at high antecedent soil moisture did however exist, although not always at the A / B boundary. Evidence included;

(i) The trial application of 50 mm dye on moist soil at site A, in which the dye tracer moved at least 1.2 meters from the application area (Figure 4.3-48).

(ii) Infiltration from ponded rings at site B and C which demonstrated lateral dye movement through the A1 horizon in the wet treatments Appendix 4.3 (Figure A10.1-1).

(iii) Observation of subsurface lateral flow within the A1 horizon or at the boundary between the A1 and A2 boundary (Figure 4.4-1, Figure 4.3-50 and Figure 4.3-49) following establishment of the wet treatment for determination of hydraulic conductivity at site B.

Figure 4.3-48 Trial application of 50 mm dye tracer at site A, wet treatment, showing considerable lateral movement of the dye tracer above the B21 and A2 horizon.

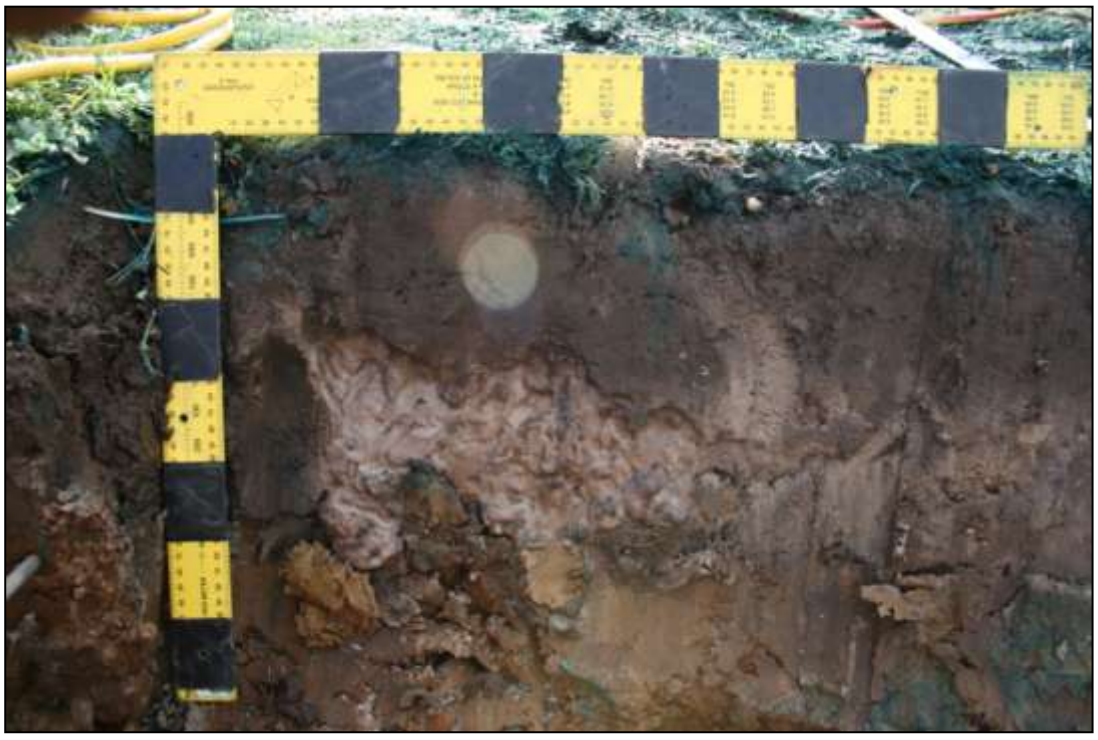

Figure 4.3-49 Site B, wet treatment. Saturation and lateral movement of the A2 horizon.

(iv) Lateral movement of the dye tracer through the mid A1 horizon from the bound area at site D. Note the area of dye staining to the right of the application area did not result from runoff, as the plot was installed 3 - 5 cm into the soil (Figure 4.4-2).

Subsurface lateral flow observed in Figure 4.4-1, 51, 52, 53 were partly induced by compaction resulting from walking around the site. Note that in Figure 4.3-50 subsurface flow resulted from saturation of the lower A1 horizon, which then spilled down onto the exposed B21 horizon. In Figure 4.3-49 the A2 horizon has started to flow (!) due to reduced consistence when saturated, and removal of confining pressure following excavation. Saturation of the lower A1 horizon and subsurface lateral flow were not observed at the other sites.

Figure 4.3-50 Saturation at the A1 / A2 boundary, site B wet treatment.

4.3.7 Effect of antecedent soil moisture on infiltration uniformity

Average infiltration uniformity over the whole soil profile (0 – 100 cm) varied significantly (p<0.05, df 37) from 55 % in the dry treatment to 70 % in the wet treatment. However antecedent soil moisture had no significant effect on infiltration uniformity in the effective root zone (0 - 30 cm), (Table 4.3-1 and Figure 4.3-51). This analysis indicates development of finger flow in the A1 horizon and bypass flow through shrinkage cracks in the B21 horizon prevented irrigation wetting up between 26.1 % to 38.0 % of the effective root zone (0 - 30 cm). Assuming similar response to rainfall or irrigation this degree of spatial variation in wetting patterns is expected to affect crop emergence, growth, and uniformity (Bauters *et al.* 2000b).

Table 4.3-1 Effect of antecedent soil moisture on infiltration uniformity

		Site A	Site B	Site C	Site D	Average all sites
Profile 0-100cm	Dry Treatment	63.17 (7.44)	59.04 (6.89)	44.01 (8.35)	55.57 (16.00)	55.45 (12.05)
	Wet Treatment	62.80 (3.43)	72.75 (3.13)	71.59 (6.50)	74.47 (2.71)	70.40 (6.03)
	Significance	ns 0.93	0.008	0.0001	ns 0.057	0.0003
Root Zone 0-30 cm	Dry Treatment	60.0 (4.1)	59.7 (7.90)	66.32 (7.10)	67.73 (11.2)	67.61 (8.41)
	Wet Treatment	59.81 (1.13)	76.72 (5.09)	72.18 (6.70)	74.85 (2.79)	70.89 (7.92)
	Significance	ns 0.075	0.009	ns 0.227	ns 0.248	ns 0.194

Brackets indicate ± standard deviation, ns = not significant. Significance at p<0.05

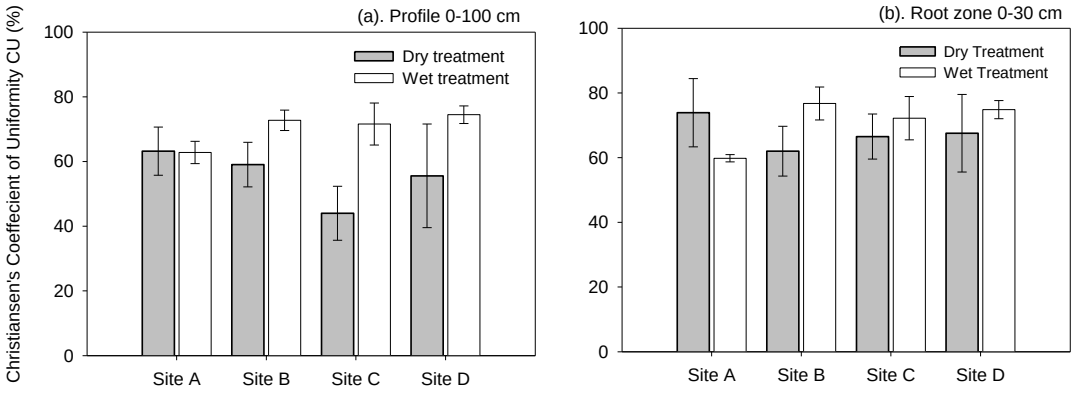

Figure 4.3-51 Effect of antecedent soil moisture on irrigation uniformity. (a) profile 0-100 cm, (b) root zone 0-30 cm.

4.4 Conclusion

Comparison between the four texture-contrast profiles demonstrated that the minor differences in soil morphology, subsoil structure, particle size, and soil chemistry between the four sites had little effect on the maximum depth or distribution of the dye tracer. Minor differences in the size, orientation and nature of dye stained soil occurred due to differences in subsoil structure and presence of sand infills. Dye staining supported field observations which indicated the A2 horizon impeded vertical infiltration when dry. However when near saturation, the A2 horizon had similar hydraulic properties to the A1 horizon and did not impede vertical infiltration.

Merdun (2008) claims researchers are in disagreement about the extent to which antecedent soil moisture influences preferential flow in soils, as higher rates of preferential flow have been reported in soil at low antecedent moisture resulting from hydrophobicity and desiccation cracks and high antecedent soil moisture due to reduced lateral losses into the soil matrix (Beven and Germann 1982; Merdun *et al.* 2008). Results presented in the Chapter 4.0 demonstrate that preferential flow was deeper and more extensive in dry soil than when soil was near field capacity.

At low antecedent soil moisture, a combination of preferential flow processes resulted in infiltration of the dye tracer to an average depth of 103 cm, while at high antecedent soil moisture the dye tracer infiltrated to an average depth of only 35 cm. These findings differ to those of Flury *et al.* (1994) who found there was no clear effect of the initial soil water content on the flow pattern and maximum penetration depth of the dye tracer, in fourteen field soils in Switzerland.

Development of preferential flow resulted in as much as 99.8 % of the soil matrix in the lower A1 horizon (site C) and 99.4 % of the B21 horizon (site A) being bypassed. At low antecedent soil moisture, preferential flow in the four texture contrast soil resulted from;

- Finger flow due to hydrophobicity in the A1 horizon.
- Funnel flow in the A2 horizon.
- Saturated ponding and lateral flow on the upper surface of the B21 horizon (< 10 cm long).
- Rivulet flow through either shrinkage cracks or down the sides of clay columns in the B21 and B22 horizons.
- Filling from the bottom up in the B22 horizon due to accumulation of dye tracer in terminal shrinkage cracks.
- Flow through cylindrical macropores created by plant roots, and burrowing fauna.

Figure 4.4-1 Site B, wet treatment. Subsurface lateral flow at A1 / A2 boundary. Flow may have been induced by compaction resulting from walking around the site.

Figure 4.4-2 Site D, wet treatment. Lateral movement of dye tracer through the A1 horizon resulting in the patch of dye stained soil to the right of the application area (white ring).

Development of perched watertables and subsurface lateral flows in texture contrast soils has been attributed to the texture and hydraulic conductivity discontinuity between the A and B horizons (Eastham *et al.* 2000). However in this study, perched watertables and subsurface lateral flow did not occur at low antecedent soil moisture due to the presence of abundant shrinkage cracks in the subsoil, and reduced hydraulic conductivity of the A2 horizon. At high antecedent soil moisture, clay swelling impeded vertical water movement through the B horizon and thus prevented displacement of existing soil water by the dye tracer. Addition of the dye tracer at application rates greater than the subsoil hydraulic conductivity resulted in saturation throughout the soil profile which resulted in the development lateral flow through the A1 horizon due to its greater porosity. Weiler and McDonnell (2004) explain in soils with a rapid decline in porosity with depth, the addition of only a small amount of new water may cause saturation above the impeding layer which results in development of rapid lateral flow at the permeability interface through the transient saturated zone or soil layer with greatest porosity. Thus saturation at the A / B horizon boundary resulted in the dye tracer moving laterally through the A1 horizon, rather than along the upper surface of the B horizon or within the A2 horizon as reported in the literature. Results demonstrated that saturation of the B2 horizons was required to induce lateral flow in the A1 horizons, as the presence of shrinkage cracks in the B21 horizon at low antecedent soil moisture, prevented ponding at the A / B horizon boundary.

The existence of preferential flow at low antecedent soil moisture invalidates the use of most Darcian or Richards equation based single pore domain soil water models, as these models are not able to simulate preferential flow processes (Simunek and van Genuchten 2007). This inability to simulate preferential flow is likely to result in underestimation of the risks posed by mobilisation of agrochemicals to shallow groundwater and waterways (Gerke 2006). At high antecedent soil moisture, inability to simulate the breakdown of the wetting front and development of flow perturbations may also limit use of Darcian based single pore domain models to simulate infiltration at high antecedent soil moisture.

Dye staining experiments in very dry and near field capacity soils have established that antecedent soil moisture had a substantial effect on the infiltration of an artificially applied dye tracer. Extrapolation of results from dye staining to rainfall events is however difficult as the soil moisture content, or soil moisture threshold at which infiltration switches from being predominantly preferential to being predominantly uniform or in equilibrium, was not able to be determined from the dye tracer experiments. The effect of antecedent soil moisture and preferential flow on rainfall effectiveness, hydraulic conductivity, velocity of the wetting front and irrigation efficiency will be investigated in the following chapters.

4.5 Key Points.

- At low antecedent soil moisture, preferential flow processes were the dominant form of water movement resulting in 99.7 % of the soil matrix being excluded from flow.
- Minor differences in soil morphology and chemistry between the three Kurosols and the single Sodosol site had little effect on the maximum depth or proportion of dye stained soil.
- Minor differences in dye staining patterns did however result from differences in subsoil structure and presence of sand infills.
- Antecedent soil moisture had a substantial effect on the distribution and maximum depth of the dye tracer.
- At low antecedent soil moisture preferential flow processes included; finger flow in the A1 horizon, funnel flow in the A2 horizon, thin film or rivulet flow in the upper B horizon, and backfilling of pores and cracks in the B horizon.
- At high antecedent soil moisture instability developed in the wetting front within the A1 horizon.
- In the subsoil, only shrinkage cracks which were hydrologically connected to soil water fingers or ponding on the upper surface of the B21 horizon participated in flow.
- At high antecedent soil moisture, lateral flow (as indicated by dye movement) appeared to occur through the A1 horizon rather than in the A2 horizon or on top of the B2 horizon.
- Lateral flow at high antecedent soil moisture is thought to have resulted from impeded vertical drainage through the B horizon due to clay swelling which prevented the dye tracer from vertically displacing old water from the lower A1 and A2 horizons.
- At low antecedent soil moisture dye staining indicated vertical flow in the A2 horizon was impeded when compared to the A1 and B21 horizons.
- At high antecedent soil moisture dye staining indicated the A2 horizon had similar hydraulic properties to that of A1 horizon.
- Results imply higher than expected risk of agrochemical contamination of shallow groundwater when soils are dry.

5.0 Soil Moisture Monitoring

5.1 Introduction

Dye staining experiments in Chapter 4.0 demonstrated that at low antecedent soil moisture, infiltration and soil moisture redistribution were dominated by preferential flow. Whilst at high antecedent soil moisture, infiltration and soil water redistribution resulted from uniform flow or equilibrium flow processes in which flow instability developed due to difficulty displacing existing soil water further down the soil profile. Dye staining experiments were not able to determine: (i) the effect of antecedent soil moisture on the rate of infiltration; (ii) the moisture content at which infiltration switch from being predominantly preferential to uniform; (iii) the change in soil moisture resulting from preferential flow; (iv) or the relative influence of rainfall intensity, rainfall amount and antecedent soil moisture on the occurrence of preferential flow.

In this chapter, high temporal frequency soil moisture monitoring will be used to determine;

I. The capacity of continuously logging soil moisture sensors to infer the presence of preferential flow,
II. The relative influence of rainfall attributes (i.e. magnitude and intensity) and antecedent soil moisture on the occurrence of preferential flow,
III. The effect of preferential flow and antecedent soil moisture on wetting fronts velocity during infiltration of dye tracer.

5.2 Methodology

5.2.1 Soil moisture monitoring

High temporal frequency soil moisture monitoring has been used to infer the presence of preferential flow and calculate the wetting front velocity following rainfall or irrigation (Blume *et al.* 2009; Hincapié and Germann 2009; Lin and Zhou 2008; Sanghyun *et al.* 2007). Allaire *et al.* (2009) however cites a number of difficulties with the use of soil moisture monitoring techniques for inferring the occurrence of preferential flow. These difficulties result from the small scale of measurement associated with most soil moisture sensors, and the inability of soil moisture monitoring techniques to distinguish between different types of preferential flow. It is postulated that the ability to relate changes in soil moisture determined from soil moisture sensors to larger scales may be inferred from binary images of infiltration pathways and determination of the Representative Elementary Volume (REV) (Bear 1972) of the infiltration pathways.

Soil moisture was monitored using a continuously logging capacitance probe (EnviroSCAN Solo - Sentek Environmental Technologies, Kent Town, South Australia). The EnviroSCAN probe consisted of a string of six to seven sensors which read a scaled frequency (S_F) at an operating frequency from 105 - 133 MHz, in which S_F values range from 0.35 in dry soil, to 0.95 in saturated soil (Evett *et al.* 2006). S_F readings were converted to volumetric soil moisture using a universal calibration equation. The EnviroSCAN probe was mounted inside a 56 mm diameter PVC plastic access tube. Access tubes were installed by ramming the tube 10 - 20 cm into the soil, then removing soil from within the tube by hand auger, before ramming the tube a further 10 - 20 cm into the soil. This procedure minimised the possibility of gaps developing between the soil and the access tube (Sentek 2003).

5.2.1.1 Dye infiltration experiments

Blume *et al.* (2009) and Weiler and Naef (2003) demonstrated that simultaneous use of dye tracers and high temporal resolution soil moisture measurements could be used to better understand preferential flow in complex soils. During the dye staining experiments the EnviroSCAN soil moisture probes were installed at sites B and D in the dry treatment, and all sites in the wet treatment. Soil moisture was recorded at 1 minute intervals, at depths of 10 cm, 20 cm, 30 cm, 40 cm, 50 cm, 70 cm, 90 cm and 110 cm following application of the dye tracer. Dye staining demonstrated that access tube installation did not cause water to flow preferentially along the sides of the access tube.

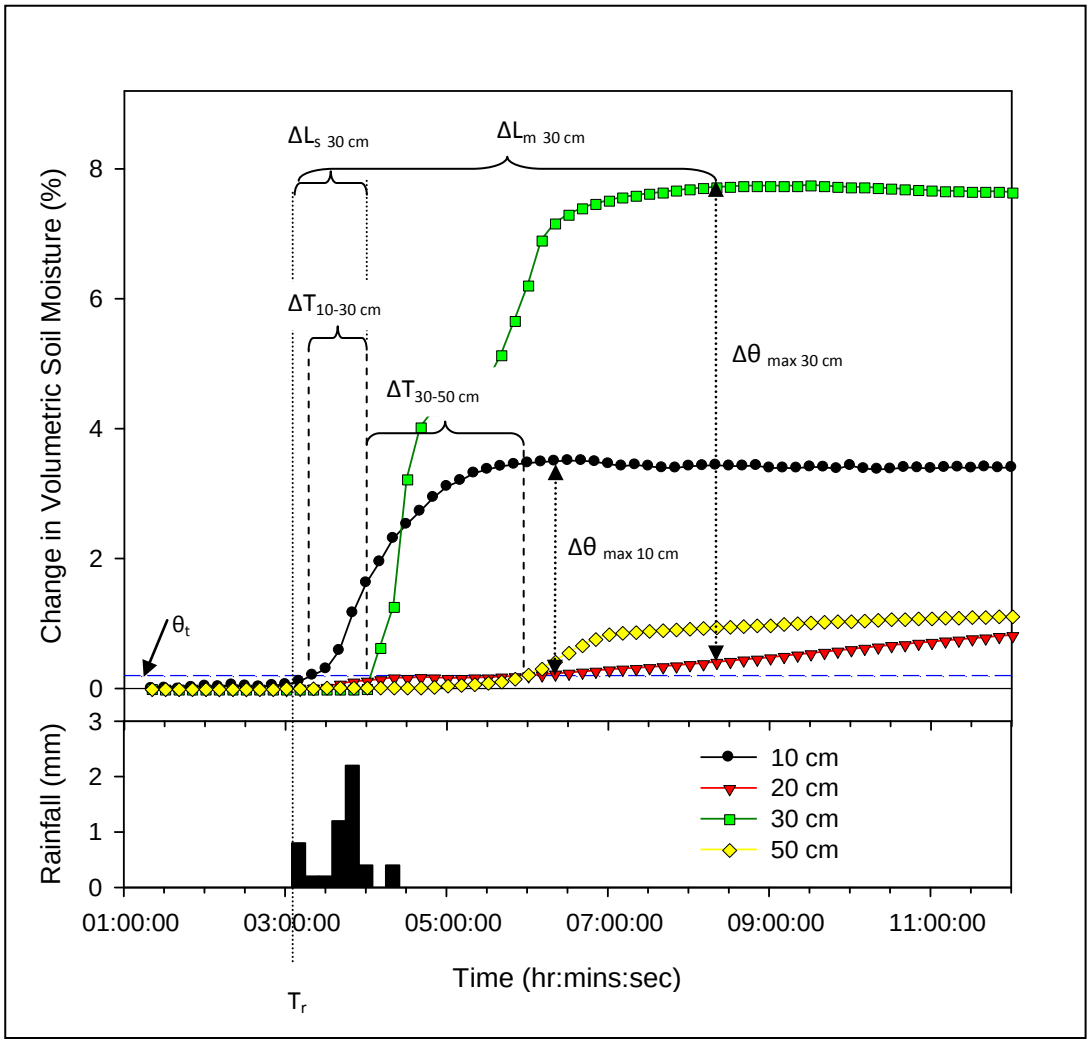

Figure 5.2-1 Example of how amplitude, lag time and velocity of the wetting front were determined from soil moisture monitoring data. Where;

T_r = Start of rainfall (rainfall >1.0 mm).

θ_t = Initial response threshold, change in soil moisture $\Delta\theta > 0.002$ m^3 m^{-3}.

$\Delta\theta_{\text{max 10 cm}}$ = Maximum amplitude for the sensor at 10 cm depth.

$\Delta T_{\text{10-30 cm}}$ = Time between initial response from sensors at 10 cm and 30 cm depth.

$\Delta L_{s\ \text{30 cm}}$ = Lag time between start of rainfall (T_r) and initial response ($> \theta_t$) for the 30 cm sensor.

$\Delta L_{m\ \text{30 cm}}$ = Lag time between start of rainfall (T_r) and maximum amplitude ($\theta_{\text{max 30 cm}}$) for the 30 cm sensor.

5.2.1.2 Rainfall events from September 2007 to July 2009, Site B

The effect of rainfall on soil moisture was monitored adjacent site B, at 10 cm, 20 cm, 30 cm, 50 cm, 70 cm, 90 cm and 130 cm depth. Logging was conducted at 60 minute intervals between 19/9/07 and 30/5/08, and 1 to 10 minute intervals between 26/6/08 and 10/7/09. Shorter time intervals were invoked to improve understanding of infiltration events into dry soils.

5.2.1.3 Estimation of soil moisture response threshold

Response to rainfall was said to have occurred when each of the soil moisture sensors had exceeded a threshold greater than the level of instrument noise. In separate studies, Blume *et al.* (2009), Lin and Zhou (2008) and Germann and Hensel (2006) determined the threshold change in soil moisture required to exceed instrument noise was 0.002 m^3m^{-3} from a range of soil moisture sensors with accuracies ranging from ±0.01 to 0.04 m^3m^{-3}. Consequently the same 0.002 m^3m^{-3} threshold was applied to the EnviroSCAN soil moisture sensors, with reported accuracies ranging from 0.009 m^3m^{-3} to 0.026 m^3m^{-3} in field soils (Paltineanu and Starr 1997), and 0.018 to 0.025 m^3m^{-3} in repacked soil (Evett *et al.* 2006). In this study, changes in soil moisture less than 0.002 m^3m^{-3} were attributed to instrument noise.

5.2.1.4 Determination of amplitude (Δθ) and lag time (ΔL) between soil moisture response

Amplitude or the change in soil moisture was determined from the maximum soil moisture (θ_{max}) minus the soil moisture threshold (θ_t) 0.002 m^3m^{-3}. Lag time to the initial soil moisture response (ΔL_s) was determined as the time between the commencement of rainfall (T_r) and the time at which the soil moisture threshold (θ_t) 0.002 m^3m^{-3} was first exceeded, i.e. for the sensor at 30 cm depth, $\Delta L_{s\ 30\ cm}$, Figure 5.2-1. Lag time to the maximum amplitude (ΔL_m) was determined as the time between the commencement of rainfall (T_r) and the time at which the maximum amplitude (θ_{max}) occurred, i.e. for the sensor at 30 cm depth, $\Delta L_{m\ 30\ cm}$,Figure 5.2-1.

5.2.1.5 Velocity of the wetting front

The velocity of the wetting front was estimated following the approach by Germann and Hensel (2006) in which the distance between sensors was divided by the time required for sensors located sequentially down the soil profile to exceed the instrument noise threshold, >0.002 m^3m^{-3}, i.e. $\Delta T_{10\text{-}30\ cm}$, Figure 5.2-1.

Figure 5.2-2 Long term soil moisture monitoring site, adjacent site B.

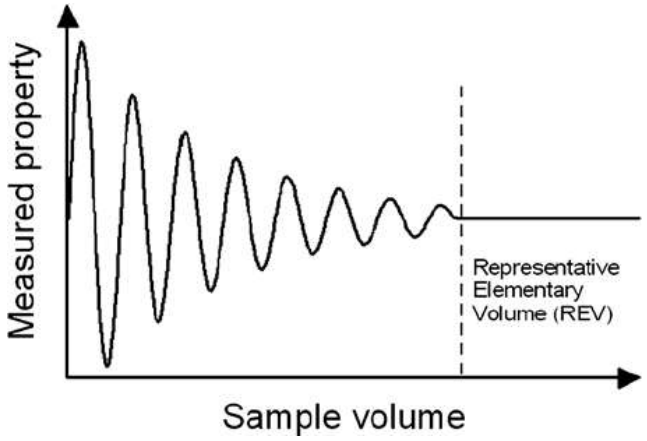

Figure 5.2-3 Schematic representation of how a measured property varies with sample volume until the Representative Elementary Volume (REV) is approached (Nordahl and Ringrose 2008).

Consequently this measure of flow rate or wetting front velocity is not equivalent to hydraulic conductivity as only a small portion of the soil participated in flow. The estimated velocity of the wetting front represents the fastest measureable component of flow within a portion of the soil that occurs within the sphere of influence of the soil moisture sensors, rather than the average flow rate through a known volume of soil.

5.2.2 Determination of representative elementary volume (REV) and area (REA)

Due to limited resources, only one EnviroSCAN probe was able to be dedicated to long term soil moisture monitoring. The extent to which results from a single probe can be related to a field site or similar soils is dependent on the sample volume of the sensors relative to the scale at which soil moisture varies in the field. In order that measured properties are not affected by localised spatial variations in soil properties, soil attributes should be measured at sample volumes greater than the representative elementary volume (REV) of the soil (Bear 1972). At the REV, fluctuations in the measured property are minimised and a representative amount of heterogeneity can be confidently averaged (Nordahl and Ringrose 2008), as presented in Figure 5.2-3.

Determination of REV in soil is difficult as scales of variability differ between different soil attributes. For example hydraulic conductivity can range over three orders of magnitude over short distances (Davis *et al.* 1999), while attributes like clay content usually vary by less than a few percent over the same distance. REV therefore needs to be considered separately for individual soil attributes. In this thesis, the REV associated with infiltration and soil water redistribution has been estimated using the following approaches:

(i) Pedological approach. Bouma (1985) considered that the REV of soil should be at least 20 peds.

(ii) Arbitrary measure of variance. Nordahl and Ringrose (2008) demonstrated the REV of permeability in a sandstone deposit occurred when the coefficient of variation (CV) from 10 measurements was less than 50 %.

(iii) Graphical approach. REV exist at the inflection point in the relationship between the reduction in coefficient of variation (CV) and sample volume.

(iv) Statistical approach. REV exists when an incremental increase in sample volume no longer produces a significant reduction in variation.

Representative elementary area (REA) was determined from the relationship between variance (CV) in the proportion of dye stained soil and the analysis width (sample area) used to determine the proportion of soil which participated in flow. The proportion of soil which participated in flow was determined from each of five 100 cm by 100 cm binary images of dye tracer infiltration, in which the binary images demonstrated the spatial variation in infiltration resulting from preferential flow. Determination of REV from two dimensional dye staining images measures the Representative Elementary Area (REA) rather than REV of the infiltration pathways, in which the width of analysis is analogous to the sample volume of the sensors in two dimensions.

The mean proportion of dye stained soil was determined using ImageJ (Abramoff *et al.* 2004) from ten measurements of each image at analysis widths of, 2 cm, 5 cm, 10 cm, 20 cm, 40 cm, 60 cm, 80 cm, and 100 cm. Analysis widths greater than 10 cm resulted in overlap of the analytical area (measurements were not mutually exclusive). As the radial sphere of influence of the EnviroSCAN sensors is approximately 10 cm (Paltineanu and Starr 1997), an analysis width of 20 cm (10 cm either side of the probe) was considered to be equivalent to the measurement area of a single soil moisture probe, 40 cm analysis width is equivalent to a two probes, 60 cm equivalent to three probes, etc. Variation in the mean proportion of dye stained soil was reported as the coefficient of variation (CV) as it provided a better estimate of variability for values with different means (Dow 1976; Lewontin 1966).

5.2.3 Inferring the presence of preferential flow from soil moisture response to rainfall

Lin and Zhou (2008) inferred the presence of preferential flow and subsurface lateral flow in the Shale Hills catchment, USA, from high frequency monitoring of soil moisture over 15 storm events using capacitance EC-10 and EC -5 soil moisture sensors. They assumed subsurface preferential flow occurred when a subsurface soil horizon responded to a rainfall input earlier than a soil horizon above it (non-sequential depth response). They considered that the rainwater had either bypassed the overlying horizon (bypass flow), or had percolated into the deeper subsoil from upslope or sideslope areas via subsurface lateral flow. Lin and Zhou (2008) inferred strong evidence for preferential flow when the change in soil moisture following rainfall (amplitude $\Delta\theta$) was greater than 0.10 $m^3\ m^{-3}$, and evidence for preferential flow was weak when the amplitude was $\Delta\theta \geq 0.002\ m^3\ m^{-3}$ but $< 0.01\ m^3\ m^{-3}$. Germann and Hensel (2006) also inferred the presence of preferential flow from soil moisture monitoring under sprinkler infiltration. Using TDR sensors logged at 5 minute intervals, they calculated the equivalent pore radii required to sustain flow using Poiseuille's Law, from the velocity of the wetting front and thus were able to infer the presence of preferential flow.

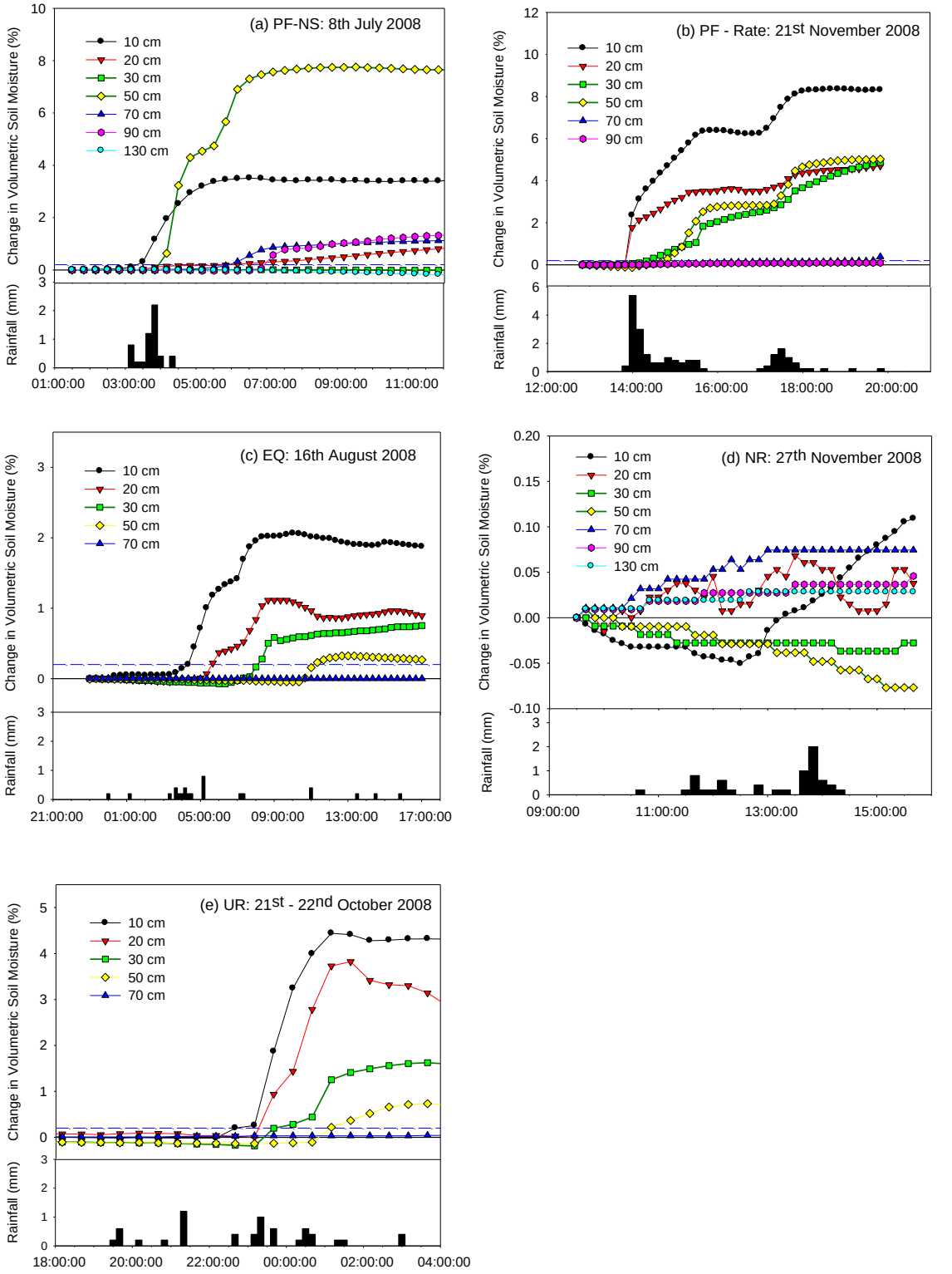

Figure 5.2-4 Examples of different infiltration types: (a) PF - NS, preferential flow - non sequential soil moisture response with depth, (b) PF - Rate, preferential flow – wetting front velocity > 500 mm hr^{-1}, (c) EQ - Equilibrium flow - wetting front velocity < 100 mm hr^{-1}, (d) NR - No response to rainfall events >5 mm, (e) UR - Unknown response, wetting front velocity between 100 mm hr^{-1} and 500 mm hr^{-1}; determination of preferential flow was not possible.
Note dashed blue line indicates 0.002 m^3 m^{-3} soil moisture response threshold.

In this study, the presence of preferential flow has been inferred from either non sequential soil moisture response with depth, similar to Lin and Zhou (2008), or wetting front velocities greater than 500 mm hr^{-1}. The 500 mm hr^{-1} threshold was chosen to infer preferential flow, as it is approximately 10 times the maximum saturated hydraulic conductivity of both the A and B horizons measured from 100 mm saturated, intact cores. Averaged maximum hydraulic conductivity of the A horizons was 52.4 mm hr^{-1} (SD ± 40.1 mm hr^{-1}) and the B2 horizons 45.9 mm hr^{-1} (SD ± 59.9 mm hr^{-1}) (Chapter 6.3.3). Little preferential flow was believed to have occurred in the 100 mm soil cores as prolonged wetting had overcome the effects of hydrophobicity in the A horizon and caused clays to swell, closing shrinkage cracks in the B2 horizons.

The effect of antecedent moisture on the occurrence of preferential flow was determined from changes in soil moisture following 44 rainfall events (> 5 mm) between 24/9/2007 and 16/8/2009. Soil moisture response to rainfall (> 5.0 mm) was classified into five infiltration types.

(i) PF-NS: Preferential flow – non sequential, evidenced by bypass flow in which first response from the soil moisture probes (> 0.002 m^3 m^{-3}) did not follow a logical sequence with depth. In Figure 5.2-4a the sensor at 50 cm depth responded before sensors at 20 cm and 30 cm depth. Dye staining experiments indicated that the PF-NS response resulted from a combination of finger flow in the A1 horizon and bypass flow via shrinkage cracks in the B2 horizons, in which infiltration resulted from flow via routes beyond the field of detection of the soil moisture sensors at one or more depths.

(ii) PF-Rate: Preferential flow, evidenced by the velocity of the wetting front in excess of 500 mm hr^{-1}. Dye staining experiments indicated that infiltration and soil water redistribution in the PF-Rate infiltration response class resulted from finger flow and flow through shrinkage cracks within the sphere of detection of the moisture sensors.

(iii) EQ: Equilibrium flow or uniform flow was evidenced by sequential soil moisture response with depth and wetting front velocities < 100 mm hr^{-1} following rainfall. The 100 mm hr^{-1} threshold was based on the mean saturated hydraulic conductivity of the soil matrix + 1 standard deviation measured from intact soil cores (Chapter 6.2.5). The rate of infiltration and soil water redistribution in equilibrium flow events (EQ) are expected to be similar to that predicted by Richards' equation for homogeneous soil.

(iv) NR: No response, despite rainfall exceeding 5 mm in a 24 hour period, soil moisture sensors failed to exceed the 0.002 m^3 m^{-3} soil moisture threshold (Figure 5.2-4e). The NR response occurred at both high and low antecedent soil moisture contents.

Figure 5.2-5 Litter dams formed from runoff following rainfall on dry hydrophobic soil.

At low antecedent soil moisture NR events are thought to have resulted from hydrophobicity induced surface runoff, as evidenced by formation of litter dams following rainfall, (Figure 5.2-5) or preferential flow via routes outside the field of detection of the whole soil moisture probe.

At high antecedent soil moisture, NR events are thought to have resulted from rainfall when soils moisture was already above field capacity or close to saturation such that the soil had little capacity to store new water. Gregory *et al.* (1992) explains that in duplex soils when perched watertables are present, or the subsoil is close to saturation, precipitation is likely to move through soil layers without any measurable change in water content, such that rainfall may enter the soil profile without being recorded by the soil moisture probe.

(v) UR: Unknown response, soil moisture response to rainfall was unable to be classified. UR events resulted from sequential soil moisture response with depth in which the velocity of the wetting front was between 100 and 500 mm hr^{-1}, and no other evidence of preferential flow existed (Figure 5.2-4f).

5.2.4 Effect of antecedent soil moisture on preferential flow

The effect of antecedent soil moisture, and rainfall on infiltration type following rainfall was investigated by one way ANOVA, with Tukey post-hoc test, with significance $p<0.05$. Comparison between the EQ and preferential flow infiltration responses (PF-NS and PF-Rate) was conducted with Independent T-test analysis with significance at $p<0.05$ and Levene's test for equality of variance at 0.1. in SPSS software Version 17.0.

5.2.5 Determination of rainfall effectiveness

Rainfall effectiveness was determined as the amplitude (change in soil moisture) divided by the amount of precipitation. Values greater than 1.0 indicate more rainfall entered the soil than actually fell on the site, presumably due to lateral flow and run-on. Whereas values less than 1.0 indicate losses due to runoff, deep drainage, and lateral flow etc.

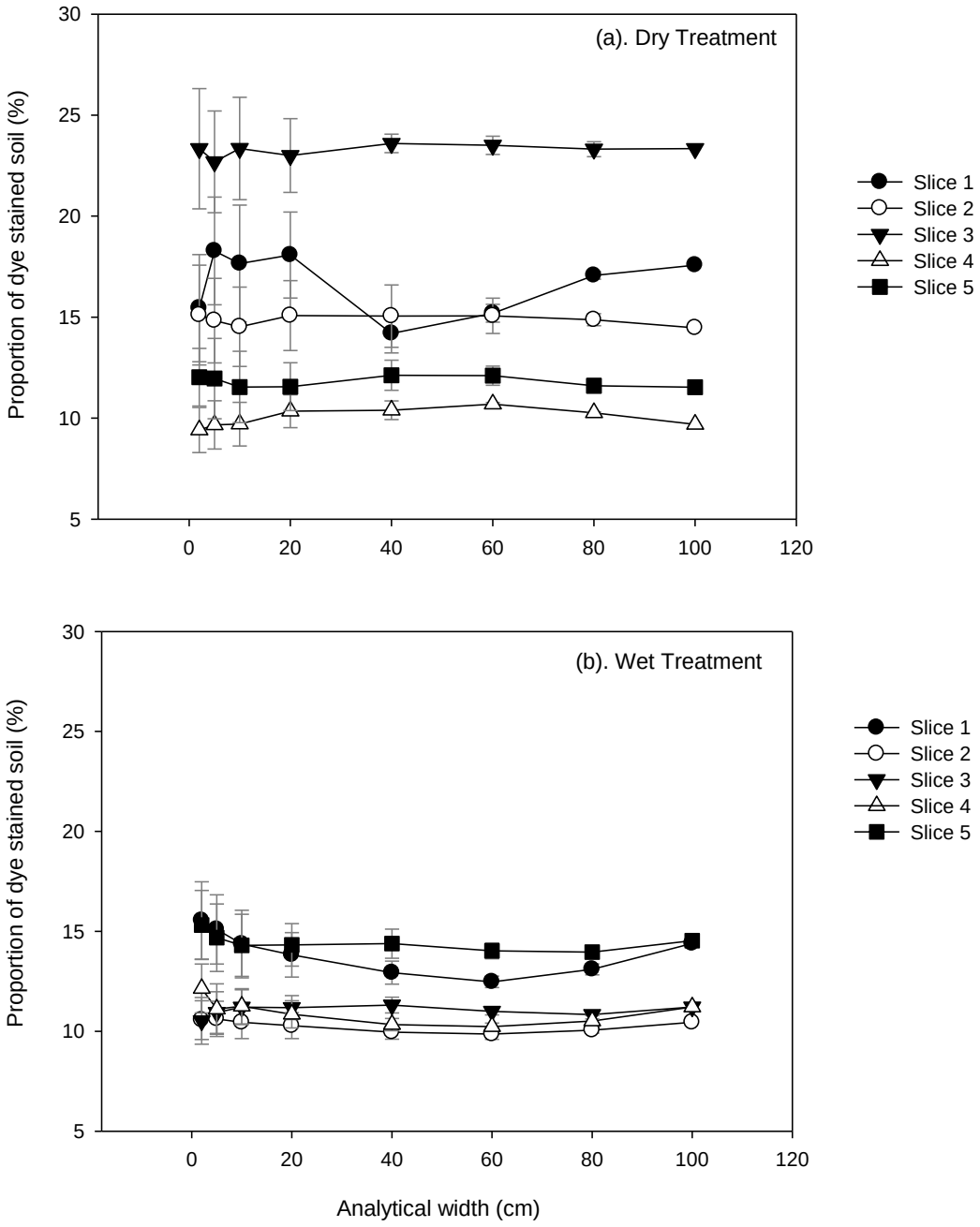

Figure 5.2-6 Change in mean and standard error of the proportion of dye stained soil with increasing analysis width. The value at 100 cm represents the true value. Slice refers to individual 100 cm x 100 cm binary image. Error bars represent ±1 standard error.

5.3 Results and discussion

5.3.1 Representative elementary volume (REV) and area (REA)

Subsoil structure at site B consisted of both primary structure consisting of clay columns separated by sand infills every 30 cm to 60 cm, and secondary structure resulting from the clay peds breaking to angular 2 cm to 5 cm diameter fragments when dry (Chapter 3.3.3). Consequently assessment of REV according to Bouma (1985) found REV existed at two length scales, in the order of 10 meters for the primary structure, and between 40 cm and 100 cm for the secondary structure. The existence of multiple REV has also been postulated by Crawford (1994) who suggested that for processes such as hydraulic conductivity, two or more REV's may exist.

Estimates of REA from dye tracer studies differed depending on analytical approach;

(i) Values of CV were less than the 50 % threshold proposed by Nordahl and Ringrose (2008) to define REV, and thus the approach was not valid in this study.

(ii) The graphical approach found a significant 2nd order polynomial relationship existed between the reduction in CV and sample volume (analytical width), in which the inflection point representing REA occurred at an analytical width of approximately 60 cm in both soil moisture treatments (Figure 5.3-2).

(iii) One way ANOVA with Tukey post hoc test demonstrated that CV did not significantly (p<0.05) change between the 60 cm analytical width and either the 40 cm or 80 cm analytical widths. This also suggested REA occurred around the 60 cm analysis width (Figure 5.3-1).

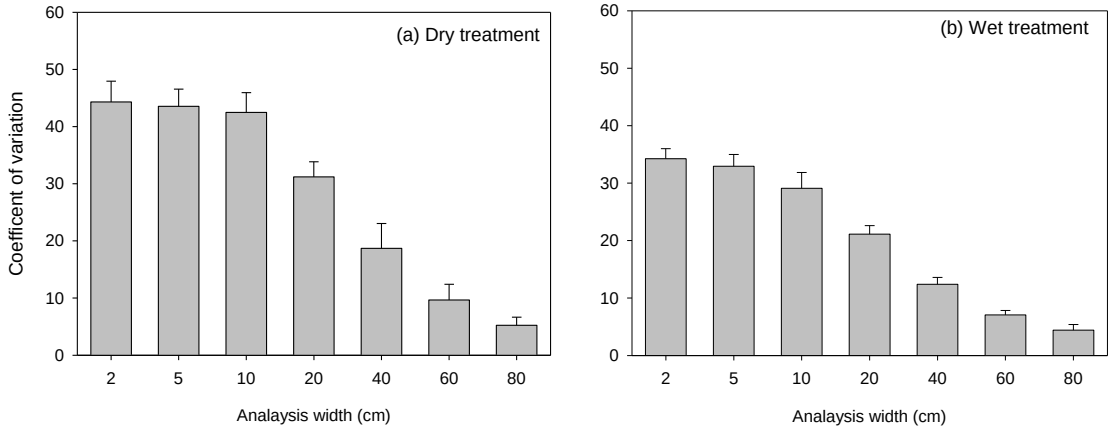

Figure 5.3-1 Reduction in the coefficient of variation in the proportion of dye stained soil with increased analysis width (sample area). Error bars represent ±1 standard error

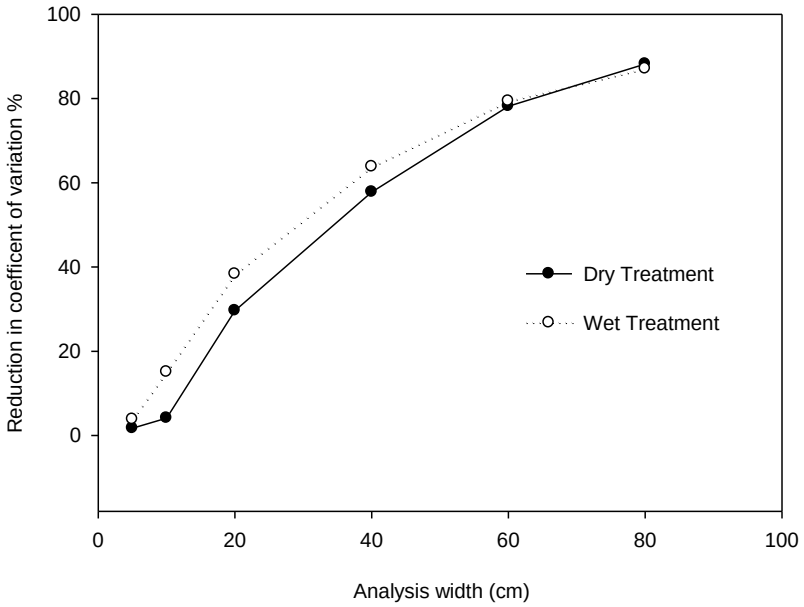

Figure 5.3-2 Reduction in the coefficient of variance with increasing analysis width for the dry and wet treatments.

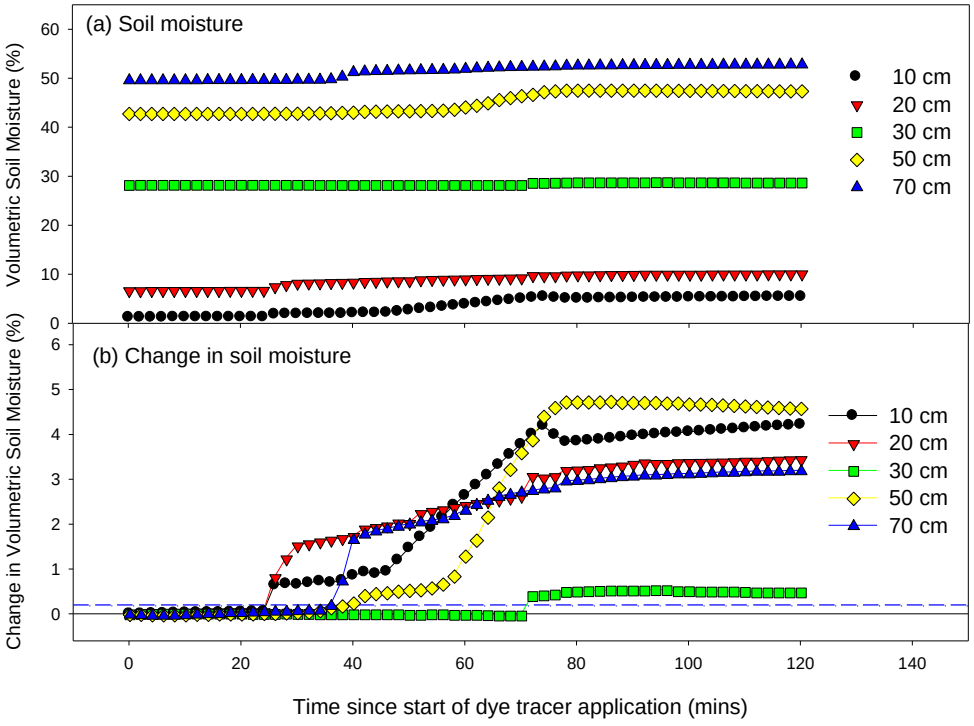

Figure 5.3-3 Soil moisture monitoring during dye tracer application at site B in the dry treatment. (a) Soil moisture. (b) Change in soil moisture. Tracer application ceased at 73 minutes. The broken blue line indicates the 0.002 m^3 m^{-3} soil moisture response threshold.

While use of a single soil moisture probe (20 cm analysis width) significantly (p<0.05) reduced CV to 31.2 % in the dry treatment and 21.1 % in the wet treatment (Figure 5.3-2, and Figure 5.2-6), the graphical and statistical approaches estimated REA occurred at an analytical width of approximately 60 cm, equivalent to the use of three soil moisture probes. Use of three soil moisture probes would have further reduced CV to 9.67 % in the dry treatment and 7.06 % in the wet treatment. Note that CV was higher in the dry treatment than the wet treatment due to the occurrence of preferential flow.

The use of a single soil moisture probe was supported for inferring relative changes in volumetric soil moisture with depth, and estimating the velocity of the wetting front. This assessment was based on the significant (p<0.05, df 18) reduction in the CV associated with the measurement width equivalent to a single soil probe (20 cm), and the high degree of similarity in the proportion of dye stained soil between the four soil profiles (Chapter 4.3, figure 4.3 – 29). However the reduction in CV associated with the use of a single soil moisture probe was not deemed sufficient to enable absolute measures of soil moisture response to rainfall, or to enable extrapolation of absolute values to other texture contrast soils with similar morphology. As such absolute values determined from the EnviroSCAN at site B are only applied to soils within the immediate vicinity of the monitoring site.

5.3.2 Soil moisture monitoring during dye staining experiments

5.3.2.1 Dry treatments – Site B

At low antecedent soil moisture, infiltration via preferential flow was evidenced by non-sequential response from the soil moisture sensors following application of 25 mm dye tracer (Figure 5.3-3). At site B the soil moisture sensor at 10 cm depth responded 25 minutes after dye application commenced, followed by the sensor at 20 cm depth one minute later. The delay in soil moisture response at 10 cm was attributed to hydrophobicity which prevented infiltration until the water repellence had broken down (similar to WDPT). Once hydrophobicity had been overcome, the wetting front rapidly penetrated via finger flow through the A1 horizon to 20 cm depth at approximately 6000 mm hr^{-1}. Soil moisture sensors at 10 cm and 20 cm demonstrated an initially rapid increase in soil moisture (0.225 m^3 m^{-3} hr^{-1}) associated with the passage of the finger flow wetting front, followed by a period of slow incremental increase in soil moisture at 0.015 m^3 m^{-3} hr^{-1} between 26 to 48 minutes.

15 mins: No response at 10 cm depth, depth of uniform wetting 2 cm, initiation of finger flow.

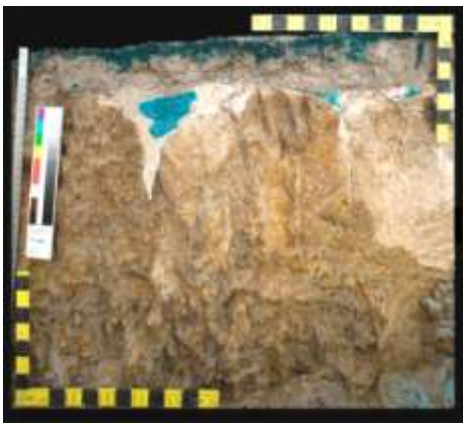

30 mins: Depth of uniform wetting 4 cm, slight ponding on B21 horizon, initiation of rivulet flow, flow into the A2 and sand infills.

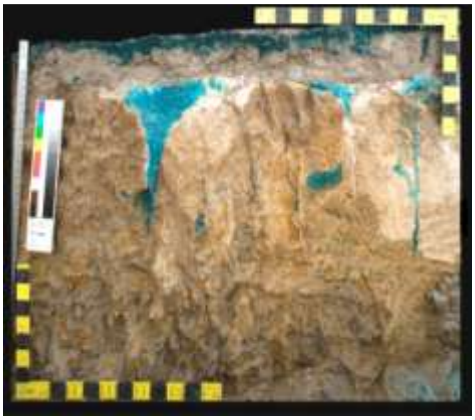

45 mins: Rivulet flow into B21 and B22 resulting in response at 50 cm, initial accumulation in dead end pores, flow through sand infills.

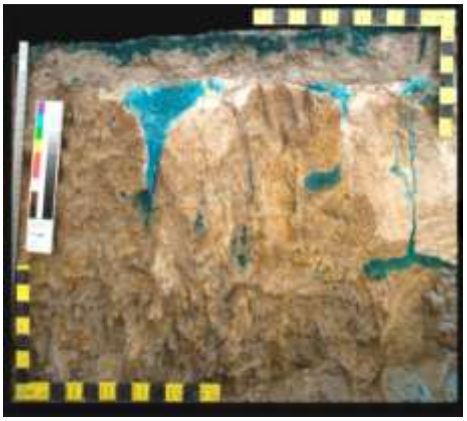

60 mins: Accumulation in dead end pores at 70 cm and 50 cm. Slow continued thickening fingers 10 cm and 20 cm depth.

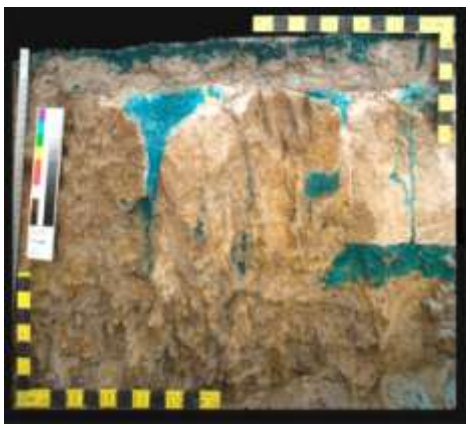

70 mins: Filling from below between clay columns and filling of smaller dead end pores in the B21 and B22 horizons. 30 cm sensor has yet to respond.

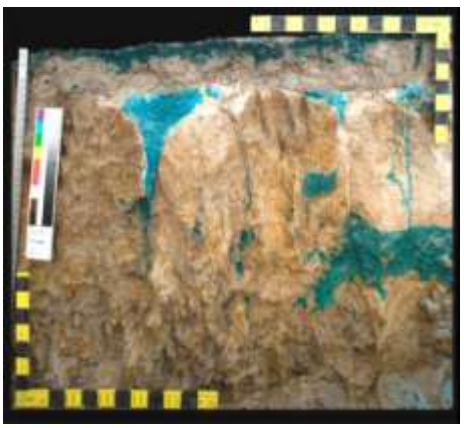

2400 mins: Image at time of excavation.

Figure 5.3-4 Conceptual reconstruction of dye tracer infiltration and redistribution into the dry soil moisture treatment at site B. Images were manipulated in Photoshop CS3 by sequentially' removing' the dye stained soil from the original image of dye staining (2400 mins) (Digital animation is presented on CD Rom, Appendix 8.1.2 and 8.1.4)

This slow increase in soil moisture was attributed to widening of the soil water fingers via lateral diffusion into the surrounding soil matrix. The sensor at 10 cm depth also demonstrated a secondary response in which amplitude increased rapidly between 47 and 73 minutes, presumably as a result of deepening of the distribution zone (Ritsema *et al.* 1993). Infiltration bypassed the field of detection of sensors at 30 cm and 50 cm depths (non-sequential infiltration), resulting in the sensor at 70 cm depth responding 37 minutes after dye application commenced. The estimated velocity of the wetting front between 20 cm and 50 cm depth was 1390 mm hr^{-1}, and was 2730 mm hr^{-1} between 20 cm and 70 cm depth (Table 5.3-1). Increased velocity of bypass flow with depth is thought to result from the reduction in transport volume with depth (Deurer *et al.* 2003).

Dye staining studies demonstrated that rapid infiltration between 20 cm and 70 cm depth resulted from thin rivulet flow down the sides of the clay columns or within the shrinkage cracks. Soil moisture at 70 cm depth increased at a moderate rate of 0.019 m^3 m^{-3} hr^{-1} as the dye tracer accumulated in dead-end shrinkage cracks and small void spaces. At 50 cm depth, soil moisture increased more slowly at 0.009 m^3 m^{-3} hr^{-1} between 42 and 56 minutes, presumably resulting from the passage of a rivulet through nearby shrinkage cracks. At 58 minutes, the rate of soil water accumulation at 50 cm depth increased tenfold to 0.127 m^3 m^{-3} hr^{-1}. Dye staining indicated this second phase of dye tracer accumulation at 50 cm depth resulted from 'filling from the bottom up' of voids fed by rivulet flow in shrinkage cracks. The estimated velocity of backfilling between 70 cm and 50 cm was 660 mm hr^{-1}.

Table 5.3-1. Time (between soil moisture response (>0.002 m^3 m^{-3}), and estimated wetting front velocity between soil moisture sensors during the dye staining experiments.

	Site A - Wet		Site B - Wet		Site B- Dry		Site C - Wet		Site D - Wet		Site D - Dry	
Infiltration Between	Time (mins)	Flow Rate (mm hr^{-1})	Time (mins)	Flow Rate (mm hr^{-1})	Time (mins)	Flow Rate (mm hr^{-1})	Time (mins)	Flow Rate (mm hr^{-1})	Time (mins)	Flow Rate (mm hr^{-1})	Time (mins)	Flow Rate (mm hr^{-1})
10 -20 cm	17	350	12	500	1	6000	34	180	376	20	3	2000
10 - 30 cm	120	100	37	330	46	260	131	90			2	6000
10 - 50 cm					14	1700					2	12000
10 - 70 cm					12	3000					25	1440
20 - 50 cm					13	1390					-1	-18000
20 – 70 cm					11	2730					23	1300
30 – 50 cm					-32	-380					0	0
30 – 70 cm					-34	-880					24	1250

* Negative values result from bypass flow resulting in an increase in soil moisture (>0.002 m^3 m^{-3}) in a deeper soil layer before an overlying layer.

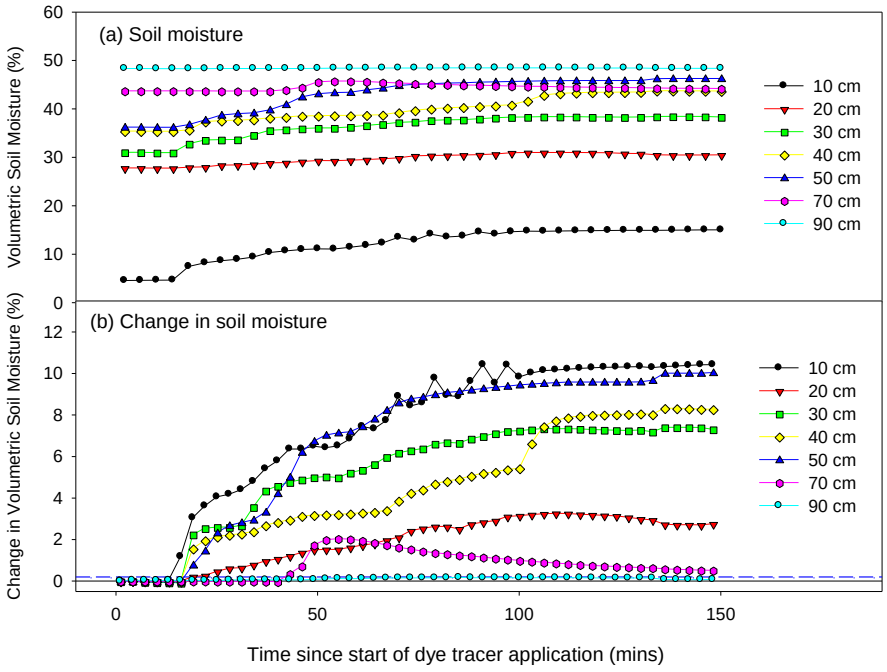

Figure 5.3-5 Soil moisture monitoring during dye tracer application at site D in the dry treatment, (a) soil moisture, (b) change in soil moisture. Tracer application ceased after 120 minutes. The broken blue line indicates the 0.002 m^3 m^{-3} soil moisture response threshold.

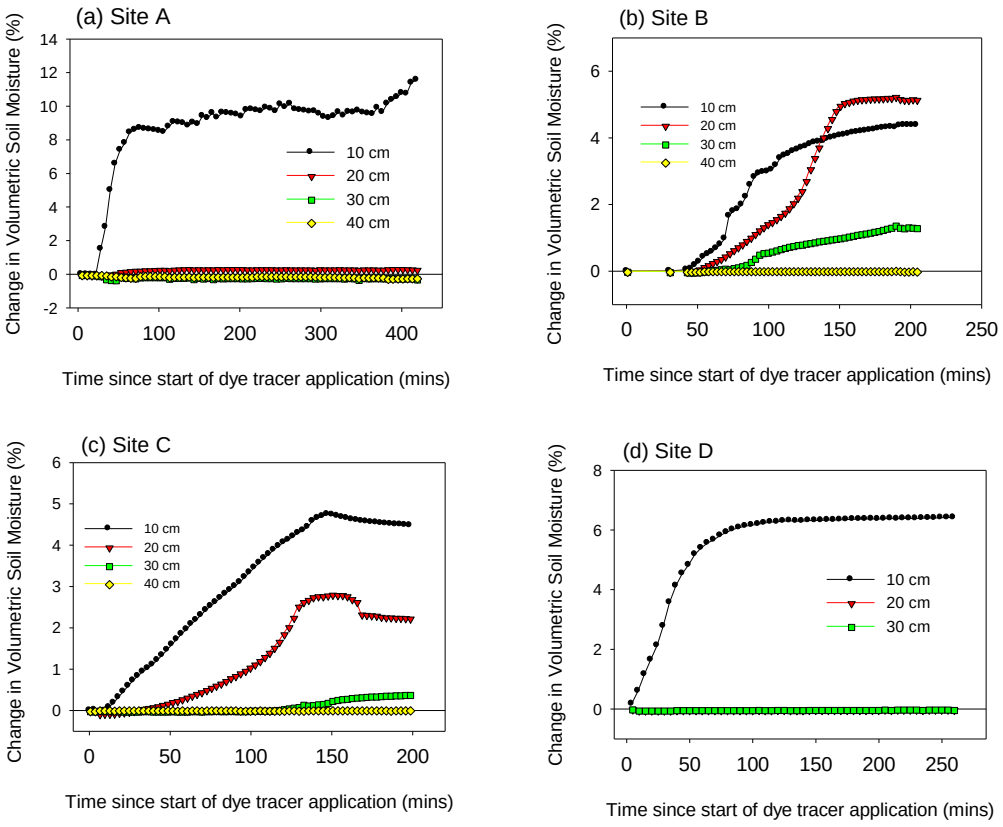

Figure 5.3-6 Change in soil moisture following application of 25 mm dye tracer to the wet treatments at (a) site A, (b) site B, (d) site D, and (c) 20 mm application at site C.

The soil moisture sensor at 30 cm depth finally responded 71 minutes after dye application commenced, and 2 minutes before dye application ceased. Soil moisture at 30 cm increased by only 0.005 m^3 m^{-3} hr^{-1} which indicated that the delayed response at 30 cm depth probably resulted from development of a bypass flow route within the sphere of influence of the soil moisture probe, rather than resulting from 'filling from below' as had occurred at 50 cm depth. A conceptual recreation of dye tracer infiltration and redistribution into the dry treatment at site B is presented in Figure 5.3-4 and on the CD Rom as a digital animation, Appendix 8.1.4.

5.3.2.2 Dry treatments – Site D

Application of 25 mm dye tracer at site D increased cumulative soil moisture by 44.5 mm (0 - 90 cm) (Figure 5.3-5). The difference between the applied volume of dye tracer and the measured change in soil moisture resulted from greater accumulation of dye tracer in the vicinity of the soil moisture probe than the surrounding soil. At site D, the soil moisture sensor at 10 cm depth responded 16 minutes after dye application commenced, which suggested hydrophobicity broke down sooner at site D than at site B as also indicated by the lower Water Drop Penetration Time (WDPT) at site D (Chapter 3.3.5). Soil moisture sensors at 20 cm, 30 cm, 40 cm and 50 cm responded 18 minutes after dye application commenced. The estimated velocity of the wetting front between 10 cm and 50 cm was 12,000 mm hr^{-1} (Table 5.3-1). Dye staining demonstrated the rapid penetration of the wetting front to a depth of 50 cm resulted from a combination of finger flow in the A1 horizon and thin rivulet flow in the B21 and B22 horizons. The greatest increase in soil moisture accumulation occurred at 10 cm and 50 cm depth, while the lowest occurred at 20 cm and 70 cm depth (Figure 5.3-5). Dye staining indicated the slow rate of soil moisture accumulation at 20 cm depth resulted from thickening of soil water fingers due to break down in hydrophobicity. While the incremental increase in soil moisture at 30 cm, 40 cm and 50 cm was attributed to filling of small voids and shrinkage cracks, rather than the 'filling from the bottom up' reported at site B.

Application of dye tracer to soil at low antecedent moisture resulted in estimated wetting front velocities ranging up to 6,000 mm hr^{-1} at site B, and 12,000 mm hr^{-1} at site D (Table 5.3-1). These wetting front velocities were 130 to 50,000 times greater than the average saturated hydraulic conductivity which ranged from 21.7 mm hr^{-1} to 46.6 mm hr^{-1} (site B and D respectively) in the A1 horizon and 0.24 - mm hr^{-1} in the B22 horizon (Chapter 6.3.3).

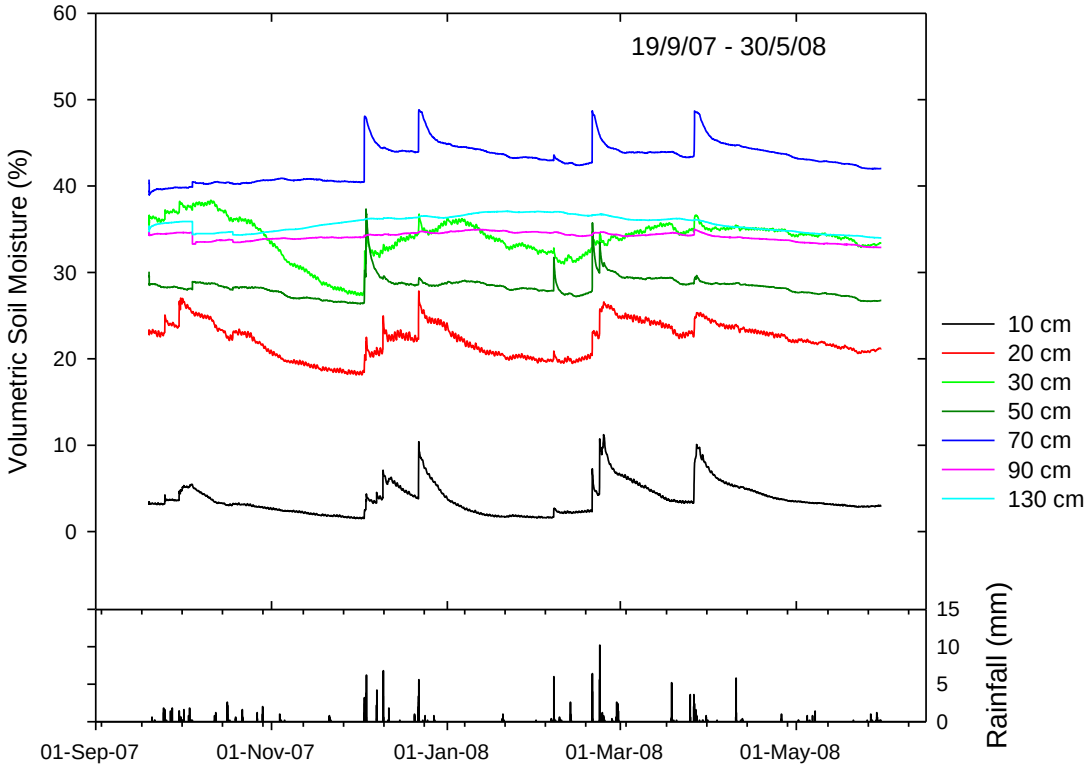

Figure 5.3-7 Soil moisture monitoring between September 07 and May 08 at 60 minute intervals.

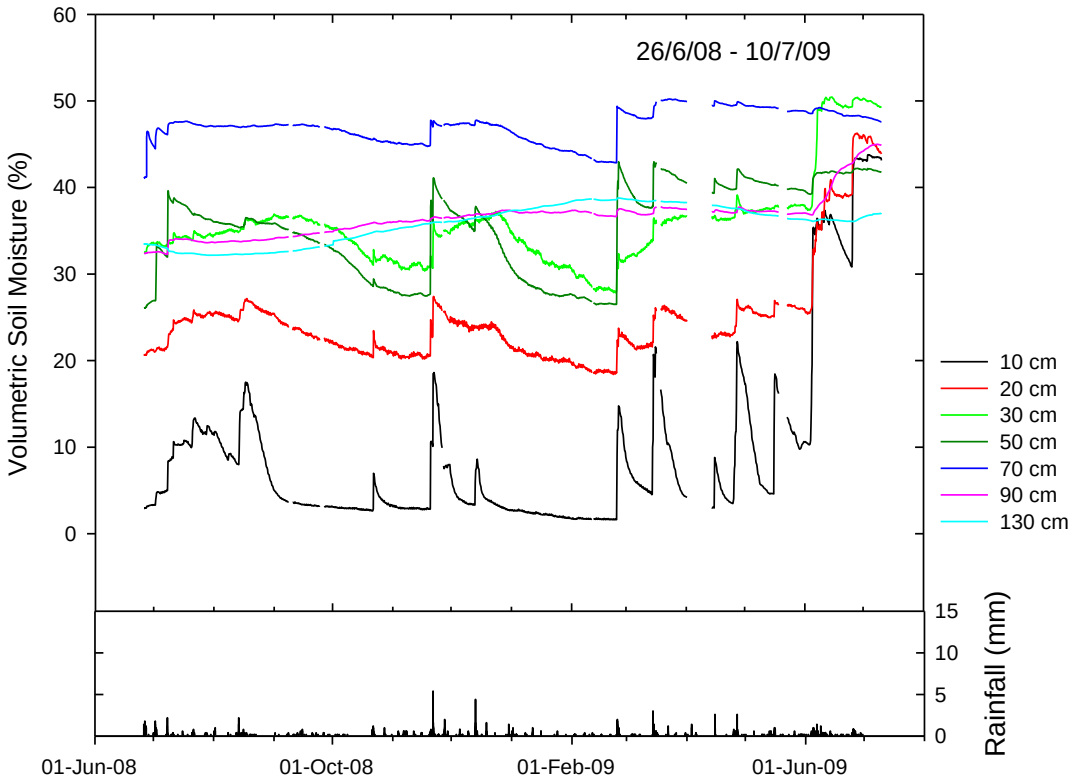

Figure 5.3-8 Soil moisture monitoring between June 08 and July 09 at 10 minute intervals.

The extreme wetting front velocities reported in this study are consistent with the literature. Germann and Hensel (2006) investigated the effect of preferential flow on wetting front velocity at twenty five undisturbed field sites in Switzerland. They found the majority of sites had wetting front velocities between 0.2 and 1.0 mm s^{-1} (720 and 3,600 mm hr^{-1}), with the highest measured velocity being 5.5 mm s^{-1} (19,800 mm hr^{-1}). Kung *et al.* (2005) similarly reported a dye tracer penetrated to 1.0 meter depth in 15 minutes, equivalent to a flow rate of 1 mm s^{-1} (4,000 mm hr^{-1}), and Hincapié and Germann (2009) report wetting front velocities between 0.3 and 4.4 mm s^{-1} (1,080 and 15,800 mm hr^{-1}) in undisturbed cores.

5.3.2.3 Wet treatments

Application of 25 mm dye tracer increased volumetric soil moisture by 12.5 % at site A, 10.9 % at site B, 10.9 % at site C (20 mm application), and 6.6 % at site D (Figure 5.3-6). At three of the four sites, amplitude was greatest at 10 cm depth. The estimated velocity of the wetting front between 0 cm and 30 cm ranged from 20 mm hr^{-1} at site D, to 330 mm hr^{-1} at site B. At all sites other than site B, the velocity of the wetting front indicated that infiltration occurred as uniform flow (EQ) (Table 5.3-1). At site B, higher wetting front velocity may have resulted from breakdown of the wetting front (noted in dye tracer experiments, Chapter 4.3.2), however the wetting front velocity was 500 mm hr^{-1} and thus infiltration was unable to be classified as being preferential.

5.3.3 Long term monitoring of soil moisture response to rainfall adjacent site B

Soil moisture monitoring between September 2007 and July 2009 (Figure 5.3-7 and Figure 5.3-8). demonstrates evidence of preferential flow including;

(i) Inability of the A1 horizon (0-10 cm depth) to reach field capacity (approx. 0.40 m^3 m^{-3}). The maximum soil moisture content at 10 cm depth never exceeded 0.12 m^3 m^{-3} prior to July 2009 despite infiltration to 50 cm depth on five occasions and a total of 577 mm precipitation between September 2007 and May 2009.

(ii) The 'spiky' (i.e. rapid increase and decrease) soil moisture response at 50 cm and 70 cm indicating rapid filling and draining of the subsoil despite the presence of clay subsoils with little porosity in the soil matrix below 30 cm depth. This spiky response is attributed to preferential flow through either sand infills (funnel flow) or bypass flow in shrinkage cracks.

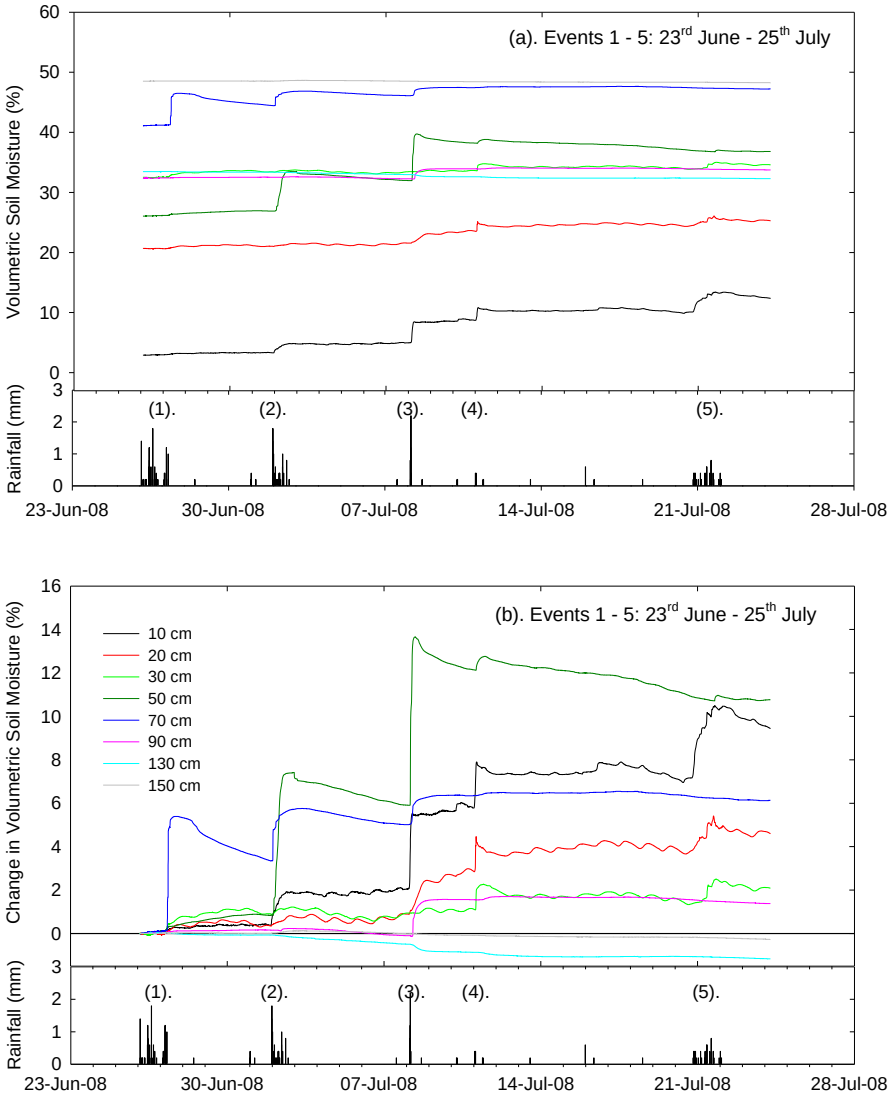

Figure 5.3-9 Site B, (a) Soil moisture monitoring and rainfall between 23rd June and 28th July 2008 (b). Change in volumetric soil moisture and rainfall. (Legend applies to both graphs). Numbers (1) to (5) refer to rainfall events.

By comparison the change in soil moisture at 90 cm and 130 cm was gradual and rounded indicating slow uniform (non-preferential) wetting below 70 cm depth. Clothier *et al.* (2008) notes similar 'spiky' response from TDR sensors at 90 cm depth in a silt loam soil in New Zealand which he attributed to either macropore flow or finger flow due to a fine-over-course texture discontinuity in the subsoil.

5.3.4 Effect of antecedent soil moisture on infiltration following rainfall between 23rd June and 28th July 2008

Soil moisture response to rainfall between 23rd June and 28th July 2008 differed as antecedent soil moisture increased with each rainfall event (Figure 5.3-9). In the first three rainfall events, non-sequential response from the soil moisture sensors resulted from preferential flow routing water to 50 cm and 70 cm depth before sensors higher in the soil profile had responded. By the fifth rainfall event, increased antecedent soil moisture resulted in uniform infiltration. Soil moisture response to rainfall is discussed for each rainfall event.

Event 1 (PF-NS): In event one, preferential flow into soil at low antecedent soil moisture resulted in infiltration of rainfall to 70 cm depth at 360 mm hr^{-1} (30 - 70 cm), which then backfilled shrinkage cracks and inter-ped voids. The first soil moisture sensor to respond was at 30 cm depth, 1720 minutes after rainfall commenced, followed by the sensor at 50 cm depth six minutes later. Sensors at 10 cm and 20 cm depth responded to rainfall 204 and 233 minutes after the sensor at 30 cm depth first responded (non-sequential infiltration). Soil moisture at sensors between 10 cm and 50 cm depth increased by less than 0.012 m^3 m^{-3}, whereas at 70 cm depth soil moisture increased by 0.054 m^3 m^{-3} (Figure 5.3-10a). The rapid increase in soil moisture at 70 cm depth, was attributed to rapid filling of terminal shrinkage cracks or 'filling from the bottom up' from rivulet flow as demonstrated by the dye staining experiments (Chapter 4.3.7).

Event 2 (PF-NS): Unlike event 1, rainfall on the 2nd of July caused the sensor at 10 cm depth to respond within 20 minutes after rainfall commenced. Sensors at 20 cm and 30 cm were bypassed resulting accumulation of water at 50 cm and 70 cm depth. The sensor at 50 cm depth responded 30 minutes after the sensor at 70 cm depth which indicated that backfilling of voids from 70 cm to 50 cm depth occurred at a rate of approximately 400 mm hr^{-1} (Figure 5.3-10b, Table 5.3-2).

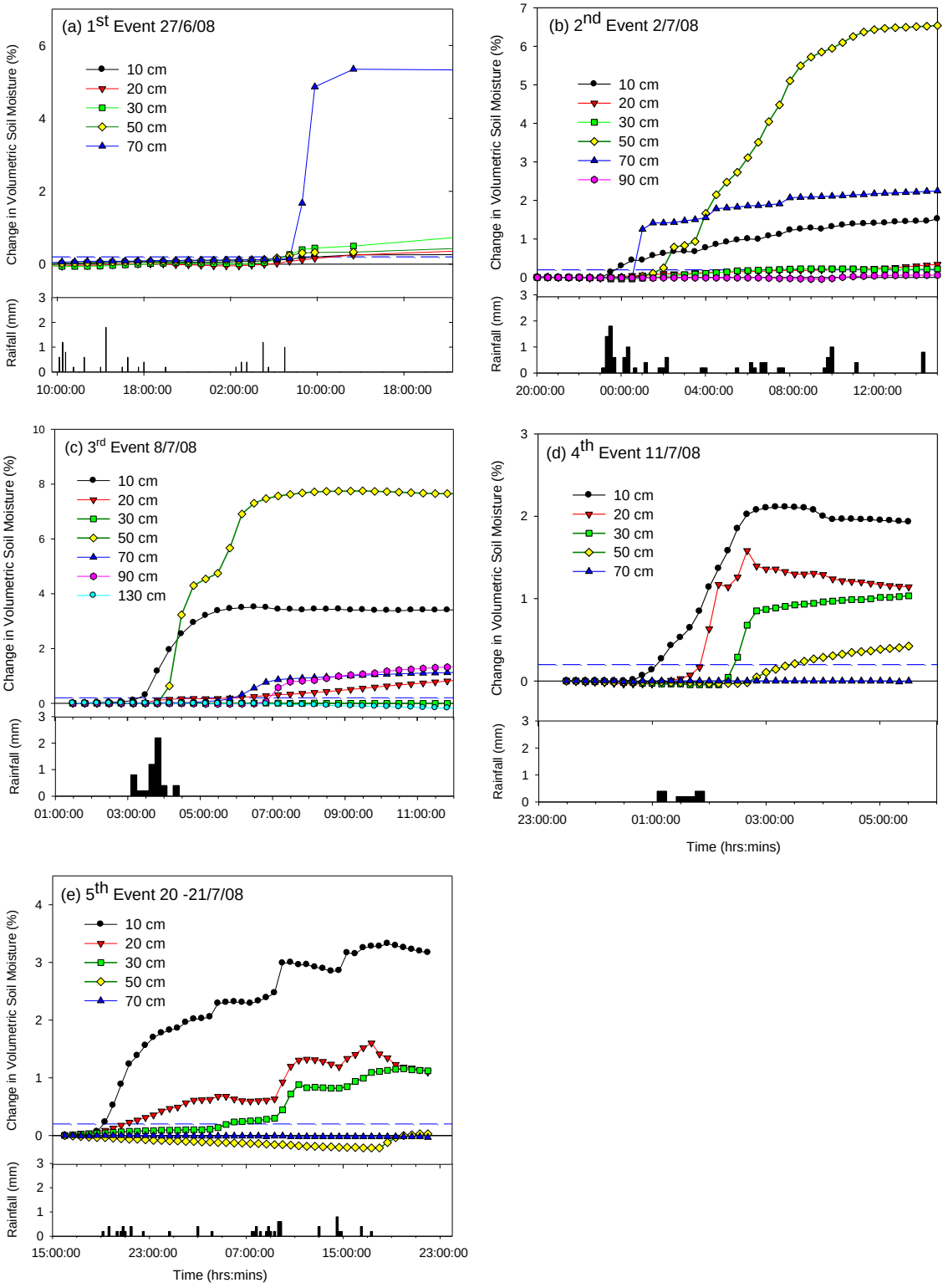

Figure 5.3-10 Change in soil moisture for five sequential rainfall events between 23rd June and 25 of July.

Note the blue line represents the $\Delta\theta$>0.002 m^3 m^{-3}soil moisture threshold.

Event 3 (PF-NS): The sensor at 10 cm depth responded less than 10 minutes after rainfall commenced, followed by the sensor at 50 cm depth, 50 minutes later (Figure 5.3-10c). Estimated velocity of bypass flow between 10 cm and 50 cm was 480 mm hr^{-1} (Table 5.3-2). The 0.35 m^3 m^{-3} increase in soil moisture at 10 cm was attributed to increased depth of uniform wetting in the distribution zone (Ritsema *et al.* 1993) or widening of soil water fingers. In the third rainfall event, higher antecedent soil moisture resulted in slower and reduced change in soil moisture at 70 cm depth (0.47 m^3 m^{-3}), presumably due to clay swelling or filling of void spaces from the two previous rainfall events.

The sensor at 90 cm depth had not responded to the previous two rainfall events. However in event three it is thought that response at 90 cm depth 240 minutes after the commencement of rainfall, may have resulted from reduced lateral infiltration from the rivulet into the soil matrix at higher soil moisture resulting in deeper infiltration down the sides of the shrinkage cracks (Beven and Germann 1982). Greve *et al.* (2010) also found that as moisture content in the soil matrix adjacent to shrinkage cracks increased from earlier rainfall events, the lateral infiltration rate decreased resulting in water flowing along the crack to successively deeper parts of the profile.

Event 4 (UR): Despite only 1.2 mm precipitation on 11/7/08, soil moisture increased by 0.06 m^3 m^{-3}. Soil moisture response was sequential with depth. Unlike all previous rainfall events, the sensor at 30 cm depth responded after the sensor at 20 cm depth and before the sensor at 50 cm depth indicating uniform flow (Figure 5.3-10d). However the velocity of the wetting front was estimated to be 150 mm hr^{-1} which indicated infiltration may have been assisted by preferential flow (Table 5.3-2). The disproportional increase in soil moisture was attributed to either greater rainfall at the monitoring site than at the Cambridge airport weather station (5.12 km from the monitoring site), or hydrophobicity induced run-on from upslope areas, as evidenced by litter dams (Figure 5.2-5).

Event 5 (EQ). Rainfall on the 20th and 21st of July 2008 resulted in sequential infiltration with depth in which the velocity of the wetting front between 10 cm and 30 cm was 20 mm hr^{-1} (Figure 5.3-10e, Table 5.3-2). Infiltration was attributed to uniform or equilibrium flow.

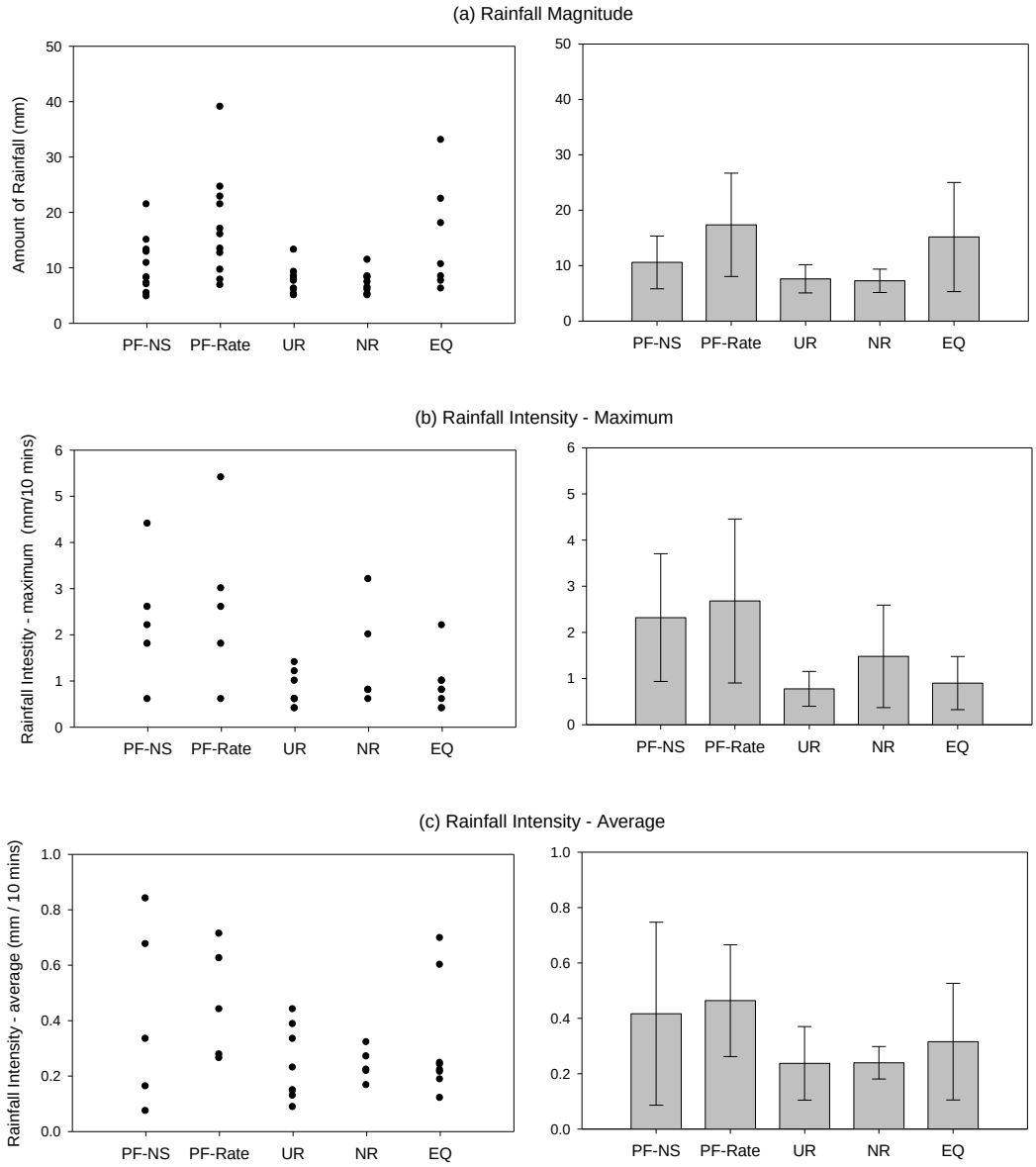

Figure 5.3-11 Effect of rainfall on infiltration type displaying plot graph of individual events and Bar chart summary (a) rainfall total, (b) rainfall intensity – maximum, (c) rainfall intensity – average. Error bars represent ±1 SD.

Table 5.3-2 Response time (ΔL_s) and estimated velocity of the wetting front between the sensor at 10 cm depth and other sensors for each flow event.

		Time (minutes) to first response and estimated velocity of the wetting front (mm hr^{-1}) between sensors at 10 cm depth and …							
		20 cm depth		30 cm depth		50 cm depth		70 cm depth	
Rainfall Event	Rainfall magnitude (mm)	Time (mins)	Velocity (mm hr^{-1})	Time (mins)	Velocity (mm hr^{-1})	Time (mins)	Velocity (mm hr^{-1})	Time (mins)	Velocity (mm hr^{-1})
1	10.6	73	80	203*	60*	197*	120*	150	240
2	11.8	600*	10*	450*	25*	120*	200*	90	400
3	5.4	160*	40*	1030*	10*	50	480	160	230
4	1.2	40	150	80	150	130	190	na	na
5	8.4	150	40	640	20	na	na	na	na

* Indicates soil horizon was bypassed

5.3.5 Analysis of rainfall events, site B between September 2007 and August 2009

5.3.5.1 Effect of rainfall magnitude and intensity on infiltration type.

Occurrence of preferential flow was not related to either the amount of rainfall or rainfall intensity, as no significant difference existed between the amount of rainfall or rainfall intensity of the EQ infiltration events, compared to the two preferential flow infiltration event types (PF-NS & PF-Rate) (Figure 5.3-11). One way ANOVA with Bonferroni post hoc test demonstrated that no significant difference in average rainfall intensity existed between any of the five infiltration types. A significant difference in rainfall magnitude existed between the PF-ns and the NR and UR infiltration types, and a significant difference in maximum rainfall intensity existed between PF rate and UR types. The absence of a relationship between rainfall intensity or rainfall magnitude and the occurrence of preferential flow contradicts previous studies in which development of preferential flow occurred above either a threshold rainfall amount (Cheng *et al.* 2007; McGrath *et al.* 2010), a rainfall duration (Heppell *et al.* 2002), or a threshold rainfall intensity (Beven and Germann 1982; Lin and Zhou 2008; McGrath *et al.* 2008). Review of the literature indicates that preferential flow in many of these studies resulted from rainfall intensity exceeding the infiltration capacity of the soil, resulting in overland flow which rapidly filled macropores which were open to the soil surface. However in this study, the A1 horizon contained few macropores, infiltration in the A1 horizon was dominated by hydrophobicity induced finger flow (Chapter 4.3.8) and subsoil macropores were not connected to the soil surface due to the sandy texture of the A1 and A2 horizons. Consequently findings and modelling approaches developed for soils with surface connected macropores are not applicable to the texture contrast soils investigated in this study, in which preferential flow was not triggered by rainfall intensity or rainfall magnitude (Figure 5.3-11).

Table 5.3-3 ANOVA Influence of antecedent soil moisture and rainfall on the occurrence of preferential flow**.**

Parameter	Depth increment / attribute	df	F	Significance	Significance level
Antecedent soil moisture	10 cm	30	21.65	0.0001	Highly Significant
	20 cm	30	17.95	0.0002	Highly Significant
	30 cm	30	10.06	0.0036	Significant
	50 cm	30	21.24	0.0001	Highly Significant
	70 cm	30	10.23	0.0033	Significant
	90 cm	30	4.51	0.0424	ns
Cumulative antecedent soil moisture	0-20 cm	30	20.95	0.0001	Highly Significant
	0-30 cm	30	18.83	0.0002	Highly Significant
	0-50 cm	30	23.86	0.0000	Highly Significant
	0-70 cm	30	25.78	0.0000	Highly Significant
	0-90 cm	30	22.90	0.0000	Highly Significant
	30-50 cm	30	20.75	0.0001	Highly Significant
	50 -90 cm	30	15.92	0.0004	Highly Significant
	30-90 cm	30	18.68	0.0002	Highly Significant
Rainfall	Event	36	0.14	0.7128	ns
	Cum. 30 days prior to event	36	2.56	0.1230	ns
	Max. Intensity /10 mins	22	7.95	0.0232	Significant
	Ave. Intensity /10 mins	22	1.20	0.2895	ns

Note the UR - unknown response and NR - no response infiltration types were removed to restrict analysis to the two preferential infiltration types and equilibrium flow. A significant difference between the EQ and two preferential flow responses indicated the parameter had a significant effect on occurrence of preferential flow.

5.3.5.2 Effect of antecedent soil moisture on infiltration type

Antecedent soil moisture content prior to rainfall significantly influenced the occurrence of preferential flow events (Figure 5.3-12, Table 5.3-3). Significant differences between the antecedent soil moisture in the equilibrium flow response (EQ) and the two preferential flow responses (PF-NS & PF-Rate) occurred at all depths other than 90 cm, which did not vary greatly over the monitoring period (Table 5.3-3). Data presented in Figure 5.3-11 and Figure 5.3-12 demonstrates the occurrence of preferential flow was influenced by antecedent soil moisture rather than rainfall intensity or the amount of rainfall. Lack of a significant relationship between rainfall attributes and occurrence of preferential flow contradicts findings by Heppell *et al.* (2002) who found the amount of rainfall and rainfall intensity are more important than antecedent conditions in generating high proportions of macropore flow.

ANOVA demonstrated that the greatest difference in antecedent soil moisture between the EQ and the two preferential flow responses (PF NS and PF-Rate) existed at 50 cm depth (p = 0.95 x10^{-4}) and cumulative soil moisture between 0 cm and 70 cm (p = 0.21 x10^{-4}), (Table 5.3-3). However Spearman bivariate correlation analysis found the monitoring depths in the topsoil (0 cm to 20 cm depth) had a higher correlation between the occurrence of preferential flow and antecedent soil moisture (correlation coefficient 0.668, p = 4.07 x10^{-5}), than the monitoring depths in the subsoil (30 cm to 70 cm) (correlation coefficient 0.577, p = 6.79 x10^{-4}).This indicates that topsoil antecedent moisture had greater influence on the development of preferential flow than antecedent moisture in the subsoil, which seems to suggest that hydrophobicity had a greater influence on the development of preferential flow than shrinkage cracks in the subsoil.

5.3.5.3 Influence of antecedent soil moisture threshold on the occurrence of preferential flow

Analysis indicated the existence of an antecedent soil moisture threshold which influenced the occurrence of preferential flow (Figure 5.3-12). When antecedent soil moisture content was below 226 mm (sum 0-70 cm) soil moisture response to rainfall was preferential (PF-NS and PF-Rate) in 17 of 22 rainfall events, two unknown (UR) events, and zero equilibrium (EQ) events. When antecedent soil moisture was above 246 mm (sum soil profile 0-70 cm) three of the nine rainfall events resulted in uniform infiltration (EQ), five responses to rainfall were unable to be classified (UR) and one no response (NR) event occurred. Preferential flow did not occur when antecedent soil moisture was above 246 mm. This analysis demonstrates that an antecedent soil moisture threshold exists between 226 -246 mm (sum 0-70 cm).

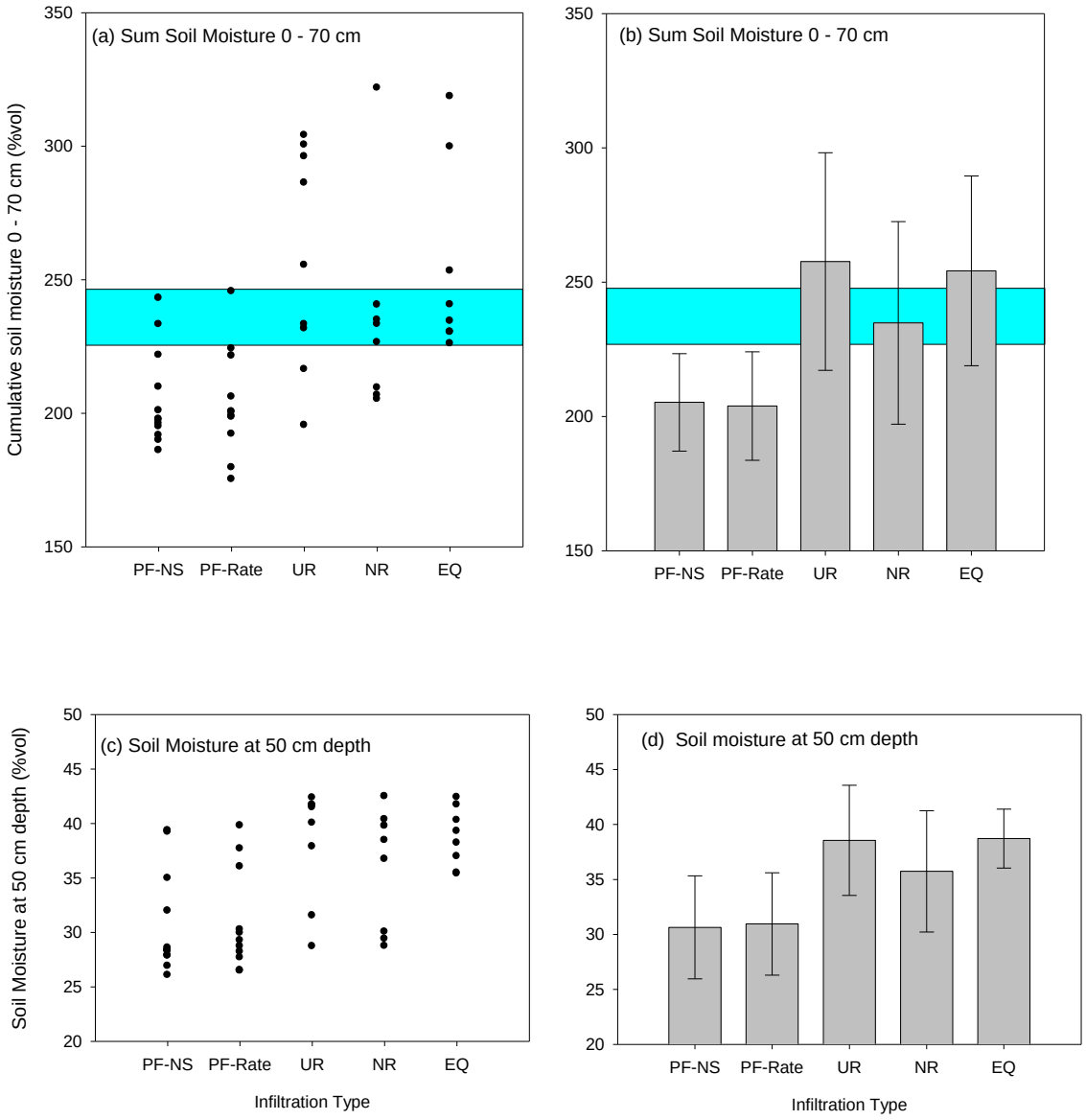

Figure 5.3-12 Effect of antecedent soil moisture on infiltration type (a & b) cumulative soil moisture between 0 cm and 70 cm, (c &d) 50 cm depth. Blue box indicates soil moisture threshold above which infiltration response is predominantly uniform, and below which is predominantly preferential. Error bars represent ±1 SD.

When soil was below the 226 mm threshold, infiltration was highly likely to result from preferential flow, while rainfall on soil above the 246 mm threshold was likely to result in uniform infiltration or unknown response to rainfall. Based on a saturated moisture content (SAT) of 322 mm, field capacity (FC) of 315 mm, and a permanent wilting point (PWP) of 141 mm (determined by suction tables and pressure chambers, Chapter 6.3.1), the soil moisture threshold corresponded to 70 - 76 % of total soil water, and 49 - 60 % of plant available water content (PAWC). PAWC determination is presented in Appendix 5.0.

The occurrence of preferential flow below a soil moisture threshold has been reported for hydrophilic soils (Bauters *et al.* 2000a; Jury *et al.* 2003; Wang *et al.* 1998b), vertic soils (Gupta *et al.* 2006), and rivulet flow in stable (non-vertic) macropores (Germann *et al.* 1997; Kutilek and Germann 2009). Sensitivity analysis with the two dimensional HILLS model also found the magnitude of subsurface lateral flow in a hillslope containing texture contrast soils was more significant when antecedent soil water content was above a threshold corresponding to 30 - 50 % of available water (Ticehurst *et al.* 2005).

In hydrophobic soil, the degree of water repellence is inversely related to soil moisture (King 1981), in which infiltration and formation of finger flow occurs during infiltration below a critical water content (Ritsema and Dekker 1994) (discussed further Chapter 7.0). In macroporous soils Kutilek and Germann (2009) and Germann *et al.* (1997) postulate the existence of a threshold volumetric soil moisture content (θ*), that defines the boundary between the preferential flow and Richards-type equilibrium flow. They suggest this threshold or transition between flow behaviours is a physical property of the soil, in which the flow-driving force of thin films within macropores is consumed by momentum dissipation as soil moisture content exceeds the threshold soil moisture content (θ*).

5.3.6 Effect of antecedent soil moisture on change in soil moisture (amplitude)

One way ANOVA demonstrated that no significant difference in amplitude (change in soil moisture following rainfall) existed between the EQ and two preferential flow infiltration response types, which indicates that preferential flow did not influence the change in soil moisture (amplitude) following rainfall. Despite the lack of a significant statistical difference between infiltration response types, the trend in amplitude with depth provides process understanding of the effect of preferential flow on infiltration and soil water redistribution (Figure 5.3-13).

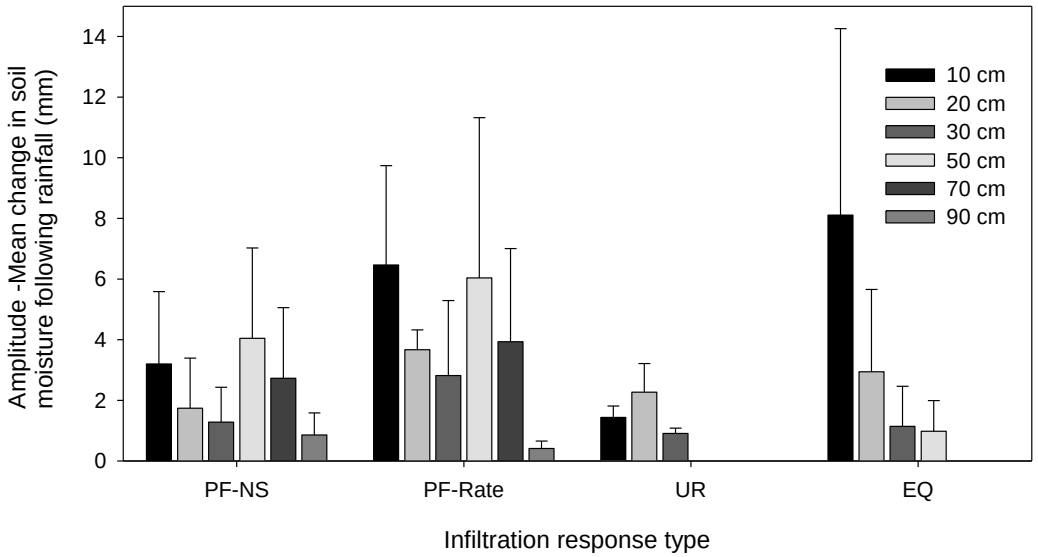

Figure 5.3-13 Relationship between infiltration response type following rainfall (>5 mm) and soil moisture redistribution (amplitude). Error bars represent ± 1 SD.

Amplitude in the EQ infiltration response decreased sequentially with depth as was expected for uniform infiltration. In the two preferential flow responses (PF- NS and PF-Rate) amplitude demonstrated a step-like reduction with depth to 30 cm, which then increased at 50 cm before declining again to 90 cm depth. Dye staining patterns at high and low antecedent soil moisture (Chapter 4.3) indicate the reduction in amplitude between 10 cm and 30 cm was due to due to finger flow in the A horizon and bypass flow in the B21 horizon. The increase in amplitude at 50 cm was attributed to accumulation of infiltration in dead-end voids, which decreased with depth within the B22 and B23 horizons due to increased soil density and a reduction in flow volume.

One way ANOVA with Tukey post hoc analysis found no significant (p<0.05, df 121) difference existed between the EQ and two preferential flow infiltration responses in either the lag time to the start of infiltration (ΔL_s) , or the lag time to the maximum soil moisture response (ΔL_m) (Figure 5.3-14). As expected the ΔL_m and ΔL_s increased with depth in the EQ infiltration response type, as the wetting front advanced sequentially with depth (the lower lag time at 50 cm depth resulted from fewer and slower infiltration events penetrating below 30 cm depth, Figure 5.3-14b). The ΔL_s at 10 cm depth was considerably lower in the PF-Rate events (78 minutes) than the PF-NS events (334 minutes), which suggests that hydrophobicity had a greater influence on the development of preferential flow in the PF-NS events than the PF-Rate events.

Time to reach maximum amplitude (ΔL_m) was also greater than ΔL_s in all infiltration response classes which indicates that although infiltration may have rapidly penetrated through the soil profile in both the preferential flow (PF) responses, the time required for soil water redistribution into the soil matrix was considerable, between 800 to 2,500 minutes (Figure 5.3-14).

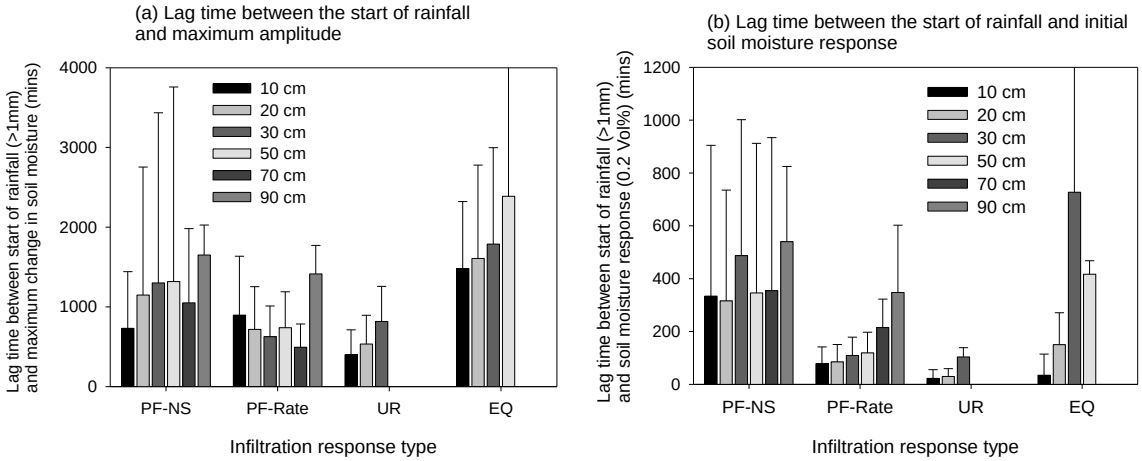

Figure 5.3-14 (a) ΔL_m- Lag time between start of rainfall (T_r) and the maximum change in soil moisture (mins). (b) ΔL_s - Lag time between start of rainfall (T_r) and initial soil moisture response (>0.002 m^3m^{-3}). Error bars represent ±1 SD.

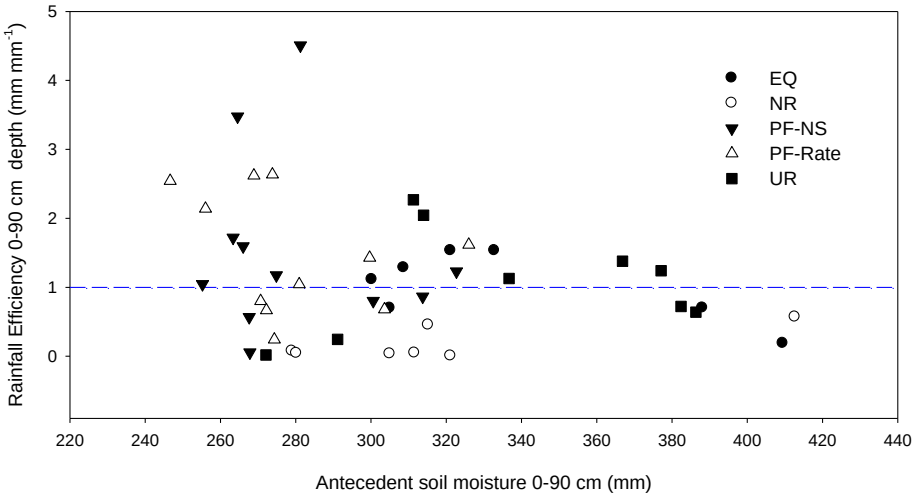

Figure 5.3-15 Relationship between antecedent soil moisture (0 – 90 cm) and rainfall effectiveness. Blue line represents rainfall effectiveness 1.0 or 100 %.

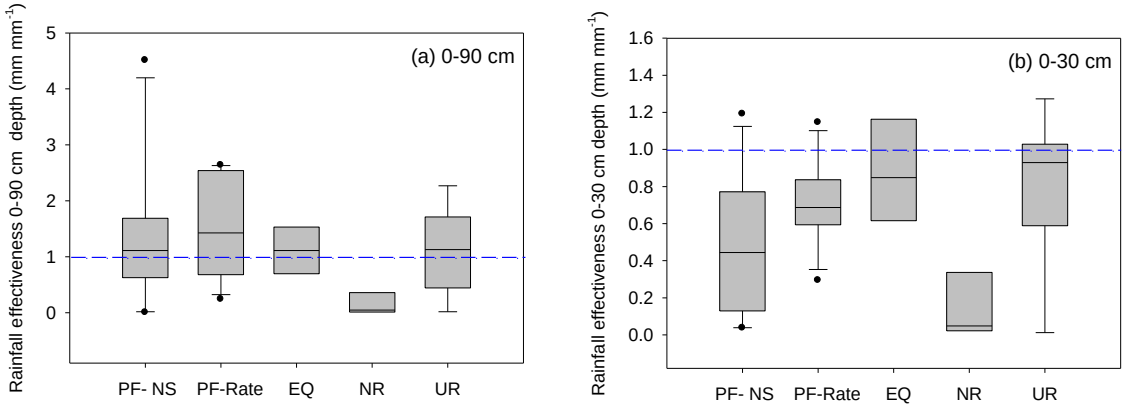

Figure 5.3-16 Effect of infiltration type on rainfall effectiveness (a) 0 – 90 cm depth, (b) 0 – 30 cm depth. Note Blue dashed line at 1.0 indicates rainfall = change in soil moisture.

5.3.7 Effect of antecedent soil moisture and preferential flow on rainfall effectiveness

A weak but significant (p<0.05, df 47) relationship existed between the amount of precipitation and amplitude (change in soil moisture following rainfall). Normally it would be expected that a 1:1 relationship with a high R^2 value would occur between rainfall and amplitude, however Figure 5.3-17 demonstrates the relationship between rainfall magnitude and the change in soil moisture was poor (R^2 0.47 at 0 - 90 cm).

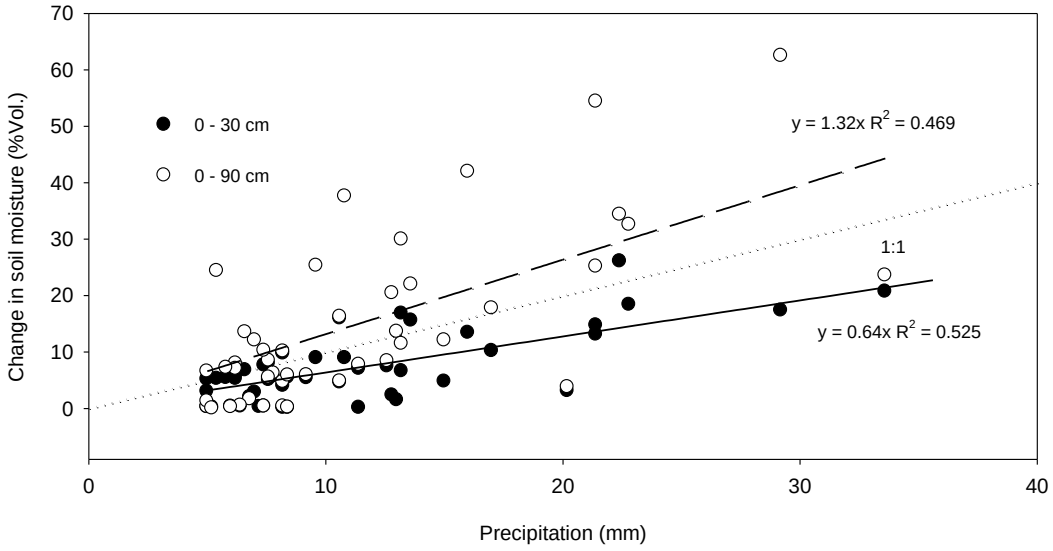

Figure 5.3-17 Relationship between precipitation and change in soil moisture. Dotted line represents the 1:1 ratio.

Rainfall effectiveness values greater than one (Figure 5.3-15) result from more water entering the soil profile than the rainfall magnitude, usually due to run-on from upslope areas, subsurface lateral flow or the location of preferential pathways within the measurement distance of the soil moisture probe. Values greater than 1.0 between September 2007 and November 2008 may also have resulted from differences in precipitation between the monitoring site and the meteorological station located 5.02 km away at Cambridge. Values lower than 1.0 were attributed to losses resulting from runoff, subsurface lateral flow and infiltration below the soil profile or root zone.

Rainfall effectiveness was not related to either antecedent soil moisture prior to rainfall or the occurrence of preferential flow. No significant relationship existed between antecedent soil moisture and rainfall effectiveness (Figure 5.3-15 and Figure 5.3-16) for either the effective rooting zone (0-30 cm – not presented) or the whole soil profile (0-90 cm).

However, variance in rainfall efficiency decreased with increased antecedent soil moisture associated with fewer preferential flow events and greater occurrence of EQ events. Multiple linear regression demonstrated that no significant relationship existed between antecedent soil moisture (0 – 90 cm) and rainfall effectiveness for any of the five infiltration response types. One way ANOVA further demonstrated that no significant difference in rainfall effectiveness existed between the two preferential flow infiltration response types (PF-NS and PF-Rate) and the equilibrium flow response (EQ) (Figure 5.3-16).

5.4 Conclusion

The ability to extrapolate results from a single soil moisture probe was limited by the small field of detection (10 cm) of the EnviroSCAN sensors. Analysis of variance in dye stained infiltration pathways demonstrated the REA or REV existed at an analytical width of approximately 60 cm, equivalent to the use of three EnviroSCAN probes. However given the similarity in the proportion of dye stained soil with depth of the four field sites, it was concluded that relative values of soil moisture could be extrapolated from a single soil moisture probe to other texture contrast soils with similar structure.

High frequency soil moisture monitoring during the dye staining experiments demonstrated that infiltration at low antecedent moisture, resulted in wetting front velocities as high as 6,000 mm hr^{-1} at site B, and 12,000 mm hr^{-1} at site D. While these values were two to four orders of magnitude higher than the saturated hydraulic conductivity of the soil, they were within the range of values reported for preferential flow in the literature. At high antecedent soil moisture, wetting front velocities did not exceed 500 mm hr^{-1} due to dominance of uniform infiltration and redistribution processes.

The sequence of five rainfall events between June 2008 and July 2008 demonstrated that as antecedent soil moisture increased with each rainfall event, the occurrence of preferential flow diminished and equilibrium flow established by the fifth rainfall event.

Soil moisture response to 47 rainfall events between September 2007 and August 2009 were able to be classified into five infiltration response types. Preferential flow was not related to the amount of rainfall or rainfall intensity, rather preferential flow demonstrated a threshold like relationship with antecedent soil moisture. When antecedent soil moisture was below approximately 225 mm (0 - 70 cm) infiltration was highly likely to result from preferential flow, however when antecedent soil moisture was above 245 mm (0 - 70 cm), infiltration was likely to result from equilibrium flow. This soil moisture threshold corresponded to 70 % - 76 % of total soil water, and 49 % - 60 % of PAWC.

The amount of rainfall was found to be poorly correlated with the change in soil moisture (R^2 0.47). Rainfall effectiveness (change in soil moisture divided by precipitation) was not significantly related to either antecedent soil moisture or the occurrence of preferential flow. This was unexpected as it was assumed that the poor relationship between the change in soil moisture and rainfall resulted from preferential flow at low antecedent conditions.

Results from the soil moisture monitoring clearly indicate that the preferential flow observed in the dye staining experiments was not an artefact of methodology, and that preferential flow occurred following rainfall when antecedent soil moisture was below approximately 50 – 60 % PAWC. The extremely rapid velocity of the wetting front at low antecedent soil moisture has implications for the offsite movement of agrochemicals.

5.5 Key Points

- Analysis of CV from dye staining patterns indicated that REA or REV existed at an analysis width of 60 cm, equivalent to the use of three EnviroSCAN soil moisture probes.
- Extrapolation of absolute values from the single soil moisture probe were limited by the small sphere of influence of the soil moisture sensors, however extrapolation of relative values from a single soil moisture probe to similarly structured texture contrast soils was supported.
- High frequency soil moisture monitoring can be used to detect the presence of preferential flow following rainfall or irrigation.
- Soil moisture response to rainfall was able to be classed into two preferential flow types (PF-NS & PF-Rate), equilibrium flow (EQ), an unknown flow response (UK) and a non response class (NR).
- Occurrence of preferential flow was not influenced by rainfall magnitude or rainfall intensity.
- Occurrence of preferential flow had a threshold based relationship with antecedent soil moisture. At the soil moisture monitoring site, preferential flow was highly likely to occur when rainfall occurred on soil with an antecedent soil moisture below 225 -245 mm, (0-70 cm depth), which corresponded to approximately 49 % - 60 % of PAWC.
- Preferential flow resulted in infiltration to 90 cm depth, whilst equilibrium flow did not occur below 50 cm depth.
- At low antecedent soil moisture content, estimated flow rates between 10 cm and 70 cm depth were as high as 6,000 mm hr^{-1} at site B, and 12,000 mm hr^{-1} at site D.
- Estimated flow rate between 10 cm and 30 cm depth at high antecedent soil moisture did not exceed 330 mm hr^{-1}.
- Preferential flow resulted in a step like reduction in amplitude (change in soil moisture) to 50 cm depth.

6.0 Effect of antecedent soil moisture and preferential flow on hydraulic conductivity and porosity

6.1 Introduction

In chapters four and five, dye staining and soil moisture monitoring demonstrated that antecedent soil moisture content had a significant effect on the occurrence of preferential flow and the velocity of the wetting front during infiltration. In this chapter the soil properties responsible for soil water storage, and soil water movement were further investigated to;

I. Determine the effect of antecedent soil moisture on soil water storage, porosity and hydraulic conductivity.
II. Assess how different analytical approaches affect measured values of porosity and hydraulic conductivity.
III. Explore how and why soil hydraulic properties vary between soil horizons and field sites.
IV. Derive input parameters for soil water modelling (reported Chapter 8).

Many methods have been developed to measure soil hydraulic properties. Differences in methodology often affect measured values due to variation in: sample volume, soil disruption, confinement (soil cores), boundary conditions, or initial soil moisture content, (Beven 2000; Davis *et al.* 1999; McKenzie and Cresswell 2002). For example Davis *et al.* (1999) found that increasing core size from 230 cm^3 to 11,700 cm^3 increased calculated values of saturated hydraulic conductivity by one to three orders of magnitude, and Cox and McFarlane (1995) found the saturated hydraulic conductivity of the B horizon in a texture contrast soil varied by as much two orders of magnitude over a 10 meter distance. Care therefore needs to be taken in the selection of methodology and presentation of results to ensure that assumptions associated with methodology are valid with respect to interpretation of results and their use in soil water models.

In this chapter, preference has been given to the selection of *in situ* techniques, or techniques which require minimal changes to the initial soil moisture content prior to measurement. The selection of both laboratory and field techniques was limited by: (i) presence of sand infills and large clay columns which restricted the use of many laboratory and small-scale field approaches, (ii) availability of existing equipment (iii) capacity to manufacture equipment from readily available materials. Where possible, field and laboratory techniques followed the procedures detailed in *Soil Physical Measurement and Interpretation for Land Evaluation* (McKenzie *et al.* 2002a) as many of the techniques presented in this book have been developed or tested using 'difficult' Australian soils.

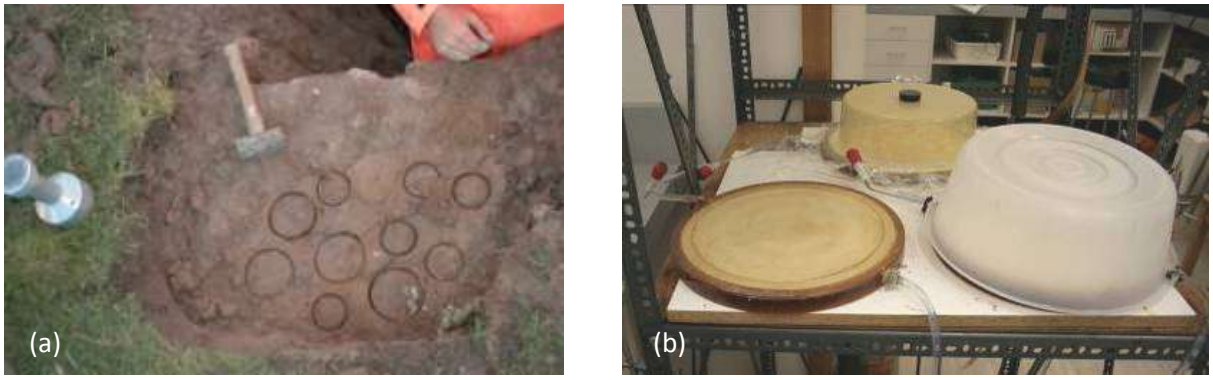

Figure 6.1-1 Determination of soil water characteristic, (a) Obtaining core samples (b) suction plates

Table 6.1-1 Selected sampling depths (cm) for determination of the soil water characteristic and hydraulic conductivity.

Depth (cm)	Site A	Site B	Site C	Site D
0-10	A1	A1	A1	A1
10-20			A2	
20-30		A2	B21	B21
30-40	B21	B21		
40-50				
60-70	B22		B22	B22
70-80		B22		
80-90				
90-100		B23	B23	
100-110				B23
110-120	B23	B23		

6.2 Methodology

6.2.1 Soil water characteristic

The soil water characteristic describes the relationship between the soil water content and matric potential. At matric potentials close to saturation (ψ = 0) soil water content is controlled by macroporosity, while at more negative potentials, water retention is controlled mainly by soil texture (particle size) and mineralogy (Cresswell 2002). The soil water characteristic may be used to predict pore size distribution (Laplace equation), hydraulic conductivity (Mualem 1976) or input parameters for soil water modelling (van Genuchten *et al.* 1991). The soil water characteristic was determined in order to derive parameters for soil water modelling (Chapter 8) and determine differences in pore size distribution, and soil water storage.

6.2.1.1 Determination using suction plates and pressure chambers

The soil water characteristic was determined using suction tables and pressure chambers according to in Cresswell (2002) and Reynolds and Topp (2008) (Figure 6.1-1). Details of sample size and equilibration potentials are provided in Table 6.2-1 and Table 6.1-1. Note: sampling was conducted on a diagnostic horizon basis rather than standard depth basis, in which soil within horizons is assumed to have similar physical properties and hydraulic characteristics (Belanger and Van Rees 2008). Further details of the procedures are provided in Appendix 6.0.

Table 6.2-1 Equilibration potentials and sample type used for determining the soil water characteristic.

Technique	Sample Type	Equilibration potential - matric potential (-kPa)									
Suction plates (desorption)	100 x 75 mm intact core	1	3	5	10						
500 kPa pressure chamber	60 x 35 mm intact core				10	30	100	300			
1500 kPa pressure chamber	<2 mm Ground sample							300	500	1000	1500

Soil moisture storage and thresholds were determined from the soil water characteristic, in which saturation (SAT) was determined as the soil moisture content at ψ =0 kPa, field capacity (FC) at ψ =10 kPa, and the permanent wilting point (PWP) at ψ =1500 kPa.

Plant available water content (PAWC) was determined as the water stored between field capacity (FC) and the permanent wilting point (PWP), and drainable porosity (DP) was determined as the soil water stored between saturation (SAT) and field capacity (FC).

Pore size distribution was approximated by the Laplace equation (Cresswell 2002),

EQ 6.1 $d = 30 / \psi_m$

d = equivalent pore diameter (μm)

ψ_m = absolute value of matric potential (meters).

The following pore size classes have been used to determine contribution to total porosity based on the pore functionally approach by Wilson *et al.* (1992);

- Macropore, ψ > -1.0 kPa, or pores > 300 μm
- Mesopores, between -1 kPa and -30 kPa, or pores between 30 – 10 μm
- Micropore, ψ < -30 kPa, or pores < 10 μm

6.2.1.2 Determination of the soil-water relationship by evaporation.

The evaporation technique has routinely been used to derive K(θ) and ψ(θ) relationships and input parameters for multiple pore domain models (Köhne *et al.* 2002; Schindler and Muller 2006; Wind 1968), however it has not been widely used in Australia. The technique is based the measurement of the water potential gradient between two tensiometers and the mean water content from a soil column during free evaporation (Richard *et al.* 2001; Wendroth and Wypler 2008). The water retention characteristic is derived from paired consecutive soil water content and matric potential gradient data using either iterative procedures (Tamari *et al*. 1993; Wendroth and Wypler 2008; Wind 1968) or inverse solutions (Eching *et al.* 1994; Simunek *et al.* 1998d). The effective range of the evaporation approach is between -5 kPa and -80 kPa depending on tensiometer accuracy, soil texture and evaporation rate (Richard *et al.* 2001). Stolte (1994) found the evaporation approach gave comparable results to four other techniques while Wendroth et al. (1993) described the technique as being simple, elegant and inexpensive (Figure 6.2-1).

The soil water characteristic was determined by the INITMH.EXE and WRET2MH.EXE software (supplied by Ole Wendroth), in which the geometric mean matric head (ψ) was calculated according to (further details Appendix 6.1.).

Figure 6.2-1 Determination of soil water characteristic and unsaturated hydraulic conductivity using the evaporation approach. (a) Core setup during initial equilibration, note use of Vaseline to provide flexible seal between the tensiometers ad the metal core, (b) Setup of logger, scales and core.
Note clamp to suspend cables (minimise their effect on cumulative weight loss), and fan to assist evaporation of sandy soils.

EQ 6.2 $\psi = 10^{\gamma}$

$$\gamma = (\log_{10} \psi 1.5(t_i) + \log_{10} (\psi 1.5(t_{i+1}) + \log_{10} \psi 4.5(t_i) + \log_{10} \psi 4.5(t_{i+1}))/4$$

and the arithmetic mean volumetric moisture content θ was calculated according to,

EQ 6.3 $\theta = (\theta 1.5(t_i) + \theta 1.5(t_{i+1}) + \theta 4.5(t_i) + 4.5(t_{i+1}))/4$

$\psi_{1.5}$ = Matric head upper tensiometer (kPa).

$\psi_{4.5}$ = Matric head lower tensiometer (kPa).

$\theta_{1.5}$ = Volumetric moisture content upper tensiometer ($m^3\ m^{-3}$).

$\theta_{4.5}$ = Volumetric moisture content lower tensiometer ($m^3\ m^{-3}$).

t_i = Initial data pair.

6.2.2 Laboratory determination of unsaturated hydraulic conductivity by evaporation

Unsaturated hydraulic conductivity (K) was calculated from evaporation data, according to Darcy-Buckinham's law (Wendroth *et al.* 1993; Wendroth and Wypler 2008). The procedure assumed quasi steady-state conditions over time in which flux and hydraulic gradient are approximately constant over time, in which the water content decreased linearly with depth (Schindler and Muller 2006).

These assumptions have been reviewed for a broad range of soil textures by Schindler and Muller (2006) and Wendroth *et al.* (1993). Due to potential errors associated with the measurement of matric potential with tensiometers, calculation of unsaturated hydraulic conductivity was restricted to matric potential gradients greater than 0.2 cm cm^{-1}. Unsaturated hydraulic conductivity was calculated by;

EQ 6.4 $K(h) = \Delta V / (2A.\Delta t.i_m)$

$$i_m = 0.5((\psi 1.5(t_i) - \psi 4.5(t_i) / \Delta z) + (\psi 1.5(t_{i+1}) - \psi 4.5(t_{i+1}) / \Delta z))^{-1}$$

i_m = Mean hydraulic gradient in the interval $cm^3\ cm^{-1}$.

ΔV = Evaporated soil water volume = mass change (g).

A = Cross sectional area of the sample (mm^2).

Δt = Time interval (min).

Δz = Vertical distance of tensiometers (mm).

ψ1.5 = Matric head upper tensiometers (1.5 cm) (hPa).

ψ4.5 = Matric head lower tensiometers (4.5 cm) (hPa).

t_i = Initial time interval (min).

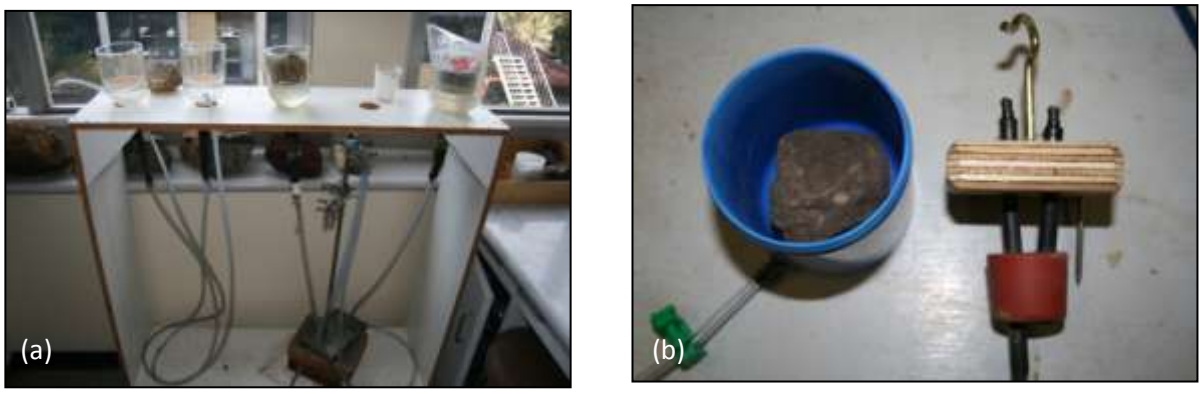

Figure 6.2-2 Preparation of samples for balloon determination of SSCC, (a) Wetting up soil clods using Haines apparatus, (b) Suction vial for getting soil clods into the balloons, and setup apparatus showing inflow and outflow tubes.

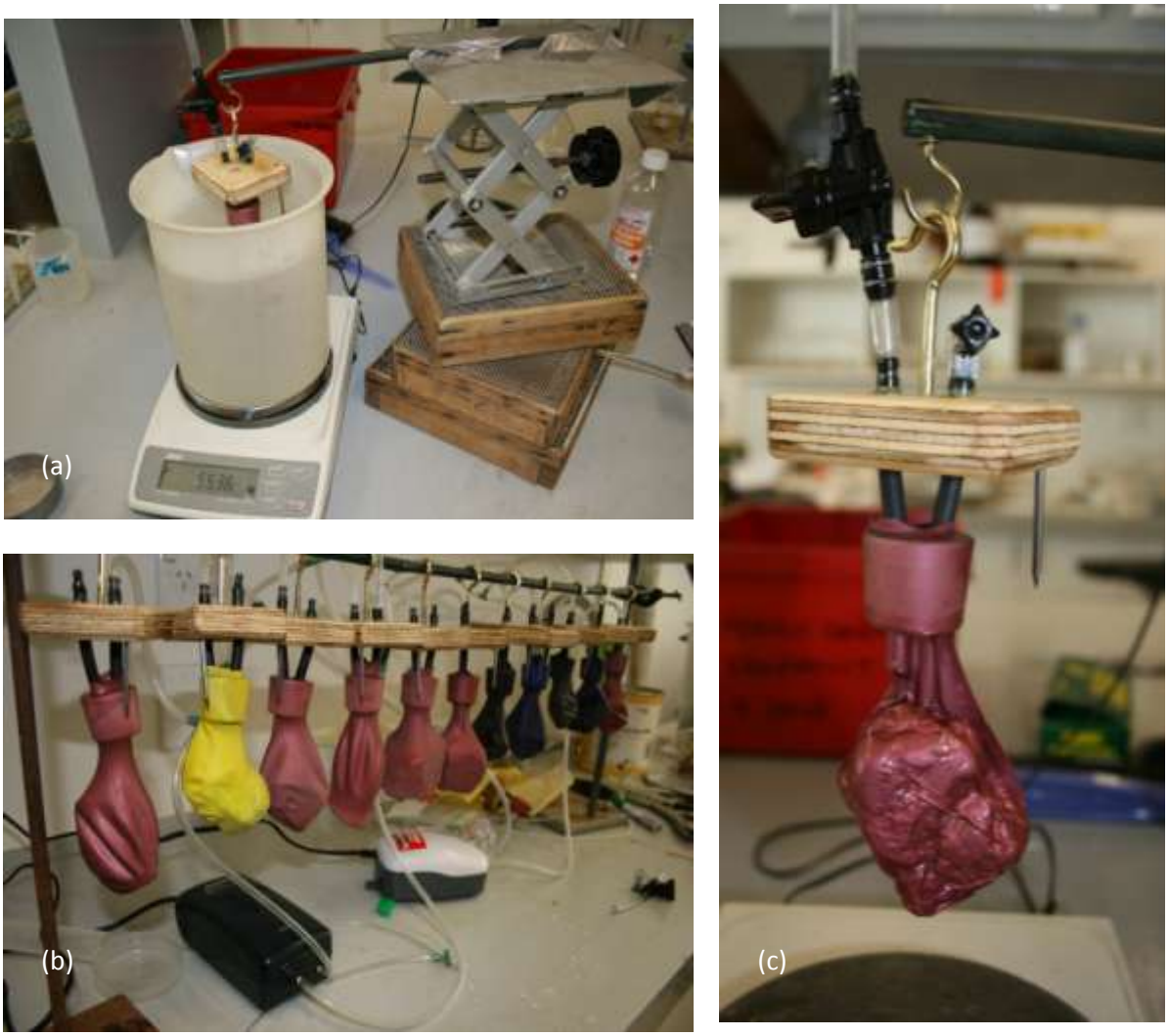

Figure 6.2-3 Balloon technique for determination of SSCC. (a) Measurement of soil clod volume by Archimedes principle. (b) Drying multiple soil clods with aquarium air pumps. (c) Air evacuated from soil clod, photographed following immersion to determine volume.

6.2.3 Effect of soil moisture content on volumetric shrinkage and soil density

Bulk density was determined to allow for calculation of soil water desorption, volumetric soil moisture content, and saturated hydraulic conductivity. However the vertic nature of the clay subsoils meant that values of bulk density were dependent on moisture content at the time of sampling.

Cresswell (2002) suggested the relationship between bulk density and soil moisture can be determined by measuring soil volume with callipers during desorption, however this approach is somewhat cumbersome and would have interfered with the measurement of the soil water characteristic and saturated hydraulic conductivity. An alternative approach was tested in which the relationship between clod density and gravimetric moisture content was determined from the soil shrinkage characteristic curve (SSCC) using the 'balloon technique' described by Tariq and Durnford (1993) and Cornelis *et al.* (2006).

Traditionally the SSCC has been determined using Saran^{tm} coated clods however Tariq and Durnford (1993) developed an alternative approach in which the soil is wrapped in a rubber balloon and dried with an aquarium air pump. Paired measures of soil mass and volume were taken over a two to three week period in which soil clods were gently dried by slow airflow over the clod supplied by an aquarium pump. Soil volume was determined by evacuating air from the balloon, causing it to shrink around the clod. The evacuated clod was immersed in water and the change in mass related to volume via Archimedes' principle (Figure 6.2-2 and Figure 6.2-3). Review of the procedure found the balloon method was simpler and in some aspects superior to other approaches (Cornelis *et al.* 2006). Analysis was conducted on five intact clods (26 to 133 cm^3) collected from each of four horizons between 20 cm and 100 cm at sites A and B. Further details of the technique including calculation of iterative clod volume and density are provided in Appendix 6.2. Clod porosity, void ratio and moisture ratio were calculated according to;

Clod porosity

EQ 6.5 $\Phi_{clod} = 1- (D_{ci} / D_p)$

Void ratio

EQ 6.6 $e = V_{pores} / V_{solids}$

$e = \Phi_{clod} / (1- \Phi_{clod})$

Moisture ratio

EQ 6.7 $v = V_{water} / V_{solids}$

$v = M_{gi\,X}\, D_p$

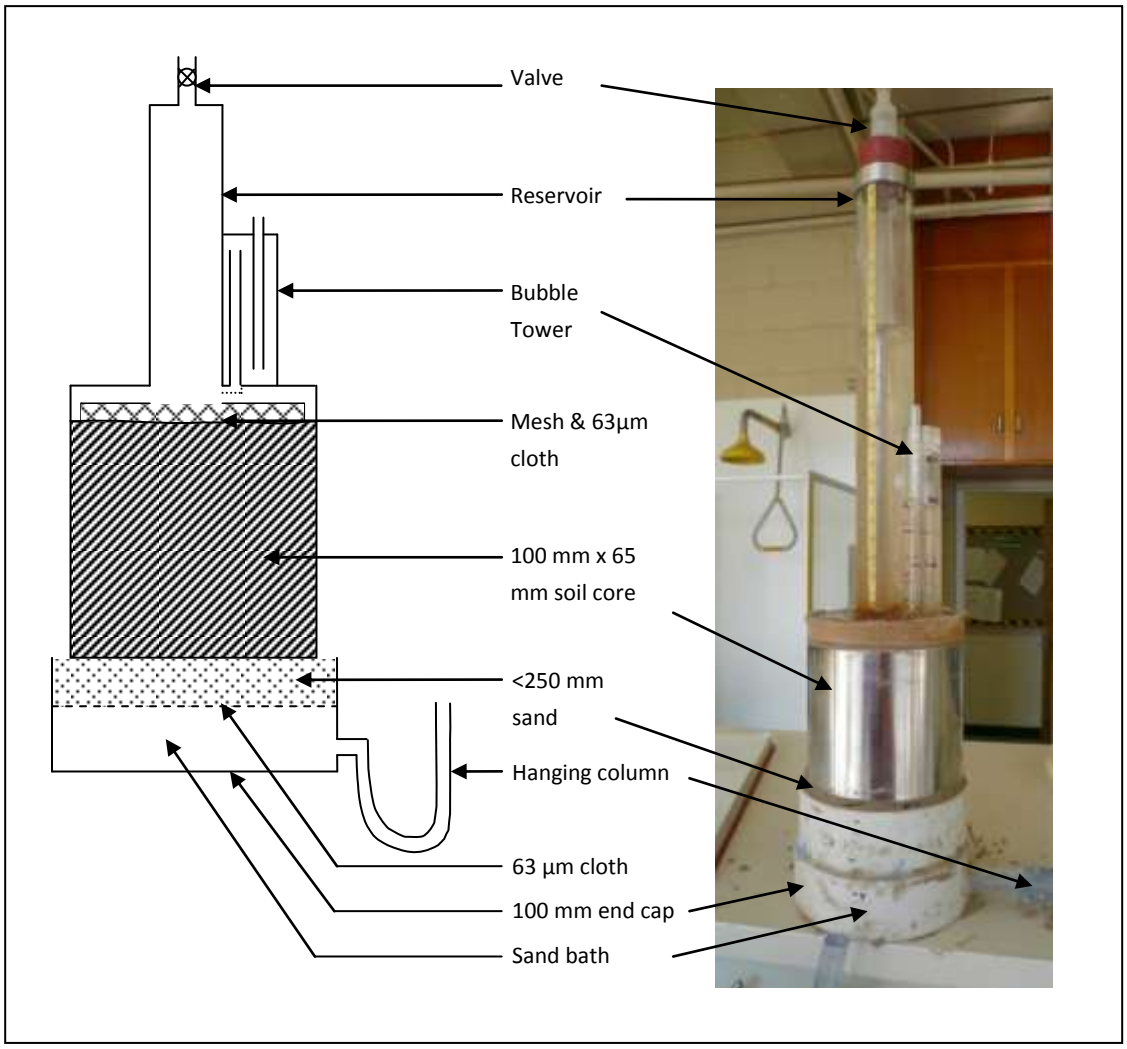

Figure 6.2-4 Measurement of unsaturated hydraulic conductivity on intact cores, using a mini disk permeameter and a sand bath hanging column apparatus to apply a constant supply potential.

Figure 6.2-5 Determination of saturated hydraulic conductivity using constant head approach on 100 mm diameter intact soil cores. Note foil to prevent evaporation on soils with slow flow rates**.**

D_p = Particle density 2.65 (g cm^{-3}).

D_{ci} = Iterative clod density on oven dried basis (g).

M_{gi} = Iterative gravimetric soil moisture (g g^{-1}).

Φ_{clod} = Iterative intra-clod porosity (cm^3 cm^{-3}).

e = Void ratio.

v = Moisture ratio.

V_{pores} = Volume of pores (cm^3).

V_{solids} = Volume of solids (cm^3).

6.2.4 Laboratory determination of unsaturated hydraulic conductivity K(ψ) - disk permeameter

Following soil water desorption, the upper and lower faces of the 100 mm x 75 mm soil cores were re-picked to expose soil pores damaged or occluded during the desorption process. Unsaturated hydraulic conductivity was determined using 100 mm diameter 'mini-disk' permeameters, based on the procedure by Cook (2008) and McKenzie *et al.* (2002c) (Figure 6.2-4). The soil was allowed to equilibrate with the supply potential over a half to five day period. Measurements were recorded over a 30 minute to three day period depending on flow rate.

By applying the same supply potential (ψ) to both the top and bottom of the core, calculation of near saturated hydraulic conductivity was simplified to the steady state water flux density or discharge rate from the hanging column (Cook 2008);

EQ 6.8 $$K\psi = q / \pi r^2 = C (R - R_i) / \pi r^2$$

$K\psi$ = Unsaturated hydraulic conductivity (mm hr^{-1}).

q = Infiltrated volume (mm^3).

r = Radius of contact material (mm).

C = Supply reservoir calibration (mm^3 mm^{-1}).

R = Sequential scale reading (mm).

R_i = Initial scale reading (mm).

$\Psi_{x,y}$ = Successive supply potentials (mm).

$q_{x,y}$ = Successive infiltrated volume (mm^3).

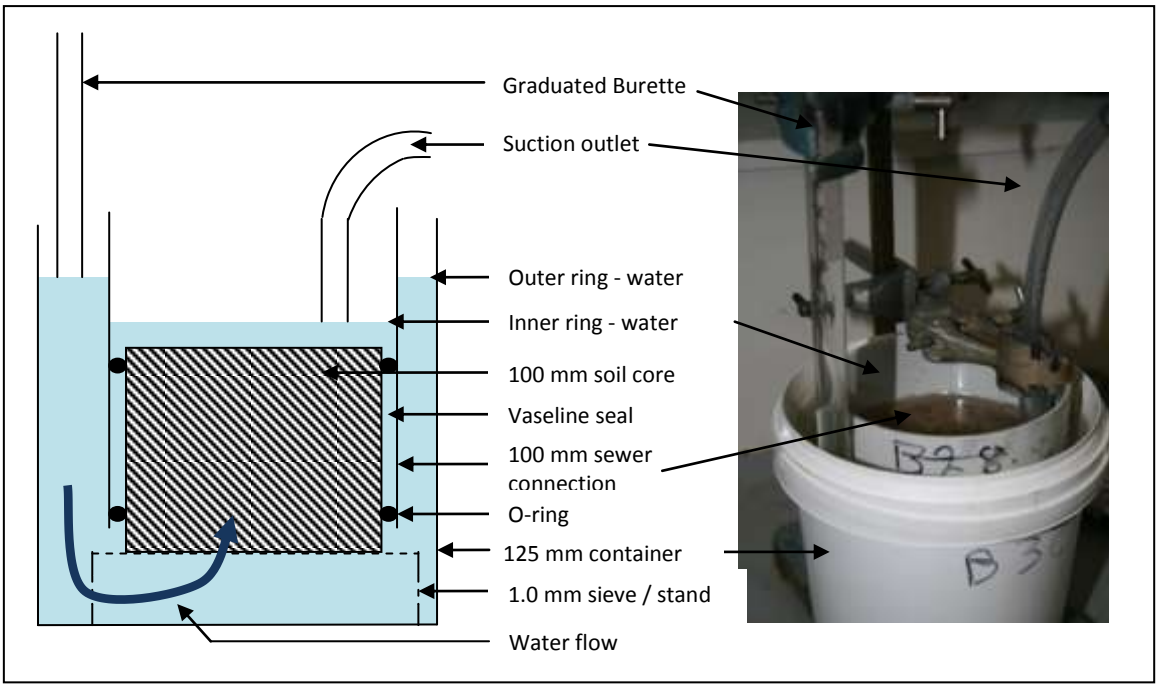

Figure 6.2-6 Design of constant head apparatus for determination of saturated hydraulic conductivity on 100 mm diameter intact cores.

Figure 6.2-7 Use of dye staining to investigate higher than expected flow rates. Note plume of dye originating from a macropore (upper left).

6.2.5 Laboratory determination of saturated hydraulic conductivity (Ksat)

Following determination of unsaturated hydraulic conductivity with the mini-disk permeameters (Chapter 6.2.4), saturated hydraulic conductivity (K_{sat} ψ = +10 mm) was determined using a simplified version of the procedure of McKenzie *et al.* (2002c) (Figure 6.2-5 and Figure 6.2-6). The 100 mm x 75 mm cores were held within a 100 mm PVC sewer pipe connection using large rubber o-rings. The space between the sewer pipe connection and the core was filled with melted Vaseline to ensure water could not pass along the outside of the core.

The core was placed on a 1.0 mm sieve inside a 120 mm diameter container. Water treated with 0.01 M $CaCl_2$ was sequentially added to raise the height of water in the outer ring (between the container and soil core) over a two day period to minimise air encapsulation and clay dispersion. Once water had emerged in the inner ring (above the core), the water level in the outer ring was maintained 10 mm above the height of water in the inner ring (Figure 6.2-6) to impose an upwards ψ +10 mm supply potential. If infiltration was faster than expected, Brilliant Blue dye tracer (C.I. Food Blue 42090) was added to the outer ring to determine if flow resulted from macropore flow or leakage along the wall of the metal core (Figure 6.2-7). Hydraulic conductivity was calculated from Darcys law as,

EQ 6.9 $$K_{sat\ (\psi\ +10mm)} = Q\Delta z / Ad$$

$K_{sat\ \psi+10mm}$ = Saturated hydraulic conductivity at +10 mm potential (mm hr^{-1}).

Q = Flow through core (mm^3 hr^{-1}).

Δz = Length of core (mm).

A = Surface area of core (mm^2).

d = Difference in height of water between inner and outer core (mm).

Values of hydraulic conductivity determined from intact soil cores are likely to differ to those obtained by *in situ* methods, as prolonged wetting and saturation were expected to overcome the effects of water repellence, and caused vertic clays to swell.

6.2.6 Field determination of unsaturated hydraulic conductivity and infiltration – disk permeameters

Disk permeameters or tension infiltrometers enable *in situ* determination of near-saturated hydraulic conductivity from quasi steady-state infiltration through a porous membrane on which a constant negative tension is applied through a secondary bubbling tower (White *et al.* 1992).

Figure 6.2-8 (a) Recently constructed tension infiltrometer with multiple tube bubble tower to enable rapid change in supply potential. Measurement of subsoil unsaturated hydraulic conductivity, (b) site C, and (c) site B.

Tension infiltrometers may also be used to estimate pore size distribution and contribution to flow using the Laplace equation (Moret and Arrué 2007), and to derive parameters for soil water modelling using inverse parameterisation techniques (Simunek *et al.* 1998c). The principle advantage of tension infiltrometers over laboratory techniques is that measurements are performed *in situ*, which allows exploration of the dependence of hydraulic properties on soil structure and antecedent soil moisture (Hussen and Warrick 1993; Vandervaere *et al.* 2000).

Four disk permeameters were constructed with a modified bubble tower containing six air tubes set to preset depths in order to enable rapid repeatable change in supply potential (Figure 6.2-8a). The bubbling towers were calibrated using a <250 µm sand tension table following the approach of McKenzie *et al*. (2002b). Unsaturated hydraulic conductivity was measured for each soil horizon in both the wet and dry soil moisture treatments using up to three of the original CSIRO disk permeameters and up to four of the newly designed tension infiltrometers (Figure 6.2-8 to Figure 6.2-10).

Cumulative infiltration was measured near the upper boundary of the A1, A2 (where present), B21 and B22, and B23 horizons at all sites at low antecedent soil moisture, and the A1, A2 (where present), B21 and B22 horizons at high antecedent soil moisture. The B23 was not measured in the wet treatment as change in soil moisture below 80 cm depth was minimal. Setup and operation of the tension infiltrometers followed a modified procedure to that described by Lin and McInnes (1995), Lin *et al.* (1997), and McKenzie *et al.* (2002b) in which apparent steady state infiltration rates were measured at supply potentials (ψ) of -1.34, -0.84, -0.54, -0.24, -0.14, and -0.12 kPa using rainwater treated with 0.01 M $CaCl_2$ to prevent dispersion (detailed Appendix 6.3).

Unsaturated hydraulic conductivity was calculated according to the procedure developed by Ankeny *et al.* (1991), and Reynolds and Elrick (1991) detailed in McKenzie *et al.* (2001). The principle advantage of the method described in McKenzie *et al.* (2001) is that unsaturated hydraulic conductivity can be calculated from infiltration at different tensions while avoiding the practical difficulties associated with estimation of sorptivity from early time flow (White and Sully 1987; White *et al.* 1992). Hussen and Warrick (1993) found the Reynolds and Elrick (1991) approach gave fast reliable results compared to four other approaches for determining hydraulic conductivity.

Infiltration was determined by linear regression of the steady state infiltration vs time (provided $R^2 > 0.995$). Unsaturated hydraulic conductivity was determined by calculation of infiltration (q), and shape parameters (α & P), for each sequential supply potential, according to EQ 6.1.

Figure 6.2-9 Picked back surface of B21 horizon , dry treatment, showing soil cracks, sand infills and red headed cockchafer beetle burrows (1 cm diameter 1 cm deep cylindrical holes).

Figure 6.2-10 Measurement of hydraulic conductivity on the upper surface of the B21 horizon at site C.

EQ 6.10 $\alpha_{x,y} = \ln (q_x / q_y) / (\Psi_x - \Psi_y)$

$P = \Psi_x / (\Psi_x - \Psi_y)$

$K_{x,y} = (G_d \alpha_{x,y} q_x) / r(1 + G_d \alpha_{x,y} \pi r) (q_x / q_y)^P$

$Q = q / \pi r^2$

$K(\Psi) = K_{x,y} \exp (\alpha_{x,y} (\Psi_x + \Psi_y)/2)$

$\alpha_{x,y}$ = Alpha (soil structure parameter).

P = Shape parameter.

$K_{x,y}$ = Average K for data pairs.

$K(\Psi)$ = Unsaturated hydraulic conductivity (mm hr^{-1}).

Q = Cumulative infiltration (cm^3).

q = Infiltrated volume (cm^3).

r = Radius of contact material (cm).

$\Psi_{x,y}$ = Successive supply potentials (cm).

$q_{x,y}$ = Successive infiltrated volume (cm^3).

G_d = Shape parameter = 0.25.

Flow weighted mean pore diameter (FWMPD) was calculated according to Philip (1987), and Clothier, (2008)

EQ 6.11 $$\mathrm{FWMPD} = 7.4 \left[\ln \frac{K_2/K_1}{\psi_2 - \psi_1} \right]$$

FWMPD = Flow weighted mean pore diameter (mm).

K_1 = Hydraulic conductivity (mm hr^{-1}) at ψ_1.

K_2 = Hydraulic conductivity (mm hr^{-1}) at ψ_2.

ψ_1 = First supply potential (mm).

ψ_2 = Second supply potential (mm).

The number of pores (NP) of equivalent diameter per unit area of infiltration surface was calculated from Poiseuille's law according to Reynolds (2006; 2008),

EQ 6.12 $$NP = \frac{128 \mu K}{\pi \rho g \, (FWMPD)^4}$$

K = Hydraulic conductivity (cm s^{-1}).

μ = Dynamic viscosity - 1.002 g cm^{-1} s^{-1}.

ρ = Pore water density - 0.9982 g cm^{-3}.

g = Gravitational acceleration -980.621 cm s^{-1}.

Based on Clothier and White (1981) and Moret and Arrué (2007) contribution to flow from macropores, mesopores and micropores was determined from infiltration at available supply potentials. Functional macroporosity was said to exist at supply potentials greater than -0.39 kPa, mesopores between ψ -0.39 kPa and ψ -1.09 kPa, and micropores less than ψ -1.09 kPa. Differences in potential between the soil water characteristic and disk permeameters meant that the same pore size classes could not be used for both techniques. Differences in porosity also result from the soil water characteristic measuring available pore space, while the disk permeameter measures functional porosity. As Beven and Germann (1982) comment '*choice of an effective size to delimit macropores is necessarily arbitrary and is often related more to details of experimental technique than considerations of flow processes'.*

Flow weighted mean pore diameter (FWMPD) and the number of pores were classed according to pore size range based on the average supply potential between sequential values of hydraulic conductivity (note different pore size range to 6.2.1), where;

- Macropores = -0.16 kPa (-0.19 to -0.13 kPa).
- Large mesopores = -0.54 kPa and -0.29 kPa, (-0.69 to -0.39 kPa) and (-0.39 to -0.19 kPa).
- Small mesopores = -0.89 kPa (-1.09 to -0.69 kPa).

Differences in unsaturated hydraulic conductivity between sites were investigated using one way analysis of variance with Tukey post hoc test in SPSS v12. Differences in unsaturated hydraulic conductivity, FWMPD, and the number of pores between soil moisture treatments were investigated for data from all sites using independent T-test with Levene's test for equality of variance, and Tukey post-hoc tests to determine at which combination of supply potentials and sites significant differences existed.

6.2.7 Rate of soil swelling

The potential for soil swelling during infiltration to affect flow rates was investigated by monitoring cumulative infiltration at five supply potentials (ψ - 1.20 kPa, -0.80 kPa, -0.56 kPa, -0.20 kPa, and -0.18 kPa) over a 6 hour period at site A. Initial soil moisture averaged 0.058 m^3m^{-3}. Disks operating at supply potentials of -0.56 kPa, -0.20 kPa, -0.18 kPa had to be disturbed to be refilled.

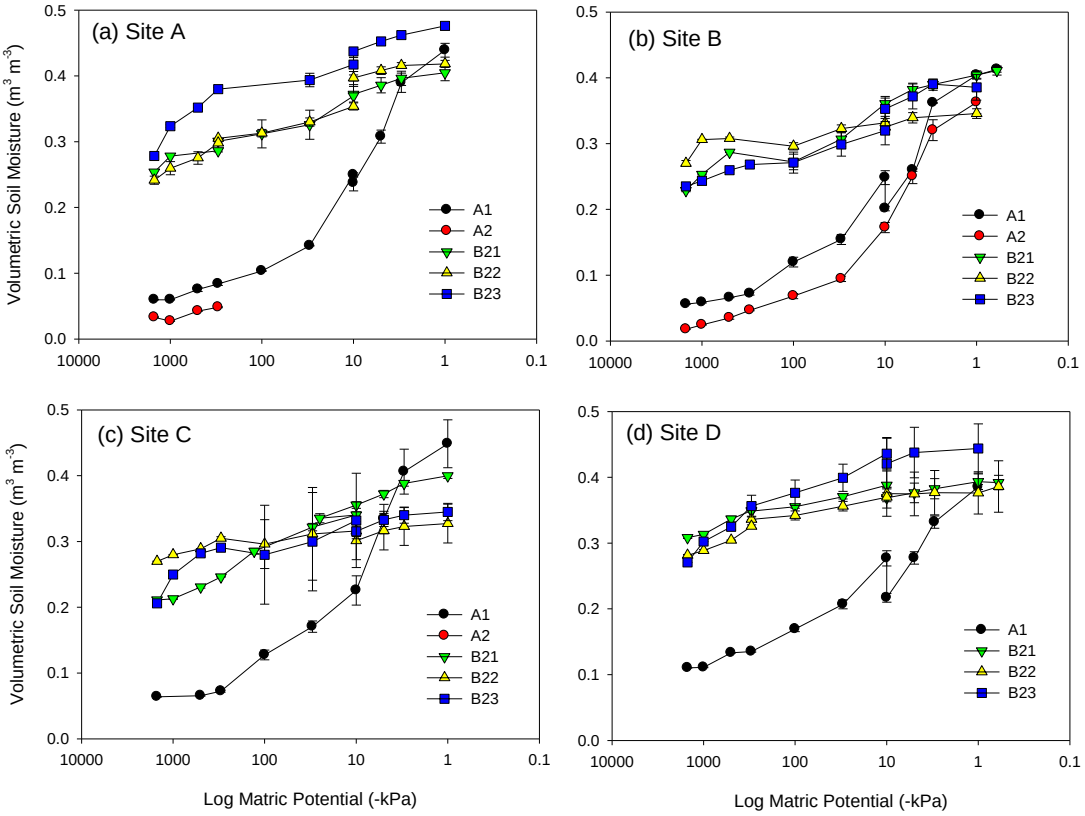

Figure 6.2-11 Soil water desorption, presented for each site (a) site A, (b) site B, (c) site C, (d) site D. Error bars represent ±1 standard error.

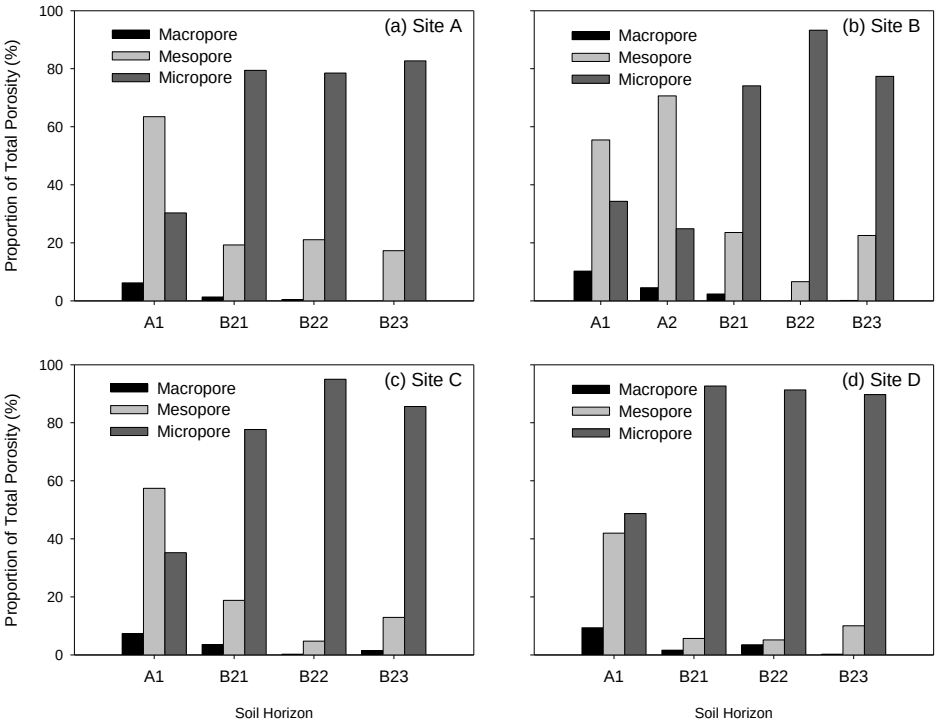

Figure 6.2-12. Macropore (0.0 <ψ >-1.0 kPa), mesopore (-1.0 <ψ > -30 kPa), and micropore (ψ<-30 kPa) contribution to total porosity (ψ = 0.0 kPa), (a) site A. (b) site B. (c) site C. (d) site D.

6.3 Results

6.3.1 Soil water characteristic - desorption ψ(θ)

The A1 horizons had a greater number of macro- and mesopores than the B2 horizons as indicated by the decrease in soil moisture with increased matric potential at all sites (Figure 6.2-11 and Figure 6.2-12). The A2 horizon (site B) had lower soil moisture content (porosity) than the A1 horizon, particularly between -10 kPa and -1500 kPa which was attributed to the lower clay content of the A2 horizon (Table 3.2-2). The soil water characteristics of the three B horizons were highly variable especially for samples determined by the 500 kPa pressure chamber. Variability was attributed to shrinkage preventing soil-plate contact in the pressure chamber, stickiness leading to loss of soil material during measurement, and difficulty wetting up vertic clays (note some clays required wetting over a 2 month period). The soil water characteristic of the three B2 horizons was relatively flat, particularly in the B22 horizon which indicated the B2 horizons had little porosity or soil water storage (Figure 6.2-11). Figure 6.2-12 demonstrated that macropores represent between 4.4 – 9.4 % of the total pore space in the A horizons and up to 3.5 % of pore space (mean 1.2 %) in the B2 horizons. Porosity in the A1 horizon was dominated by mesopores at sites A, B and C, however the higher clay and lower sand content at site D increased the proportion of micropores at site D.

Significant differences (p<0.05, df 15) in the average permanent wilting point (PWP), field capacity (FC) and drainable porosity (DP) existed between the five soil horizons. However one way ANOVA demonstrated that no significant difference (p<0.05, df 15) existed between the mean PAWC or mean saturated water content (SAT) of the five soil horizons (Figure 6.3-1). This analysis suggests that while all horizons had similar total porosity, the A1 and A2 horizons had greater drainable porosity (DP) (resulting from the presence of macropores between ψ 0 and -10 kPa) and lower PWP(due to lower clay content), than the B2 horizons. The plant available water content (PAWC) at site D differs to the other three sites, in the A1 horizon, the PAWC at site D (11.03 % vol.) was approximately twice that of the other three sites (5.60 – 6.39 % vol.), while the PAWC of the B21 horizon was approximately half (6.04 %vol.) that of the other three sites (11.84 - 14.41 % vol.). Data for each site and horizon is presented in Table 6.3-1.

Tennant *et al.* (1992) and McCown *et al.* (1976) argue that the traditional concept of available water as defined by the water held between field capacity and the permanent wilting point does not apply in texture contrast soils, as the water content in the A horizon is influenced by low subsoil permeability and development of perched watertables. Data presented in Table 6.3-1 was determined from the soil water characteristic rather than *in situ* monitoring and thus represents the available water in the absence of perched water tables.

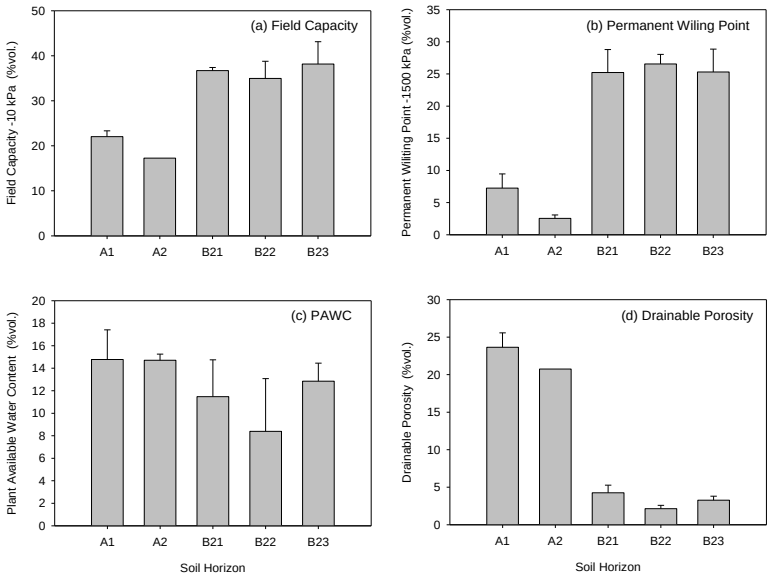

Figure 6.3-1 Mean values for all four sites; (a) Field capacity (FC). (b) Permanent wilting point (PWP). (c) Plant available water content (PAWC). (d) Drainable porosity (DP). Error bars represent ±1 SD.

Table 6.3-1 Soil water storage, PAWC and drainable porosity (% Vol.)

Site	Horizon	Saturation SAT (0 kPa)	Field capacity FC (1.0 kPa)*	Permanent Wilting Point PWP (1500 kPa)	Plant Available Water Content PAWC (1.0 -1500 kPa)	Drainable Porosity DP (0.0 – 1.0 kPa)
A	A1	46.80	23.71	5.97	17.74	23.09
	B21	41.00	37.21	25.37	11.84	3.79
	B22	42.00	39.68	24.14	15.54	2.32
	B23	47.60	43.73	30.04	13.69	3.87
B	A1	45.00	20.13	5.60	14.53	24.87
	A2	38.00	17.25	1.78	15.48	20.75
	B21	41.40	37.21	23.59	13.62	4.19
	B22	34.60	32.51	27.00	5.51	2.09
	B23	38.60	35.27	23.51	11.76	3.33
C	A1	48.40	22.55	6.39	16.17	25.85
	B21	41.43	35.53	21.13	14.41	5.90
	B22	32.80	30.12	26.97	3.15	2.68
	B23	35.00	31.54	20.60	10.94	3.46
D	A1	42.50	21.69	11.03	10.65	20.81
	B21	40.00	36.87	30.83	6.04	3.13
	B22	39.00	37.52	28.16	9.36	1.48
	B23	44.50	42.07	27.06	15.02	2.43
Average	A1	45.68	22.02	7.25	14.77	23.65
	A2	38.00	17.25	2.54	14.71	20.75
	B21	40.96	36.70	25.23	11.48	4.25
	B22	37.10	34.96	26.57	8.39	2.14
	B23	41.43	38.15	25.30	12.85	3.27

*Field capacity was determined from suction table data rather than the 5 bar pressure chamber ,as difficulty maintaining pressure was thought to have resulted in a 'jump' in values at -10 kPa.

Available water (0-100 cm) ranged from approximately 100 mm m^{-1} at site D, to 145 mm m^{-1} at site A. Tennant *et al.* (1992) notes there is little information available on the available water of texture contrast soils. Williams (1983) reported the PAWC of texture contrast soils ranged from as little as 25 – 100 mm in soils with sodic B horizons, and 120 – 230 mm in non-sodic texture contrast soils. As subsoils at all four sites were sodic (ESP>6) the amount of available water reported for the four texture contrast soils in this study are considerably greater than that determined by Williams (1983). Williams however notes that the main determinant of water storage was the water entry properties of the A and B horizons rather than their 'true' water holding capacities. Consequently values cited by Williams (1983) are likely to under predict the available water.

6.3.2 Soil-water relationship – evaporation technique

Comparison between soil water characteristics determined by desorption (Chapter 6.2.1.1) and evaporative approaches (Chapter 6.2.1.2) is presented for site B in Figure 6.3-2. Analysis of all sites indicated the evaporative approach predicted higher volumetric soil moisture in the A1 horizon between ψ -1.0 and -10 kPa, suggesting the evaporation approach was more sensitive to macroporosity than the desorption approach. In the B21 horizon, the two methods predicted similar soil water characteristics, although at site D, the evaporative approach resulted in lower soil water contents between -10 kPa and -100 kPa than the desorption approach. Discussion of the implications of methodology on prediction of van Genuchten parameters is presented in Chapter 8.0 on soil water modelling and parameterisation. The relationship between unsaturated hydraulic conductivity and matric potential is presented in Appendix 6.4.

6.3.3 Laboratory determination of saturated and unsaturated hydraulic conductivity

The hydraulic conductivity of the four B21 and B23 horizons demonstrated considerable variability between and within sites. Estimates of hydraulic conductivity differed by up to 2 orders of magnitude in the B21 horizon (Figure 6.3-4 b). Variability resulted from the flow through shrinkage cracks or pockets of sand infill within the core sample (Figure 6.3-3).

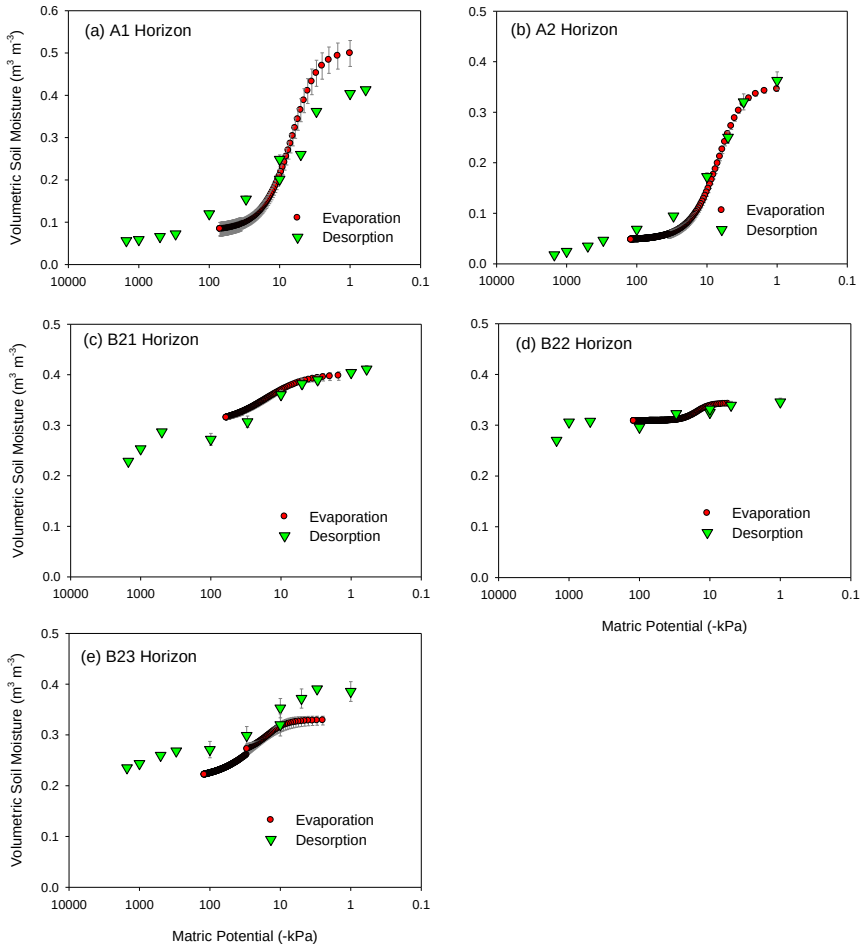

Figure 6.3-2 Comparison of soil water characteristics determined by desorption and evaporation. Data is presented for site B.

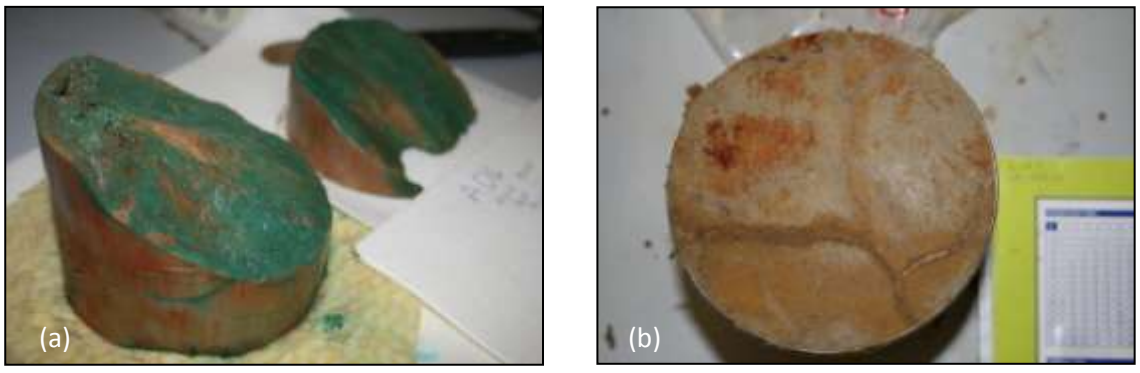

Figure 6.3-3 Difficulty with core based techniques (a) Dye tracer staining showing preferential flow through a shrinkage crack B21 horizon, during Ksat determination (ψ +10 mm). Estimated saturated hydraulic conductivity in this core was 29.7 mm hr^{-1} compared to 1.02 mm hr^{-1} (SD 1.21 mm hr^{-1}) for the other three cores. (b) Soil variability indicated by differences in colour resulting from sampling a sand infill.

Tennant *et al.* (1992) partly attributed the high variability in hydraulic conductivity of the B horizon in texture contrast soils to the presence of vertical and horizontal preferred pathways rather than differences in clay content. Dye staining demonstrated that in some cores, high values of hydraulic conductivity resulted from flow through large shrinkage cracks or slickensides which had not completely closed during prolonged saturation. Beven and Germann (1982) also reported cracks between structural peds may not close, even after prolonged wetting.

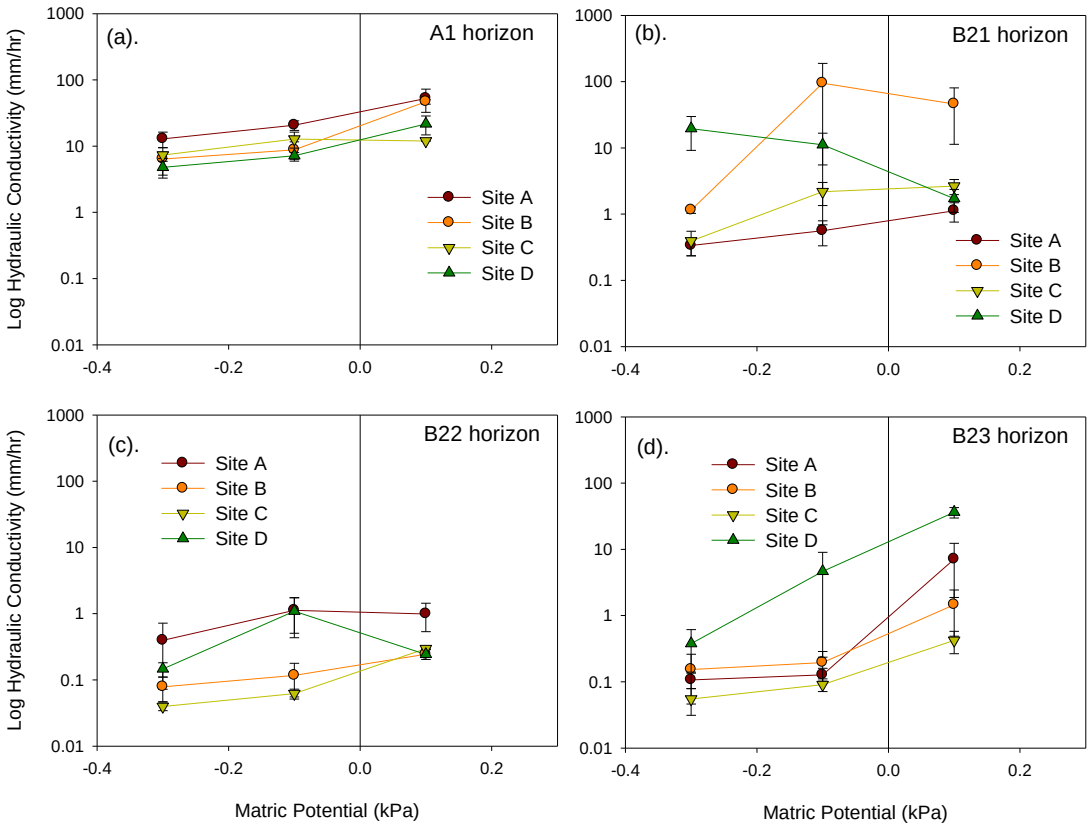

Figure 6.3-4 Saturated (ψ = +0.1 kPa) and unsaturated (ψ= -0.1 kPa & -0.30 kPa) hydraulic conductivity of 100mm diameter cores presented by horizon; (a) A1 horizon (b) B21 horizon (c) B22 Horizon (d) B23 horizon. Error bars represent ±1 standard error.

In the B21 horizon, hydraulic conductivity decreased between measurement of unsaturated (-0.1 kPa) and saturated hydraulic conductivity (+0.1 kPa) at sites D and B (also site D in the B22 horizon) (Figure 6.3-4). Possible explanations for this anomaly include; (i) clay swelling at higher soil moisture, (ii) blockage of pores by dispersed clay particles, (iii) blockage of pores by microbial growth. However soil was near field capacity prior to measurement at +0.1 kPa, and infiltrating water was treated with 0.01 M $CaCl_2$, and biological growth inhibitors.

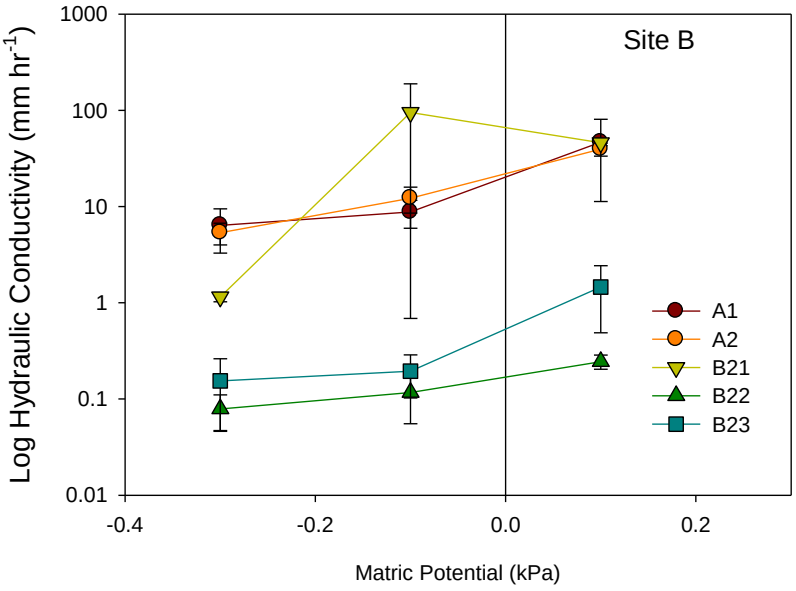

Figure 6.3-5 Saturated (ψ =+10 mm) and unsaturated (ψ= -10 &-30 mm) hydraulic conductivity of 100mm diameter cores at site B. Error bars represent ±1 standard error.

Figure 6.3-6 Development of finger flow beneath a tension infiltrometer during infiltration into soil at low antecedent soil moisture.

The A2 horizon at site B had a similar hydraulic conductivity to the A1 horizon, which indicates the two A horizons had similar proportions of functional macroporosity (Figure 6.3-5). This finding is supported by Figure 6.2-11 and Table 3.3-2 which demonstrated the A1 and A2 horizons had similar pore size distribution and particle size range despite having distinctly different consistence and structure (Chapter 3.3.2). The saturated hydraulic conductivity of the B22 and B23 horizons were approximately two orders of magnitude lower than that of the A1 and A2 horizons due to reduced macro and mesoporosity (Figure 6.2-12). However the hydraulic conductivity of the B21 horizon were generally higher than the other two B horizons, despite the similarity in particle size. The greater variability and higher rate of water movement in the B21 horizon were attributed to preferential flow through partly closed shrinkage cracks and sand infills (Figure 6.3-3). Detail of results from the 100 mm cores is presented in Appendix 6.5.

6.3.4 Rate of clay swelling resulting from infiltration from disk permeameters

The rate of cumulative infiltration from disk permeameters at five supply potentials did not influence infiltration over the six hour measurement period (Figure 6.3-7). Consequently values of hydraulic conductivity in vertic clay soils were not affected by volume change during infiltration.

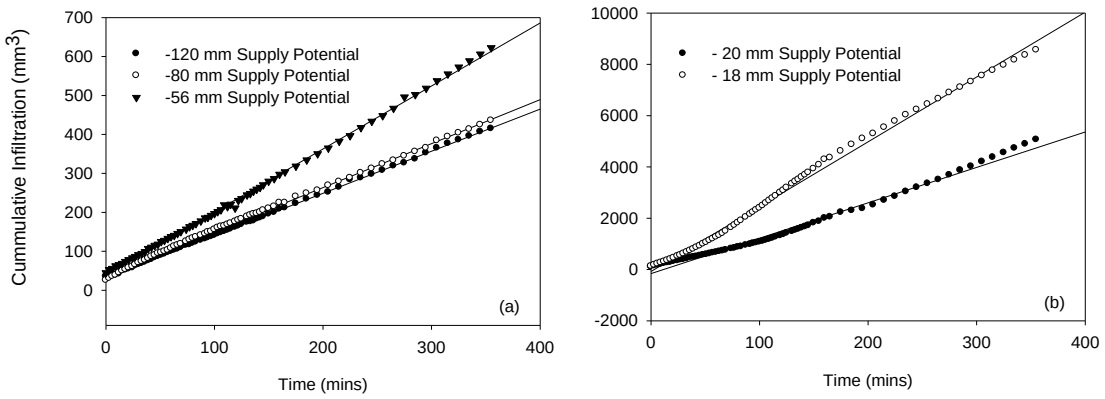

Figure 6.3-7 Change in infiltration over time (a) supply potentials ψ -1.20 kPa to -0.56 kPa, (b) supply potentials ψ -0.20 kPa to -0.18 kPa.

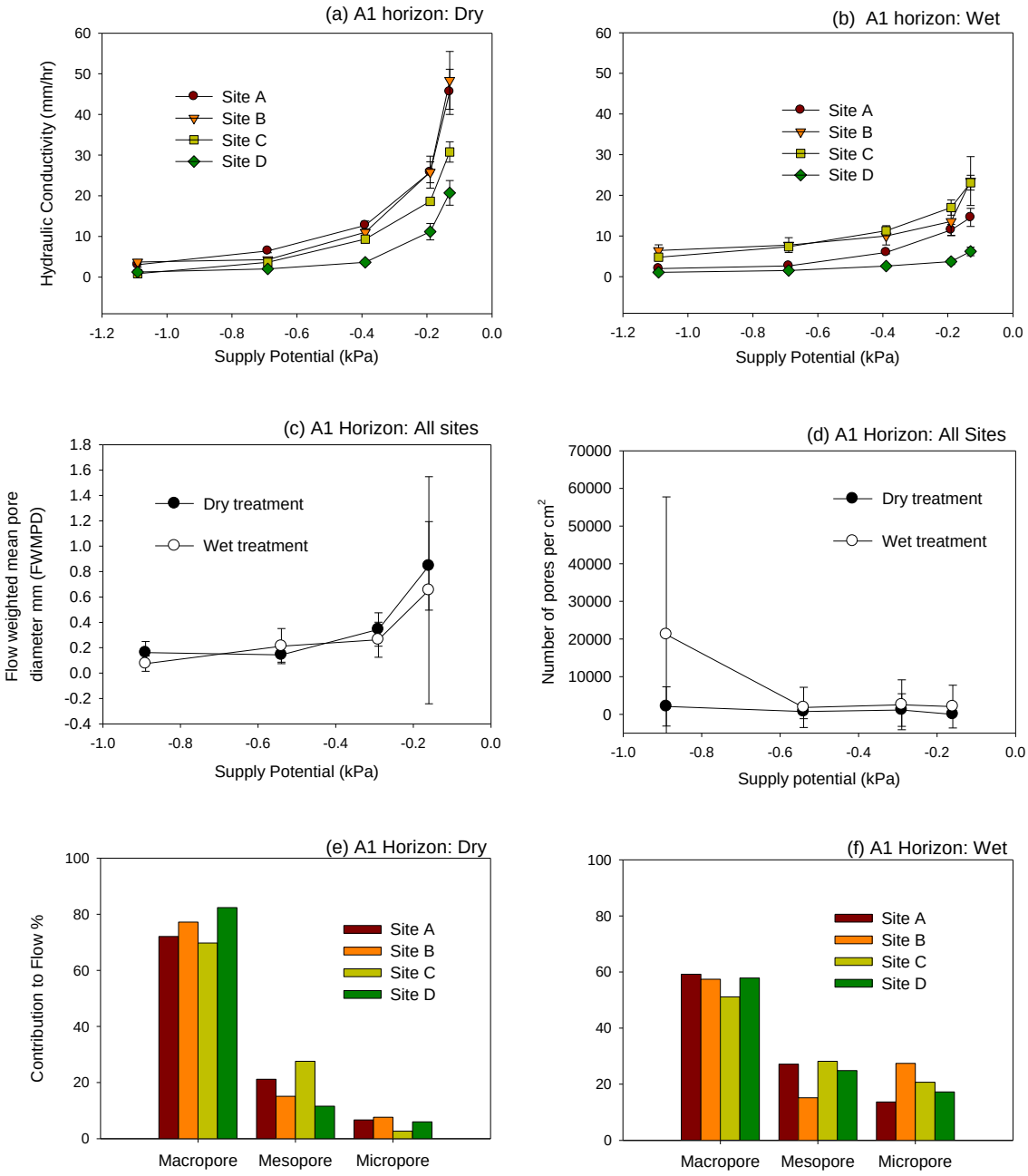

Figure 6.3-8 A1 horizon; Effect of antecedent soil moisture on unsaturated hydraulic conductivity (a) dry treatment, (b) wet treatment, (c) flow weighted mean pore size, (d) number of pores per square cm, (e) contribution to flow from pore size classes– dry treatment, (f) contribution to flow from pore size classes– wet treatment. Error bars in (a & b) represent ± 1 SE. Error bars in (c & d) represent ± 1 SD.

6.3.5 Effect of antecedent moisture on unsaturated hydraulic conductivity and functional macroporosity.

6.3.5.1 A1 horizon

The unsaturated hydraulic conductivity of large macropores (ψ -0.19 and -0.13 kPa) was significantly (p<0.05, df 41-43) lower in the wet treatment compared to the dry treatment. The FWMPD within the average macropore size range (ψ -0.29 kPa) was also significantly lower (p<0.05, df 25-36) in the wet treatment than in the dry treatment. However, no significant difference in the number of pores existed between the two soil moisture treatments. Lower macropore flow and pore diameter in the wet treatment was unexpected as hydrophobicity at low antecedent soil moisture (Chapter 3.3.3) has been demonstrated to decrease infiltration and hydraulic conductivity (Dekker and Ritsema 2000; Lamparter *et al.* 2006). Four explanations are proposed for the reduction in unsaturated hydraulic conductivity in the wet treatment;

(i) Clay swelling in the B2 horizons restricted vertical water movement from the A1 horizon into the B horizon. Restricted flow into the B horizon prevented new water from the disk permeameter displacing existing pore water further down the soil profile by piston flow (Hillel 1998). Thus the B2 horizon acted as a throttle to vertical infiltration reducing infiltration of new water into the A1 horizon.

(ii) Compaction associated with sheep grazing reduced the proportion of macropores and thus reduced hydraulic conductivity in the wet treatments. While sheep grazing occurred in both soil moisture treatments, compaction and loss of macropores was greater in the wet treatment due to lower soil strength. This hypothesis is supported by decreased macropore and increased mesopore contribution to flow in the wet treatments (Figure 6.3-8 e & f).

(iii) In the dry treatment, values of hydraulic conductivity are likely to be invalid due to water repellence. Use of approaches such as Reynolds and Elrick (1991) and the Laplace equation assume that wetting patterns beneath the infiltrometer are homogeneous and that water entry into pores is controlled exclusively by matric potential according to Richards equation. However in hydrophobic soils, the matric potential of dry soil during infiltration is positive rather than negative (hydrophilic soils), consequently the largest pores fill before smaller pores (Bauters *et al.* 2000b), and water entry into dry soil must also overcome the water-entry potential ($h$we) or wait until the persistence of water repellence is overcome (Jury *et al.* 2003).

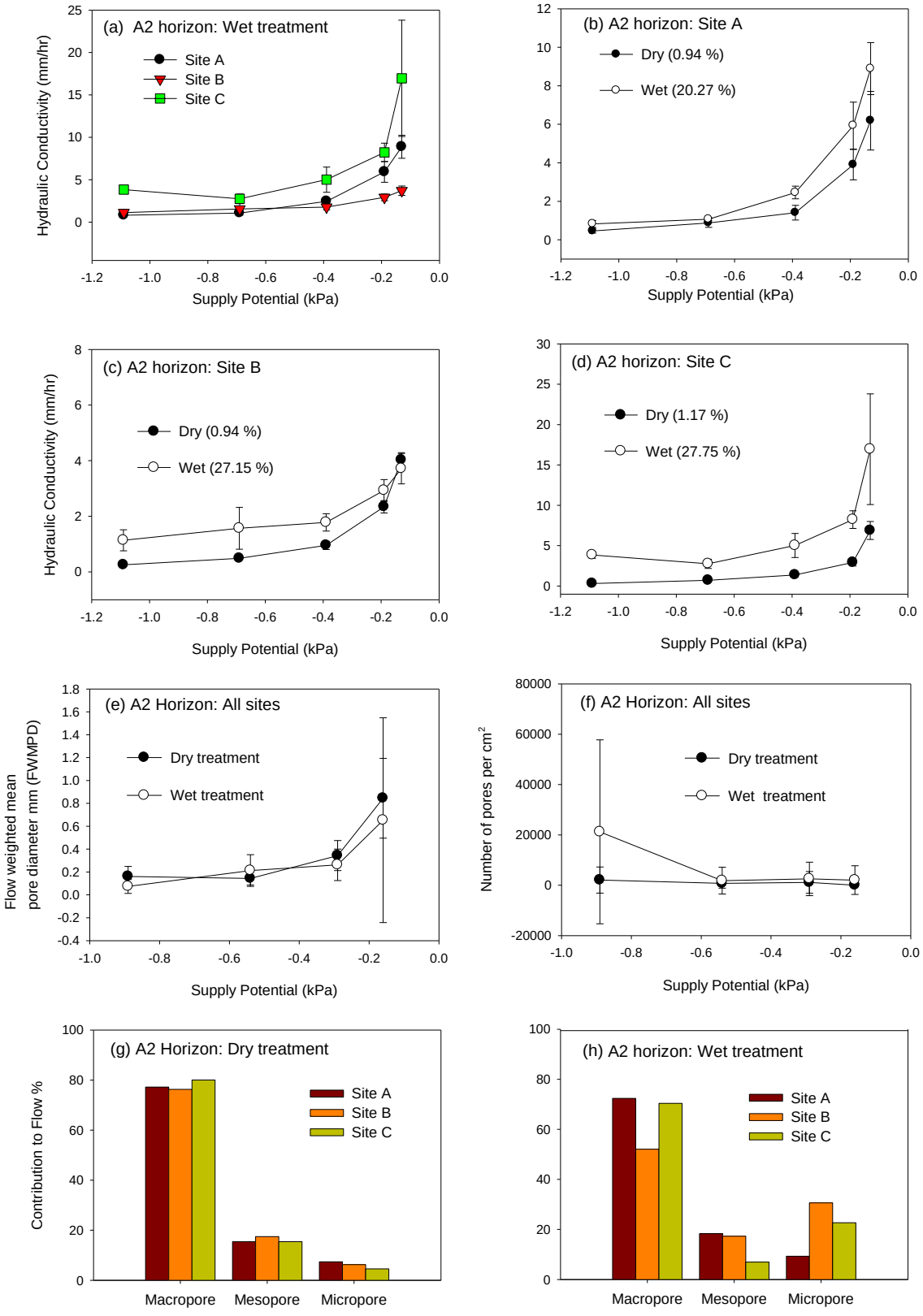

Figure 6.3-9 A2 horizon: (a) Variation in hydraulic conductivity between sites in the wet treatment. Effect of antecedent soil moisture on unsaturated hydraulic conductivity, (b) site A. (c) site B. (d). site C. (e) Flow weighted mean pore size. (f) Number of pores per square cm, (g) Contribution to flow from pore size classes– dry treatment. (h) Contribution to flow from pore size classes– wet treatment. Error bars in (a, b, c &d) represent ± 1 SE. Error bars in (e & f) represent ± 1 SD.

Furthermore development of finger flow reduces the area of soil participating in flow (Figure 6.3-6) which invalidates assumptions of homogeneity required by the Reynolds and Elrick (1991), and thus reported hydraulic conductivity values may be invalid. Further discussion is presented in Chapter 7.0.

(v) Dixon and Linden (1972) and Linden and Dixon (1976) report that air entrapment created by ponding of water, may decrease infiltration rates by up to two orders of magnitude. However air entrapment under the relatively small infiltration area of the tension infiltrometers (20 cm diameter) is considered plausible but not very likely.

6.3.5.2 A2 horizon

Unlike all other soil horizons, the unsaturated hydraulic conductivity of the A2 horizon was significantly (p<0.05, df 24-35) higher in the wet treatment than in the dry treatment at all supply potentials other than -0.13 kPa (Figure 6.3-9). This suggests that increased antecedent soil moisture increased flow through the micropores and mesopores (pores < 230 μm) within the A2 horizon (Figure 6.3-9 b, c & d). The FWMPD but not the number of pores were significantly (p<0.05, df 7-12) higher in the wet treatment than the dry treatment at ψ -0.89 kPa. This suggests the reduction flow may have resulted from a reduction in the size or connectivity of the smaller mesopores and micropores.

Leaching studies by Chartres *et al.* (1990) indicate the reduction in mesopore and micropore flow in the A2 horizon at low antecedent soil moisture may have resulted from precipitation of amorphous silica within menisci between coarse particles. In a hardsetting E (A2) horizon of a solodic texture contrast soil, Chartres *et al.* (1990), found cementation principally resulted from amorphous silica in which the cementing agent occurred as very thin layers, probably coatings and very small bridges between adjacent grains in which the likely points of precipitation were the soil mesopore and micropores where menisci form. Norton (1994) explains that unlike duripan, and fragipan cementation in which insoluble silica enriched hard pans form hardsetting in A / E horizons, the cementation in hardsetting in A / E horizons "*dissolve reversibly and precipitate resulting in their characteristic low strength when wet and high strength when dry*" as observed in the consistence of the A2 horizons reported in this study (Chapter 3.3.2).

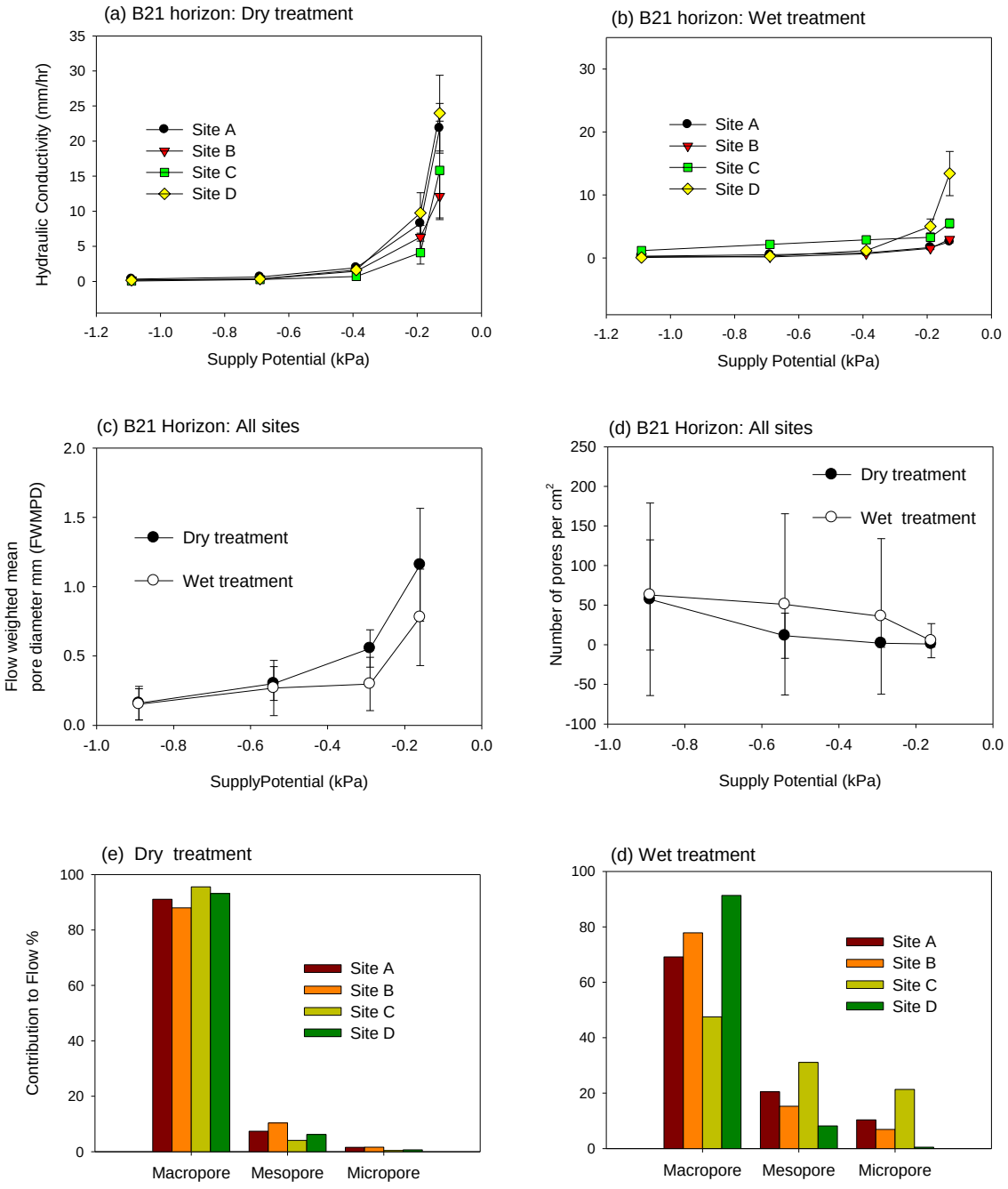

Figure 6.3-10 B21 horizon: Effect of antecedent soil moisture on unsaturated hydraulic conductivity (a) dry treatment, (b) wet treatment. (c) Flow weighted mean pore size. (d) Number of pores per square cm. (e) Contribution to flow from pore size classes– dry treatment. (f) Contribution to flow from pore size classes– wet treatment. Error bars in (a & b) represent ± 1 SE. Error bars in (c & d) represent ± 1 SD.

6.3.5.3 B21 Horizon

Drying of clays in the B21 horizon resulted in the formation of large shrinkage cracks which significantly increased macropore hydraulic conductivity and FWMPD without increasing the number of pores participating in flow. The hydraulic conductivity resulting from flow through macropores (1580 – 2310 μm) was significantly (p<0.05, df 35-43) higher in the dry treatment than in the wet treatment (Figure 6.3-10). FWMPD was also significantly higher in the dry treatment 1.16 mm (sd 0.41 mm) than the wet treatment 0.78 mm (sd 0.34 mm) at ψ-0.16. Increased macropore size in the dry treatment increased the macropore contribution to flow by 20 % (Figure 6.3-10 e & d). These findings are consistent with observations that the B21 horizon consisted of very dense clay peds with minimal intra-ped porosity, and large (0.5 – 2.0 mm wide) inter-ped shrinkage cracks when dry.

At high antecedent moisture content these shrinkage cracks had mostly closed due to clay swelling (Chapter 4.3.7). However water movement through large macropores did not completely stop as also noted by Waller and Wallender (1991) and Greve *et al.* (Greve *et al.* 2010). Wallender (1991) and Greve *et al.* (2010) found flow through shrinkage cracks decreased dramatically but did not stop following clay swelling as some pores remained open allowing water to move slowly through the soil. Antecedent soil moisture control on macropore flow has been reported by Gupta *et al.* (2006) who also used tension infiltrometers to measure infiltration in a Vertisol at different antecedent soil moisture. Gupta *et al.* (2006) found that infiltration was bimodal consisting of preferential flow through shrinkage cracks and matrix flow. The hydraulic conductivity close to saturation were positively correlated with antecedent moisture conditions, resulting from activation of flow in biological and structural macropores.

6.3.5.4 B22 Horizon

Results for the B22 horizon differed to that of the B21 horizon. Antecedent soil moisture had no significant effect on unsaturated hydraulic conductivity of the B22 horizon or the number of pores participating in flow at any supply potential. The FWMPD significantly (p< 0.05, df 39) increased at both -0.16 kPa and -0.29 kPa supply potentials resulting in a 17 % increase in the proportion of flow through macropores. This increase in macropore size did not significantly affect the unsaturated hydraulic conductivity (Figure 6.3-11). Detailed results from *in situ* tension infiltrometers are presented in Appendix 6.6.

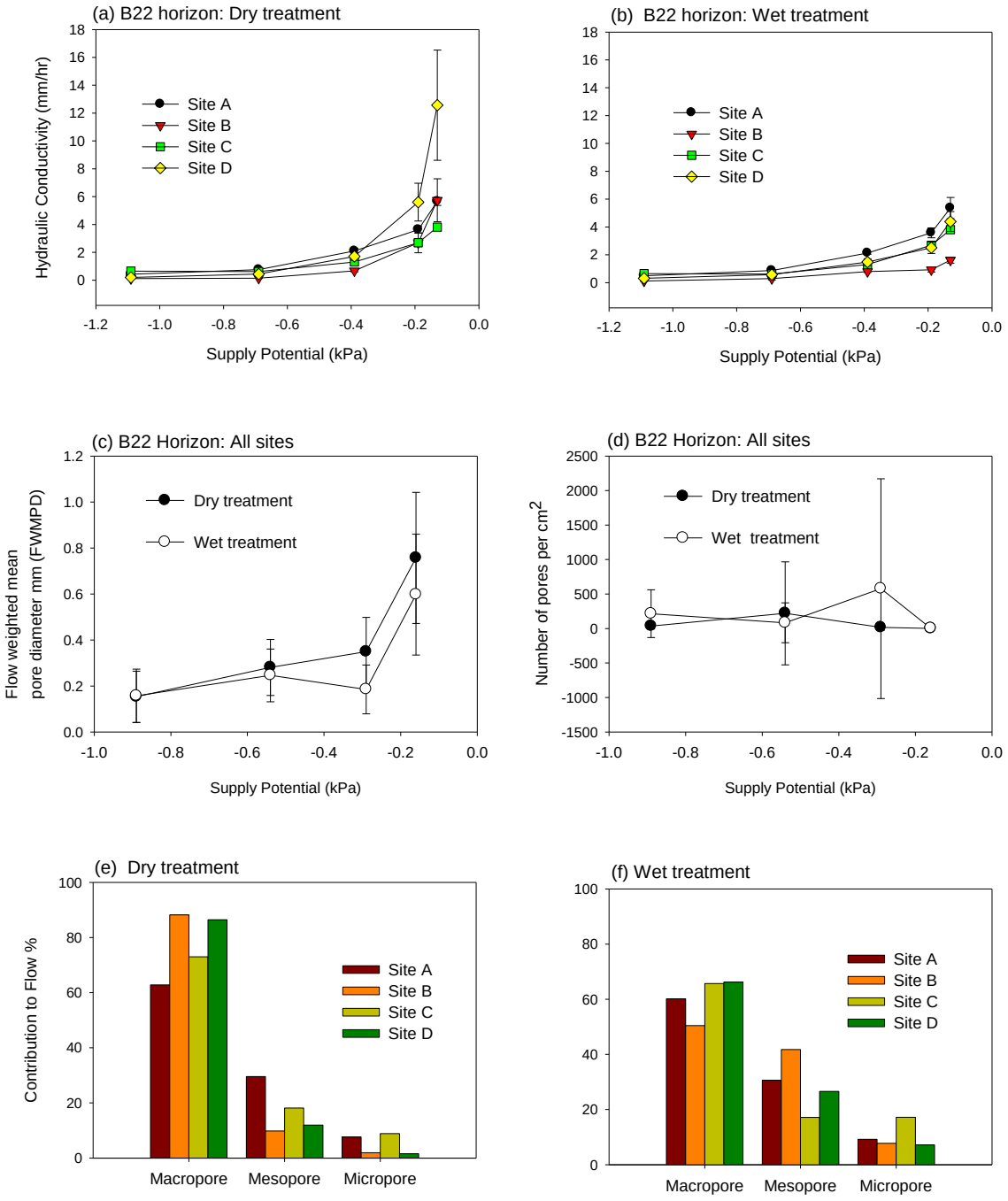

Figure 6.3-11 B22 horizon: Effect of antecedent soil moisture on unsaturated hydraulic conductivity (a) dry treatment, (b) wet treatment. (c) Flow weighted mean pore size. (d) Number of pores per square cm. (e) Contribution to flow from pore size classes– dry treatment. (f) Contribution to flow from pore size classes– wet treatment. Error bars in (a & b) represent ± 1 SE. Error bars in (c & d) represent ± 1 SD.

6.3.6 Prediction of ponding and subsurface lateral flow based on soil hydraulic conductivity

Waterlogging in duplex soils depends on rainfall quantity, slope, position in landscape, the ratio of saturated hydraulic conductivity between the A and B horizons, and the water storage capacity of the horizons above the perching layer (McFarlane and Williamson 2002).Restricted permeability in the subsoil is thought to occur when the conductivity of the subsurface horizon is at least two orders of magnitude lower than that of the surface soil (Devillers and Guyon 1979). However Tennant *et al.* (1992) cites evidence of restricted permeability causing the development of perched watertables in texture contrast soils in which the difference in conductivity between the A and B horizons was less than one order of magnitude. At low antecedent soil moisture (dry treatments), differences in unsaturated hydraulic conductivity indicate the greatest impediment to vertical infiltration existed at the A1 / A2 horizon boundary, not within the A2 horizon or upper surface of the B horizon as commonly cited in the literature (Cox and McFarlane 1995; Eastham *et al.* 2000; Ticehurst *et al.* 2007). The unsaturated hydraulic conductivity of the A2 horizon was significantly lower than the A1 and B21 horizons at ψ -0.19 kPa and -0.13 kPa, and an order of magnitude lower than the A1 horizon at all supply potentials (Figure 6.3-12).

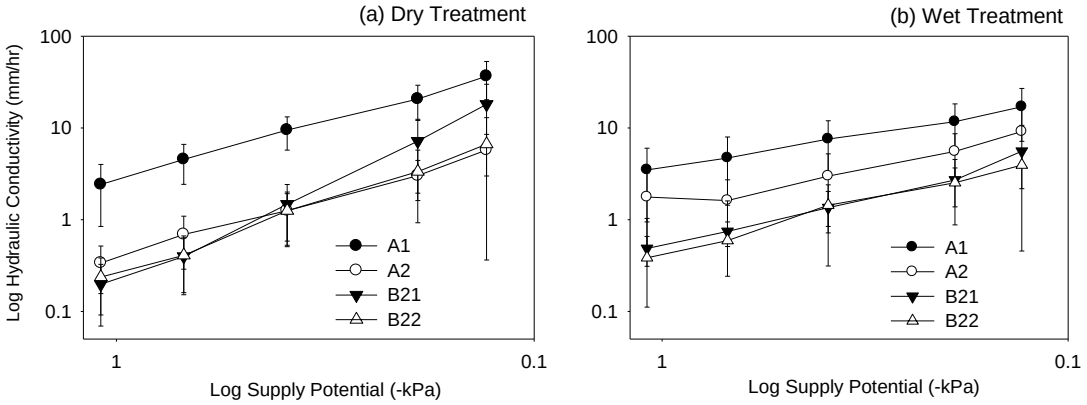

Figure 6.3-12 Mean log unsaturated hydraulic conductivity of each soil horizons (a) dry treatment, (b) wet treatment. Error bars represent ±1 SD

At low antecedent soil moisture the presence of shrinkage cracks resulted in the B21 horizons having significantly (p<0.05, df 19) higher hydraulic conductivity than the A2, B22 and B23 horizons at ψ-0.19 kPa and -0.13 kPa. Analysis indicates vertical infiltration via mesopores (ψ -0.39 to -1.09 kPa) would be impeded on the upper surface of the A2 horizon as the unsaturated hydraulic conductivity at ψ -0.69 kPa decreased 85 % from 4.52 mm hr^{-1} (sd 2.09) in the A1 horizon to 0.69 mm hr^{-1} (sd 0.40) in the A2 horizon.

Figure 6.3-13 Site B, wet treatment. Subsurface lateral flow at A1 / A2 boundary.

Vertical flow through macropores (ψ -0.13 kPa to -0.19 kPa) is also likely to be impeded by the A2 horizon, as the hydraulic conductivity at the -0.13 kPa supply potential was 84 % lower in the A2 horizon 5.73 mm hr^{-1} (sd 2.74) than in the A1 horizon 36.6 mm hr^{-1} (sd 16.3). In the absence of an A2 horizon, infiltration is likely to penetrate into the B22 and B23 horizons via shrinkage cracks thus preventing the development of a perched watertable and subsurface lateral flow, as also observed in a texture contrast soil in the Adelaide hills by Smettem *et al*. (1991).

When soil was near field capacity, the reduction in subsoil hydraulic conductivity was expected to result in ponding and accumulation above the B2 horizons or within the A2 horizon as predicted by Eastham *et al.* (2000) and Cox and McFarlane (1995). Tennant *et al.* (1992) suggests that a 10 fold reduction in hydraulic conductivity is required between soil layers to generate perched water tables in texture contrast soils. However at high antecedent soil moisture, the hydraulic conductivity of the A2 horizon was only 1.9 to 2.5, and the B21 horizon only 3.1 to 7.2 times lower than the A1 horizon (Figure 6.3-12). Consequently the difference in hydraulic conductivity between the A1 horizon and either the A2 or B21 horizons was not considered to be sufficiently great to generate perched watertables and subsurface lateral flow. However at high antecedent soil moisture, the restriction to vertical infiltration caused by precipitation of amorphous silica in the mesopores and micropores of the A2 horizon at low antecedent soil moisture was not longer apparent.

Lateral flow within the A1 horizon was however observed when the entire soil profile became saturated (Figure 6.3-13). It is postulated that clay swelling following prolonged wetting resulted in impeded water movement through the B2 horizons which created anisotropic conditions in the A1 horizon. Consequently rainfall or dye tracer application at rates greater than the hydraulic conductivity of the least conductive layer (3.9 mm hr^{-1} at ψ -0.13 kPa in the B22 horizon) resulted in saturation throughout the soil profile. Continued rainfall or dye tracer application at rates less than the surface soil infiltration rate but greater than the hydraulic conductivity of the least conductive layer resulted in lateral flow through the zone of highest conductivity, the A1 horizon (Figure 6.3-12). A similar process was invoked by Weiler and McDonnell (2004) to explain the development of subsurface lateral flow in steep forested catchments in which lateral flow develops at the soil-bedrock or soil-impeding layer interface due to the rapid decline in porosity with depth. They postulated that the addition of only a small amount of new water resulted in saturation above the impeding layer which resulted in rapid lateral flow at the permeability interface through the transient saturated zone.

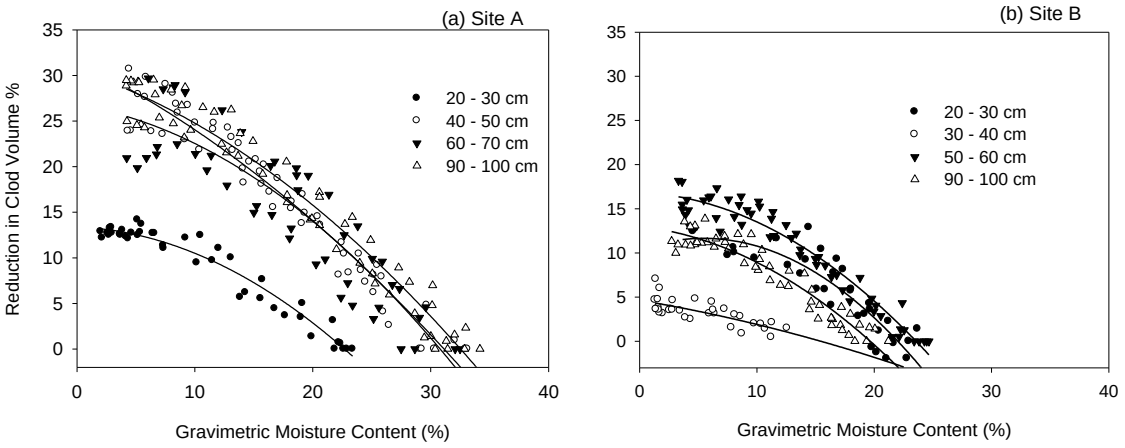

Figure 6.3-14 Relationship between soil moisture and clod volume (a) site A, (b) site B.

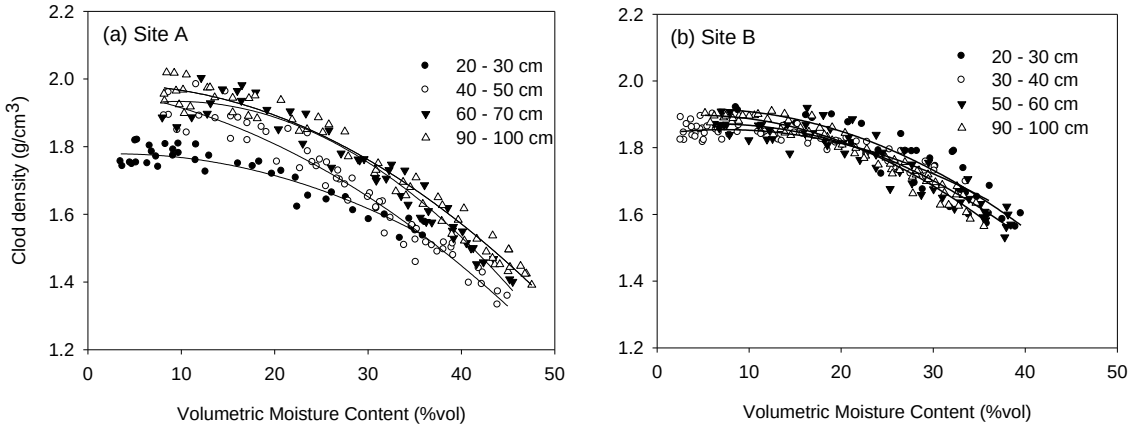

Figure 6.3-15 Relationship between volumetric soil moisture and clod density.

6.3.7 Soil shrinkage characteristic curve - effect of soil moisture on porosity

Clod volume and clod density were significantly (p<0.05 df 33-55) related to moisture content at both site A and B (Figure 6.3-15). Clod density ranged from approximately 1.4 g cm^{-3} to 1.5 g cm^{-3} near saturation, to 1.8 g cm^{-3} to 2.0 g cm^{-3} following desiccation.

Analysis of the soil shrinkage characteristic curve SSCC (Appendix 6.7) demonstrated that with the exception of a small amount of moisture loss near saturation, normal shrinkage occurred between void ratios of 0.25 and at least 0.8, however continued drying below a void ratio of 0.25 (0.10 g g^{-1} or 0.15 m^3 m^{-3}) resulted in residual shrinkage in which further loss of soil water caused little reduction in soil volume, as the soil matrix was strong enough to resist further contraction (Cornelis *et al.* 2006; Kirby *et al.* 2003).

Change in clod density following drying was greater at site A (except 20 – 30 cm) than site B (Figure 6.3-15). At site A desiccation in the B22 and B23 horizons resulted in 25 % to 30 % reduction in clod volume, whereas in the upper B21 horizon (20 – 30 cm depth) desiccation reduced clod volume by approximately 13 % (Figure 6.3-14). Values of clod density around 1.90 g cm^{-3} and 2.00 g cm^{-3} are substantially higher than values of bulk density reported in the literature for texture contrast soils. For example, Cotching *et al.* (2001) report the average bulk density of subsoil Sodosols in northern Tasmania ranged from 1.39 g cm^{-3} under long term pasture to 1.50 g cm^{-3} following cropping. Greenwood *et al.* (2006) reported bulk density of a Red Sodosol from northern Victoria was 1.71 g cm^{-3} at 30 - 35 cm depth, clod density was 1.58 g cm^{-3} at 30 - 40 cm depth, which increased to 1.63 g cm^{-3} following drainage. Differences between bulk density determined from soil cores, and clod density determined by laboratory drying, result from differences in sample size and soil moisture content. Field determination of soil density using cores (Cresswell and Hamilton 2002) is likely to sample both clods and interclod voids, whereas SSCC determination of clod density does not sample interclod voids resulting in higher density. Soil strength in texture contrast soils also tends to be very high at low soil moisture content, such that core sampling for bulk density is usually only able to be conducted on moist soils when strength is low.

6.4 Conclusion

Soil hydraulic properties were affected by methodology and antecedent soil moisture resulting in differences between *in situ* and laboratory measures of porosity and hydraulic conductivity.

Little difference existed between the soil water characteristic of the A1 and A2 horizons. Both A horizons had similar values for field capacity, permanent wilting point, PAWC and drainable porosity, which supports the proposition that both A horizons are derived from aeolian deposition. Lower PWP in the A2 horizon resulted from lower clay content. Comparison between sites found that the A1 horizon at site D had less drainable porosity due to lower levels of macroporosity, and lower PAWC and PWP than the other sites due to higher silt and clay content associated with weathering of Tertiary sediments.

Despite the presence of hydrophobicity at low antecedent soil moisture, the unsaturated hydraulic conductivity of the A1 horizon was significantly higher in the dry treatment than the wet treatment. Explanations for this observation include; reduced air and water flow due to swelling of clay subsoils at high antecedent soil moisture, greater compaction due to sheep grazing on moist soil, and uncertainty with the calculation of unsaturated hydraulic conductivity and other soil properties at low antecedent moisture due to hydrophobicity.

The unsaturated hydraulic conductivity of the A2 horizon was significantly higher in the wet treatment than in the dry treatment. This was attributed to precipitation of soluble amorphous silica in the menisci between sand grains (Chartres *et al.* 1990) which is thought to have restricted flow through the mesopores and micropores in the A2 horizon at low antecedent soil moisture.

The three B2 horizons had similar soil water characteristics, resulting in similar values for PAWC, permanent wilting point and drainable porosity. The unsaturated hydraulic conductivity at supply potentials close to saturation was significantly lower in the wet treatment than the dry treatment due to the almost complete closure of shrinkage cracks at high antecedent soil moisture. Volumetric shrinkage of soil clods demonstrated that clays within the three B2 horizons were able to undergo up to 30 % reduction in volume following desiccation, although under field conditions a 10 - 15 % reduction in clod volume is more likely due to difficulty drying subsoil clays. At low antecedent soil moisture, desiccation resulted in the formation of shrinkage cracks which significantly increased macropore hydraulic conductivity and FWMPD at supply potentials between -0.19 an -0.13 kPa. At high antecedent soil moisture, prolonged wetting resulted in clay swelling and closure of shrinkage cracks, however infiltration decreased with increased antecedent soil moisture but did not stop completely ,as water movement still occurred through partly open pores, as noted by Waller and Wallender (1991) and Greve *et al.* (Greve *et al.* 2010).

At low antecedent soil moisture (dry treatment), ponding and lateral flow were predicted to occur at the A1 / A2 horizon boundary due to the reduction in micropore and mesopore flow which was attributed to amorphous silica precipitation between sand grains in the A2 horizon. The upper surface of the clay B21 horizon did not present a restriction to vertical infiltration at low antecedent soil moisture due to the presence of shrinkage cracks. Similar phenomenon was reported by Smettem *et al*. (1991) who found that soil macroporosity and bypass flow were responsible for preventing subsurface lateral flow at the A / B horizon boundary of a texture contrast soil in the Adelaide Hills.

Development of bypass flow resulted in the near saturated hydraulic conductivity of B2 horizons being considerably higher than would otherwise have been predicted from particle size analysis. Brower and Fitzpatrick (2002b) also found that macroporosity resulting from root holes and inter pedal cracks in the B horizon of a texture contrast soil provided sufficient hydraulic connectivity to prevent the development of subsurface lateral flow on a series of texture-contrast soils in the Dundas Tablelands, Western Victoria. In the absence of an A2 horizon, vertical infiltration would be required to fill the shrinkage cracks and voids in the subsoil before ponding could occur on the surface of the B2 horizon.

At high antecedent soil moisture saturated hydraulic conductivity (intact cores) and *in situ* unsaturated hydraulic conductivity decreased sequentially with depth. Ponding and lateral flow were predicted to occur at the A1 / A2 horizon boundary or in the absence of an A2 horizon, at the A1 / B21 boundary. At low rates of rainfall or infiltration through the A1 horizon, saturation was predicted to occur at a range of depths depending on antecedent soil moisture. At high rates of infiltration ponding and lateral flow are predicted to occur within the most conductive soil layer (Weiler and McDonnell 2004), the A1 horizon. Results from both the wet and dry soil moisture treatments differ from that of Eastham *et al.* (2000), Cox and McFarlane (1995) and Ticehurst *et al.* (2007) who suggest that development of subsurface lateral flow in texture contrast soils principally occurs in the A2 horizon or at the A2 / B2 horizon boundary due to differences in particle size of the two horizons.

6.5 Key points

- Measurement of soil hydraulic properties was influenced by choice of methodology, type of soil sample (i.e. disturbed, ground repacked) and boundary or initial conditions including soil moisture content and supply potential.
- At site B, the A1 and A2 horizons had similar soil water retention curves, PAWC and DP due to similar particle size distribution.
- At all sites the B2 horizons had similar soil water retention curves, resulting in similar SAT, PAWC and DP.
- Differences in porosity, pore size distribution, PAWC and hydraulic conductivity, between site D and the other three sites principally resulted from differences in particle size associated with highly weathered Tertiary sediments at site D.
- In the A1 horizon, lower hydraulic conductivity in the wet treatment was unexpected as hydrophobicity was expected to reduce infiltration into the dry treatment. Explanations include; reduced air and water flow due to swelling of clay subsoils, compaction due to sheep trampling on moist soil, and uncertainty with the calculation of unsaturated hydraulic conductivity for hydrophobic soils.
- In the A2 horizon, lower hydraulic conductivity in the dry treatment was attributed to precipitation of amorphous silica in micro and meso pores.
- When saturated, the B2 horizons contained little porosity resulting in reduced PAWC, and drainable porosity than would otherwise be expected.
- Desiccation caused clod volume to decrease by up to 35 % and bulk density to increase above 1.8 g cm^{-3}, although these extreme values are unlikely to result from in-field seasonal changes in subsoil moisture.
- In dry antecedent soil moisture conditions ponding is predicted to occur at the A1 / A2 horizon boundary and lateral flow is likely to occur within the A1 horizon.
- In low antecedent soil moisture the absence of an A2 horizon, ponding would not occur due to shrinkage cracks in the B21 horizon.
- In wet antecedent soil moisture conditions hydraulic conductivity decreased sequentially with increasing depth.
- At high antecedent soil moisture, lateral flow in the A1 horizon is expected in the A1 horizon when the infiltration rate exceeds the hydraulic conductivity of the B21 horizon.

7.0 Effect of water repellence on infiltration and preferential flow

7.1 Introduction

The occurrence of water repellence or finger flow in texture contrast soils has been reported in a limited number of studies including; Chittleborough *et al.* (1992), Crabtree and Gilkes (1999), Gardner *et al.* (1992), and Hall *et al.* (2010). Given that around 80 % of agricultural regions in southern Australia are comprised of texture contrast soils (Chittleborough *et al.* 1994), the existence of water repellence and finger flow in texture contrast soils represents a potential risk to agricultural production due to uneven wetting patterns and the environment by rapid mobilisation of agrochemicals from the biologically and chemically reactive topsoil to shallow groundwater and waterways (Ritsema and Dekker 2000).

Water repellence in the A1 horizon was noted in previous chapters. Soil characterisation and pedological investigations in Chapter 3.0 found the aeolian derived A1 horizon was water repellent at three of the four sites. At low antecedent soil moisture, dye staining experiments in Chapter 4.0 indicated that water repellence resulted in the development of finger flow. Finger flow was responsible for bypassing between 74 % – 89 % of the A1 horizon (Chapter 4.3). Hydrophobicity induced finger flow also exerted control on the location of ponding on the upper surface of the B21 horizon and which subsoil shrinkage cracks were able to participate in flow. In Chapter 6.0 water repellence was suspected to have influenced infiltration into the A1 horizon at low antecedent soil moisture, however infiltration into the A1 horizon was unexpectedly higher when antecedent soil moisture was low.

Given the potential importance of water repellence on the occurrence of preferential flow, a series of experiments were conducted to better understand the nature of water repellence and its influence on the development of preferential flow, studies investigated:

- Seasonal variation in water repellence.
- If winter rainfall was able to remove water repellent coatings from the soil.
- The effect of antecedent soil moisture and water repellence on infiltration and intrinsic permeability.
- The relative contribution of soil moisture, water repellence, and air and water entrapment on the development of finger flow.

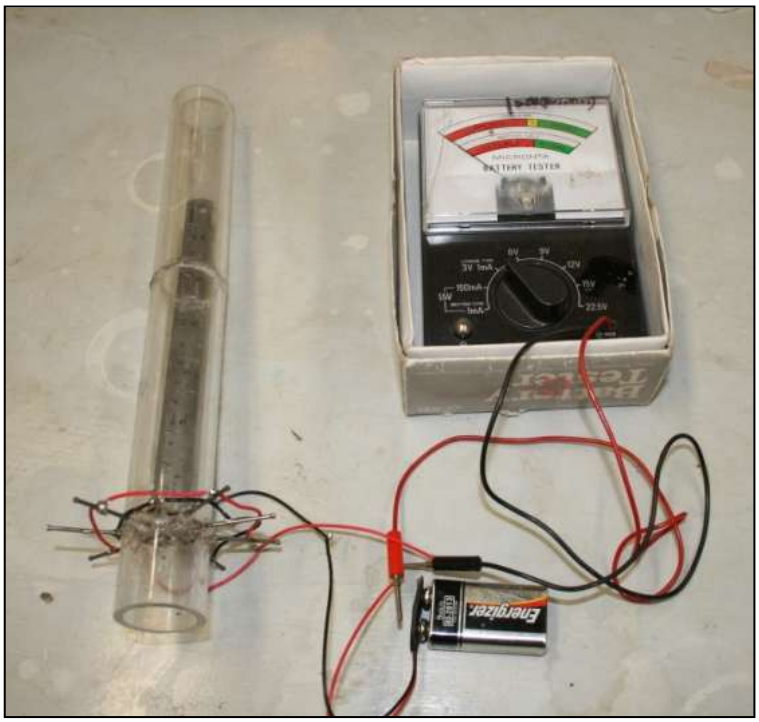

Figure 7.1-1 Water entry value (WEP) device in WEP is determined as the height of water immediately prior a sudden rise in volts following infiltration 0.5 cm below the soil surface.

7.2 Methodology

7.2.1 Determination of Water Repellence

The persistence of water repellence was determined by the WDPT approach (Chapter 3.2.4). The physical severity of water repellence was measured using the Water Entry Potential (WEP *or* h_{we}) which is equivalent to the soil water potential at which infiltrating water starts to displace air in a hydrophobic porous medium (Wang *et al.* 2000a). WEP is a function of both moisture content and the soil pore radius (Letey *et al.* 2000). WEP was determined following the procedure of Wang *et al.* (2000a) in which the height of water required to instantaneously breakdown water repellence and enable infiltration to commence is equivalent to the water entry value. A simplified version of the device developed by Carrillo *et al.* (1999) was constructed in which soil was packed into a transparent tube, 0.5 mm above a series of metallic pins (Figure 7.1-1). The tube was treated with Teflon dry film lubricant to prevent preferential flow down the edge of the tube. Air flow from the base of the tube was not restricted. Distilled water was initially applied slowly to prevent disruption of the soil surface, once the depth of water exceeded 1 cm depth, the tube was rapidly filled (15 mm sec^{-1}) until breakdown of water repellence caused infiltration to close the electrical circuit, as indicated by a sudden rise in volts. The height of water at the time voltage started to rise was equivalent to the WEP (Wang *et al.* 2000a).

Unless otherwise stated, all tests were conducted on soils which had been dried at 40 ^{o}C for 24 hours, passed through a 2 mm sieve to remove roots, and allowed to cool to room temperature.

7.2.2 Effect of antecedent soil moisture on water repellence

The relationship between antecedent soil moisture and WDPT was determined following a similar approach to Ritsema *et al.* (1998b) in which a 1 kg sample of extremely hydrophobic (WDPT 120 + mins) soil was wet to saturation. The sample was obtained from 0 - 10 cm depth, at site B in April 2008, air-dried and archived for 15 months prior to analysis. The soil and water were mixed using a rotary shaker for 24 hours to ensure even wetting (difficult in hydrophobic soil). Subsamples were dried at 40°C (or 60 °C after a colleague inadvertently reset the oven) for durations ranging from 6 to 140 hours to produce a range of soil moisture contents. Soil samples were cooled to room temperature and the WDPT determined from five replicate samples. Animation of WDPT test on extremely water repellent soil is presented on the CD Rom (Appendix 8.2) in which the water droplets actually evaporate over the three hour measurement period.

7.2.3 Effect of leaching on water repellence

The effect of leaching on water repellence was investigated by measuring WDPT and WEP following sequential leaching of an archived, extremely hydrophobic (WDPT 120 + mins) soil collected in April 2000. Approximately 1200 cm^3 air dried soil was placed in a 120 mm diameter tube mounted on a freely draining sand bath to which 1.0 L distilled water was added. The leached soil was dried at 40°C for 24 hours, allowed to cool to room temperature before determining WDPT and WEP on a minimum of three replicates. The remaining dried soil was returned to the leaching apparatus and the procedure repeated another four times. Leachate was collected and analysed for dissolved organic carbon by Analytical Services Tasmania using a Skalar segmented flow analyser with phenolphthalein indictor determined spectrophotometrically at 550 nm. Differences in WDPT and WEP between leaching events were analysed using T-test with $p<0.05$ in SPSS v12 software.

7.2.4 Seasonal variation in water repellence

Seasonal monitoring of WEP and WDPT was conducted nine times between July 2009 and June 2010, adjacent site B. Approximately 1 kg bulk samples were obtained every 1-2 months from 0 - 5 cm depth, sampling was conducted around a fixed monitoring point adjacent site B. Bulk soil samples were mixed, dried at 40°C for 24 hours, passed through a 2 mm sieve and allowed to cool to room temperature before analysis. The gravimetric soil moisture content was determined at the time of sampling and time of analysis by drying at 105°C for 24 hours. As WDPT and WEP were determined on air dried 40°C samples, results represent seasonal changes in 'potential water repellence' rather than changes in 'actual water repellence' as discussed by Dekker and Ritsema (1994). Changes in water repellence are therefore related to seasonal changes in the type or amount of water repellent compounds within the soil, rather than seasonal differences in soil moisture at the time of analysis.

The association between water repellence and climate attributes measured at the Hobart airport (Bureau of Meteorology 2009) were investigated using Spearman pairwise bivariate correlation analysis. Comparisons were made with both WDPT and WEP against soil moisture at the time of sampling, soil moisture following air drying at 40°C, and cumulative climate attributes in the 10, 30, 60, and 90 days prior to analysis, climate attributes include; rainfall (mm), relative humidity (% 9 am), average temperature (°C), sunshine hours (hrs), pan evaporation (mm) and soil water deficit (rainfall – evaporation).

Table 7.2-1 Physical properties of water, ethanol and 40 % ethanol solution.

	100% Water	40% Ethanol	100% Ethanol
Specific Density (kg m^{-3})	998	935	789
Surface Tension (mN m^{-1})	72.75	30.69	22.31
Dynamic Viscosity (kg m^{-1} s^{-1})	0.001002	0.002846	0.001203

All values per sea level at 20°C (Lide 2005; Vazquez *et al.* 1995)

Table 7.2-2 Radius of largest water filled pore and equivalent tension for water, ethanol, and the 7M ethanol solution

	Radius of largest water filled pore (m)			Equivalent ethanol supply potential (kPa)	
Water Supply Potential (kPa)	100% Water	100% Ethanol	40 % Ethanol	100% Ethanol	40% Ethanol
1.34	1.09E-04	4.30E-05	4.99E-05	0.52	0.603
0.84	1.75E-04	6.86E-05	7.96E-05	0.326	0.378
0.54	2.72E-04	1.06E-04	1.23E-04	0.209	0.243
0.24	6.12E-04	2.40E-04	2.78E-04	0.093	0.108
0.14	1.05E-03	4.11E-04	4.78E-04	0.054	0.063
0.12	1.22E-03	4.80E-04	5.57E-04	0.047	0.054

7.2.5 Effect of water repellence and antecedent soil moisture on infiltration and intrinsic permeability

In water repellent soils, measurement of hydraulic properties with water may be erroneous as different water content exist at an equal capillary pressure (Bauters *et al.* 2000b). Consequently the effect of water repellence on infiltration and intrinsic permeability was determined by infiltration of both rainwater and a 7M ethanol solution (40.75 %). Use of ethanol solution assumes the contact angle between the soil particle and the water was zero such that infiltration of the ethanol solution instantaneously overcame the effects of water repellence, consequently infiltration was not influenced by hydrophobic pore surfaces (Lamparter *et al.* 2006). A 7M ethanol solution was used in preference to a pure ethanol solution (Jarvis *et al.* 2008; Lamparter *et al.* 2010) as MED analysis (Chapter 3.3.5) demonstrated water repellence was overcome at ethanol molarities between 1.75 and 5.0, and the 7M solution did not dissolve the polycarbonate tension infiltrometers (Chapter 6.2.6).

When evaluating the conductivity of porous media using tension infiltrometers with ethanol as the infiltrating liquid, the specific physicochemical properties of the ethanol solution have to be considered, as differences in the surface tension and density (Table 7.2-1) of the ethanol solution to that of water, effect the maximum pore size which is able to conduct the two fluids (Jarvis *et al.* 2008; Lamparter *et al.* 2010). In addition in order to ensure a valid comparison between the two solutions, the equivalent supply potential of the ethanol solution to that of the water was calculated from the capillary equation, following a similar approach to Jarvis *et al.* (2008) in which the supply potential (ψ) of 7M ethanol solution = (ψ) water x 2.2 (Table 7.2-2). The validity of scaling measurements by supply potential for different infiltrating liquids was validated by Lamparter *et al.* (2010).

Setup and operation of the tension infiltrometers was similar to Lin *et al.* (1997) and McKenzie *et al.* (2002b) detailed in Chapter 6.2.6. In both the wet and dry treatments, three disks containing rainwater were operated at the same time, approximately three meters away from three disks containing the 7M ethanol solution. The 'wet' soil moisture treatment was established via pop-up sprinklers, which operated for 40 minutes every second day over a three week period, while the adjacent 'dry' treatment was established under ambient conditions over summer. The average gravimetric soil moisture content (0 - 10 cm) of the wet treatment was 0.385 $m^3\ m^{-3}$ (sd 0.024 $m^3\ m^{-3}$), and the dry treatment 0.013 $m^3\ m^{-3}$ (sd 0.007 $m^3\ m^{-3}$).

Differences in the dynamic viscosity of water and the ethanol solution lead to different infiltration rates, even at equal liquid contents (Lamparter *et al.* 2010). To account for these differences, intrinsic permeability was calculated from the hydraulic conductivity to enable valid comparison between the soil porosity infiltrated by the two solutions. Unsaturated hydraulic conductivity was determined according to McKenzie *et al.* (2002b) and Reynolds and Elrick (1991) detailed in Chapter 6.2.6, in which the equivalent ethanol tension (Table 7.2-2) was used to calculate the soil structure parameter α and exponent P for the ethanol solution. Intrinsic permeability was determined from hydraulic conductivity for the two solutions in which,

EQ 7.1 $K_i = K.\eta / p.g$

k_i - Intrinsic permeability (m^2).

K – hydraulic conductivity ($m\ s^{-1}$).

η – dynamic viscosity ($kg\ m^{-1}\ s^{-1}$).

ρ – fluid density ($kg\ m^{-3}$).

g – gravitation constant ($m\ s^{-1}$).

Flow weighted mean pore diameter was calculated according to Philip (1987) described in Chapter 6.2.6. Differences in infiltration and intrinsic permeability of the two solutions and antecedent soil moisture treatments were compared using SPSS version 12, independent T – test (2-tailed) with Levene's test for equality of variances, significant differences existed where $p< 0.05$.

7.2.6 Effect of soil moisture, air flow and water repellence on finger flow

Unlike other forms of preferential flow, Jury *et al.* (2003) considered finger flow to be a fluid phenomenon, resulting from spatial heterogeneity in water repellence or moisture content (Keizer *et al.* 2007; Lemmnitz *et al.* 2008) rather than soil structure. Consequently finger flow may be investigated using repacked soils in large glass walled Hele-Shaw tanks (Miyazaki 2006; Wang *et al.* 2003; Wang *et al.* 2000b). Following a similar approach to Carrillo *et al.* (2000a), a 700 mm x 1000 mm x 20 mm Hele–Shaw tank was constructed to enable 2D visualisation of infiltration into a repacked soil (Figure 7.2-1). The tank consisted of two layers of 5 mm plexiglass held 2 cm apart. Ten drainage valves were installed in the base of the tank to control air / water flow. Water was supplied by a constant head mariotte bottle via either a supply tube or 10 constant rate drippers. Water flow down the sides of the glass panes was prevented by coating the glass with either Teflon spray (moist soil) or thinly smeared Vaseline (dry soil).

Figure 7.2-1 Hele –Shaw tank. Note reservoir chamber with bubble tube (left), adjustable stand to level the depth of ponding (bottom), supply tube with drippers inside the tank, and collection vials beneath the tank to capture leachate.

Sieved (<2 mm) dried soil was uniformly packed into the tank in 10 x 50 mm layers and gently compacted with a large bar, and the sides of the tank were gently tapped with a rubber mallet. The soil surface was levelled, and excess soil removed by vacuum. Once water was released from the reservoir, the tank was re-levelled to ensure even depth of ponding across the soil surface. The head of water was maintained between 0.5 cm and 0.8 cm by adjusting the bubble tube in mariotte bottle. Infiltration rate was recorded as outflow from the reservoir. Visualisation of infiltration into wet soil was aided by application of 15 g L^{-1} Brilliant Blue FCF (C.I. Food Blue 42090) to the infiltrating water. Infiltration was recorded by still camera every 1 to 5 minutes depending on rate of infiltration. Images of dye stained soil were digitally enhanced using procedures described in Chapter 4.2.4 to improve visualisation of water movement. Animation and sequential grey scale figures of infiltration were produced using Photoshop CS3 software and SigmaPlot 10.0.

The degree of fingering or extent of unstable flow was calculated from the slope of the linear relationship between the depth of infiltration (cm) and the proportion of infiltrated soil (%) at each time interval. In uniform flow, the slope was close to zero as virtually all the soil behind the horizontal wetting front was wetted. In unstable flow, portions of the wetting front advanced ahead of other areas, such that the proportion of infiltrated soil behind the maximum wetted depth increased as flow instability increased. Consequently the slope of the relationship between the depth of infiltration (cm) and the proportion of infiltrated soil (%) increased with increased flow instability.

Infiltration experiments compared the effects of air entrapment, soil moisture content and water repellence on the rate of infiltration, flow patterns and the extent of unstable flow. Treatments included (Table 7.2-3);

(i) Antecedent soil moisture: Dry treatments were established by oven drying at 40°C for 24 – 96 hrs, or oven drying at 105 °C for 24 hrs to induce water repellence. The wet treatments were established by flooding soil within the tank, then allowing water to drain from the base of the tank for at least 24 hours following saturation.

(ii) Water repellence: The degree of water repellence varied between soil collected in winter (July 2009) which had a WDPT between 11 sec and 38 sec, compared to archived soil collected from the same location at the end of summer (April 2008) which had a WDPT greater than 7200 sec.

(iii) Air / water flow: Valves at the base of the Hele-Shaw were either (i) open, allowing free movement of air and water through the base of the tank or (ii) closed, resulting in air entrapment. During run C the valves became blocked which greatly restricted but did not totally prevent air flow.

Table 7.2-3 Hele-Shaw tank treatments and level of water repellence for each infiltration event.

Run	Run Date	Soil collection Date	Soil Moisture Treatment	Initial Soil Moisture ($\%_{grav}$)	Air Flow	WDPT (sec)	WEP (cm)
A	26/6/9	Summer 08	Oven dried 40 °C 24 hrs	1.01	Open	4800	11.7
B	2/7/09	Winter 09	Field Moisture	26.6	Closed	0	0
C	7/7/09	Winter 09	Saturated and drained following Run B	25.4	Restricted	0	0
D	15/7/09	Winter 09	Oven dried 45 °C 96 hrs	0.37	Open	38	?
E	16/70/9	Winter 09	Saturated and drained following Run D	28.1	Open	0	0
H	28/7/09	Summer 08	Oven dried 105 °C 24 hrs	0.01	Open	4860	19

7.3 Results and discussion

7.3.1 Effect of antecedent soil moisture on water repellence

No significant relationship existed between WDPT and moisture content for samples dried at 60 °C. A significant power relationship existed between gravimetric soil moisture and WDPT for samples dried at 40 °C, although the relationship was highly dependent on two extreme values which were subjected to measurement difficulties. When values less than 3 seconds were excluded from the analysis, no significant relationship existed between gravimetric soil moisture and WDPT of samples dried at 40 °C (Figure 7.3-1). Results in Figure 7.3-1 also demonstrated that higher values of water repellence may be induced by drying at temperatures above 40 °C. Dekker *et al.* (1998) also reported water repellency was greater after drying at 65 °C compared to drying at 25 °C, which Doerr *et al.* (2000) attributed to an increase in the alignment of the hydrophobic molecules.

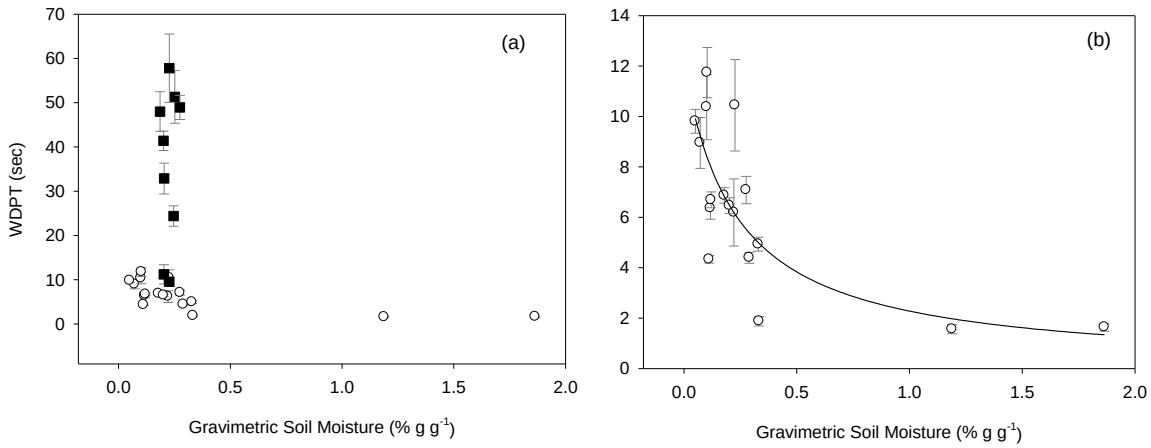

Figure 7.3-1 Relationship between gravimetric soil moisture and water repellence (WDPT): (a) samples wet to saturation then dried at 40 °C (open circles) and 60 °C (closed squares), (b) samples wet to saturation then dried at 40 °C. Power regression $r^2 = 0.70$. Error bars represent ±1 standard deviation.

Results from the laboratory drying experiment indicate that methodology may have influenced results. As extreme water repellence (WDPT 120-150 minutes) occurred in field soils at soil moisture contents greater than 0.5 % g g^{-1}, the lack of water repellence in soils at soil moisture contents greater than 0.5 % g g^{-1} in the laboratory drying experiment were attributed to the effects of saturation and end over end shaking.

Consequently it is considered that the process of saturating the soil prior to analysis either removed the water repellent coatings from the sand grains, or caused the water repellent coating to become non-repellent. Notably water repellence did not return with drying at either 40 °C or 60 °C. This analysis suggests that the change from repellent to wettable behaviour may have resulted from saturation changing the orientation of soluble amphiphilic molecules in which the hydrophobic polar ends switched from being bonded to the soil surface to being bonded to the water droplet (Doerr *et al.* 2000).

Inability of water repellent soil to return to pre-wetting levels of repellence following drying has been reported by Crockford *et al.* (1991) and Doerr and Thomas (2000). Doerr and Thomas (2000) reported that water repellancy did not return to a forest soil even when samples were dried to near the air dried moisture content and allowed to equilibrate for several weeks. It is speculated that if soil had been wet-up to a range of moisture contents between air dried and field capacity without saturation, a stronger relationship between soil moisture and water repellence may have existed.

7.3.2 Seasonal variation in water repellence

Water repellancy varied significantly (p<0.05) from winter (July 2009) in which WDPT was 0.19 mins (SD ± 0.02 mins) and WEP 0.0 cm, to a maximum WDPT of 53.9 mins (SD ± 13.3 mins) and a WEP of 14.4 cm (SD ± 0.52 cm) in May 2010, before decreasing significantly again in June 2010 (Figure 7.3-2). Seasonal variation in water repellence has been reported by Crockford *et al.* (1991), Doerr and Thomas (2000; 2003), Keizer *et al.* (2007; 2008) Leighton-Boyce *et al.* (2005), and Lemmnitz *et al.* (2008). However, many of these studies were conducted on field soils at ambient soil moisture contents, such that variation in water repellence is likely to have been confounded by soil water content at the time of analysis. Consequently there is uncertainty as to whether the change in water repellence resulted from changes in actual water repellence or potential water repellence associated with seasonal changes in soil moisture and rainfall. By determining WDPT on air dried samples Doerr and Thomas (2000) also found water repellancy did not return to a forest soil even when samples were dried to near the air dried moisture content and allowed to equilibrate for several weeks. Results presented in Figure 7.3-1 and Figure 7.3-2 support findings by Doerr and Thomas (2000) who postulated that for at least some soils, the relationship between soil moisture and water repellence is hysteretic, and that water repellence is not re-established after seasonal rainfall, unless input of new hydrophobic substances occurs.

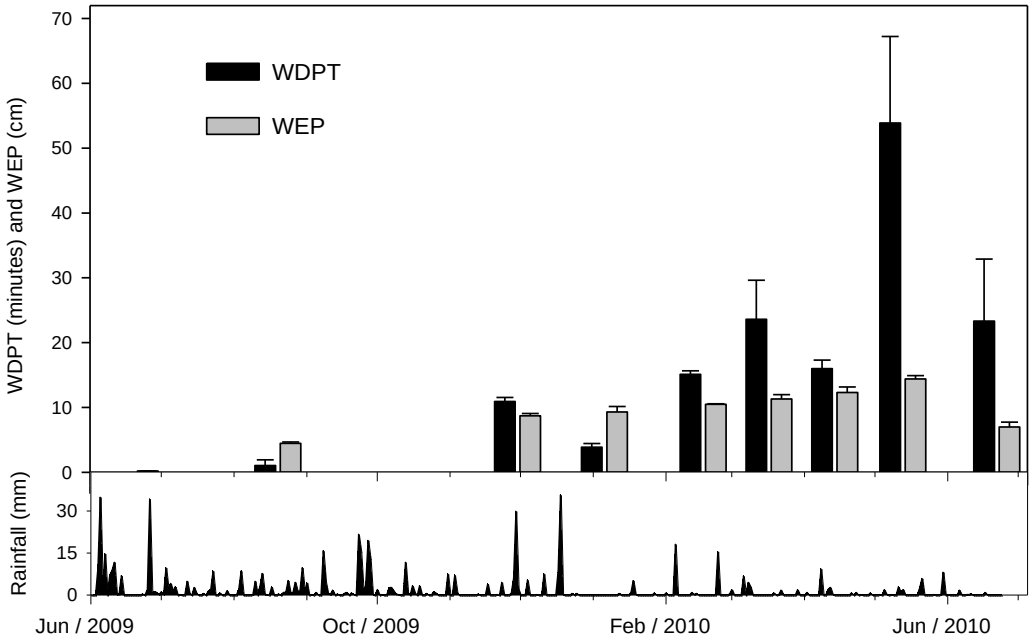

Figure 7.3-2 Seasonal variation in water repellence, measured as WDPT and WEP, and daily rainfall. Error bars represent + 1 SD.

The rate of increase in water repellence between July 2009 and May 2010 in WDPT was 10.2 sec day^{-1}, and for WEP 4.2 mm day^{-1} (Figure 7.3-2). While increased sampling interval may have revealed that accumulation and loss of water repellent compounds occurred over shorter periods, the rates of change in water repellence are generally slower than those reported in the literature. Leighton-Boyce *et al.* (2005) reported that soil in a Eucalyptus globules plantation in Portugal went from being wettable to entirely repellent within two months, Crockford *et al.* (1991) found that breakdown of water repellency required several weeks of consistently wet weather, however soil repellency was re-established after one week of hot dry weather. Keizer *et al.* (2007) also found that within a potato maize fallow rotation large temporal variations in the severity of repellence occurred within periods as short as two weeks. Differences in the rate of repellence loss and reestablishment between studies are likely to be due to input of different types and rates of water repellent compounds under different landuse, vegetation and climates.

7.3.2.1 Effect of climate attributes and soil moisture on water repellence

Accumulation and loss of water repellent compounds resulted from monthly to seasonal (30 – 90 days) changes in climate attributes, rather than short-term climate events such as frosts, or individual rainfall events.

WDPT and WEP were not correlated with soil moisture ($m^3\ m^{-3}$), pan evaporation (mm), or sunshine (hrs). Significant correlations (p<0.05) between WDPT existed with cumulative rainfall in the 30, 60 and 90 days prior to analysis, cumulative average temperature in the 90 days prior to analysis, and cumulative soil water deficit in the 90 days prior to analysis.

Neither WDPT nor WEP were correlated with any climate attribute in the 10 days prior to analysis. Significant negative correlations between WEP existed with soil moisture at the time of sampling, cumulative rainfall in the 60 days prior to analysis, cumulative humidity in the 60 and 90 days prior to analysis, and cumulative soil water deficit in the 30, 60 and 90 days prior to analysis (Table 7.3-1). WEP was also positively correlated with cumulative average temperature in the 60 and 90 days prior to analysis. The high degree of correlation between WEP and average temperature (positive) and soil water deficit (negative) in the 90 days prior to analysis, indicates that accumulation of compounds responsible for the severity of water repellence are likely to have resulted from microbial or plant processes which responded to seasonal changes in both soil moisture and temperature.

Table 7.3-1 Significant (p<0.05) correlations between water repellence and climate attributes.

		Soil moisture at analysis	Cumulative Rainfall			Average air temperature		Humidity		Soil water deficit		
Period prior to sampling			30 days	60 days	90 days	60 days	90 days	60 days	90 days	30 days	60 days	90 days
WDPT	Correlation		-0.833	-0.850	-0.883		0.667					-0.700
	Significance		0.005	0.004	0.002		0.050					0.036
WEP	Correlation	-0.929		-0.733		0.750	0.867	-0.700	-0.700	-0.683	-0.767	-0.817
	Significance	0.003		0.025		0.020	0.002	0.036	0.036	0.042	0.016	0.007

Non significant (p>0.05) correlations have been excluded from the table.

While seasonal monitoring demonstrated the general case that an inverse relationship existed between antecedent soil moisture and water repellency, the reduction in both WEP and WDPT between May 2010 and June 2010 occurred during a period in which only moderate rainfall occurred (21 mm in 39 days). Although the laboratory experiments demonstrated that saturation and leaching may reduce repellence, particularly the persistence of water repellence, the moderate level of rainfall over this period suggests factors other than rainfall may have attributed to the reduction in water repellence.

Leighton-Boyce *et al.* (2005) and Keizer *et al.* (2008) also found that factors other than antecedent rainfall may play a role in determining temporal changes in water repellency, factors included; rainfall intensity, temperature, root activity and microbial activity. For example, Roper (2005) found that constant soil moisture (-10 kPa) in the laboratory and frequent irrigation in the field, decreased water repellence (MED) by increasing the population of wax degrading bacteria (*Rhodococcus* spp. and *Mycobacterium* spp.). A high degree of correlation between water repellence severity (WEP) and soil water deficit has also been reported by Leighton-Boyce *et al.* (2005) who found the relationship between water repellence (MED) and soil moisture was stronger than the relationship with antecedent rainfall.

7.3.3 Effect of leaching on water repellence

Leaching significantly reduced both the severity (WEP) and persistence of water repellence (WDPT) (Figure 7.3-3). WEP significantly (p<0.05) decreased between the dried soil and the 1st, 1st and 2nd, and 3rd and 4th leaching events (Figure 7.3-3), however there was no significant difference between the WEP of the 4th and 5th or 2nd and 3rd leaching events. The first leaching event also significantly (p<0.05) reduced the WDPT between the air dried soil and the 1st leaching event, and between the,2nd and 3rd, and 3rd and 4th events, however no significant reduction in WDPT occurred between the 1st and 2nd events or between the 4th and 5th events. The first leaching event had the greatest effect on WDPT, in which WDPT was reduced by 95 % from 10108 seconds (SD 3208 seconds) to 466 seconds (SD 91 seconds), while the WEP was reduced by only 9.3 %.

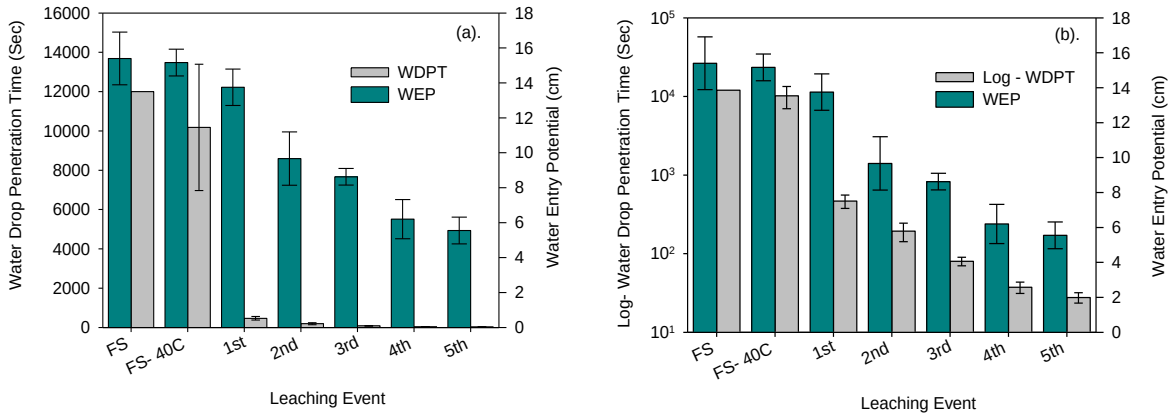

Figure 7.3-3 (a) Effect of leaching on water drop penetration time (WDPT), and water entry potential (WEP), (b) Effect of leaching on the log of water drop penetration time (log-WDPT), and water entry potential (WEP). FS = Archived prior to air drying, FS-40°C = Archived soil dried to 40°C for comparison with leached samples.

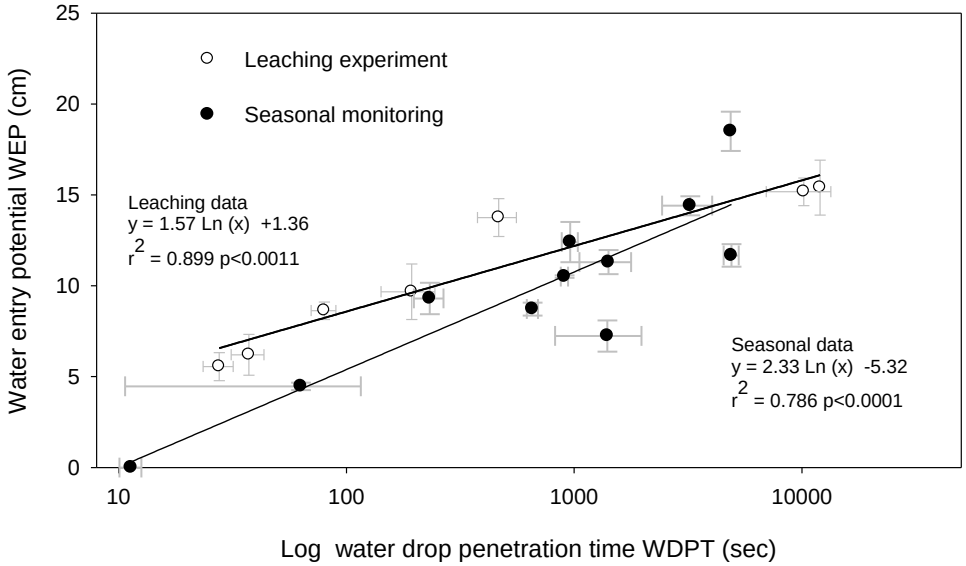

Figure 7.3-4 (a) Relationship between log-WDPT and WEP from the leaching experiment (open) and seasonal monitoring (closed). Error bars represent ±1 standard deviation.

Figure 7.3-5 Organic staining (brown colour) in shrinkage cracks, ped faces and macropores in the B21 horizon, site B.

This suggests that leaching had a greater effect on the water repellent compounds responsible for persistence of water repellence than severity of water repellence. The relationship between water repellence persistence (WDPT) and physical severity (WEP) was described by logarithmic relationship R^2 = 0.90 - 0.79 (Figure 7.3-4).

The amount of dissolved organic carbon in the leachate was sequentially lower with each leaching event (Figure 7.3-6). A significant (p<0.05, df 4) linear regression existed between dissolved organic carbon content (DOC) of the leachate and both WDPT (p = 0.0001) and WEP (p = 0.0139). The stronger relationship between WDPT and DOC indicates the reduction in WDPT, and to a lesser extent WEP, resulted from the leaching of soluble water repellent organic components from the soil. Pedological evidence of organic coatings on ped faces and within macropores in the B21 horizon (Chapter 3.3.2), (Figure 7.3-5) provides further independent field based evidence that soluble organic compounds have leached from the hydrophobic A1 horizon into the B21 horizon.

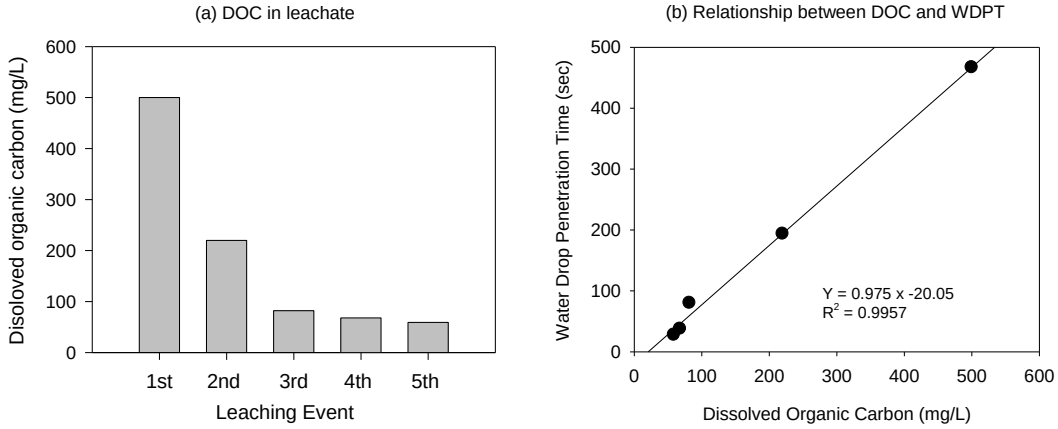

Figure 7.3-6 (a) Concentration of dissolved organic carbon in leachate following each leaching event, (b) Relationship between dissolved organic carbon in leachate and water repellence WDPT.

The high organic carbon content of the leachate indicated the reduction in persistence of water repellence resulted from the permanent, sequential, removal of soluble amphiphilic compounds from either the surface of the sand grains or interstitial spaces between sand grains (Doerr *et al.* 2000). The laboratory experiments indicate that water repellence at the University of Tasmania Farm is mainly caused by a coating of amphiphilic molecules on soil particles. When these soils are saturated the attraction of water to the polar ends of these molecules is thought to weaken the soil-molecule bond leading eventually to the displacement f the organic compounds from the soil particles resulting in a wettable soil (Doerr *et al.* 2000).

7.3.4 Effect of soil moisture and water repellence on infiltration

The effect of prolonged soil saturation on leaching of water repellent compounds from the soil was not understood at the time that the infiltration experiments were conducted. Consequently the wet treatments represent both the effects of high antecedent soil moisture and leaching on the actual water repellence.

7.3.4.1 Antecedent soil moisture

Infiltration of water appeared to be greater in the dry treatment than the wet treatment, however the only significant (p<0.05, df 4) difference between the two soil moisture treatments occurred at the ψ -0.84 kPa supply potential (Figure 7.3-7a). This finding contradicts findings in Chapter 6.3.5.1 in which the unsaturated hydraulic conductivity through macropores (ψ -0.19 and -0.13 kPa) was significantly (p<0.05, df 41-43) lower in the wet treatment than in the dry treatment. Discrepancy between the two results was attributed to the reduced number of replicates (three) compared to Chapter 6.3.5.1 (six).

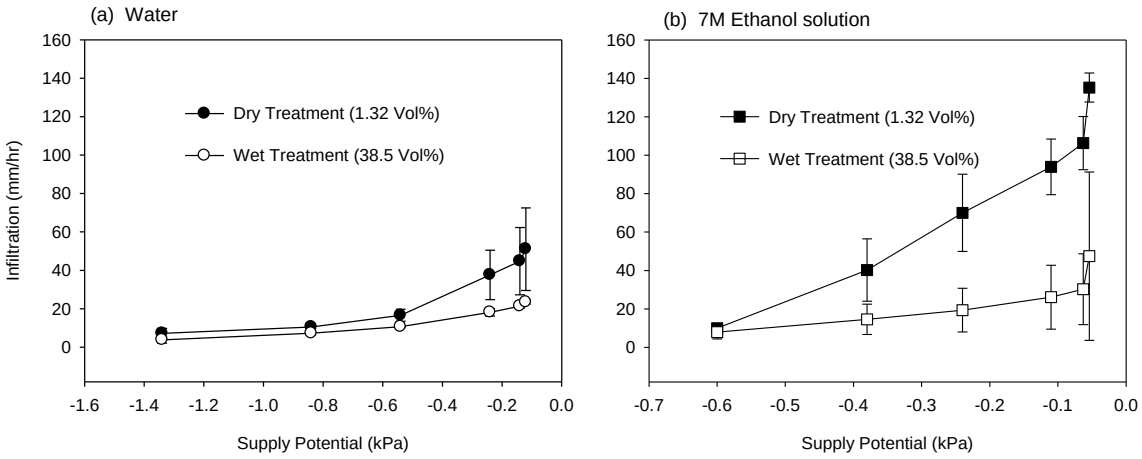

Figure 7.3-7 Effect of antecedent soil moisture at site B on (a) infiltration of water (b) infiltration of 7M Ethanol solution. Error bars represent ±1 standard deviation.

Infiltration of the 7M ethanol solution was significantly (p<0.05, df 4) higher in the dry treatment than the wet treatment at supply potentials between saturation ψ =0 and -0.24 kPa (Figure 7.3-7b). The intrinsic permeability of the 7M ethanol solution was also significantly higher in the dry treatment than the wet treatment at all supply potentials other than -0.49 kPa (Figure 7.3-8b). As intrinsic permeability was not influenced by sorptivity or matric potential gradients, results indicate the effect of water repellence was overcome by the ethanol solution.

Consequently fluid movement through pores larger than 610 µm was restricted by pre-existing soil water in the wet treatment. This result does not concur with Lamparter *et al.* (2010) who found initial soil moisture content had little effect on infiltration of ethanol, and that the pre-existing water was completely displaced via piston flow by ethanol after less than 1.25 pore volumes.

However, Lamparter *et al.* (2010) used artificially hydrophobic sand grains in repacked columns with free air and water movement at the base of the column, in contrast to this study in which fluid movement in the A1 horizon was restricted by near saturated conditions in the A2 horizon and low permeability of the B2 horizons.

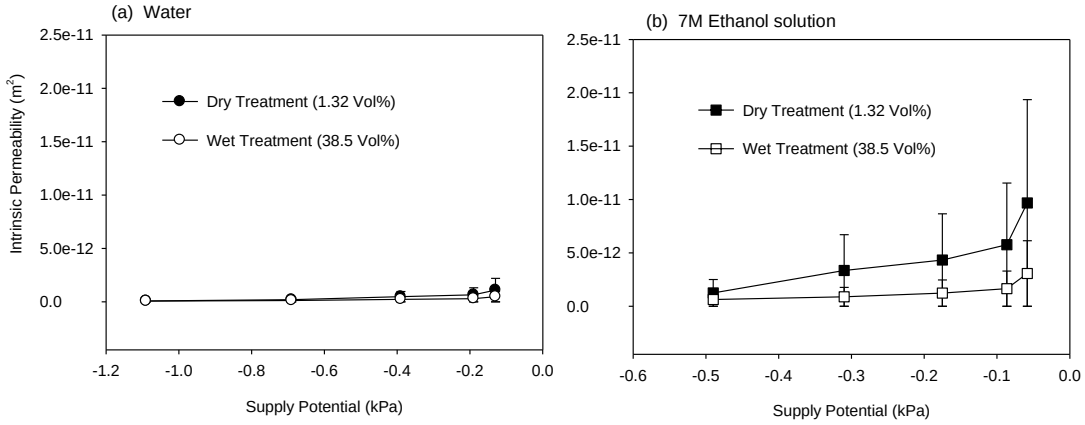

Figure 7.3-8 Site B: Effect of antecedent soil moisture at site B on (a) intrinsic permeability of water (b) intrinsic permeability of 7M Ethanol solution. Error bars represent ±1 standard deviation.

The reduction in the intrinsic permeability and infiltration of the 7M ethanol solution at high antecedent soil moisture provides additional evidence to the dye staining in Chapter 4.0 that vertical infiltration into the A1 horizon was impeded due to difficulty displacing existing soil water further down the soil profile.

7.3.4.2 Water repellence

Comparison between the 7M ethanol solution and water was complicated by differences in effective supply potential of the two fluids (Jarvis *et al.* 2008). Infiltration was able to be directly compared between the two fluids at supply potentials of -0.24 kPa and between -0.12 kPa for water and -0.11 kPa for ethanol. Intrinsic permeability and FWMPD were best compared between water at a supply potential of -0.19 kPa and the 7M ethanol solution at -0.175 kPa.

In the wet treatment, no significant difference existed between the infiltration rate of the two solutions (Figure 7.3-9a). However the intrinsic permeability of the 7M ethanol solution was significantly (p<0.05) higher than water between the -0.175 and -0.19 kPa supply potentials (Figure 7.3-9b). No significant difference existed between the FWMPD of the two fluids between -0.175 and -0.19 kPa in either soil moisture treatment. This suggests that although the two soil moisture treatments had similar porosity, prolonged saturation in the wet treatment overcame the effect of water repellence by either (i) leaching of soluble water repellent compounds (Chapter 7.3.3), (ii) increased microbial consumption of water repellent waxes (Roper 2004; 2005), or (iii) exceeding the critical soil moisture content of the soil (Dekker and Ritsema 1996b; King 1981).

In the dry treatment, infiltration of the ethanol solution was significantly (p<0.05, df 4) higher than the water at the -0.12 to -0.11 kPa supply potential, however differences at -0.24 kPa supply potential were not significant. The intrinsic permeability of the ethanol solution was also significantly (p<0.05, df 4) higher than the water at the -0.175 to -0.19 kPa supply potentials (Figure 7.3-10). This indicates water repellence restricted water movement through macropores in the dry treatment. Figure 7.3-10 indicates that the different infiltration and intrinsic permeability of the two fluids increased towards saturation from a supply potential of approximately -0.6 kPa. Near saturation, water repellence appeared to have reduced infiltration by approximately 57 % and intrinsic permeability by a factor of 10. This result differs to that of Jarvis *et al.* (2008) who found that water repellence reduced infiltration of water by a factor of approximately 15 compared to infiltration of ethanol.

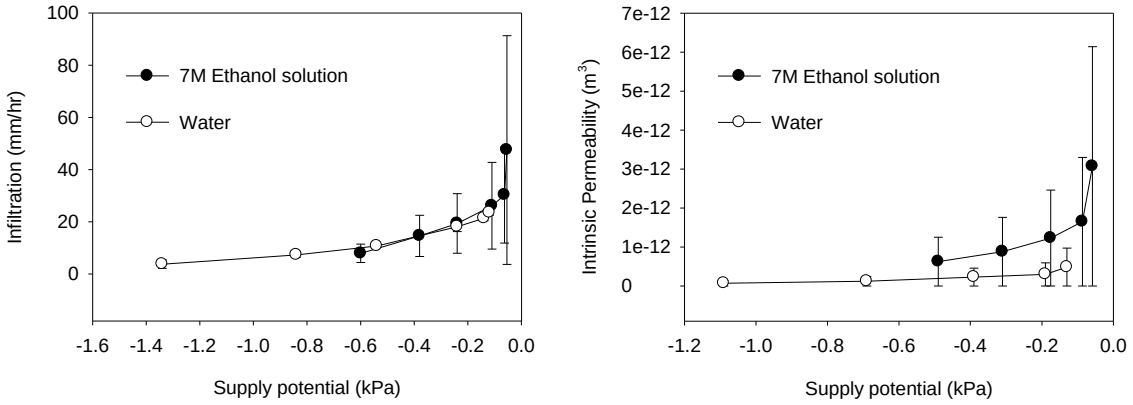

Figure 7.3-9 Comparison of (a) infiltration and (b) intrinsic permeability of water and 7M ethanol solution in the wet treatment. Error bars represent ±1 standard deviation.

The significantly higher intrinsic permeability of the 7M ethanol solution in both soil water treatments demonstrated that differences in infiltration were not attributed to sorptivity, or fluid properties, rather water repellence impeded water entry into pores larger than 500 µm (ψ -0.6 kPa). Lamparter *et al.* (2006) attributed differences in infiltration of water and ethanol to water repellence reducing the capillary force required for water to enter individual pores with narrow throats (bottlenecks) which resulted in a local stop of the advancing wetting front. Jarvis *et al.* (2008) also found that water repellence resulted in many structural pores being inactive during infiltration.

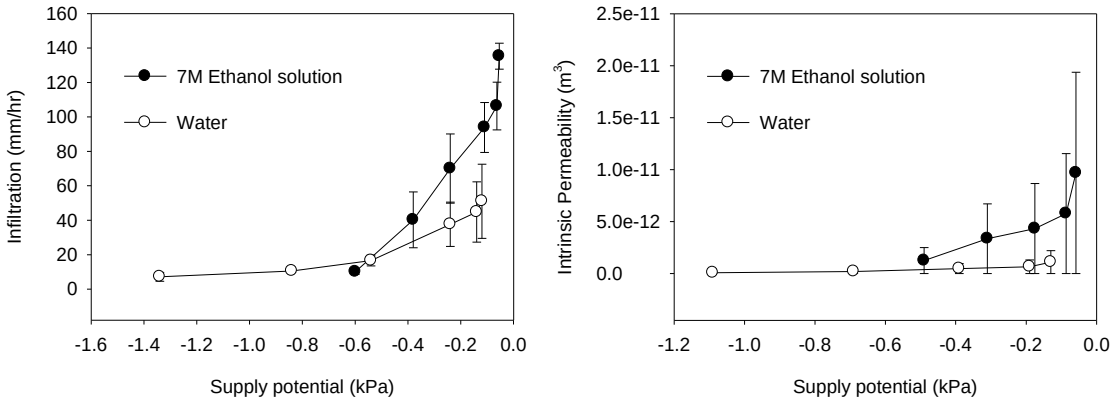

Figure 7.3-10 Comparison of (a) infiltration and (b) intrinsic permeability of water and 7M ethanol solution in the dry treatment. Error bars represent ±1 standard deviation.

7.3.5 Effect of soil moisture, leaching, and air entrapment on infiltration rate

Run B and C, in which air flow at the base of the Hele-Shaw tank was restricted or closed, resulted in the slowest infiltration rates (Figure 7.3-12). The highest infiltration rates occurred for runs with free air movement and non water repellent soil (Runs D & E). In hydrophilic soil, air entrapment reduced infiltration from an average of 206 mm hr^{-1} to 10.4 mm hr^{-1}. Whilst with free air flow, high antecedent soil moisture decreased the infiltration rate from 240 mm hr^{-1} (Run D) to 172 mm hr^{-1} (Run E), and water repellence decreased infiltration from 206 mm hr^{-1} (Runs D and E) to 85 mm hr^{-1} (Runs A and H). The twin rate of infiltration rate in Run H (Figure 7.3-12a) indicated that infiltration increased after overcoming the initial effects of water repellency approximately 90 minutes after infiltration commenced, which was very similar to WDPT 80 mins. Analysis suggests that air / water entrapment at the base of the soil profile had a greater effect on infiltration into a hydrophobic soil than either the degree of water repellence or the antecedent soil moisture content. Wang *et al.* (1998b) also demonstrated that the speed of finger propagation in water repellent soil was always higher in soil with free air flow than when air flow was confined.

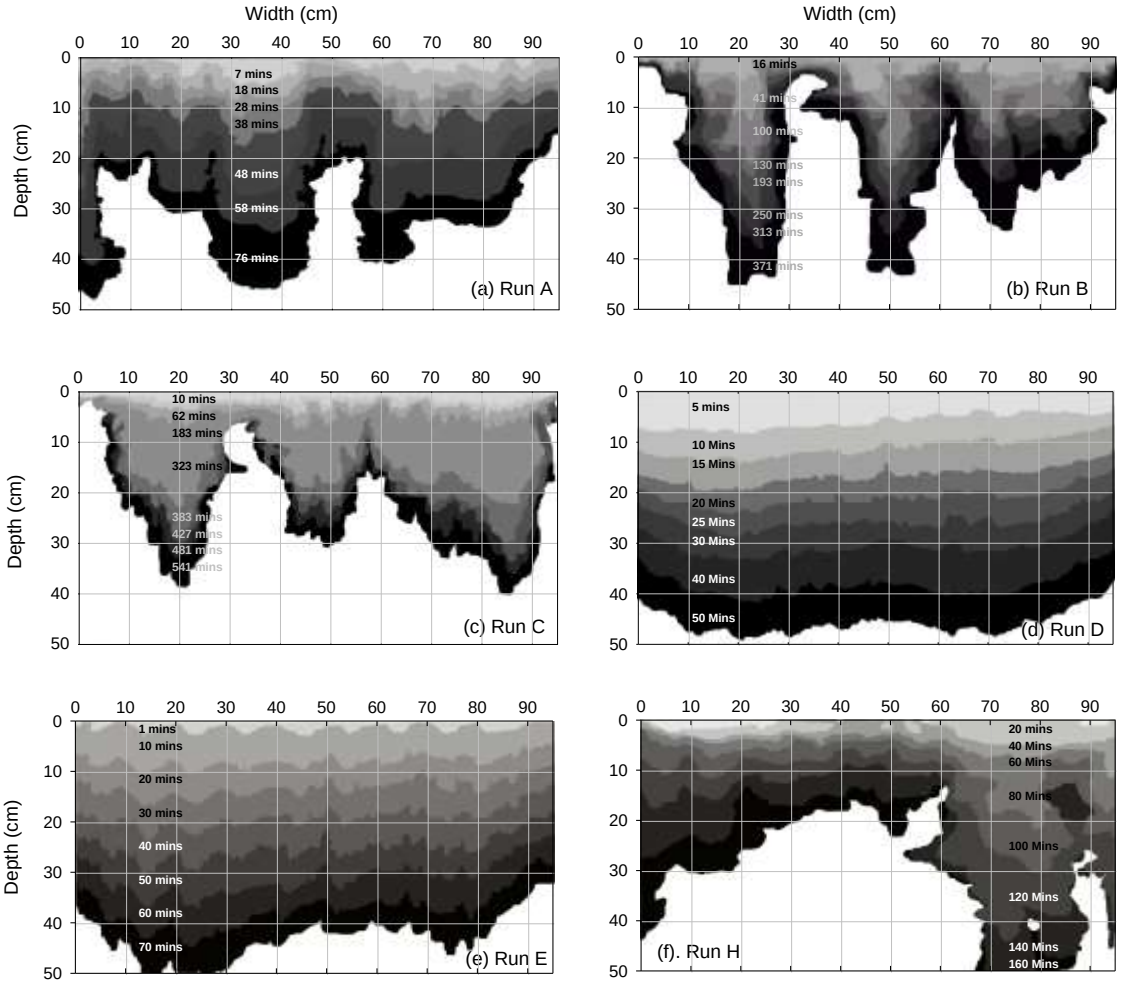

Figure 7.3-11 Sequential infiltration over time;

(a) Run A, collected April 08, hydrophobic, dried 40°C 24 hrs, open air flow, WDPT 4800 sec

(b) Run B, collected June 09, hydrophilic, dried 40°C 24 hrs, air entrapment, WDPT 0 seconds.

(c) Run C, collected June 09, hydrophilic, saturated and drained following Run B, restricted air flow, WDPT 0 sec.

(d) Run D, collected July 2009, hydrophilic, dried 45° C 96 hours, open air flow, WDPT 38 sec.

(e) Run E, collected July 2009, hydrophilic, saturated and drained following run D, open air flow. WDPT 0 sec.

(f) Run H, collected April 2008, hydrophobic, dried at 105° C for 24 hours, open air flow, WDPT 4860 seconds.

Animations of Hele-Shaw infiltration experiments are presented on the CD-Rom (Appendix 8.3, Figure A8.6 – A8.11).

Wang *et al.* (1998c) found that the infiltration rate was equal to and controlled by the rate of air outflow, and that the infiltration rate varied inversely with the air pressure ahead of the wetting front.

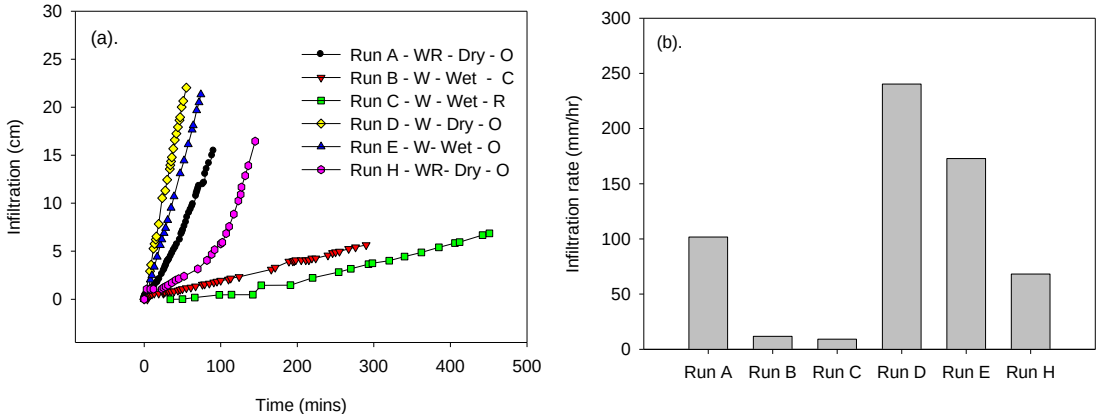

Figure 7.3-12 Effect of soil moisture, air entrapment and leaching on (a) cumulative infiltration over time (b) average infiltration rate. Note: WR water repellent, W - wettable, Dry = oven dried 40 – 105 °C, Wet = saturated and drained for 24 hrs, O = open - no air entrapment, C = closed – air entrapment.

7.3.5.1 Effect of soil moisture, leaching, and air entrapment on the degree of flow instability

In the absence of air / water entrapment wetting front instability and fingers formed in water repellent soil (WDPT 4800, Runs A and H) but not the hydrophilic soil (WDPT 0, Run D). These results are in agreement with Carrillo *et al.* (2000b) who reported that the degree of finger formation increased with greater water repellence (WDPT). Finger width and finger depth increased with time, indicating that lateral movement of soil water into the soil matrix (from the infiltrating fingers) occurred once the localised persistence of water repellence (WDPT) was overcome. In Run A, lateral flow along the sides of the glass may have broadened the infiltrating fingers below 40 cm depth resulting in a lower than expected degree of wetting front instability (Figure 7.3-13). Run H was performed to confirm the results from run A in which flow down the sides of the tank was prevented. Animation of Hele-Shaw infiltration experiments are presented on the CD Rom (Appendix 8.3).

Soil collected in July 2009 after prolonged rainfall was found to be wettable (hydrophilic, WDPT 0), which in the absence of air entrapment, resulted in uniform flow as indicated by the horizontal wetting front and low degree of wetting front instability 0.131 cm $\%^{-1}$ (SD 0. 015 cm $\%^{-1}$) Run D, and 0.127 cm $\%^{-1}$ (SD 0.018 cm $\%^{-1}$) Run E (Figure 7.3-11 and Figure 7.3-13).

The occurrence of uniform flow in the hydrophilic soil was not influenced by initial soil moisture content. In hydrophilic soil (WDPT 0), restricted (Run C) or closed air / water (Run D) flow at the base of the tank resulted in development of finger flow regardless of antecedent soil moisture.

Comparison between Run B (no air flow) and Run E (air flow) demonstrated that air / water entrapment at the base of the Hele-Shaw tank resulted in a similar degree of instability 0.377 cm $\%^{-1}$ to that which developed in dry hydrophobic soil with open air flow 0.244 – 0.400 cm $\%^{-1}$ (Runs A and H respectively). Using a similar experimental approach Wang *et al.* (1998b) also demonstrated that large fingers or wetting front perturbations (7-15 cm wide) could be induced during infiltration into wettable (hydrophilic) sand by restricting air flow at the base of a Hele-Shaw chamber (similar to Runs B and C).

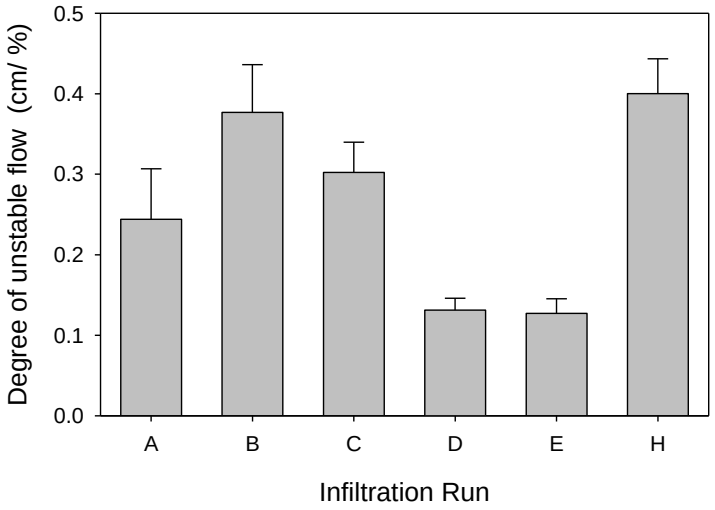

Figure 7.3-13 Degree of unstable flow, measured as the mean slope between the depth of infiltration and proportion of infiltrated soil for the final three time intervals. Error bars represent ±1 standard deviation.

Wang *et al.* (1998b; 1998c) found that as water infiltrated into the soil, soil air was displaced and became compressed ahead of the wetting front resulting in decreased infiltration and formation of soil water fingers. However when air flow at the base of the tank was not restricted Wang *et al.* (2003) found that finger development was highly dependent on antecedent moisture, which affected the timing of finger formation, finger width, and the rate of finger propagation. In dry soil, finger development and propagation stopped as soon as infiltration stopped, but continued to form and propagate in the wet soil.

Finger width ranged from an average of 4.5 cm in dry soil to 17 cm when soil was very wet, and finger propagation velocity decreased from 4.5 cm min^{-1} in dry soil to 2.9 cm min^{-1} in wet soil. Ritsema *et al.* (1998b) also noted that that infiltration into an extremely water repellent soil at high antecedent soil moisture resulted in the wetting front developing perturbations which did not grow into fingers. Perturbations were believed to have formed in places where the soil was wetter, or potentially less water repellent, resulting in slightly deeper protrusion of the wetting front which either propagated or dissipated depending on antecedent soil water.

Infiltration into wet, highly water repellent soil was not able to be replicated in this study as soil was not able to be wet-up without severely reducing both the potential (when re-dried) and actual (when moist) water repellence, as demonstrated by the leaching experiment.

Hele-Shaw experiments demonstrated that air / water entrapment at the base of the Hele-Shaw tank had a greater effect on the development of flow instability, than water repellence or antecedent soil moisture. Antecedent soil moisture was not significantly related to the degree of flow instability explaining only 0.2 % of the variance (p = 0.859), compared to 13.4 % for water repellence (p = 0.136) and 22 % for air flow (p = 0.47). These findings differ to Wessolek *et al.* (2008) who found that development of finger flow in a water repellent sandy soil was seasonally dependant on antecedent moisture content, and Taumer *et al.* (2006) who demonstrated that water content had greater influence on occurrence of finger flow, than climate or rainfall attributes.

Based on the results from the Hele-Shaw experiments, it is postulated that occurrence of finger flow in the dry treatment of the dye staining experiment (Chapter 4.3) resulted from accumulation of water repellent compounds in the spring and summer prior to dye tracer infiltration. In the dry treatment there was a lack of air entrapment or compression below the wetting front due to the large volume of open pores and shrinkage cracks below the A1 horizon. However in the wet treatment, instability in the wetting front resulted from infiltration of the dye tracer compressing existing soil water and air within the A1 horizon, as demonstrated in Run C. Entrapment of the existing soil water and air within the A1 horizon caused by clay swelling in the B2 horizons reduced the subsoil hydraulic conductivity (Chapter 5.3) and prevented displacement of existing soil water and entrapped air further down the soil profile.

7.4 Conclusion

7.4.1 Effects of antecedent soil moisture on water repellence, flow rate and wetting front instability

The laboratory drying experiment (Chapter 7.3.1) demonstrated that soil moisture had little influence on water repellence (WDPT) of a previously extremely hydrophobic soil. However the leaching experiment (Chapter 7.3.3) indicated that saturation prior to analysis, leached the water repellent coatings from the soil, consequently the true nature of the relationship between soil moisture and water repellence prior to saturation was not replicated in the experiment.

In situ infiltration from disk permeameters demonstrated that antecedent soil moisture significantly influenced infiltration of both water and the 7M ethanol solution, for at least one supply potential, however antecedent soil moisture had no effect on the intrinsic permeability of water. The lack of a significant difference in the infiltration rate of the two solutions in the wet treatment, suggested prolonged saturation had overcome the effects of water repellence as a result of (i) leaching of soluble water repellent compounds (Chapter 7.3.3), (ii) increased microbial consumption of water repellent waxes (Roper 2004; 2005), or (iii) exceeding the critical soil moisture content of the soil (Dekker and Ritsema 1996b; King 1981).

The significantly higher intrinsic permeability of the 7M ethanol solution in the dry treatment compared to the wet treatment, indicated that once water repellence had been overcome, pre-existing soil water in the wet treatment restricted flow through pores larger than 610 µm. The Hele-Shaw tank experiments also demonstrated that antecedent soil moisture had less effect on the development of flow instability than both air entrapment and water repellence. Although with free air flow, high antecedent soil moisture decreased the infiltration rate from 240 mm hr^{-1} to 172 mm hr^{-1}.

Even after accounting for differences in the fluid property of the ethanol solution, a degree of caution must be taken in the interpretation of results from the disk permeameter experiments. The validity of hydraulic conductivity and intrinsic permeability values calculated from approaches such as Reynolds and Elrick (1991) are questioned for hydrophobic soils (Clothier *et al.* 2000; Logsdon 1997) in which it is assumed that participation in flow is exclusively controlled by the supply potential.

Furthermore development of finger flow under the infiltrating disk surface reduced the area of soil participating in flow (Figure 7.4-1), which resulted in lower than expected values of hydraulic conductivity or intrinsic permeability in the dry treatment.

Figure 7.4-1 Wetting (dark) pattern under disk permeameter demonstrating a 43 % reduction in flow area under the disk permeameter at 2 cm depth, site D.

As Buczko *et al.* (2006) demonstrated, reduced hydraulic conductivity in a water repellent soil due to incomplete wetting beneath a hood infiltrometer, in which only single flow paths contributed to the measured 'apparent' saturated hydraulic conductivity. Error with the calculation of hydraulic conductivity and intrinsic permeability in hydrophobic soil may also result from vapour flow rather than fluid flow (Doerr *et al.* 2002), or be an artefact of infiltration time as demonstrated by Clothier *et al.* (2000) in which the apparent steady state infiltration rate of a water repellent silt loam topsoil increased steadily after 100 minutes observation.

7.4.2 Seasonal variation in water repellence

Seasonal monitoring of potential water repellence (air dried soil) demonstrated that both the severity (WEP) and persistence (WDPT) of the potential water repellence varied seasonally. Results were similar to Doerr and Thomas (2000) in that water repellence was not re-established after seasonal rainfall (leaching) unless new input of hydrophobic substances occurred.

The significant correlation between WEP with both soil water deficits in the 30 to 90 days prior to sampling, soil moisture at the time of sampling, and air temperature and humidity in the 60 to 90 days prior to sampling, indicated that accumulation of hydrophobic compounds was likely to have resulted from microbial process or accumulation of plant residues.

Rainfall in the 60 to 90 days prior to sampling was significantly correlated with WDPT which indicated that prolonged winter rainfall may have reduced the severity of water repellence, however this was not associated with rainfall within the 10 days prior to sampling. Laboratory leaching experiments demonstrated that water repellent compounds were removed from the soil by successive leaching events which caused a disproportional reduction in the persistence of water repellence (WDPT) compared to the severity of water repellence (WEP). The highly significant relationship between the dissolved organic carbon content of the leachate and WDPT indicated that leaching disproportionally removed the soluble amphiphilic organic compounds responsible for the persistence of water repellence.

7.4.3 Effects of water repellence on water movement and flow instability

The significantly higher intrinsic permeability of the 7M ethanol solution in both soil water treatments demonstrated that differences in infiltration were not attributed to sorptivity, or fluid properties. Rather, water repellence impeded water entry into pores larger than 500 µm (ψ -0.6 kPa).

Hele-Shaw tank experiments supported findings from the dye staining experiments (Chapter 4.0) in which unstable flow developed in the water repellent A1 horizon at both high and low antecedent soil moisture. The mechanism for flow instability at high antecedent soil moisture was not previously understood. Results from the Hele-Shaw tank experiments demonstrated that by not allowing air / water flow through the base of the soil profile, infiltration of new water into both wettable and water repellent soil resulted in similar levels of flow instability to that observed during infiltration into dry water repellent soil.

Leaching of soluble organic compounds from topsoils has previously been reported by Artiola and Walworth (2009), Laegdsmand *et al.* (2005) and Vinther *et al.* (2006). Ritsema *et al.* (1998a) speculated that the commonly observed re-wetting of existing flow pathways or fingers in water repellent soils was due to leaching of hydrophobic compounds from the pores along the finger flow pathways. They speculated that leaching of soluble water repellent compounds would change the water retention functions of the soil and rendered the soil within the flow paths more wettable than the surrounding soil. Thus it was thought that as time progresses, these pathways would develop into permanent preferential flow pathways. However reestablishment of water repellence between August 2009 and May 2010 confirmed the study by Doerr and Thomas (2000) in which they postulated that for at least some soils, the relationship between soil moisture and water repellence is hysteretic, and that water repellence is not re-established after seasonal rainfall, unless input of new hydrophobic substances occurs.

Further research is required to better understand the effects of seasonal rainfall and microbial processes on the accumulation and depletion of water repellent compounds in the sandy loam topsoil of texture contrast soils. It is expected that this research would facilitate a better understanding of the effects of seasonal water repellence on hydrological processes at the pedon scale so that further progress can be made on simulating the effects of water repellence and occurrence of finger flow in soil water models (Bachmann *et al.* 2007).

7.5 Key points

- A poor relationship existed between soil moisture and WDPT due to the effects of initial soil wetting on WDPT.
- Water repellence varied seasonally from a WDPT of 11.3 sec and WEP of 0 cm in winter (July 2009), to a maximum WDPT of 906 sec and a WEP of 14.4 cm in May 2010, before decreasing in June 2010.
- Seasonal changes in WDPT were greater than WEP indicating that persistence of water repellence varied more than severity.
- Seasonal change in WDPT and WEP were significantly related to prior rainfall, temperature and soil water deficit, (at different time periods) indicating that accumulation of water repellent compounds is likely to have resulted from microbial processes or plant inputs.
- Leaching preferentially removed the soluble organic compounds responsible for the severity of water repellence rather than the compounds responsible for the severity of water repellence.
- Antecedent soil moisture had no effect on the intrinsic permeability of water, however the intrinsic permeability of the 7M ethanol solution was significantly higher in the dry treatment at all but one supply potential.
- In the wet treatment, pre-existing soil water restricted flow through pores > 610 µm.
- In the wet treatment, no significant difference existed between the infiltration of the two solutions, which suggested prolonged saturation overcame the effect of water repellence on infiltration via either leaching of soluble water repellent compounds, increased microbial consumption of water repellent waxes, or exceeding the critical soil moisture content.
- In the dry treatment, water repellence reduced infiltration through macropores by approximately 57 % and intrinsic permeability by approximately one order of magnitude.
- Water repellence impeded water entry into pores larger than 500 µm (ψ -0.6 kPa).
- Air entrapment had greater effect on flow instability than either the degree of water repellence or antecedent soil moisture.
- In hydrophilic soil air entrapment reduced infiltration from an average of 206 mm hr^{-1} to 10.4 mm hr^{-1}.
- In the absence of air entrapment, wetting front instability and fingers formed in water repellent soil (WDPT 4800), but not the hydrophilic soil (WDPT 0).
- Air entrapment induced similar levels of wetting front instability and fingering in hydrophilic (wettable) soil as observed in hydrophobic soil with free air flow.

8.0 Soil-water modelling, parameter estimation and simulation of infiltration and seasonal response to rainfall.

8.1 Introduction

A number of modelling approaches have been developed to simulate water and solute movement in soil (Jarvis 2007). However in most soil water models, preferential flow is not explicitly simulated (Simunek and van Genuchten 2007). Over the last two decades, a relatively large number of commercially available models have been developed that consider preferential flow. These models range from relatively simplistic bi-modal dual-porosity models to complex dual-permeability, and multi-region models. Review of preferential flow modelling is presented by Köhne *et al.* (2009a), Simunek *et al.* (2003), Simunek and van Genuchten (2007; 2008).

Model choice is not straightforward as models differ in relation to sophistication, parameterisation requirements, preferential flow capability, flow conceptualisation, access to software, access to technical support, and data output. A review of commercially available models indicated the HYDRUS suite of models (Simunek *et al.* 2003; Simunek *et al.* 2008) and MACRO 5.1 (Jarvis 1994) offered the best combination of model sophistication, ease of parameterisation and technical support (Table 8.1-1). Model choice was limited by recognition that no single model was able to adequately simulate the full range of preferential flow processes observed in Chapter 4.0, or account for the threshold like control on the occurrence of preferential flow (Chapter 5.0). In addition, one dimensional models such as HYDRUS-1D and MACRO 5.1 are not able to simulate lateral flow, funnel flow or finger flow (Bachmair *et al.* 2010; Beulke *et al.* 2001; Dubus and Brown 2002). Consequently different models or model conceptualisations have been employed to explore different research questions. Further discussion of model choice and capability is presented in Appendix 7.0.

Whilst a number of multiple pore domain models have been developed to simulate preferential flow their use is currently limited by; difficulty simulating finger flow in water repellent soil (Bachmann *et al.* 2007; Doerr and Thomas 2000), the large number of parameters required to characterise the hydraulic properties of both the macropore and micropore flow domains (Simunek *et al.* 2003), difficulty representing changes in soil structure associated with soil shrinkage, and difficulty simulating film flow or non-saturated flow in macropores (Gerke *et al.* 2010).

Discussions with Dr Brent Clothier, Dr Markus Deurer, and Dr Steve Green, (*pers. comm*. Plant and Food Research, New Zealand), authors of the SPASMO model, and Simunek (2008 pers. comm.) author of HYDRUS, indicated that the range of processes demonstrated in the previous chapters were not able to be explicitly simulated with the current range of commercially available soil water models such as MACRO 5.1, and HYDRUS-1D-2D/3D. In response the scope and intent of the modelling studies presented here was limited to validation of model performance in relation to:

I. Direct and inverse approaches for determining van Genuchten parameters and saturated hydraulic conductivity.
II. Effect of different parameterisation approaches on simulated infiltration into soil at high and low antecedent soil moisture (simulation of the dye staining experiments).
III. Effect of different parameterisation approaches and model sophistication on changes in soil water content adjacent to site B between September 2007 and September 2009.
IV. Effect of sand infills on simulated infiltration at high and low antecedent soil moisture.
V. Effect of lateral flow on simulation of infiltration into soil at high antecedent soil moisture.

Table 8.1-1 Comparison of soil water model functionality and ability to simulate preferential flow processes

Model	**HYDRUS 1D**			**HYDRUS 2D/3D**			**MACRO**
Module / Component	van Genuchten-Mualem	Mobile-Immobile	Dual Permeability	van Genuchten-Mualem	Mobile-Immobile	Dual Permeability	Dual Permeability
Single Porosity	✓			✓			
Dual Porosity		✓			✓		
Dual Permeability 1D	✓	✓	✓				✓
Dual Permeability 2D /3D				✓	✓	#	
Fracture / Crack			✓			#	✓
Finger flow						*	
Funnel flow				✓	✓	#	
Calculation of E & T	✓	✓	✓				
Calculation of ET							✓

*May be represented by altering hydraulic conductivity of the A1 horizon, # restricted access.

8.2 Methodology

8.2.1 Determination of change in soil moisture from images of dye stained soil

In order to evaluate the ability of the models to simulate the dye tracer experiments, the change in soil moisture predicted by the models and the change in soil moisture following dye tracer infiltration had to be determined. Given analysis in Chapter 5.3.1 indicated that changes in soil moisture at site B should be determined from at least three EnviroSCAN soil moisture probes (equivalent to 60 cm analysis width) to ensure that variations in infiltration pathways are accounted for. As only one soil moisture probe was available, a procedure was developed to determine the change in soil moisture from 1.0 x 1.0 meter binary images of dye tracer infiltration (Chapter 4.0). The 'dye staining approach' estimated changes in volumetric soil moisture by relating the proportion of soil which participated in flow to the pore space available for infiltration.

8.2.1.1 Determination of available pore space for infiltration of the dye tracer

In the dry treatment, the volume of pores (ϕ_a) available for dye infiltration was calculated as the saturated water content (θ_{sat}) plus the porosity of the shrinkage cracks (Φ_{crack}), minus initial soil moisture ($\theta_{initial}$), minus drainable porosity between saturation (θ_{sat}) and field capacity at ψ-10 kPa (θ_{fc}). The change in volumetric soil moisture was calculated as the proportion of dye stained soil (D) multiplied by the available porosity (ϕ_a).

EQ 8.1 Change in soil moisture $(\Delta\theta_{dry}) = \phi_a \times D = (\theta_{sat} - \theta_{initial}) - (\theta_{sat} - \theta_{fc}) + \Phi_{crack} \times D$

In the wet treatment, drainable porosity was not considered as the initial soil moisture content ($\theta_{initial}$), was greater than field capacity (θ_{fc}). Available porosity (ϕ_a) and the change in volumetric soil moisture in the wet treatment was calculated as;

EQ 8.2 Change in soil moisture $(\Delta\theta_{wet}) = \phi_a \times D = \theta_{sat} - \theta_{initial} + \Phi_{crack} \times D$

In order to accurately compare results from the dye staining approach to the soil moisture probe, the proportion of dye stained soil 10 cm either side of the soil moisture probe was also determined, referred to as the 'probe area'. Field capacity and saturation were determined from desorption analysis of 100 mm diameter intact cores (Chapter 6.2.1.1).

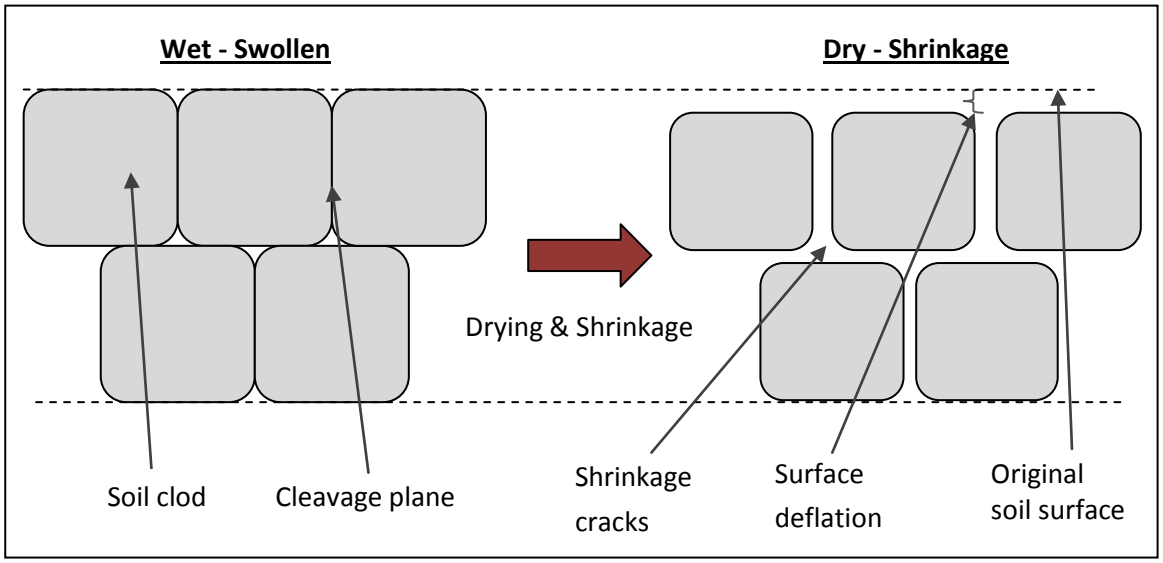

Figure 8.2-1 Conceptual diagram of soil shrinkage, surface deflation and creation of inter clod porosity – shrinkage cracks.

8.2.1.2 Determination of shrinkage cracks volume

The pore volume associated with the creation of shrinkage cracks was estimated from the soil shrinkage characteristic curve (SSCC) by assuming the reduction in clod volume during desiccation was proportional to the volume of cracks formed between soil clods / peds minus the effect of desiccation on surface deflation. The SSCC was determined by the 'balloon approach' (Chapter 6.2.3) in which intact clods were wrapped in a rubber balloon and sequentially dried with an aquarium air pump (Cornelis *et al.* 2006; Tariq and Durnford 1993). Surface deflation was determined following the approach of Bronswijk (Bronswijk 1988; 1989) in which shrinkage was assumed to be three-dimensional and isotropic. Iterative volume of shrinkage cracks and gravimetric soil moisture was determined according to,

Volume of cracks or inter- clod porosity (no deflation)

EQ 8.3 $$\Phi_{crack} = (V_{sat} - V_{ci}) / V_{sat}$$

$$M_{gi} = M_i - A - M_{cd} / M_{cd}$$

$$D_f = (V_{ci} / V_{sat})^{1/3}$$

$$\Phi_{crack\text{-}sd} = (V_{sat} - V_{ci}) / (V_{sat} \times D_f)$$

Where,

Φ_{crack} = Porosity resulting from intra-ped cracks (crack porosity) ($cm^3\ cm^{-3}$).

V_{ci} = Iterative clod volume (cm^3) determined by Archimedes principal.

V_{sat} = Clod volume at -1.0 kPa (saturation) (cm^3).

D_f = Surface deflation factor (Bronswijk 1988; 1989)

M_{gi} = Iterative gravimetric soil moisture ($g\ g^{-1}$).

M_i = Iterative clod and apparatus mass (g).

A = Mass of apparatus (g),

M_{cd} = M mass of oven dried (105^oC) clod (g).

D_c = Final clod density (g/cm^3).

D_p = Particle density 2.65 (g/cm^3).

8.2.1.3 Assumptions

The change in soil moisture determined from images of dye tracer infiltration, the soil water characteristic and soil shrinkage characteristic curves required a number of assumptions to be acknowledged, for which the following observations were made;

- Sorption of the dye tracer to the soil particles did not retard dye movement. During excavation of the dry treatments it was noted the wetting front had moved ahead of the dye tracer in the A1 horizons (not observed in other soil layers), discussed by Flury and Fluhler (1995).
- Dye staining was isotropic, i.e. equally distributed in both horizontal and vertical dimensions. Dye staining indicated this assumption was invalid in the B horizons, in which dye staining occurred in fissure shaped voids rather than symmetrical isotropic pores (Chapter 4.3.8).
- Soil excavation did not occur preferentially along cleavage plains, or preferred dye tracer pathways. This is partly invalid, as soil hardness in the dry treatment resulted in some of the B21 horizon having to be excavation along cleavage plains.
- Confined field soils shrink in a similar manner to unconfined laboratory clods, consequently the reduction in clod volume following drying is proportional to the volume of shrinkage cracks in the field (after accounting for surface deflation). Unable to be tested.
- That soils did not swell during infiltration of the dye tracer. This assumption is supported by infiltrometer data (Chapter 6.3.4).
- That piston flow did not occur, i.e. infiltrating dye tracer did not displace pre-existing soil water held below field capacity further down the soil profile. The approach assumed the volume of pores occupied by initial soil water was not available for infiltration of new water. Tension infiltrometer data suggested that in the wet treatment, displacement of existing pore water by new water was restricted, but not entirely prevented (Chapter 6.3.5.1).
- In the dry treatment, infiltrated dye tracer retained in macropores and shrinkage cracks drained between field capacity ψ -10 kPa and saturation within 48 hours.
- That dye drained from macropores was available to fill other pores.
- Following drainage, the volume of dye tracer on the walls of stained pores was negligible (van Dam *et al.* 2004).

A1 Horizon: Desorption

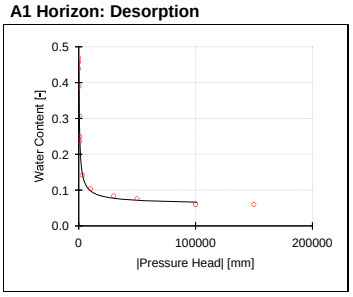

A1 horizon: Evaporation

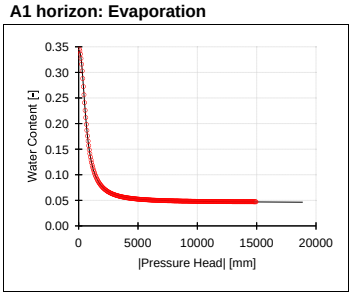

A2 horizon: Desorption

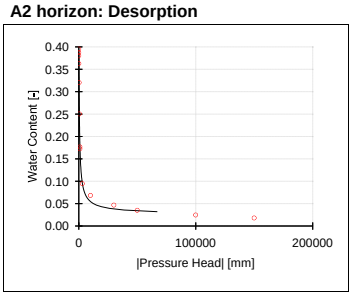

A2 Horizon: Evaporation

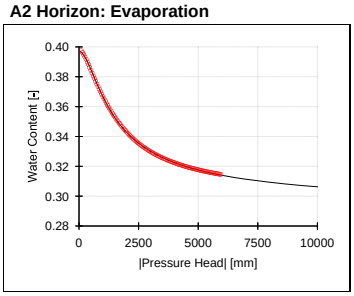

B21 Horizon: Desorption

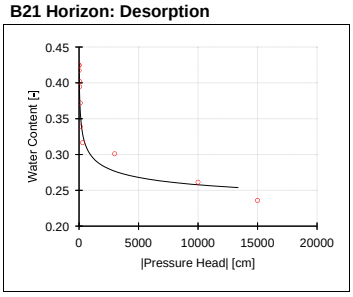

B21 Horizon: Evaporation

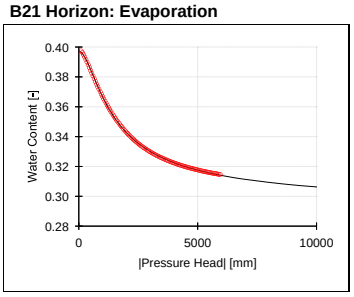

B22 Horizon: Desorption

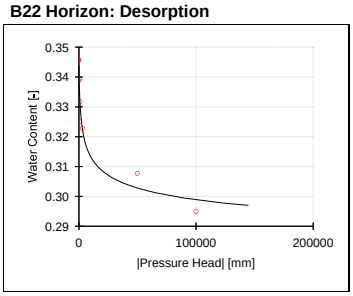

B22 Horizon: Evaporation

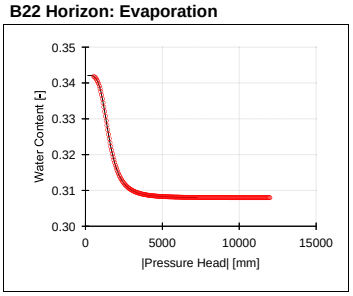

B23 Horizon: Desorption

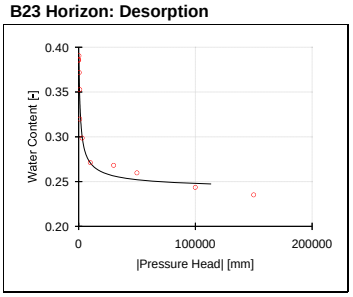

B23 Horizon: Evaporation

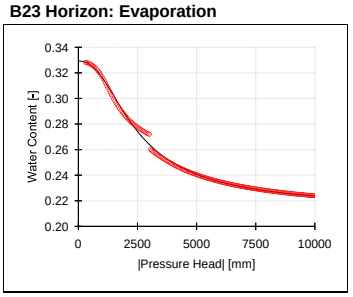

Figure 8.2-2 Curve fitting (RETC) approximation of retention data using van Genuchten equation.

- That -10 kPa was a reasonable approximation of field capacity. However, soil water retention curves derived from the evaporation approach suggest the threshold between mesopore and macropore function ranged from ψ-6.0 to -15.5 kPa.
- In the wet treatment, water held between field capacity and saturation did not drain to field capacity due to low hydraulic conductivity in the B2 horizons. This was supported by soil monitoring data which showed soil water contents above field capacity before and after infiltration of the dye tracer (Chapter 5.3.5).

8.2.2 Estimation of van Genuchten parameters for single pore domain modelling

The van Genuchten-Mualem equation used in single pore domain models requires determination of the five van Genuchten parameters; residual soil moisture content (Qr), saturated water content (Qs), shape parameters alpha (α) and (*n*), pore tourtuosity factor *(l*), and the saturated hydraulic conductivity (K_{sat}). Separate sets of van Genuchten parameters were derived for each soil layer at site B, based on three inverse and two laboratory drying approaches, parameterisation approaches included:

I. **Desorption**: van Genuchten parameters were determined from the soil water characteristic using suction plates and pressure chambers in which volumetric soil moisture was determined from the bulk density at saturation (Chapter 6.3.1). van Genuchten parameters were solved using the curve fitting software RETC (van Genuchten *et al.* 1991) using the m=1-1/n assumption (Figure 8.2-2). Multiple runs were performed with differing starting texture to minimise the likelihood on non-uniqueness.

II. **Desorption – vBD**: Similar to the desorption approach (above) in which calculation of volumetric soil moisture accounted for increased density at sequentially lower matric potential. Using the SSCC data, and the procedure outlined in Chapter 6.2.3, a polynomial relationship between gravimetric soil moisture and clod density (Appendix 6.7) was employed to determine density at each equilibration point in which,

EQ 8.4 $$BD_i = a(\theta_i)^2 - b(\theta_i) + C$$

$$C = BD_s - a(\theta_{sat})^2 - b(\theta_{sat})$$

C = Intercept, equivalent maximum density of the desorption sample.

BD_s= Bulk density of the desorption sample at saturation.

θ_s = Gravimetric moisture content of the desorption sample at saturation.

Table 8.2-1 Relative change in soil moisture following inverse simulation of infiltration from tension infiltrometers after 180 minutes

	Dry	Wet	Comments
A1 Horizon	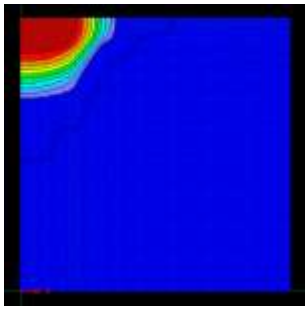	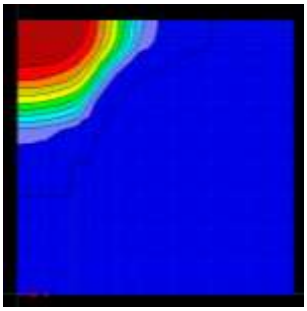	Higher initial soil moisture in the wet treatment resulted in deeper infiltration and displacement of existing soil water further down the soil profile. Note the potential effect of the low hydraulic conductivity in the b21 horizon was not represented in the simulation.
A2 Horizon	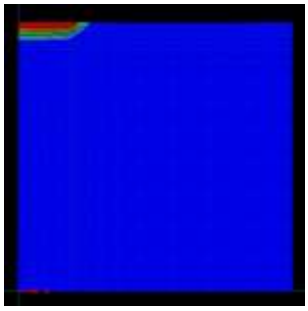	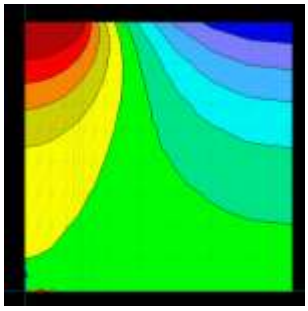	Infiltration was limited by the low hydraulic conductivity and absence of macropores in the dry treatment. In the wet treatment, existing soil water drained by gravity prior to and during infiltration (blue-right). The infiltrating water also displaced existing soil water further down the soil profile.
B21 Horizon	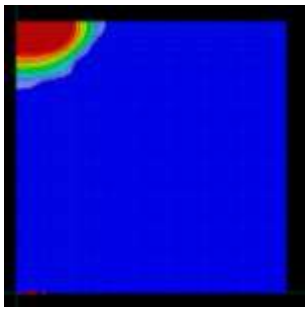	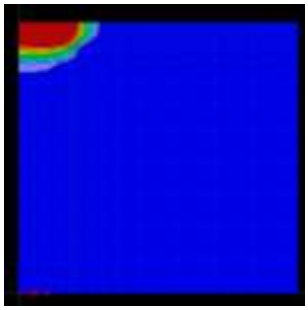	Infiltration into the wet treatment was shallower than the dry treatment due to diffiulty displacing existing soil water further down the soil profile following clay swelling which reduced the hydraulic conductivity of the B2 horizons.
B22 Horizon	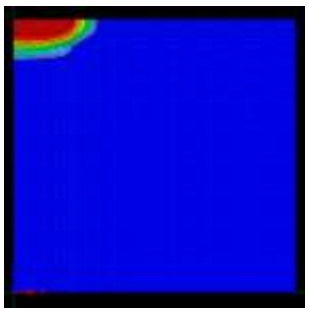	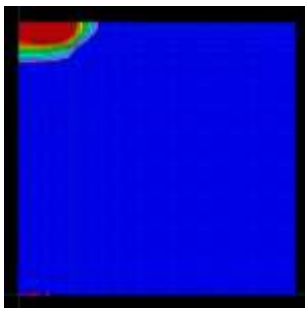	Infiltration into the B22 was minimal due to low hydraulic conductivity. Antecedent soil moisture had little effect on infiltration.

Colours represent differences in soil moisture following infiltration from tension infiltrometers after 180 minutes. Note colour scale differs between simulations due to differences in initial soil moisture between horizons and treatments. For example starting soil moisture in B21 – dry was 0.18 m m^{-3}, while the same colour blue in A1 horizon wet treatment was 0.35 m m^{-3}.

BD_i = Bulk density of the desorption sample at each measurement interval.

a = Slope of the clod density vs gravimetric soil moisture relationship.

b= Slope of the clod density vs gravimetric soil moisture relationship.

Following recalculation of volumetric soil moisture, the van Genuchten parameters were determined using RETC as above. This approach assumed; (i) that shrinkage of soil clods used to determine the SSCC data was identical to shrinkage of the core samples and disturbed samples within the pressure chambers, and (ii) no water was held within desiccation cracks, i.e. cracks formed after drainage had occurred.

III. **Evaporation:** van Genuchten parameters were determined from the evaporative approach (Chapter 6.2.1.2) in which the water potential gradient between two tensiometers and the mean water content from a soil core during free evaporation were used to derive the water retention characteristic (Wendroth *et al.* 1993; Wendroth and Wypler 2008; Wind 1968). van Genuchten parameters were determined using RETC (van Genuchten *et al.* 1991) for each soil core, and the parameters averaged and reported on a horizon basis (Figure 8.2-2).

IV. **Disk VG:** Inverse parameterisation of tension cumulative infiltration data from tension infiltrometers using HYDRUS-2D/3D. Inverse parameterisation of tension infiltration data has been used to derive soil hydraulic parameters for single porosity models from both field (Ramos *et al.* 2006; Simunek *et al.* 1998a; Simunek *et al.* 1998c) and laboratory data (Simunek *et al.* 1999b). Inverse parameterisation was conducted in HYDRUS-2D/3D following the procedure by Simunek *et al.* (1998c) which employed the van Genuchten - Mualem soil water model with no hysteresis. The objective function was defined in terms of the average measured cumulative infiltration from 4 - 6 tension infiltrometers, operated for 30 minutes at six sequential supply potentials. Initial and final volumetric soil moisture were specified from measured data using the EnviroSCAN soil moisture probe. The five Mualem-van Genuchten parameters (Qs, Qr, α, n and Ks) were estimated simultaneously by numerical inversion in which initial estimates of the parameters were iteratively improved during the minimisation process until a desired precision was obtained (Hopmans *et al.* 2002; Ramos *et al.* 2006). Note the pore connectivity parameter (*l)* was set at 0.5 to reduce the number of variables in the parameter function. The inverse tension infiltrometer approach was limited to single pore domain applications as HYDRUS 2D/3D does not provide inverse capabilities for the dual permeability model (Kodesova *et al.* 2010). Example of inverse infiltration using Hydrus 2D/3D is provided in Table 8.2-1, additional details of the procedure are supplied in Appendix 7.1.

V. **Disk VG – Qr set**: Similar to Disk VG parameterisation approach, in which the residual water content (Qr) was set to the value determined by the desorption approach (above). The remaining van Genuchten parameters; alpha, *n*, and Qs were inversely solved using HYDRUS 2D/3D from infiltration data (as above). The Disk-Qr set approach was conducted as infiltration from tension infiltrometers occurs primarily through macropores and mesopores at supply potentials close to saturation (ψ – 0.134 kPa to -0.012 kPa). Consequently inverse solution of tension infiltration data is somewhat insensitive to flow through smaller mesopores and micropores resulting in uncertainty in the estimation of Qr and to a lesser extent *n*. By setting the Qr parameter, the number of parameters in the objective function was reduced resulting in increased sensitivity of the inverse solution and decreased likelihood of non-uniqueness (Hopmans *et al.* 2002).

8.2.3 Estimation of saturated hydraulic conductivity

The van Genuchten-Mualem equation requires knowledge of the saturated hydraulic conductivity (Ksat). However specifying an appropriate value of hydraulic conductivity can be problematic in a macroporous soil, as typical methods for measuring Ksat, sample too small a volume of soil to capture the representative elementary volume (Davis *et al.* 1999; Hutchinson and Moore 2000), or measure Ksat at unrepresentative soil moistures or boundary conditions (Beven 2000; McKenzie and Cresswell 2002). Additionally in soils with vertic or hydrophobic properties, hydraulic conductivity may be influenced by soil moisture content (Jarvis *et al.* 2008; Lamparter *et al.* 2006; Lin *et al.* 1998). Consequently saturated hydraulic conductivity was estimated using both direct laboratory approaches from saturated intact cores, and *in situ* infiltration from tension infiltrometers (disk permeameters). Approaches for estimating Ksat included;

(i) **Direct:** Measurement of K_{sat} from 3 x 100 mm diameter saturated cores at ψ+10 mm (Chapter 6.2.5).

(ii) **Evaporation**: Linear extrapolation of K(ψ) relationship to ψ = 0 determined from the evaporation approach using data presented in Chapter 6.2.2. (Wendroth and Wypler 2008).

(iii) **Disk – Inverse - Dry**: Inverse parameterisation of cumulative infiltration from tension infiltrometers into soil at low antecedent soil moisture (Chapter 6.2.6) using HYDRUS 2D/3D following the approach by Simunek *et al.* (1998c) in which saturated hydraulic conductivity was included in the objective function.

(iv) **Disk – Inverse - Wet**: As per Disk - Inverse - Dry, except infiltration was into soil at high antecedent soil moisture.

(v) **Disk – RETC - Dry**: Extrapolation of the K(ψ) relationship to ψ=0 using RETC (van Genuchten *et al.* 1991). In which the K(ψ) relationship was determined by cumulative infiltration from tension infiltrometers at multiple tensions following the approach in Chapter 6.2.6 and solved using the approach by Reynolds and Elrick (1991) at low antecedent soil moisture.

(vi) **Disk - RETC - Wet**: As per Disk – RETC-Dry, except infiltration was into soil at high antecedent soil moisture.

8.2.4 Estimation of additional macropore parameters for multiple pore domain modelling with MACRO 5.1

In addition to the van Genuchten parameters Qr, Qs, α and n, and Ksat, the multiple pore domain model MACRO 5.1 required parameterisation of an additional 10 soil parameters to characterise the macropore domain and enable water movement between the micropore (matrix) and macropore domains. Parameterisation of the subsoil was difficult as there are few physically based approaches for determining the hydraulic properties of cracking clay soils (Haws *et al.* 2005). The boundary matric potential between the macropore and matrix domains (CTEN) was inferred from the inflection point in the k(ψ) relationship determined by infiltration from tension infiltrometers (Chapter 6.3.5). CTEN values ranged from -5 to -9 cm compared to the assumed value of -10 cm (Jarvis 2007). The minimum saturated hydraulic conductivity i.e. without flow in macropores (KSATMIN) was determined from saturated 100 mm cores in which flow through shrinkage cracks was minimised. The hydraulic conductivity at the macropore / micropore boundary (KSM) was determined directly from tension infiltrometers at CTEN. The permanent wilting point (WILT) was determined by pressure chamber apparatus at 1500 kPa. The pore tourtuosity factor in the micropore domain (ZM) was set to default value of 0.5. The shrinkage characteristic (ZP) was determined by linear regression of the normal or basic shrinkage phase of the SSCC curve (Chapter 6.2.3, Appendix 6.7). The exponent relating macropore hydraulic conductivity to macroporosity (ZA) was determined from the power relationship describing the difference in hydraulic conductivity at CTEN compared to at saturation. The saturated water content (TPORV), residual water content (RESID), and van Genuchten *n* and α (ALPHA) were determined from either desorption data, or inverse infiltration from tension infiltrometers. The boundary water content (XMPOR) was determined at CTEN after fitting the van Genuchten parameters determined by desorption or inverse infiltration data.

Based on advice from Dr Nicholas Jarvis (pers. comm.) the pore size / tourtuosity distribution factor (Zn) was estimated to be 2.0 for the A horizons and 3.0 for the B2 horizons, and the effective diffusion path length (ASCALE) was estimated to be 50 mm in the A1, 10 mm in the A2, and 300 in the B2 horizons.

8.2.5 Validation of 1D simulation of dye staining experiments

HYDRUS-1D and MACRO 5.1 simulations of the dye staining experiments at site B were conducted by simulating 25 mm precipitation on soil at high and low antecedent soil moisture (Chapter 4). In both modelling approaches, the soil profile was discretized into 150 equally spaced 1 cm deep layers in which; A1 horizon was 0 - 15 cm, A2 horizon was 15-20 cm, B21 horizon was 20 - 35 cm, B22 horizon was 35 - 85 cm, B23 horizon was 85 - 150 cm. Simulations were run for 48 hours at an initial time step of 1.4 minutes. The 25 mm dye tracer (precipitation) was applied 1.0 hour after the simulation had commenced at a rate of 12.5 mm hr^{-1} for 2.5 hours in the wet treatment, and 25 mm hr^{-1} for one hour in the dry treatment (Chapter 4.2.2). Evaporation and rainfall were ignored as the soil surface was covered following dye application to prevent evaporation. Additional details of the procedure and issues encountered with establishing the initial soil moisture (θi) are discussed in Appendix 7.2.

Validation of model and parameterisation performance was conducted by calculation of the root square mean error (RMSE) between the change in soil moisture predicted by the models, and the change in soil moisture determined from dye staining approach (Chapter 8.2.3) or the EnviroSCAN soil moisture probe, in which;

EQ 8.5 Root mean squared error (RMSE) = $\sqrt{\frac{\sum(\text{Observed } - \text{Estimated })^2}{n(\text{observations }) - n(\text{parameters })}}$

Observed = soil moisture recorded by soil moisture probe or dye staining approach.

Estimated = soil moisture determined by simulation.

n(observed) = number of observed data.

n(parameters) = number of parameters required to estimate soil moisture.

8.2.6 Validation of modelling - soil moisture monitoring data 2007 – 2009

Changes in soil moisture adjacent to site B, between September 2007 and September 2009, were simulated using MACRO 5.1 and HYDRUS-1D (air entry value at -2.0 cm).

Both models were operated at a daily time step, the soil profile was discretized into 150 x 1 cm deep layers with five soil layers as per Chapter 8.2.5.

Initial soil moisture (θi) was determined by the EnviroSCAN soil moisture probe when θi was greater than Qr and less than Qs. If θi was greater than Qs or less than Qr, the θi was adjusted to be either 0.05 m^3 m^{-3} less than Qs or 0.05 m^3 m^{-3} greater than Qr. Climate parameters were determined from the Hobart Airport (Bureau of Meteorology 2009) in which evapotranspiration was determined using the Penman-Montheith equation for pasture with a constant height of 10 cm, and maximum root depth of 50 cm (Appendix 4.2).

MACRO 5.1 parameterisation was conducted for desorption data and inverse infiltration from tension infiltrometers into soil at low antecedent soil moisture using a range of methods for determining K_{sat} and either inclusion or exclusion of Qr from the objective function.

In MACRO 5.1 an extreme preferential flow simulation (High PF) was conducted to induce maximum drainage from the A1 horizon into the B2 horizons. The high preferential flow simulation (High PF) was invoked by changing van Genuchten *n* to 2.5, Qr to 0.05, CTEN to 10.0 and recalculating XPORV at a CTEN of 10 in the A1 and A2 horizons. In the B2 horizons ASCLE was changed to 500. Otherwise all other parameters were set as per the Disk VG-Q r set, inverse K simulation.

8.2.7 Evaluation of the effect of sand infills on infiltration.

The dye staining experiments (Chapter 4.0) were simulated using HYDRUS -2D to explore the effects of sand infills and lateral flow on infiltration into soil at high and low antecedent soil moisture. These infiltration features were unable to be represented or simulated using one dimensional models such as MACRO 5.0 and HYDRUS -1D.

In both soil moisture treatments sand infills were represented by two 12 cm to 3 cm wide 'funnel' shaped extensions of the A2 horizon which extended to approximately 70 cm depth through the B21 and into the upper B22 horizons (based on soil morphology, Chapter 3.3.2). Simulations were conducted using van Genuchten parameters determined by inverse solution of infiltration data from tension infiltrometers in which Qr had been previously determined by desorption. Saturated hydraulic conductivity was estimated by either (i) direct measurement on saturated 100 mm diameter cores (Chapter 6.2.5) (ii) RECT extrapolation of the K(ψ) relationship to ψ = 0, or (iii) inverse infiltration (i.e. Disk VG – Qr set, core / RETC K / inverse K).

8.2.8 Evaluation of the effect of high antecedent soil moisture on lateral flow within the A horizons

In the wet treatment, infiltration of the dye tracer was simulated in a 4.0 x 1.5 meter area to assist visualisation of lateral flow in the A1 horizon. Van Genuchten parameters were determined by inverse infiltration from tension infiltrometers at high antecedent soil moisture in which the Qr parameter had previously been defined from desorption data using RETC, (DiskVG- Qr set). Simulations were conducted using saturated hydraulic conductivity values determined by (i) direct measurement, (ii) inverse infiltration from tension infiltrometer data (iii) RETC interpolation of the $K(\psi)$ relationship to $\psi = 0$.

8.3 Results and discussion

8.3.1 Determination of crack volume from desiccation of unconfined clods

The SSCC data was able to be reinterpreted to derive a relationship between inter-clod volume (proportion of shrinkage cracks) and volumetric soil moisture. This relationship was employed to determine the potential volume of shrinkage cracks prior to application of the dye tracer. An example is presented for site B for clods sampled at 60 - 70 cm (Figure 8.3-1). Desiccation had little effect on total pore volume (intra clod and inter clod pore volume – closed circles), however desiccation decreased the intra-clod pore volume (open circles) from 0.42 cm^3 cm^{-3} at 0.38 m^3 m^{-3} to 0.28 cm^3 cm^{-3} at 0.07 m^3 m^{-3}, whilst increasing inter- clod pore volume (shrinkage cracks) from 0.00 cm^3 cm^{-3} to 0.16 cm^3 cm^{-3} over the same soil moisture range. Surface deflation had minimal effect on inter clod pore volume (0.008 cm^3 cm^{-3} difference at 0.07 m^3 m^{-3}).

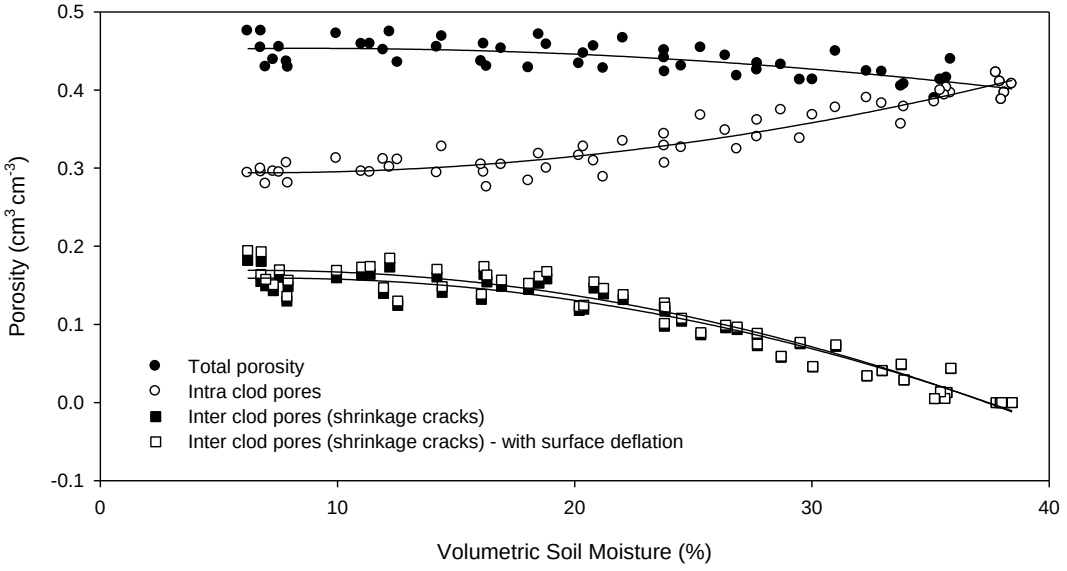

Figure 8.3-1 Site B, 60 - 70 cm: Example of the effect of soil moisture on total porosity, intra clod porosity, volume of shrinkage cracks (inter clod porosity), and surface deflation.

8.3.2 Comparison between the change in soil moisture determined by dye staining and the EnviroSCAN soil moisture probe

Despite the number of assumptions inherent with the dye staining approach (Chapter 8.2.1.3) Figure 8.3-2 demonstrates that differences between the 'probe area' (change in soil moisture was determined by the dye staining approach) and the EnviroSCAN were minor.

The low RMSE between the two approaches validates the use of the dye staining approach for determining change in soil moisture in soils with heterogeneous infiltration pathways (dry treatment RMSE 0.023, wet treatment 0.025 at 48.0 hrs). In the dry treatment (Figure 8.3-2a), differences between the two approaches at 20 cm depth, resulted from dye accumulation at the A / B boundary due to the staining of a thin sand infill between 20 cm to 30 cm depth. This resulted in a disproportionally greater area of dye staining than the change in soil moisture recorded by the EnviroSCAN soil moisture probe.

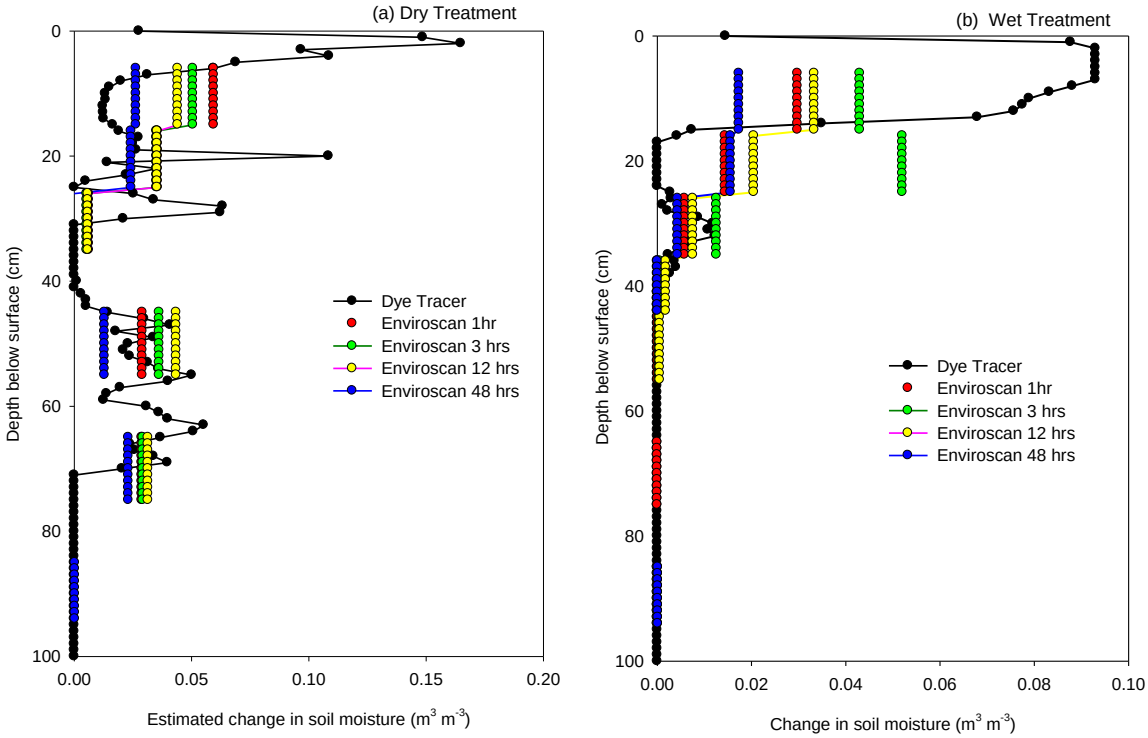

Figure 8.3-2 Comparison between the estimated change in soil moisture from the EnviroSCAN probe at four time intervals and the estimated change in soil moisture determined from dye staining (probe area) at site B, (a) dry treatment, (b) wet treatment.

In the wet treatment (Figure 8.3-2b) values from the soil moisture probe were considerably higher than the dye approach at 20 cm depth due to a lack of dye staining between 17 and 24 cm. Data from the soil moisture probe indicated that infiltration below 20 cm depth principally occurred 12 to 48 hours after dye application ceased. This suggests that the discrepancy between the two approaches resulted from displacement of pre-existing pore water down the soil profile via 'piston flow' following infiltration of the dye tracer. This displaced flow occurred below the depth of dye staining and thus was not able to be 'observed' by the dye staining approach.

In addition Gregory *et al.* (1992) explains that in strong texture contrast soils when perched watertables are present, or the subsoil is close to saturation, precipitation is likely to move through soil layers without any measurable change in water content. Differences between the 'recovered' volume of infiltrated dye tracer estimated by the dye staining approach, the EnviroSCAN and the applied volume of dye tracer are presented in more detail in Appendix 7.3.

8.3.3 Comparison between parameterisation techniques - van Genuchten parameters

Model parameterisation approach and antecedent soil moisture had considerable influence on parameter values (Table 8.3-1) which resulted in differences in the predicted soil water characteristics (Figure 8.3-3). Direct approaches using suction tables and pressure apparatus (desorption) have traditionally been used to derive parameter inputs or compare values produced by alternative approaches (Ramos *et al.* 2006; Simunek *et al.* 1998c). However the extent to which parameter values in Table 8.3-1 varied between approaches raises questions about the validity of all approaches used to estimate van Genuchten parameters, not just the inverse approaches. Uncertainty in parameter values derived from direct approaches resulted from unrepresentative boundary conditions associated with saturation of intact cores prior to analysis. Saturation is thought to have overcome water repellence in the A1 horizon (Chapter 7.3.1), reduced silica cementation in the A2 horizon (Chapter 6.3.5.2) and minimised the occurrence of shrinkage cracks in the B2 horizons following clay swelling (Chapter 6.3.3). Consequently soil parameters derived from approaches that dry soil from saturation (desorption and evaporation approaches) are only likely to represent water movement in field soils following saturation. van den Berg (1989) also identified problems associated with calculating porosity and hydraulic conductivity from the soil water retention curve in swelling soils, due to the loss of soil volume during pre-treatment. They found antecedent soil moisture had considerable influence on estimated parameter values derived from both the inverse solution and laboratory drying approaches.

Simunek *et al.* (1999b) has argued that retention data determined by inverse solution of infiltration data from tension infiltrometers should be more useful for determining hydraulic properties of field soils than those obtained from steady state laboratory methods. Improved parameterisation results from the larger infiltrating surface area of the tension infiltrometer compared to other approaches which acts to integrate properties of the porous media including the influence of local-scale heterogeneity, differences in soil structure and texture irregularities, and preferential pathways.

Differences in parameter values between the wet and dry treatments presented in Table 8.3-1 and Figure 8.3-3 also demonstrate that inverse solution of infiltration data from tension infiltrometers is able to discern differences in soil hydraulic properties at different antecedent soil moisture contents. Discussion of the effect of parameterisation on estimated van Genuchten parameter values is presented for each soil horizon.

8.3.3.1 A1 horizon

In the A1 Horizon, the saturated water content (Qs) varied from 0.44 to 0.58 depending on parameterisation method (Table 8.3-1), the desorption approach produced the lowest estimate of Qs 0.444 m^3 m^{-3}, and inverse solution of infiltration data from the tension infiltrometers into dry soil produced the highest estimate of Qs 0.580 m^3 m^{-3}. The Qs value determined by desorption 0.444 m^3 m^{-3} was lower than would normally be expected for a moderatly structured sandy loam which suggests the possibility that soil within the core was compacted during sampling.

Inverse solution of infiltration data from the tension infiltrometer into dry soil resulted in higher values of Qs (0.580 m^3 m^{-3}) than the final saturated water content of soil below the tension infiltrometers (θ_{final} = 0.46 m^3 m^{-3}), which indicates error in the inverse solution. Potential for divergence between Qs and θ_{final} was anticipated by Ramos *et al.* (2006) who applied a weighting factor of 10 to the θ_{final} value (compared to 1 for infiltration data) to force the inverse solution to solve Qs near θ_{final}. However re-running simulations (Disk VG-Inverse K- Dry) in which θ_{final} was assigned a 10 weighting factor, did not substantially alter the estimated van Genuchten parameters (Qs 0.5815, α 0.484, n 1.321 cf Qs 0.580, α 0.482, n 1.321).

Differences in Qs determined by inverse solution of evaporation data and total porosity have also been reported by Wessolek *et al.* (1994), who found removing Qs from the objective function and setting Qs to total porosity resulted in over prediction of soil water content in the wet range. Error resulted from differences in the field saturation of the soil and the true saturation or total porosity determined from core samples (Richard *et al.* 2001; Wessolek *et al.* 1994). While Hillel (1998) attributes differences in Qs values to entrapped or dissolved air. In the A1 horizon overestimation of Qs is more likely to have resulted from either the inverse infiltration extrapolating results beyond the measurement range of the tension infiltrometer (<-0.13 kPa) (Simunek and van Genuchten 1997) or invalidation of the inverse solution due to water repellence at low antecedent soil moisture (discussed Chapter 7.4.1).

Table 8.3-1 Effect of parameterisation technique on van Genuchten parameters

Parameterisation Method			**Results van Genuchten Parameters**				
Van Genuchten Parameters	Ksat	Antecedent Soil Moisture	Qr	Qs	alpha	n	R squared
					A1 Horizon		
Desorption	Direct	From sat.	0.0359	0.4442	0.0505	1.452	0.9882
Evaporation	Evaporation	From sat.	0.0778	0.5016	0.0189	2.677	0.9999
Disk VG	Inverse K	Low	0.0001	0.5796	0.4821	1.321	0.9989
Disk VG - Qr set	Inverse K	Low	0.0359	0.5707	0.4801	1.324	0.9988
Disk VG	Inverse K	High	0.0001	0.4750	0.0413	1.193	0.9994
Disk VG - Qr set	Inverse K	High	0.0359	0.4573	0.0422	1.194	0.9994
					A2 Horizon		
Desorption	Direct	From sat.	0.02456	0.3870	0.0293	1.736	0.9971
Evaporation	Evaporation	From sat.	0.04566	0.3427	0.0197	2.652	0.9999
Disk VG	Inverse K	Low	0.00010	0.4242	0.9990	1.541	0.9964
Disk VG - Qr set	Inverse K	Low	0.02456	0.4608	1.0443	1.643	0.9961
Disk VG	Inverse K	High	0.2549	0.2713	0.0151	1.359	0.9999
Disk VG - Qr set	Inverse K	High	0.02456	0.2756	0.0082	1.3117	0.9991
					B21 Horizon		
Desorption	Direct	From sat.	0.23576	0.4211	0.0177	1.497	0.9789
Desorption - vBD	Direct	From sat.	0.26813	0.4185	0.0149	1.464	0.9813
Evaporation	Evaporation	From sat.	0.29090	0.3973	0.0107	1.814	0.9998
Disk VG	Inverse K	Low	0.17610	0.4963	0.9460	1.691	0.9997
Disk VG - Qr set	Inverse K	Low	0.26813	0.3591	1.0528	1.432	0.9997
Disk VG	Inverse K	High	0.2178	0.3197	0.7693	1.171	0.9988
Disk VG - Qr set	Inverse K	High	0.26813	0.3244	0.5234	1.449	0.9981
					B22 Horizon		
Desorption	Direct	From sat.	0.2604	0.3437	0.0251	1.139	0.9452
Desorption - vBD	Direct	From sat.	0.3114	0.3443	0.0017	1.486	0.9559
Evaporation	Evaporation	From sat.	0.3079	0.3421	0.0071	4.640	0.9999
Disk VG	Inverse K	Low	0.1746	0.5964	3.1846	1.618	0.9989
Disk VG - Qr set	Inverse K	Low	0.2435	0.5530	3.1448	1.589	0.9995
Disk VG	Inverse K	High	0.00001	0.4313	0.9496	1.035	0.9994
Disk VG - Qr set	Inverse K	High	0.2435	0.4126	0.2377	1.125	0.9974
					B23 Horizon		
Desorption	Direct	From sat.	0.2396	0.3919	0.0155	1.576	0.9699
Desorption - vBD	Direct	From sat.	0.2613	0.3906	0.0155	1.424	0.0971
Evaporation	Evaporation	From sat.	0.2126	0.3292	0.0053	2.401	0.9974
Disk VG	Inverse K	Low / High	0.0009	0.4720	0.6466	1.198	0.9991
Disk VG - Qr set	Inverse K	Low / High	0.2613	0.5422	1.0812	1.478	0.9968

From sat. refers to laboratory drying techniques in which initially saturated soil is dried to derive retention data.

Antecedent soil moisture had a large effect on the two van Genuchten shape parameters alpha (α) and n. Infiltration into the dry treatment resulted in α values which were an order of magnitude higher than estimates of α determined by desorption and inverse infiltration into the wet treatment. Values of *n* determined by inverse infiltration in the dry treatment were lower than all other approaches. As the n parameter is thought to be sensitive to small aggregates, and α related to larger pores (Porebska *et al.* 2006), it is likely that higher α and lower *n* resulted from higher sensitivity of the inverse approach to infiltration into macropores than micropores.

Variations in α and *n* between the two soil moisture treatments had a substantial effect on the predicted soil water retention curves (Figure 8.3-3). Schwartz and Evett (2002) also found initial soil moisture content influenced parameter values. They found inverse parameterisation from infiltration into soil with initially high water content had better fit to drying retention data, than soil at initially low water content. They found that at low initial water content, a good fit between inverse estimation of the retention curve and measured values only occurred when the retention curves exhibited hysteresis. However in this study, differences in α an *n* between the two soil moisture treatments did not result from hysteresis, as the wetting curve produced by inverse infiltration occurred at a higher rather than lower moisture content than the draining curves produced by the two laboratory drying approaches.

Determination of van Genuchten parameters determined by inverse solution of tension infiltration data at low antecedent soil moisture are likely to be invalid due to hydrophobicity. Development of finger flow at low antecedent soil moisture (Figure 7.4-1) reduced the proportion of soil participating in flow and thus invalidated the assumption of homogeneity required for the inverse solution in HYDRUS-2D (Hopmans *et al.* 2002).

8.3.3.2 A2 horizon

In the A2 horizon, parameterisation approach and antecedent soil moisture had a substantial effect on estimated van Genuchten parameters and the soil water characteristic (Figure 8.3-3 and Table 8.3-1). The Qs parameter was substantially lower for the two inverse solution approaches at high antecedent soil moisture than either the two laboratory drying approaches, or the inverse solution at low antecedent soil moisture. However the final soil moisture under the tension infiltrometers at high antecedent soil moisture (0.255 – 0.27 m^3 m^{-3}) was considerably lower than the volumetric soil moisture content at saturation (0.38 m^3 m^{-3}) determined by desorption. Consequently the Qs determined by desorption was substantially higher than Qs determined by inverse solution at high antecedent soil moisture.

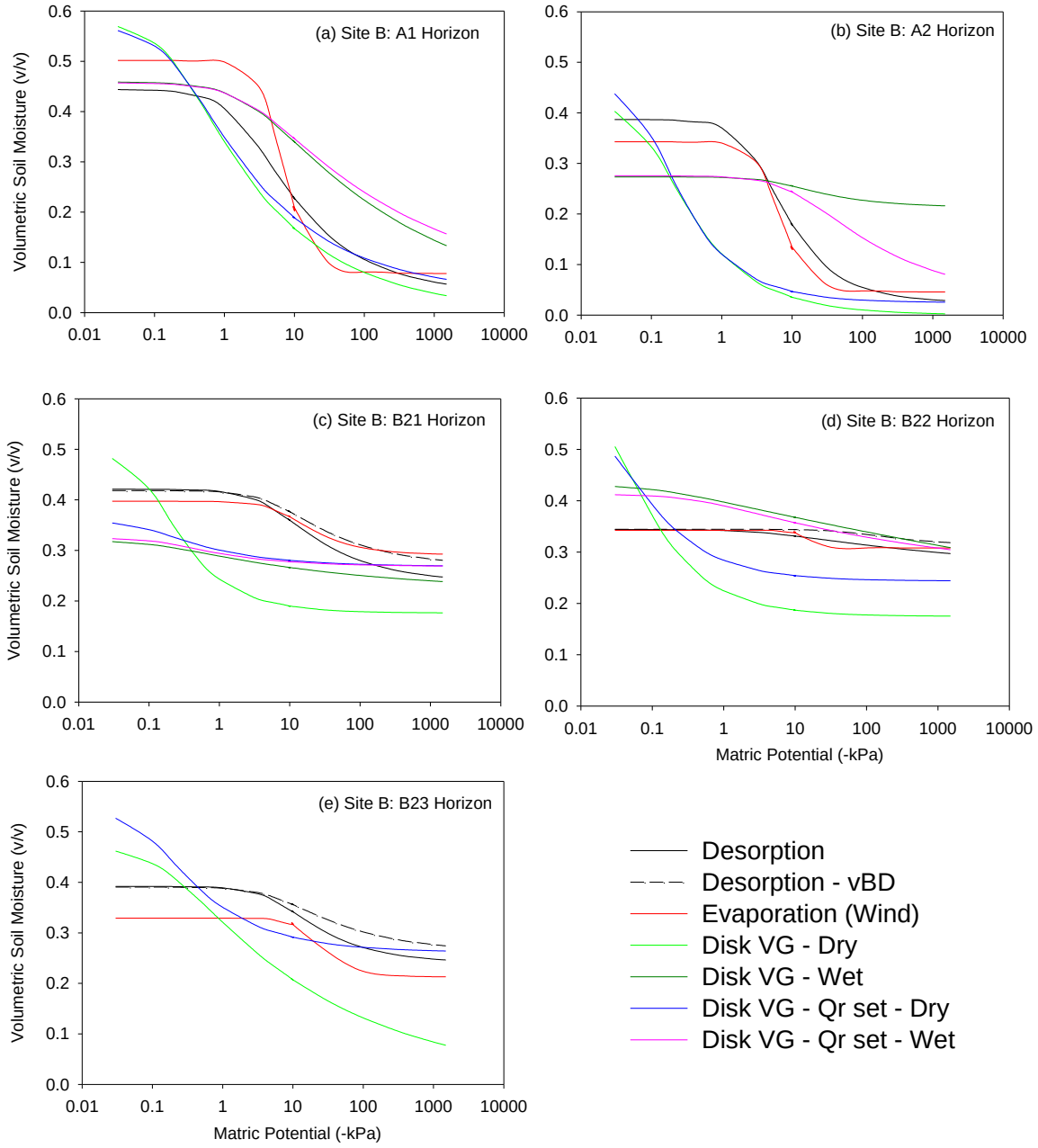

Figure 8.3-3 Effect of parameterisation technique on the soil water characteristic (a) A1 Horizon, (b) A2 Horizon, (c) B21 Horizon, (d) B22 Horizon, (e) B21 Horizon. Figure nomenclature is derived from Chapter 8.2.2. Desorption –suction tables and pressure chambers, Desorption –vBD correction for shrink swell soils. Disk VG – inverse parameterisation from tension infiltrometer data. Wet /Dry -antecedent soil water treatments. Qr set –Qr set to desorption value and removed from the objective function.

This discrepancy is likely to have resulted from inability of the tension infiltrometer to fill macropores between the maximum matric potential supplied by the tension infiltrometer (-0.13 kPa) and saturation (Simunek and van Genuchten 1997). Linden and Dixon (1976) also report that air entrapment created by ponding of water, may decrease infiltration rates by up to two orders of magnitude, and thus field based infiltration may also result in lower saturated water content than would otherwise be measured from laboratory samples which were subjected to prolonged wetting.

Inverse solution of infiltration data from the tension infiltrometer into the wet treatment failed or struggled to solve to a unique local minimum when the Qr parameter was included in the object function. However by setting the Qr to the value determined by desorption and removing Qr from the objective function, infiltration into the wet treatment was able to be solved. Difficulty obtaining local minima for Qr was attributed to tension infiltrometers being highly sensitive to flow in macropores, whilst being rather insensitive to flow in micropores represented by the Qr parameter. Local minima were established after setting the Qr value to that determined by desorption and removing the Qr parameter from the objective function. Ramos *et al.* (2006) also found that inverse estimation of parameters improved when independently measured water contents at -10 and -1585 kPa were added to the objective function.

Similar to the A1 horizon, inverse solution of infiltration data from the tension infiltrometer into the dry treatment resulted in α values which were approximately 50 times higher than those determined from the two laboratory drying approaches or inverse solution of infiltration data into the wet treatments. Higher *n* values derived by the laboratory drying approaches were attributed artificial creation of many fine pores during hammering of cores into the weakly cemented A2 horizon. Similar shattering and creation of fine artificial pores has been reported by Stone (1991).

8.3.3.3 B2 horizons

Prediction of van Genuchten parameters in the B2 horizons was less variable than in the A1 and A2 horizons, as the three laboratory drying approaches predicted similar van Genuchten parameter values in all three horizons (Table 8.3-1). Accounting for soil shrinkage and increased density with drying (desorption –v BD) had a relatively minor influence on van Genuchten parameters as demonstrated by the minimal difference in values between the desorption and the desorption - vBD parameterisation approaches. For example in the B21 horizon, Qr increased by only 0.03 m^3 m^{-3}, and *n* decreased by 0.04 m^3 m^{-3} (Table 8.3-1). In the B23 horizon, differences between the desorption and evaporation approaches were attributed to small scale variability associated with sampling of weathered sand clasts near the base of the soil profile.

In the B21 and B22 horizons, antecedent soil moisture had little influence on Qs, Qr and n. However inverse infiltration into soil at low antecedent soil moisture when Qr had been removed from the objective function (Qr set) resulted in substantially higher values for α in the dry treatment compared to the wet treatment. Qs values determined by inverse infiltration data were lower than values determined by the two laboratory drying approaches. This was unexpected as soil cracking in the upper B2 horizons at low antecedent soil moisture was expected to have resulted in substantially higher Qs than that determined from saturated soil cores. Lower values of Qs predicted by inverse solution are likely to have resulted from extrapolating results beyond the measurement range of the tension infiltrometer (<-0.13 kPa) as discussed by Simunek and van Genuchten (1997).

8.3.3.4 Comparative studies

Few studies have compared soil hydraulic properties determined by direct laboratory approaches to field based inverse solution of tension infiltrometer data (Ramos *et al.* 2006). Most of these studies have investigated hydrologically 'simple' sandy loam soils, (Ramos *et al.* 2006; Simunek *et al.* 1998b; Simunek *et al.* 1999b) or fine textured soil (Schwartz and Evett 2002) in which the hydraulic properties do not vary with soil moisture (i.e. hydrophilic and non-vertic). Despite the relative hydrological simplicity of these soils compared to the current study, most studies also report poor agreement between van Genuchten parameters determined by inverse infiltration from tension infiltrometers to other approaches (Schwartz and Evett 2002). Simunek *et al.* (1999b) found that retention curves estimated from the infiltration experiments on a sieved loamy sand were quite different and usually underestimated from those determined using the evaporation approach (Wind 1968). Simunek *et al.* (1998b; 1998c) also found relatively poor agreement between retention curves obtained by numerical inversion of infiltration data and independently measured laboratory data.

Schwartz and Evett (2002) found simultaneous determination of van Genuchten parameters in a fine textured soil was difficult to perform due to insensitivity of the objective function over a wide range in saturated hydraulic conductivities, and enhanced capillary flow from the unconfined tension infiltrometers. They recommended that α be determined independently from water retention data. However this would defeat the principal objective of inverse approaches, rapid, repeatable determination of van Genuchten parameter values from easily obtained field data.

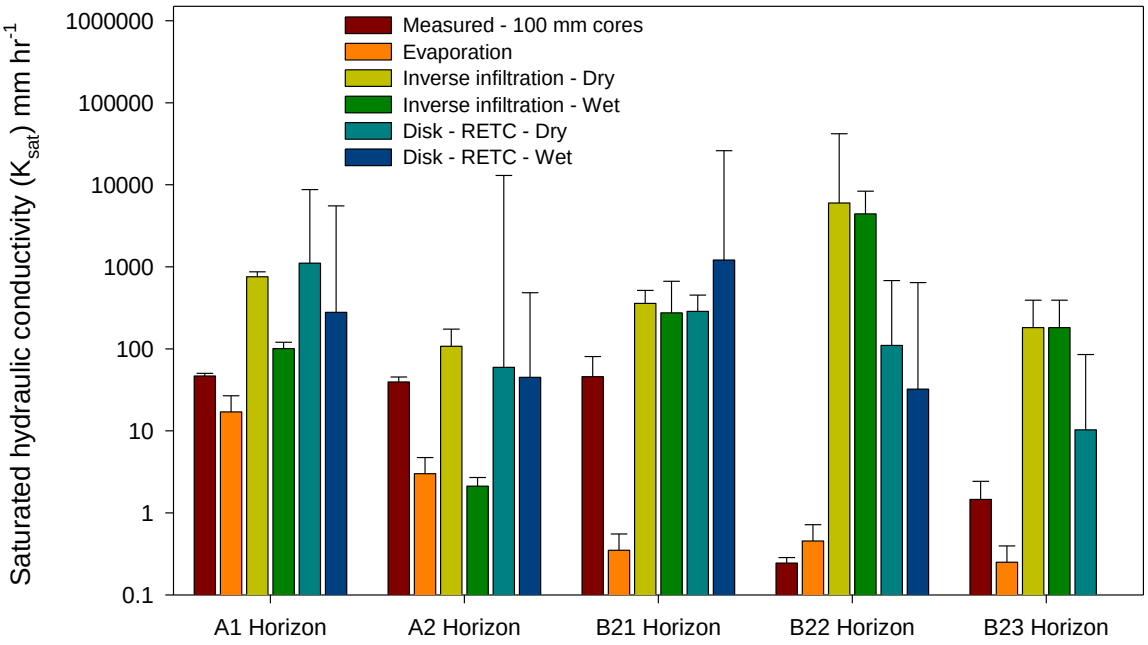

Figure 8.3-4 Effect of parameterisation approach on saturated hydraulic conductivity. Error bars represent ± 1 standard deviation.

In contrast to previous studies and this study, Ramos *et al.* (2006) found close agreement between the water retention curves derived from evaporation technique, desorption and pressure chamber analysis, with those derived by numerical inversion of cumulative infiltration from a tension infiltrometer on a series of A horizons (Gleyic Luvisols and Haplic Fluvisol). In contrast to this study they concluded that inverse infiltration from tension infiltrometers provided a relatively simple and reliable method for determining van Genuchten parameters.

8.3.4 Estimated saturated hydraulic conductivity

Values of saturated hydraulic conductivity (K_{sat}) proved to be considerably more variable than expected. Parameterisation approach and antecedent soil moisture were found to influence estimates of saturated hydraulic conductivity by two to three orders of magnitude (Table 8.3-2 and Figure 8.3-4).

Direct measurement by constant head ψ = +10 mm on 100 mm diameter cores generally resulted in lower values of saturated hydraulic conductivity than the two tension infiltrometer approaches. This finding contradicts many studies in which higher estimates of hydraulic conductivity have been obtained by saturated approaches compared to tension infiltrometers (Kodesova *et al.* 2010) due to inclusion of larger macropores in the infiltration process (Jarvis 2007). However, in this study however lower K_{sat} values with the laboratory core approach resulted from (i) smaller sample size (3 x 100 – 65 mm diameter) which reduced the likelihood of sampling a large macropore compared to the tension infiltrometers (4-6 x 200 mm diameter) (Davis *et al.* 1999), (ii) prolonged saturation of the soil cores prior to analysis resulting in clay swelling and incomplete sealing of shrinkage cracks (Greve *et al.* 2010; van den Berg 1989; Waller and Wallender 1991), and (iii) biological gumming of pores (Ragusa *et al.* 1994) due to prolonged saturation. Use of traditional laboratory core methods for deriving K_{sat} in hydrophobic and vertic soils is thought to have underestimated the contribution to flow from preferential processes compared to the field based approach and thus resulted in lower values of K_{sat} than that experienced in the fields (except perhaps after prolonged rainfall or inundation).

Linear extrapolation of the K(ψ) relationship determined by evaporation (Wind 1968) produced lower estimates of saturated hydraulic conductivity than the other techniques (except B22 horizon, Figure 8.3-4) due to the smaller core size (3 X 60 mm diameter), and limited data near saturation to enable extrapolation to ψ=0. Extrapolation of the K(ψ) relationship to ψ = 0 using RETC from tension infiltrometers at multiple supply potentials (Chapter 6.2.6) resulted in higher estimates of K_{sat} than the desorption approach.

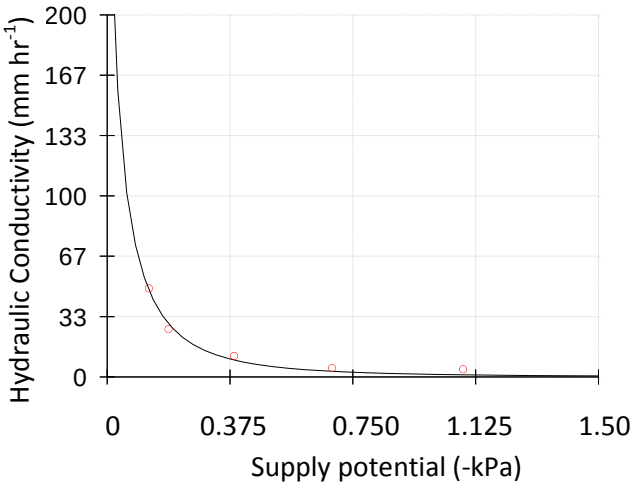

Figure 8.3-5 RETC output. Example of exponential relationship between supply potential (pressure head) and hydraulic conductivity making estimation of hydraulic conductivity at saturation difficult, site B, A1 horizon, dry treatment. Red circles indicate measured values. Black line represents the RETC interpolation.

However very large standard errors resulted from difficulty extrapolating the K(ψ) relationship to ψ = 0 as the relationship became exponential near saturation (Figure 8.3-5).

Inverse parameterisation of cumulative infiltration from the tension infiltrometers into the dry treatment using HYDRUS-2D resulted in substantially higher values of saturated hydraulic conductivity than other approaches. Estimated saturated hydraulic conductivity from inverse parameterisation in the wet treatment was higher than expected. Results suggest that despite wetting of the site for approximately 30 days, shrinkage cracks had only partly closed and continued to contribute to flow. Preferential flow through shrinkage cracks after the initial surface crack network had completely closed has also been reported by Waller and Wallender (1991) and Greve *et al.* (2010).Kodesova (2010) found that numerical inversion of a multistep outflow experiment using a single porosity model also resulted in significantly higher K_{sat} values than those determined by constant head method on the same soil samples.

Table 8.3-2 Variation in estimated saturated hydraulic conductivity

	A1 Horizon		A2 Horizon		B21 Horizon		B22 Horizon		B23 Horizon	
Approach	Mean ($mm\ hr^{-1}$)	SE	Mean ($mm\ hr^{-1}$)	SE	Mean ($mm\ hr^{-1}$)	SE	Mean ($mm\ hr^{-1}$)	SE	Mean ($mm\ hr^{-1}$)	SE
Measured - 100mm cores ψ +10 mm	46.7	3. 7	39.4	5.9	45.9	34.6	0.2	0.01	1.4	0.9
Evaporation- Linear	17.0	9.8	3.0	1.7	0.3	0.2	0.5	0.2	0.2	0.1
Disk – Inverse - Dry	760	110	110	70	360	160	6000	35880	180	210
Disk – Inverse - Wet	100	20	3.4	1.5	270	390	4430	3920		
Disk – RETC - Dry	1100	7650	60	12930	290	170	110	570	10	75
Disk – RETC - Wet	280	5260	45	440	1210	24800	32	610		

SE+ standard error

8.3.5 Model simulation of the dye staining experiment at site B.

The two soil water models HYDRUS-1D and MACRO 5.1 were unable to adequately simulate infiltration of the dye tracer (25 mm precipitation) in either the wet or dry soil water treatments (Figure 8.3-6 a&c and Figure 8.3-7a). Notably neither MACRO 5.1 nor HYDRUS-1D were able to simulate the maximum depth of infiltration demonstrated by the dye staining experiments in the dry treatment (~40 cm c.f. ~82 cm). Bachmair *et al.* (2010) also reported MACRO 5.1 underestimated flow depth in soils with a water repellent sandy A horizon. Inability of one dimensional dual permeability models to accurately simulate preferential flow in tile drained field soils has also been reported by Kohne and Gerke (2005) and Haws *et al.* (2005).

Table 8.3-3 Effect of parameterisation approach on degree of fit (RMSE) between the change in soil moisture predicted by HYDRUS 1D and estimates based on dye staining and the EnviroSCAN soil moisture probe, 48 hours after infiltration commenced.

Model	Soil Moisture Treatment	Parameter Estimation Approach		Root Square Mean Error 0 - 30 cm		Root Square Mean Error 0 - 50 cm		Root Square Mean Error 0 – 100 cm	
		van Genuchten Parameters	Saturated Hydraulic Conductivity	Dye Staining Profile	Enviro SCAN	Dye Staining Profile	Enviro SCAN	Dye Staining Profile	Enviro SCAN
HYDRUS-1D single pore domain	**Direct Approaches**								
	Dry	Desorption	Measured +10mm	0.074	0.064	0.057	0.049	0.043	0.035
		Desorption vBD	Measured +10mm	0.075	0.066	0.058	0.050	0.043	0.036
		Evaporation	Extrapolation	0.068	0.044	0.054	0.036	0.042	0.028
	Wet	Desorption	Measured +10mm	0.087	0.062	0.068	0.049	0.047	0.034
		Desorption vBD	Measured +10mm	0.110	*0.076*	*0.084*	*0.059*	*0.058*	*0.040*
		Evaporation	Evaporation	0.061	0.032	0.046	0.025	0.032	**0.017**
HYDRUS-1D single pore domain	**Inverse Approaches**								
	Dry	Disk-VG	Disk - Inverse	0.059	0.053	*0.060*	*0.051*	*0.074*	0.056
		Disk-VG – Qr set	Disk - Inverse	0.054	0.045	0.045	0.037	0.053	0.041
		Disk-VG	RETC	0.058	0.051	0.047	0.040	0.052	0.046
		Disk-VG – Qr set	RETC	**0.053**	**0.042**	**0.043**	**0.034**	**0.034**	**0.027**
	Wet	Disk-VG	Disk - Inverse	0.031	0.043	0.024	0.033	0.017	0.023
		Disk-VG – Qr set	Disk - Inverse	0.027	0.029	0.026	0.027	0.022	0.021
		Disk-VG	RETC	0.029	0.039	0.022	0.030	**0.016**	0.021
		Disk-VG – Qr set	RETC	0.028	**0.026**	0.024	**0.023**	0.018	**0.017**
MACRO 5.1 single pore domain	**Dual Permeability**								
	Dry	Desorption vBD	Measured +10mm	0.086	0.071	*0.066*	0.054	0.048	0.137
		Disk -VG – Qr set	Measured +10mm	*0.100*	*0.085*	*0.078*	*0.066*	0.058	0.048
		Disk -VG – Qr set	Disk -Inverse	0.098	0.083	0.078	0.065	0.061	0.049
		High PF	Measured +10mm	0.073	0.050	0.078	0.048	0.058	0.036
	Wet	Desorption vBD	Measured +10mm	0.075	*0.024*	0.061	0.045	0.043	0.041
		Disk -VG – Qr set	Measured +10mm	0.027	0.036	**0.020**	*0.027*	*0.027*	*0.027*
		Disk -VG – Qr set	Disk -Inverse	**0.026**	0.035	0.021	*0.027*	0.038	0.032
		High PF	Measured +10mm	*0.121*	0.046	*0.091*	0.035	0.066	0.031

Bold indicates lowest RSME (best fit) and Italics represent highest RSME (worst fit) for each soil moisture treatment and root zone increment. Note RMSE values are comparable between rows not columns as sample number differs between root depth and the two measures of soil moisture.

Caution is expressed when comparing the change in soil moisture estimated from dye staining and the two soil water models. Potential error results from inability of the dye staining approach to (i) determine a positive change in soil moisture resulting from displacement of existing soil moisture further down the soil profile, (ii) determine a negative change in soil moisture resulting from drainage of the initial soil moisture during infiltration of the dye tracer.

The single pore domain model HYDRUS-1D predicted higher RMSE (RMSE 0.0496) or a poorer fit between the modelled and measured change in soil moisture in the dry treatment compared to the wet treatment (RMSE 0.040), (Table 8.3-3). Simulations based on parameterisation by laboratory drying approaches had poorer fit (RMSE 0.038) to both the EnviroSCAN data and the dye staining approach, than parameterisations based on inverse infiltration from *in situ* tension infiltrometers (RMSE 0.034). However considerable differences in model performance existed between parameterisation approaches, particularly in the dry treatment (Figure 8.3-6c and Table 8.3-3).

MACRO 5.1 produced poorer prediction of the change in soil moisture following 25 mm precipitation (RMSE 0.050) than the single pore domain model HYDRUS-1D (RMSE 0.039), (Table 8.3-3 and Figure 8.3-7). MACRO 5.1 prediction of the change in soil moisture was better (lower RMSE) in the wet treatment (RMSE 0.043) than the dry treatment (RMSE 0.70). Higher RMSE in the dry treatment with both models resulted from preferential flow which resulted in infiltration to 80 cm depth, whereas the models did not simulate infiltration below approximately 40 cm. Bachmair *et al.* (2010) also reported poor prediction of infiltration and dye staining experiments with MACRO 5.1 in forest and agricultural soils. They attributed poor model performance to inadequate simulation of flow initiation caused by inability to represent spatial variation in microtopography and water repellence at the soil surface.

8.3.5.1 Dry treatment

In the dry treatment, the lowest RMSE occurred between the change in soil moisture determined by dye staining and the Disk-VG, Qr set, RETC K parameterisation (RMSE 0.034) in which the van Genuchten parameters had been determined by inverse infiltration of tension infiltrometer data in which the Qr parameter had been determined by desorption and removed from the objective function, and saturated hydraulic conductivity was determined by RETC extrapolation of K(ψ) to ψ = 0, (Table 8.3-3). The poorest approximation (highest RMSE) occurred for the HYDRUS-1D Disk-VG –inverse K approach in which Qr and K_{sat} parameters were included in the objective function (RMSE 0.74).

Laboratory drying approaches

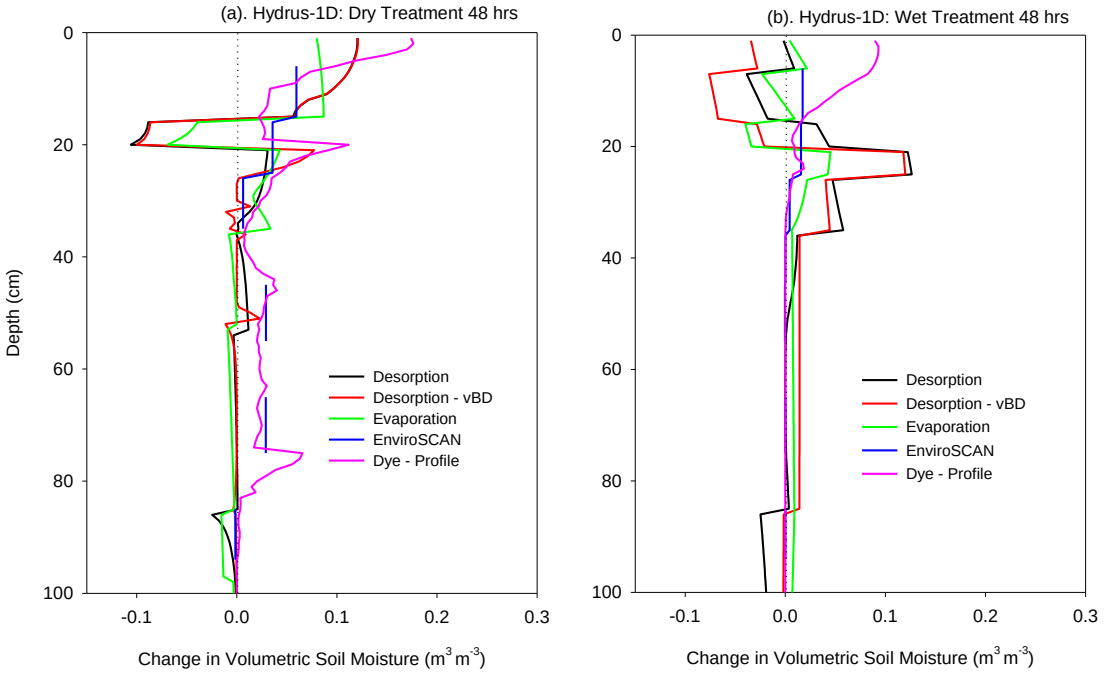

Field inverse approaches

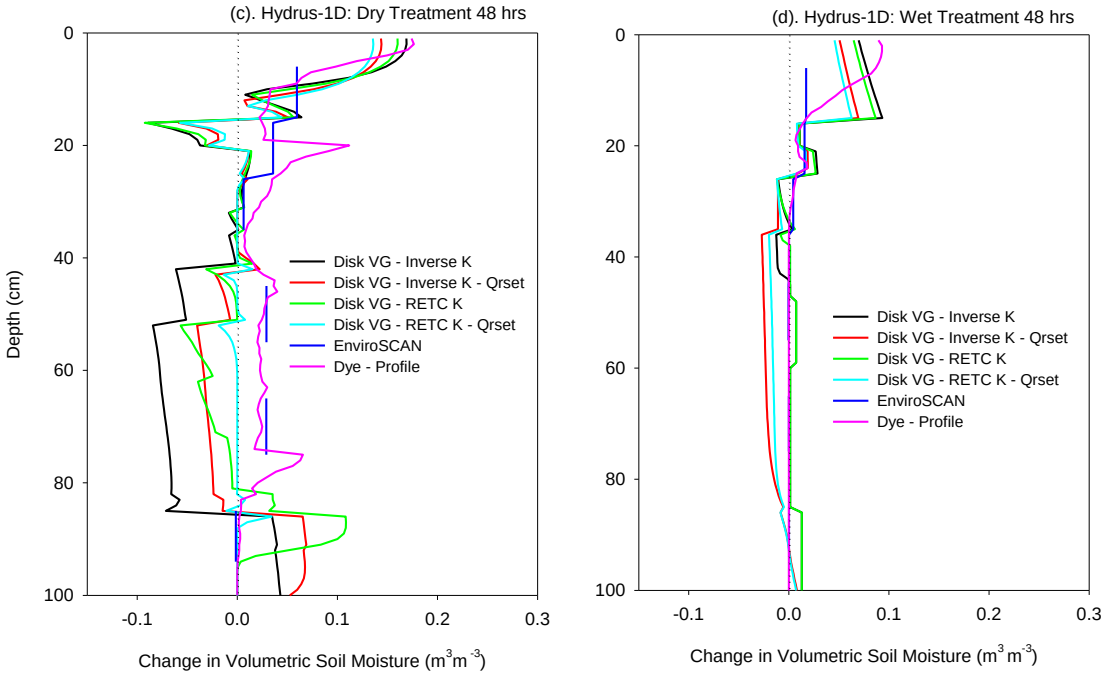

Figure 8.3-6 Effect of parameterisation techniques on predicted change in soil moisture using HYDRUS-1D following 25 mm infiltration into soil at high (b & d) and low (a & c) soil. van Genuchten parameters determined by (a & b) laboratory drying approaches, (c & d) field based inverse infiltration of tension infiltrometers data. Disk VG, inverse infiltration from tension infiltrometers. Inverse K, K_{sat} estimation by inverse parameterisation of tension infiltrometer data. RETC K, K_{sat} estimation by extrapolation of K(ψ) to ψ = 0. Qrset determined by desorption and removed from the objective function.

Of the dual permeability approaches in MACRO 5.1 the Disk-VG, Qr set, Inverse K parameterisation in which the Qr parameter had been removed from the objective function had the poorest fit (RMSE 0.061).

In the dry treatment, differences between the change in soil moisture predicted by the models and that estimated by either the EnviroSCAN soil moisture probe or the dye staining approach principally resulted from inability of both HYDRUS-1D and MACRO 5.1 to simulate the effects of water repellence on the development of finger flow. Dye staining experiments in Chapter 4.0 demonstrated that at low antecedent soil moisture finger flow resulted in as little as 7.1 % of the A1 horizon participating in flow (Chapter 4.3.2.2) consequently a large proportion of the applied tracer was available to infiltrate further down the soil profile. However the models were unable to simulate finger flow consequently the majority of the applied dye tracer was retained in the A1 horizon, which limited infiltration into the subsoil layers.

Model error also resulted from prediction of drainage (negative change in soil moisture) from the A2 horizon (15-20 cm), due to high initial soil water content (Figure 8.3-6a&b and Figure 8.3-7a). Neither modelling approach (including the MACRO 5.1 – High PF simulation) was able to simulate the type or extent of bypass flow and soil water accumulation at low antecedent soil moisture. Similarities between model predictions and the change in soil moisture determined by the EnviroSCAN or the dye staining approach did not result from the models accurately representing infiltration processes. Rather, the lack of soil water accumulation predicted by the models resulted from the majority of the infiltrating water being retained in the A1 horizon, whereas dye staining experiments (Chapter 4.3.2) demonstrated the absence of dye staining in the B21 horizon resulted from rivulet flow through shrinkage cracks.

8.3.5.2 Wet treatment

In the wet treatment, prolonged wetting by irrigation was expected to reduce the occurrence of preferential flow resulting in more uniform infiltration as predicted by Richards equation. Consequently it was expected the models would be able to accurately simulate infiltration into the soil at high antecedent soil moisture. However Table 8.3-3 and Figure 8.3-6 b&d and Figure 8.3-7b demonstrate a poor fit (high RMSE) between the simulated change in soil moisture and that determined by both the EnviroSCAN soil moisture probe and the dye staining approach. Dye staining demonstrated infiltration did not extend into the B21 horizon or below 40 cm depth, however both models predicted slight accumulation of soil water or drainage in the B22 and B23 horizons depending on parameterisation approach (Figure 8.3-6b&c and Figure 8.3-7b).

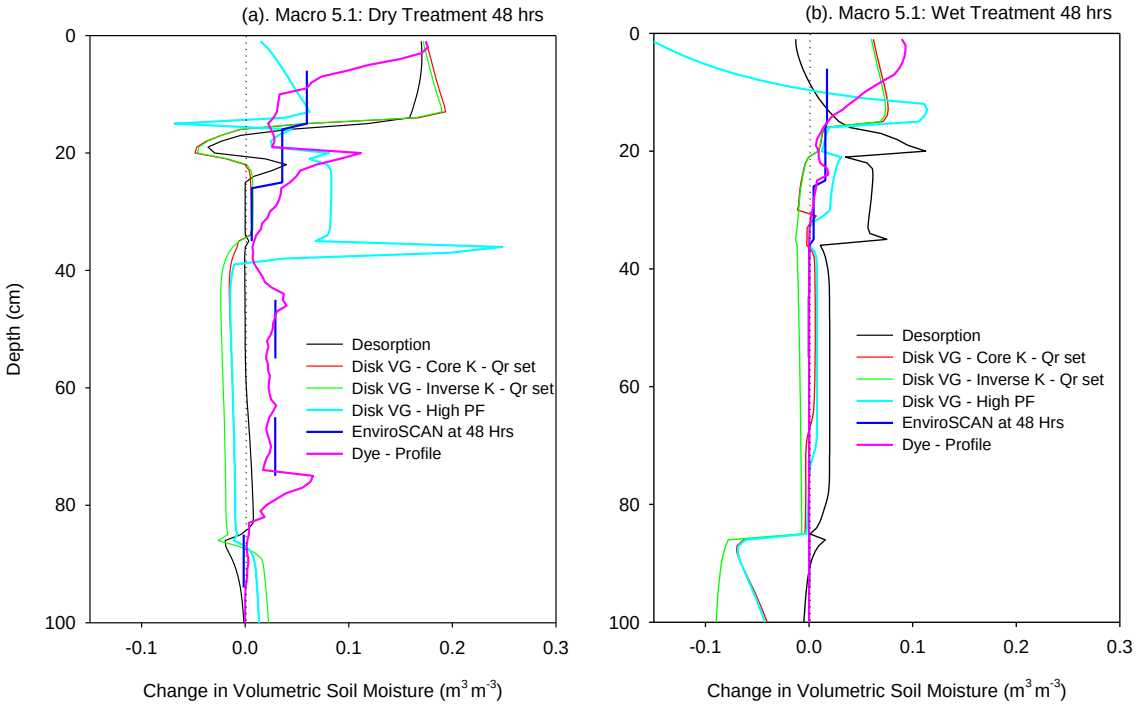

Figure 8.3-7 Effect of parameterisation techniques on predicted change in soil moisture using MACRO 5.1 following 25 mm infiltration into soil at(a) low, and high (b) antecedent soil moisture. van Genuchten parameters determined by desorption and inverse infiltration of tension infiltrometers data. Disk VG, inverse infiltration from tension infiltrometers. Inverse K, K_{sat} estimation by inverse parameterisation of tension infiltrometer data. Core K, K_{sat} determination on 100 mm diameter saturated cores. Qr set determined by desorption and removed from the objective function.

In the wet treatment, parameterisation by inverse solution of tension infiltration data tended to result in closer approximation (lower RMSE) of the change in soil moisture following application of dye tracer than parameterisation approaches based on laboratory drying. Parameterisation based on laboratory drying approaches resulted in HYDRUS-1D predicting drainage from the A1 and A2 horizons and accumulation of soil water in the B21 horizon to a depth of 35 cm (Figure 8.3-6b). Whereas parameterisation based on inverse solution of tension infiltration data resulted in HYDRUS-1D predicting accumulation of the dye tracer in the A1 horizon and minimal increase in soil moisture in the A2 and B21 horizons. A small amount of drainage was predicted from the B22 and B23 horizons (Figure 8.3-6d). The duel permeability model MACRO 5.1 parameterisation based on inverse solution of tension infiltration data (RMSE 0.027 – 0.038) resulted in accumulation of the dye tracer in the A1 horizon (similar to HYDRUS-1D), however parameterisation based on desorption (RMSE 0.043) resulted in drainage of the A1 horizon and considerable soil water accumulation in the A2, B21 and upper B22 horizon to a depth of approximately 38 cm (Figure 8.3-7). The High PF (extreme preferential flow simulation), (RMSE 0.066) resulted in considerable drainage in the upper A1 horizon, accumulation in the lower A1 horizon, and a small amount of soil water accumulation in the B21 horizon (Table 8.3-3).

8.3.6 Simulation of changes in soil moisture adjacent site B, 9 / 2007 to 9 / 2009

Neither HYDRUS-1D nor MACRO 5.1 were able to adequately simulate the changes in soil moisture recorded by the EnviroSCAN soil moisture probe between September 2007 and September 2009 (Table 8.3-4,Figure 8.3-8, Figure 8.3-9, and Figure 8.3-10). Parameterisation approach had a greater influence on RMSE than model choice. Determination of van Genuchten parameters by laboratory drying approaches resulted in the lowest RMSE for both the effective root zone (0 - 30 cm) and the whole soil profile (0 - 150 cm, Table 8.3-4). Differences between modelling and parameterisation approaches are further investigated for selected soil horizons.

8.3.6.1 A1 horizon 10 cm

MACRO 5.1 produced better simulation of soil moisture at 10 cm depth than HYDRUS-1D. The closest approximation with the EnviroSCAN data occurred for the desorption parameterisation approach with hydraulic conductivity determined from 100 mm cores in MACRO 5.1 (RMSE 0.060). The highest RMSE values resulted from inverse infiltration from tension infiltrometers into soil at high antecedent soil moisture, indicating the worst fit to the measured data (Table 8.3-4).

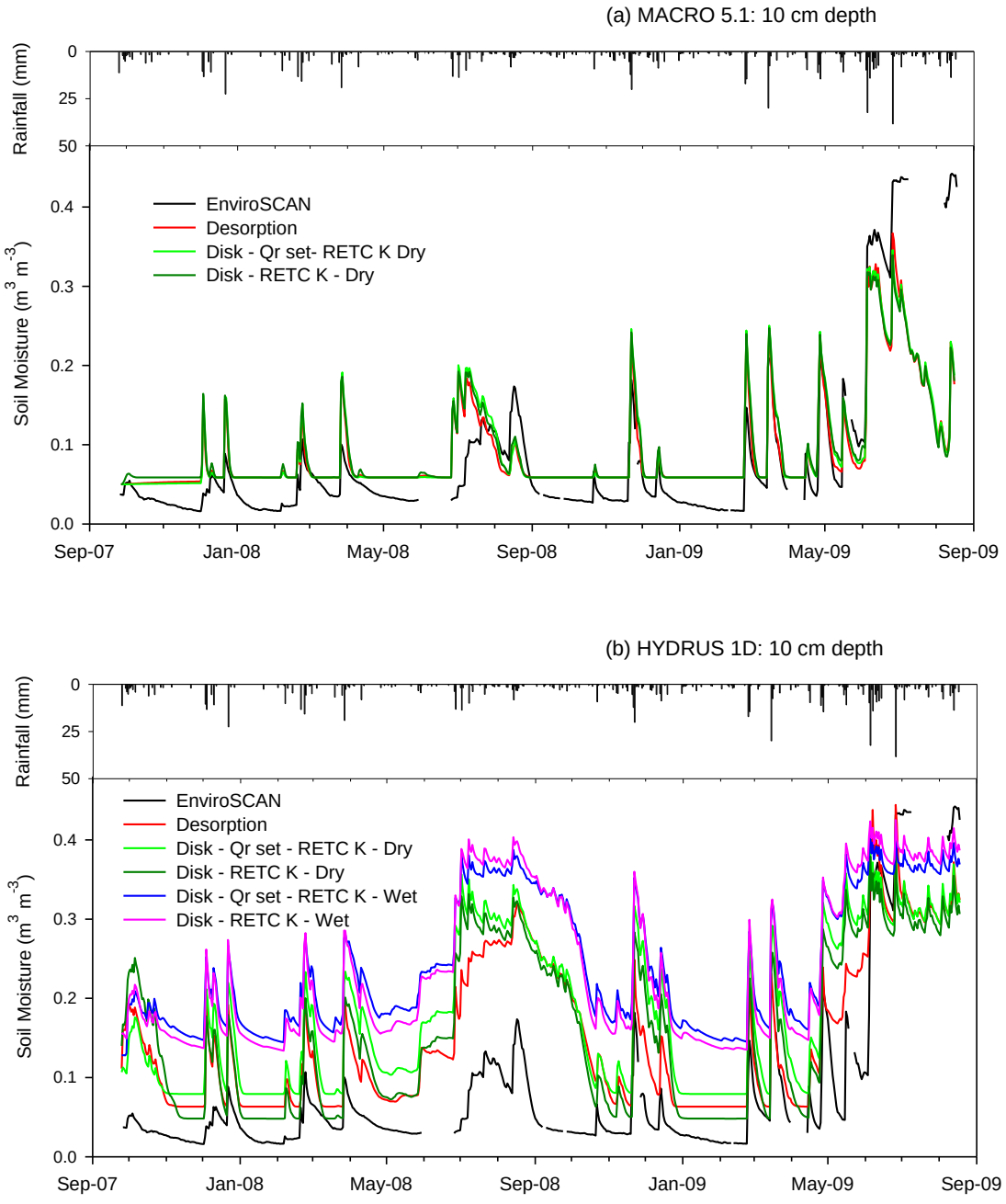

Figure 8.3-8 Comparison between EnviroSCAN recorded change in soil moisture and simulated change in soil at 10 cm depth (a) MACRO 5.1, (b) HYDRUS 1D.

Differences between the change in soil moisture measured by the EnviroSCAN and model predictions resulted from: (i) over-estimation of soil moisture storage in the A1 horizon following rainfall, (ii) over-estimation of the residual soil moisture content (Qr) (iii) underestimation of drainage and / or soil water extraction by evapotranspiration (Figure 8.3-8).

All parameterisation approaches over-estimated the maximum soil water content following rainfall due to inability to simulate finger flow when the antecedent soil moisture was below the threshold soil moisture content. As discussed in Chapter 7.4, finger flow reduced the volume of soil within the A1 horizon which participated in infiltration, the change in soil moisture recorded by the EnviroSCAN soil moisture probe was substantially lower than the potential change in soil moisture that would have occurred in a similar hydrophilic soil. It is thought that after July 2009, hydrophobicity broke down due to either persistently high soil moisture or early winter rainfall leaching the hydrophobic substances from the soil (Chapter 7.3.3). Breakdown in hydrophobicity after July 2009 resulted in a greater proportion of the A1 horizon participating in flow which resulted in closer agreement between the simulated and measured change in soil water content at 10 cm depth with both models. Residual water content (Qr) values higher than the minimum measured soil moisture content also contributed to higher simulated moisture content in the A1 horizon, as the models are unable to extract water below the residual soil water content (Figure 8.3-8).

An additional simulation was conducted with an artificially shallow A1 horizon (0-10 cm cf 0-15 cm) to mimic the effect of finger flow by reducing the volume of soil through which infiltration was able to occur. This shallow A1 simulation reduced the RMSE (0-30 cm) from 0.158 to 0.098, the lowest of all parameterisation approaches (Table 8.3-4). This additional simulation supported the previous proposition that inability to adequately simulate the effects of water repellence on the proportion of soil which participated in flow was responsible for a substantial component of the error between the measured and simulated change in soil moisture.

8.3.6.2 B21 horizon - 30 cm depth

Dye staining (Chapter 4.3) and soil moisture monitoring (Chapter 5.3) demonstrated that at low antecedent soil moisture, infiltration frequently bypassed the B21 horizon resulting in little change in soil moisture at 30 cm depth. It was expected that inability to simulate bypass flow in the single porosity model (HYDRUS-1D) would result in overestimation of soil moisture at 30 cm depth.

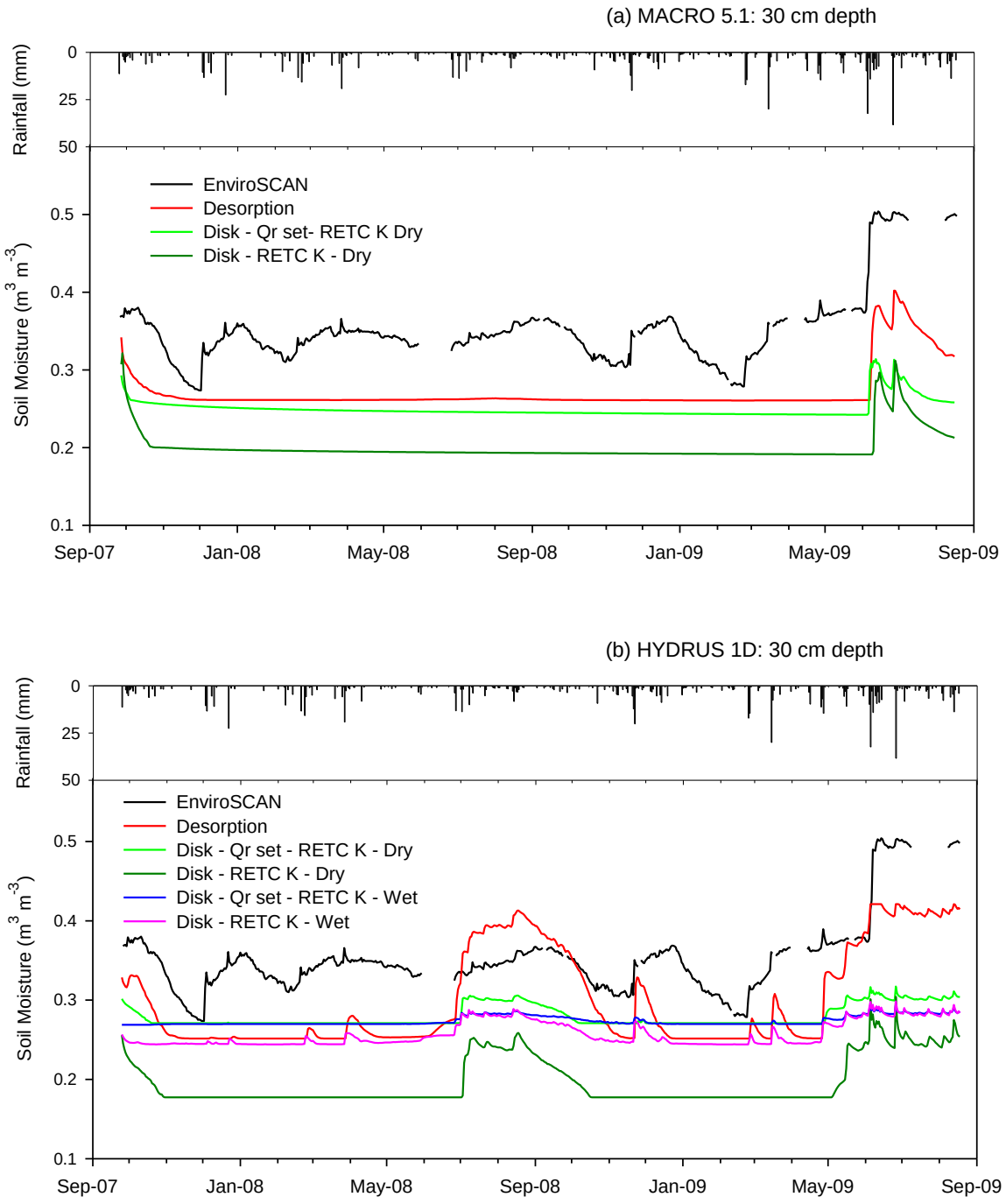

Figure 8.3-9 Comparison between EnviroSCAN recorded change in soil moisture and simulated change in soil at 30 cm depth (a) MACRO 5.1, (b) HYDRUS 1D.

However Figure 8.3-9 demonstrates that both models underestimated the frequency and magnitude of infiltration into the B21 horizon. Model failure was attributed to the rainfall being retained in the A1 horizon as a consequence of the inability to simulate finger flow and high Qr.

MACRO 5.1 was unable to simulate infiltration to 30 cm depth prior to July 2009, while the degree of infiltration to 30 cm depth simulated in HYDRUS-1D was highly dependent on the parameterisation approach. Omitting the residual soil water content from the parameter function (Qr set) substantially reduced RMSE from 1.66 to 0.085, while different parameterisation approaches for determining K_{sat} had little effect on the RMSE (i.e. 0.160 cf 0.166) (Table 8.3-4).

8.3.6.3 B22 Horizon - 70 cm depth

Neither modelling approach was able to adequately simulate bypass flow from the A horizons into the B2 horizons as observed by the dye staining experiments. At low antecedent soil moisture, dye staining experiments (Chapter 4.3) and soil moisture monitoring (Chapter 5.3.3) demonstrated that infiltration bypassed the B21 horizon resulting in soil water accumulation in dead-end pores in the B22 and B23 horizons. This flow behaviour was also observed in the 'spiky' (rapid rise and fall) response to rainfall recorded by the EnviroSCAN at 70 cm depth (Chapter 5.3.3, Figure 8.3-10). However, HYDRUS-1D only simulated infiltration to 70 cm depth when the whole soil profile was between saturation and field capacity in August 2008, and after June 2009, while MACRO 5.1 only simulated infiltration at 70 cm depth after June 2009.

8.3.6.4 Deep drainage

Traditional approaches for determining deep drainage which use Darcy's Law, such as the zero plane flux method, were also not able to be used in this study as they do not account for preferential flow. While Fernandez-Galvez *et al.* (2007) demonstrated that deep drainage could be determined from high frequency soil moisture monitoring, in this study the change in soil moisture at 70 cm depth is presented as a conservative surrogate for deep drainage. Whilst it is acknowledged that true deep drainage is usually represented by flow beneath the soil profile, typically greater than 1.0 meter depth. At site B the maximum rooting depth was 50 cm such that soil water accumulation below 70 cm depth is expected to contribute to deep drainage. It is also anticipated that the change in soil moisture at 70 cm depth is likely to differ to the magnitude of deep drainage as the flux of water moving below a specified depth cannot be directly determined from changes in soil moisture content, as soils near field capacity are capable of transmitting water without recording a change in soil moisture content (Gregory *et al.* 1992).

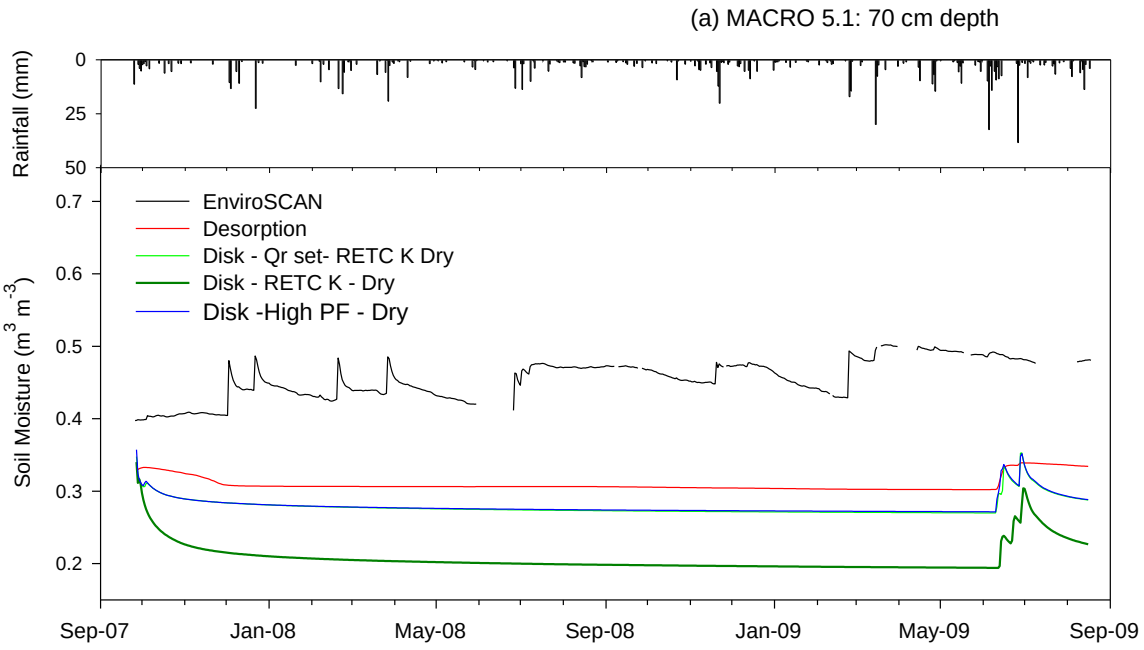

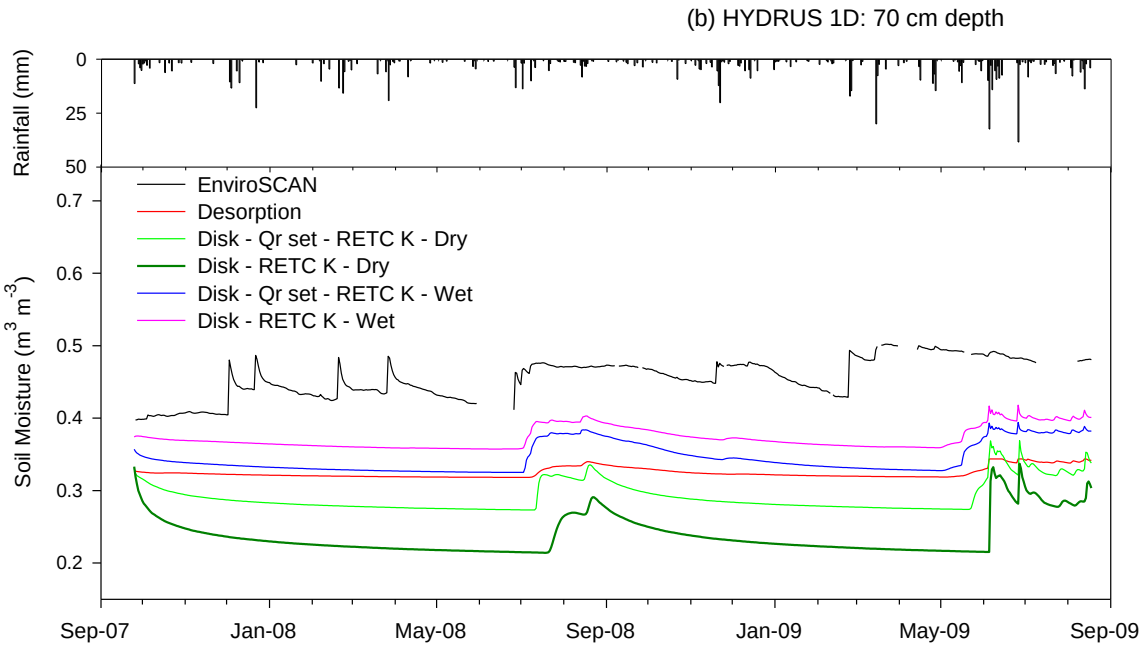

Figure 8.3-10 Comparison between EnviroSCAN recorded change in soil moisture and simulated change in soil at 70 cm depth (a) MACRO 5.1, (b) HYDRUS 1D.

The EnviroSCAN recorded 17 days in which soil moisture at 70 cm depth increased by >0.002 m^3 m^{-3} d^{-1} including 8 days in which soil moisture increased by >0.02 m^3 m^{-3} d^{-1}. These events increased soil moisture by a total 46.27 mm at 70 cm depth (5.2 % of rainfall) between September 2007 and September 2009. Prior to March 2009 these events predominantly resulted from preferential flow. After March 2009 infiltration to 70 cm depth was dominated by equilibrium flow resulting from saturation of the whole soil profile. Of the infiltration to 70 cm depth, 92.9 % resulted from preferential flow.

The two soil water models were not able to predict either the frequency or magnitude of infiltration events which resulted in soil water accumulation at 70 cm depth. Depending on parameterisation approach, HYDRUS-1D predicted accumulation of soil water below 70 cm depth ($\Delta\theta$ >0.002 m^3 m^{-3} d^{-1}) on 13 to 32 days, and on 4 occasions when $\Delta\theta$ >0.02 m^3 m^{-3} d^{-1}. These events increased soil moisture by 2.07 – 25.65 mm at 70 cm depth. MACRO 5.1 predicted accumulation of soil water below 70 cm depth on up to 9 occasions in which soil moisture increased by >0.001 m^3 m^{-3} d^{-1}, and up to 4 occasions in which soil moisture increased by >0.02 m^3 m^{-3} d^{-1}. These infiltration events below 70 cm depth were predicted to have increased soil moisture at 70 cm depth by 3.06 - 13.36 mm depending on parameterisation approach. Differences between the measured and modelled change in soil moisture at 70 cm depth were attributed to inability of the two models to adequately simulate the magnitude and frequency of preferential flow processes, specifically finger flow in the A1 horizon and rivulet flow in the B2 horizons.

Few studies have measured deep drainage in texture contrast soils, Ward *et al.* (1998) reported that between 11-21 mm deep drainage occurred during a single storm event on a texture contrast soil in south-western Australia. Ticehurst (2004) reported vertical drainage beneath the root zone constituted 9.5 % of rainfall in texture contrast soils in N.S.W. Dowling *et al.* (1991) estimated deep drainage from furrow irrigation of a sodic duplex soil ranged from 98 mm yr^{-1} to 0 mm yr^{-1}. Using the tipping bucket soil water model SoilWAT within APSIM, Lisson *et al.* (2005) estimated deep drainage on texture contrast soils at the University of Tasmania Farm ranged from 9 mm ha^{-1} yr^{-1} under rainfed management to approximately 40 mm ha^{-1} yr^{-1} with irrigated production. The estimated change in soil moisture at 70 cm depth in this study (~23 mm yr^{-1}) was approximately seven times greater than the magnitude of rainfed deep drainage estimated by Lisson *et al.* (2005). However comparison between the two approaches is limited by differences in seasonal variations in rainfall, inability of APSIM to simulate preferential flow, and differences between deep drainage and infiltration to 70 cm depth.

Table 8.3-4 Comparison of change in soil moisture measured by the EnviroSCAN with simulated change in soil moisture using MACRO 5.1 and HYDRUS-1D at site B between Sep. 2007 - Sep. 2009.

	Parameterisation methodology				Root Mean Square Error (RMSE) for each monitored soil depth (cm)								Average RMSE	
	Van Genuchten parameters	Qr	Ksat	Moist. Treat.	10	20	30	50 c	70	90	130	150	**0 - 30 cm**	**0 -150 cm**
MACRO 5.1	Desorption	RETC	Core	Sat	*0.060*	*0.203*	*0.092*	*0.062*	*0.153*	0.080	0.076	0.219	**0.119**	**0.118**
	Inverse	Set	RETC	Dry	0.062	0.215	0.113	0.077	0.183	0.073	0.068	0.212	**0.130**	**0.125**
	Inverse – High PF	Set	RETC	Dry	0.062	0.214	0.114	0.077	0.182	*0.073*	*0.068*	*0.210*	**0.130**	**0.124**
	Inverse	Inverse	RETC	Dry	0.062	0.216	0.160	0.139	0.254	0.174	0.142	0.329	**0.146**	**0.184**
HYDRUS – 1D	Desorption	RETC	Core	Sat	*0.094*	0.155	*0.069*	0.049	0.133	0.052	0.054	0.192	**0.106**	**0.100**
	Inverse	Set	RETC	Dry	0.122	0.196	0.083	0.061	0.167	0.095	0.092	0.230	**0.134**	**0.131**
	Inverse	Set	Inverse	Dry	0.124	0.198	0.085	0.075	0.186	0.132	0.132	0.273	**0.136**	**0.151**
	Inverse	Inverse	RETC	Dry	0.109	0.205	0.160	0.105	0.221	0.094	0.091	0.229	**0.158**	**0.152**
	Inverse	Inverse	Inverse	Dry	0.105	0.207	0.166	0.134	0.254	0.146	0.147	0.288	**0.159**	**0.181**
	Inverse	Set	RETC	Wet	0.176	0.107	0.089	*0.048*	0.114	*0.046*	*0.033*	*0.159*	**0.124**	**0.097**
	Inverse	Set	Inverse	Wet	0.182	*0.102*	0.090	0.051	0.121	0.062	0.055	0.191	**0.124**	**0.107**
	Inverse	Inverse	RETC	Wet	0.109	0.205	0.160	0.105	0.221	0.094	0.091	0.229	**0.158**	**0.152**
	Inverse	Inverse	Inverse	Wet	0.161	0.058	0.105	0.055	*0.106*	0.190	0.174	0.314	**0.108**	**0.145**
	Shallow A1	Inverse	RETC	Dry	0.075	0.061	0.159	0.103	*0.219*	0.092	0.090	0.228	**0.098**	**0.128**

Italics indicates lowest RMSE (best fit) for each model and depth increment.

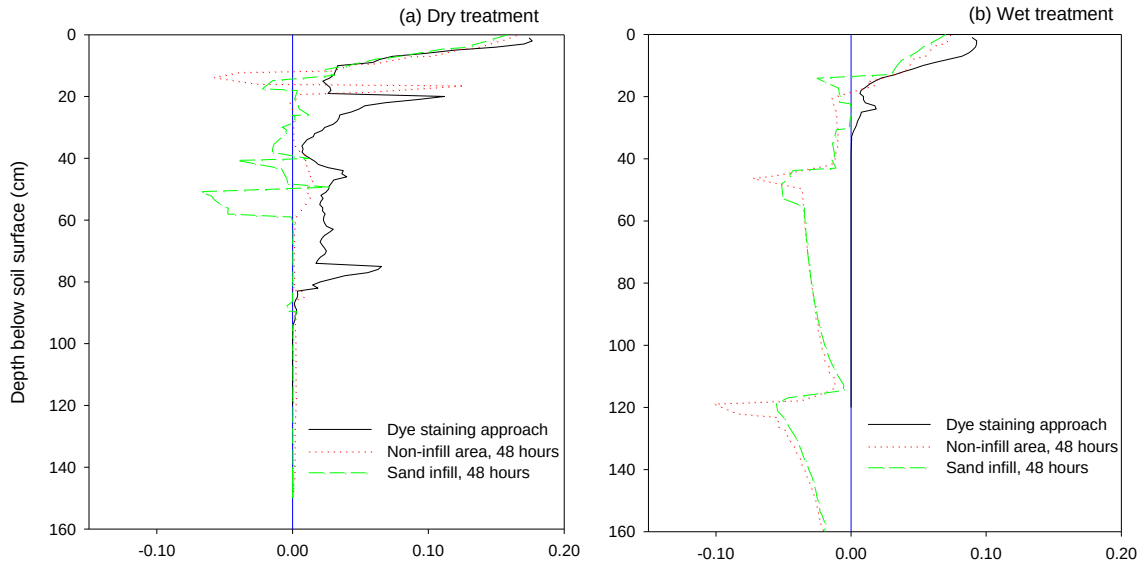

Figure 8.3-11 Change in soil moisture following infiltration of 25 mm dye tracer at site B (a) dry treatment, (b) wet treatment. Simulations were conducted with HYDRUS 2D in which sand infills were represented as extensions of the A2 horizon into the B21 and B22 horizons.

8.3.7 Two dimensional simulations of dye tracer infiltration using HYDRUS-2D/3D.

8.3.7.1 Effect of sand infills on infiltration of 25 mm dye tracer

Creation of sand infills had little effect on two dimensional simulated infiltration into soil at low antecedent soil moisture (Figure 8.3-12). Similar to the one dimensional simulation, the majority of the dye tracer was retained within the A1 horizon. HYDRUS-2D/3D predicted gravitational drainage of initial soil water from the sand infills into the surrounding soil B21 and B22 horizons (Figure 8.3-11) and lateral movement of soil water from the sand infills into the surrounding soil matrix (Figure 8.3-12). In the non-sand infill areas, the soil moisture in the A2 horizon drained under gravity into the upper B21 horizon as indicated by development of red areas in Figure 8.3-12. Within the A1 horizon, HYDRUS-2D/3D predicted a similar change in soil moisture to that estimated by dye staining within both the sand infill and non sand infill areas (Figure 8.3-11 b). Within the non-sand infill areas, infiltration of the dye tracer extended to 60 cm depth which resulted in RMSE 0.037, similar to the one dimensional simulation in HYDRUS-1D without sand infills (RMSE 0.034). Discrepancy between the simulated and measured change in soil moisture was in part attributed to drainage (negative change in soil moisture) from within the sand infills which was not able to be inferred from the dye staining experiments (Digital animation presented on CD Rom, Appendix 8.3.2).

8.3.7.2 Lateral flow at high antecedent soil moisture

In the wet treatment, HYDRUS-2D predicted the dye tracer spread at least 1.6 meters laterally from the side of the application area through the A1 horizon or along the A1 / A2 boundary (Figure 8.4-1). Sequential HYDRUS-2D simulations demonstrated the development of lateral flow following dye application, resulted from a combination of the infiltrating precipitation and lateral displacement of the existing soil water by piston flow (Figure 8.4-1). The lateral movement of infiltration predicted by HYDRUS-2D was greater than that observed by the dye tracer, due to the model predicting displacement of existing soil water (not dye stained) beyond the area of dye staining (Digital animation presented on CD Rom, Appendix 8.3.2).

Although HYDRUS-2D was unable to simulate the wetting front instability observed by dye staining in the lower A1 horizon (Chapter 4.0), HYDRUS-2D simulations confirmed the lack of dye staining below 40 cm depth (Chapter 4.3.6), resulted from lateral flow of the dye tracer through the A1 horizon (Figure 8.4-1). Lateral flow occurred as unsaturated flow (ψ -3 to -9 kPa) above the B21 horizon in which new water (dye tracer) moved laterally through the A1 horizon above the A2 horizon.

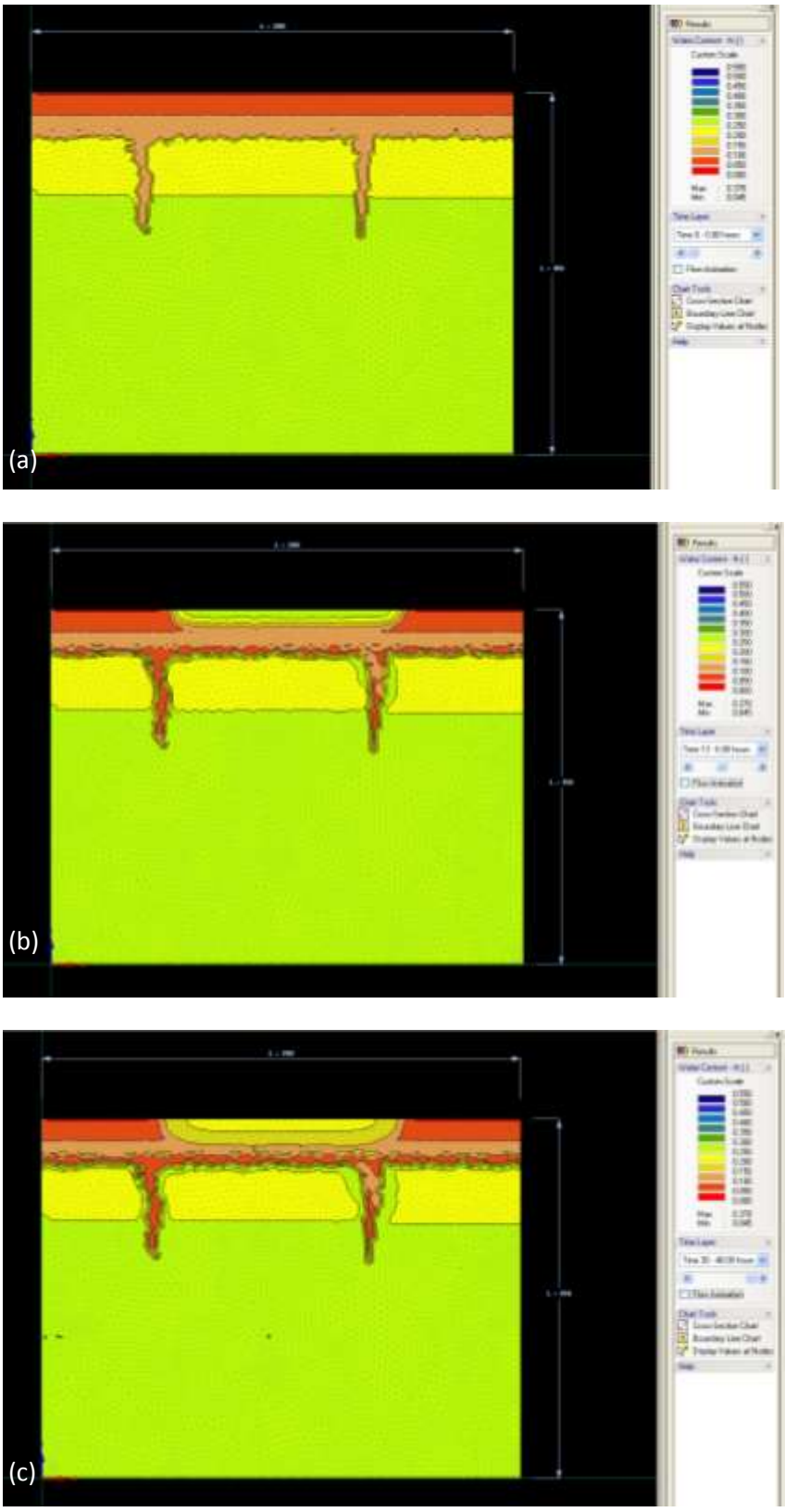

Figure 8.3-12 Effect of sand infills on infiltration of 25 mm dye tracer into soil at low antecedent soil moisture, Disk VG, Qr set, RETC-K. Soil moisture at (a) zero hours, (b) 6 hrs, (c) 48 hours after dye application. Digital animation presented on CD Rom, Appendix 8.3.1.

8.4 Conclusion

Traditionally, soil hydraulic parameters have been determined by laboratory drying approaches, however data presented in this chapter indicates that prolonged saturation required by laboratory drying methods, resulted in parameter values which were not representative of field conditions. In soils which exhibit changes in hydraulic properties with antecedent soil water content such as hydrophobic soils (A1 horizon), vertic soil (B2 horizons), or soils with soluble amorphous silica bridging (A2 horizon), determination of soil hydraulic properties by *in situ* approaches such as inverse solution of infiltration data from tension infiltrometers should provide better estimates of the soil hydraulic properties than traditional laboratory drying approaches (Simunek *et al.* 1999b). However inverse infiltration from tension infiltrometers struggled to reach local minima when the residual soil water parameter (Qr) was included in the objective function (Ramos *et al.* 2006). This difficulty was attributed to the tension infiltrometers being relatively insensitive to flow in micropores. Removing Qr from the objective function improved the inverse solution, however, separate determination of Qr is required by other methods such as pressure chamber analysis or pedotransfer approaches (Patil and Rajput 2009). Use of additional approaches to determine Qr detracts from the intended purpose of the inverse approach, to derive representative soil hydraulic parameters from rapid, *in situ* techniques.

Despite the use of a range of soil parameterisation approaches, neither HYDRUS-1D nor MACRO 5.1 were able to adequately reproduce the dye tracer experiments (Chapter 4.3) or long term soil moisture monitoring data (Chapter 5.3.3). In the dry treatments, discrepancy between modelled and measured changes in soil moisture principally resulted from an inability to simulate hydrophobicity induced finger flow which led to overestimation of soil water accumulation in the A1 horizon. Error is also thought to have resulted from overestimation of Qr which prevented adequate drying of the A1 horizon by evapotranspiration. Bachmair *et al.* (2010) also found MACRO 5.1 predicted greater change in topsoil water content than measured values, which resulted in underestimation of changes in soil moisture further down the soil profile, as observed in this study.

Use of single pore domain models to derive soil hydraulic properties by inverse solution of tension infiltration data in soils known to contain preferential flow is not supported, as Crescimanno and Garofalo (2005) also found with the SWAP (van Dam *et al.* 2008) soil water model, changes in soil moisture resulting from rainfall and evapotranspiration over a two year period were not able to be reproduced due to the inability of the van Genuchten function to adequately simulate macropore flow when matric potential was near saturation (Greco 2002; Larsbo and Jarvis 2005).

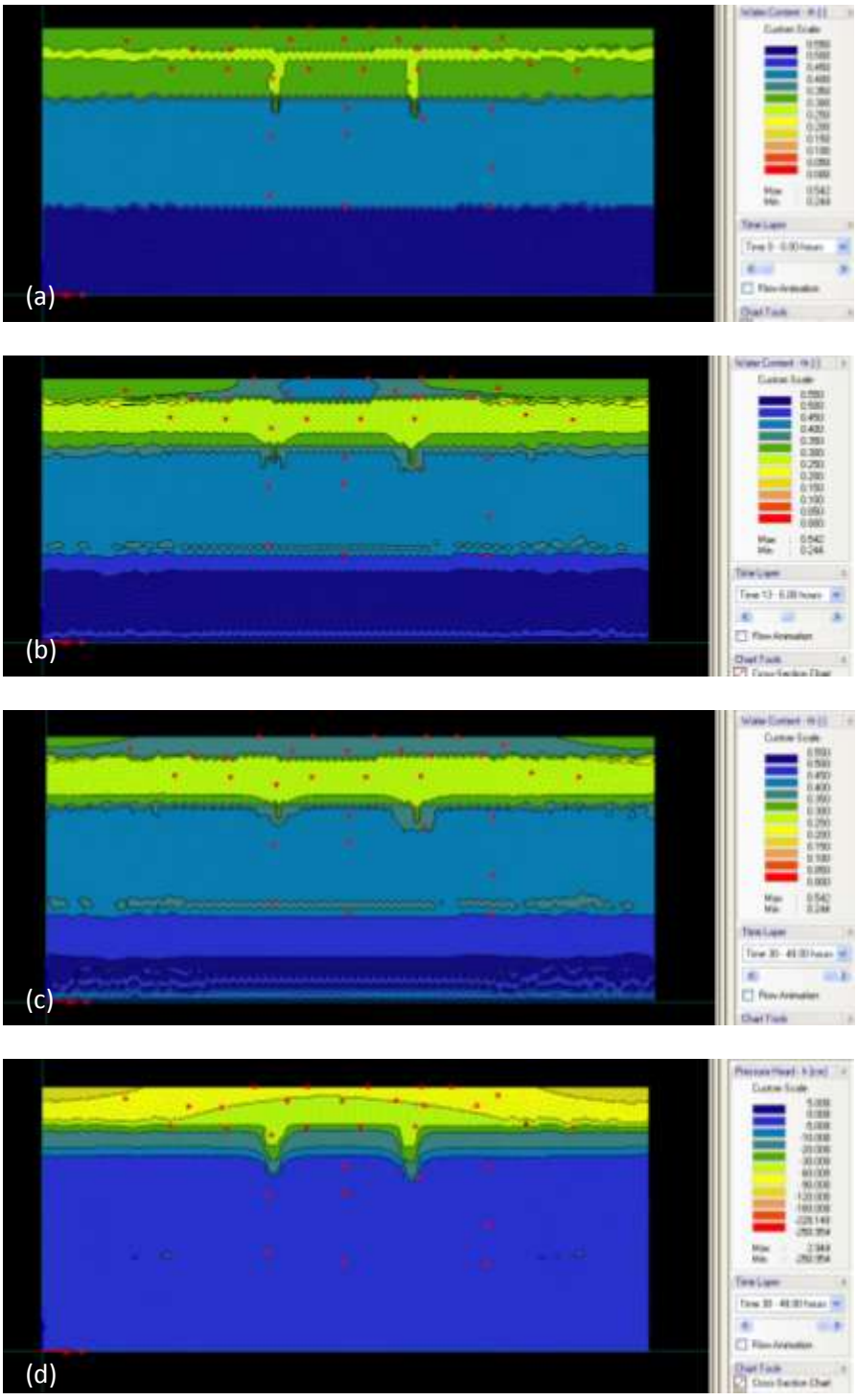

Figure 8.4-1 HYDRUS-2D representation of 25 mm infiltration into wet treatment using Disk VG-Qr set van Genuchten parameters, with K_{sat} defined by laboratory measurement on 100 mm diameter cores. Soil moisture distribution, (a) prior to infiltration, (b) 6 hours after application commenced, (c) 48 hours after application commenced. (d) Representation of pressure head six hours after infiltration commenced. Digital animation presented on CD Rom, Appendix 8.3.2.

As Coppola *et al.* (2009) laments "if the effects of structure and preferential flow are not explicitly accounted for, only false interpretations of reality can be achieved and modelling becomes a purely academic practice".

In the A2 horizon, differences between parameter values were attributed to artificial creation of macropores by soil shattering during sampling (Stone 1991). Differences between in parameter values determined from inverse infiltration at alternate soil moisture content were attributed to precipitation of soluble amorphous silica (Chartres *et al.* 1990) which restricted mesopore and micropore flow at low antecedent soil moisture (Chapter 6.3.5). In the B2 horizons neither HYDRUS-1D nor MACRO 5.1 were able to adequately simulate bypass flow through shrinkage cracks (Gerke *et al.* 2010) or represent the accumulation of soil water within dead end voids as demonstrated by dye staining at low antecedent soil moisture. For example, infiltration to 70 cm was only simulated when the soil profile was between field capacity and saturation, however dye staining and soil moisture monitoring (Chapter 5.3.3) demonstrated the majority of infiltration to 70 cm occurred by preferential flow when soil moisture was below the threshold soil moisture content (< 70 - 76 % total soil moisture).

In the wet treatments, the effect of clay swelling and difficulty displacing existing soil water further down the soil profile resulted in the inverse infiltration approaches producing 'flatter' soil water retention curves (lower α and *n)* than other approaches. Differences between modelled and measured changes in soil moisture resulted from difficulty determining appropriate values for saturated hydraulic conductivity. Differences also resulted from inability of the dye staining approach to 'observe' changes in soil moisture resulting from changes in soil moisture below the depth of dye staining associated with either drainage of the B2 horizons or displacement of existing soil water higher in the soil profile. The two dimensional analysis (HYDRUS-2D/3D) confirmed previous evidence that infiltration into texture contrast soils at high antecedent soil moisture resulted in lateral unsaturated flow within the A1 horizon or along the upper surface of the B21 Horizon.

In relation to the risk of agrochemical mobilisation beneath the root zone, the EnviroSCAN indicated that changes in soil moisture at 70 cm occurred on 17 days resulting in a 46.27 mm increase in soil moisture below 70 cm depth. However HYDRUS-1D and MACRO underestimated the frequency and magnitude of these infiltration events, predicting infiltration to 70 cm depth occurred on 3 to 32 days and increased soil moisture between 3.06 mm and 25.65 mm, depending on parameterisation approach. Poor model performance was attributed to difficulty accurately simulating hydrophobicity induced finger flow in the A1 horizon, and rivulet flow through antecedent soil moisture controlled shrinkage cracks in the B2 horizons.

The presence of sand infills had little influence on infiltration through the B2 horizons. Poor model performance limited ability to further explore the effects of preferential flow, land use and management on the occurrence of deep drainage and solute leaching.

The inability to adequately simulate infiltration and changes in soil moisture using a range of parameterisation approaches and levels of model sophistication indicates that different modelling and parameterisation approaches may be required for simulating soil water movement in soils in which the hydraulic properties vary with antecedent soil moisture. This includes separate conceptualisation of flow in shrinkage cracks to that of biopores (Haws *et al.* 2005) and improved simulation of finger flow in water repellent soil (Bachmann *et al.* 2007).

Although outside the scope of this thesis, opportunities exist to explore different model conceptualisations based on data presented in this thesis. Results indicate that in vertic or hydrophobic soils, parameterisation is required at both high and low antecedent soil moisture content in order to represent the potential range of hydraulic properties of both the micropore and macropore flow domains. This study indicated that parameterisation at high and low antecedent soil moisture may be conducted by inverse solution of infiltration from tension infiltrometers provided soils are not hydrophobic, and Qr is independently determined.

Results presented in this study indicate consideration may also need to be given to the effect of antecedent soil moisture on the porosity and flow within the micropore domain. Current dual permeability models assume the hydraulic properties of the micropore domain (soil matrix) do not vary with moisture content. However evidence presented in this thesis demonstrated the hydraulic properties of the soil matrix varied with antecedent soil moisture, evidence includes: (i) a significant difference (p<0.05, df 29-35) between the hydraulic conductivity of the wet and dry treatments in the A2, B21 and B22 horizons at ψ =-1.09 kPa (average of all sites) (Chapter 6.3.5), (ii) changes in intra-clod density and porosity with moisture content (Chapter 6.3.7), and (iii) variation in parameter values, especially Qr and n, derived by inverse solution of tension infiltration at alternate soil moisture contents.

8.5 Key points

- Parameterisation approach and antecedent soil moisture had considerable influence on predicted parameter values.
- Parameter values derived from laboratory drying methods were not representative of field conditions due to saturation prior to assessment which altered soil structure, water repellence, and silica cementation.
- Inverse solution of infiltration data from tension infiltrometers struggled to reach local minima when the residual soil water parameter (Qr) was included in the objective function.
- In the wet treatments, difficulty displacing existing soil water resulted in the inverse solution predicting 'flat' soil water retention curves with low α and *n* values.
- Hydrophobicity reduced the proportion of soil participating in flow which invalidated assumptions of homogeneity required for inverse solution of infiltration data in HYDRUS-2D
- Use of single porosity models to derive van Genuchten parameters by inverse solution in soils known to contain preferential flow is not supported by evidence presented in this thesis.
- Parameterisation approach and antecedent soil moisture was found to affect saturated hydraulic conductivity values by two to three orders of magnitude.
- Neither HYDRUS-1D nor MACRO 5.1 were able to adequately simulate changes in soil moisture demonstrated by the dye tracer experiments or long term soil moisture monitoring data.
- Despite a range of parameterisation approaches, neither MACRO 5.1 nor HYDRUS-1D were able to simulate the maximum depth of infiltration demonstrated by the dye staining experiments at low antecedent soil moisture.
- In the dry treatments, discrepancy between modelled and measured changes in soil moisture resulted from inability to simulate hydrophobicity induced finger flow, which led to overestimation of soil water accumulation in the A1 horizon.
- In wet treatments, differences between modelled and measured changes in soil moisture resulted from, inability of 1D model conceptualisations to simulate lateral flow, and inability of the dye tracer to 'observe' displacement of existing soil water.
- In the wet treatment, HYDRUS-2D predicted the dye tracer spread at least 1.6 meters laterally from the application area, through the A1 horizon or along the A1 / A2 boundary.
- The frequency and magnitude of infiltration to 70 cm depth was not able to be simulated by either MACRO 5.1 nor HYDRUS-1D resulting in under prediction of contaminate risk.

9.0 General discussion

9.1 Effect of antecedent soil moisture on preferential flow

Merdun *et al.* (2008) claims that researchers are in disagreement about the extent to which antecedent soil moisture influences preferential flow in soils. Increased preferential flow has been reported in dry water repellent and vertic soils (Lin *et al.* 1998; Merdun *et al.* 2008; Shipitalo and Edwards 1996), whilst increased preferential flow has also been reported in macroporous soils at high antecedent soil moisture content (Beven and Germann 1982; Greve *et al.* 2010; Jarvis 2007). This study found antecedent soil moisture strongly influenced the type, depth and rate of preferential flow in a series of texture contrast soils at the University of Tasmania Farm near Hobart. When soil was close to field capacity, dye tracer infiltrated to only 24 – 40 cm depth. When soils were dry, up to five different forms of preferential flow resulted in the same volume of dye tracer infiltrating to 85 – 119 cm depth. In dry soil, water repellence induced finger flow resulted in as little as 12 % of the A1 horizon participating in flow at 10 cm depth. When soil was near field capacity, the effects of water repellence were no longer apparent, and infiltration into the upper A1 horizon was mostly stable. However infiltration into soil near field capacity was impeded by difficulty displacing existing soil water further down the soil profile which resulted in saturation above the impeding soil layers, in either the A2 or B21 horizons, causing lateral flow through the A1 horizon.

Preferential flow is commonly thought to occur when rainfall intensity or magnitude exceed a particular threshold (Beven and Germann 1982; Cheng *et al.* 2007; Heppell *et al.* 2002; Lin and Zhou 2008; McGrath *et al.* 2010). However soil moisture monitoring following 44 rainfall events, over a two year period, found the occurrence of preferential flow was not significantly related to either rainfall intensity or rainfall magnitude. Rather, occurrence of preferential flow was significantly related to soil moisture content at the time of rainfall. When total stored moisture (0 - 70 cm) was below approximately 225 mm (49 % PAWC), occurrence of preferential flow was significantly more prevalent than when antecedent soil moisture was above 245 mm (60 % PAWC). Threshold like relationships between preferential flow and antecedent soil moisture has been reported for hydrophilic soils (Bauters *et al.* 2000a; Jury *et al.* 2003; Wang *et al.* 1998b), vertic soils (Gupta *et al.* 2006), and rivulet flow in macroporous soils (Germann *et al.* 1997; Kutilek and Germann 2009).

Unlike the other soil horizons, the A2 horizon had lower hydraulic conductivity when dry, than when near field capacity. Reduced hydraulic conductivity through mesopores and micropores in dry soil was attributed to precipitation of soluble amorphous silica in the menisci between sand grains which restricted flow through smaller pores (Chartres *et al.* 1990; Norton 1994).

At high antecedent soil moisture, clay swelling and closure of shrinkage cracks in the B2 horizons decreased the number, size and hydraulic conductivity of macropores. However, as noted by Waller and Wallender (1991) and Greve *et al.* (2010), closure of shrinkage cracks severely reduced but did not completely stop flow through the macropores. The effect of antecedent soil moisture on pore volume was considerable. Volumetric shrinkage experiments demonstrated that subsoil clods underwent a 5 - 25 % reduction in volume during drying from near saturation to around 0.05 g g^{-1} moisture content. In dry soil, flow through shrinkage cracks resulted in infiltration bypassing around 99 % of the soil matrix in the B21 horizon and 94 % of the soil matrix in the B22 horizon. At low antecedent soil moisture, the infiltrating dye tracer accumulated in small depressions on the upper surface of the B21 horizon, which then spilled down the sides of the very large clayey soil columns as rivulets or film flow. Rivulet flow down the side of the shrinkage cracks and ped faces occurred at rates estimated to be between 2000 - 3000 mm hr^{-1}, which was up to three orders of magnitude greater than the measured saturated hydraulic conductivity. At low antecedent soil moisture the majority of the infiltrating dye tracer accumulated in voids and terminal shrinkage cracks between 50 cm and 70 cm depth. Variation in subsoil dye staining patterns was related to differences in subsoil structure between the four sites.

9.2 Importance of water repellence

In dry soil, dye staining experiments demonstrated finger flow was initiated by water repellence at the soil surface. Extensive research has demonstrated that water repellence and development of finger flow is inversely related to antecedent soil moisture content (Bauters *et al.* 2000a; Jury *et al.* 2003; Wang *et al.* 1998b). However as predicted by Doerr *et al.* (2007), the effect of antecedent soil moisture on water repellence was not as simple as expected. Water repellence was found to vary with both antecedent soil moisture and wetting history. While a number of studies have reported that actual water repellence (field moist) varies seasonally with rainfall or soil moisture (Keizer *et al.* 2007; Keizer *et al.* 2008; Leighton-Boyce *et al.* 2005; Lemmnitz *et al.* 2008). This study demonstrated that potential water repellence (dried 40 °C) varied seasonally in relation to wetting history, independent of soil moisture content at the time of sampling. Mechanisms for the accumulation and loss of water repellent compounds were not adequately understood.

Water repellence (WDPT) was found to be highly correlated with rainfall history (60 to 90 days prior to analysis) but not antecedent soil moisture, nor rainfall or any other climate attribute within the 10 days prior to sampling. Leaching studies demonstrated the soluble compounds responsible for the persistence of water repellence (WDPT) and to a lesser extent severity of water repellence (WEP), were able to be leached from the A1 horizon. Consequently after saturation soil did not return to previous levels of water repellence following drying. The extent to which accumulation or loss of water repellent compounds can be attributed to specific soil or climate attributes is somewhat uncertain, however it appears that accumulation of water repellent compounds is likely to have resulted from microbial or plant inputs between August 2009 and May 2010. Whilst after May 2010, reduction in water repellence may have resulted from either leaching of water repellent compounds following winter rainfall, or microbial consumption from organism such as wax degrading bacteria (Roper 2005).

Water repellence in texture contrast soils at the University of Tasmania Farm appeared to be similar to forest soils investigated by Doerr and Thomas (2000), in which a hysteretic relationship between soil moisture and water repellence exists that requires input of new hydrophobic substances is required to re-establish water repellence following saturation.

Water repellence decreased infiltration through macropores by 57 % and decreased intrinsic permeability by an order of magnitude. Restricted infiltration into larger pores also occurred when soils were near field capacity due to difficulty displacing existing soil water further down the soil profile. The Hele-Shaw experiments demonstrated that inability to displace existing soil moisture resulted in a similar level of flow instability to that caused by finger flow in dry water repellent soil. Restricted ability to displace existing soil moisture further down the soil profile also explained the lack of dye staining in the B2 horizons, and development of flow perturbations or unstable flow in the A1 horizons at high antecedent soil moisture content. Development of finger flow in the A1 horizon influenced other preferential flow processes further down the soil profile by determining the location of ponding on the upper B21 horizon, and by determining which shrinkage cracks were able to participate in flow. Water repellence and development of finger flow was also largely responsible for poor infiltration uniformity and poor model performance.

9.3 Occurrence of perched watertables and subsurface lateral flow

Development of perched watertables and subsurface lateral flows in texture contrast soils has been attributed to the discontinuity in texture and hydraulic conductivity between the A and B horizons Eastham *et al.* (2000) and Cox and McFarlane (1995). However at the University of Tasmania Farm sites perched watertables and subsurface lateral flows did not develop when soil moisture was low due to the presence of bypass flow through shrinkage cracks, and to a lesser extent sand infills, in the upper B2 horizons.

When soil moisture was close to field capacity, clay swelling was expected to result in ponding and accumulation of the dye tracer at the A / B boundary as reported by Eastham *et al.* (2000) and Cox and McFarlane (1995). However at high moisture content, dye staining indicated the impeded drainage of the B horizons resulted in dye tracer moving laterally through the A1 horizon rather than through the A2 horizon or along the upper surface of the B horizon as reported in the literature. *In situ* infiltration studies demonstrated the near saturated hydraulic conductivity of the B21 horizon decreased from 18.04 mm hr^{-1} to 5.56 mm hr^{-1} as soil moisture increased to near field capacity. However even following prolonged wetting, the B horizon was not impermeable, as clay swelling did not completely prevent flow through shrinkage cracks at high soil moisture content (Greve *et al.* 2010). Furthermore, at high antecedent soil moisture, hydraulic conductivity decreased sequentially with depth down the soil profile, consequently the discontinuity in hydraulic conductivity between the A and B horizons was no longer apparent. As explained by Weiler and McDonnell (2004) development of lateral flow through the A1 horizon at high antecedent soil moisture resulted from the decline in hydraulic conductivity with depth, such that rainfall or dye tracer application at rates greater than the hydraulic conductivity of the least conductive layer (3.9 mm hr^{-1} at ψ -0.13 kPa in the B22 horizon) resulted in saturation throughout the soil profile. Continued rainfall or dye tracer application at rates less than the surface soil infiltration rate but greater than the hydraulic conductivity of the least conductive layer resulted in lateral flow through the zone of highest porosity, the A1 horizon.

In forested catchments with shallow bedrock, development of subsurface lateral flow is facilitated by macropore flow through the overlying regolith, and along the upper surface of the impeding layer (McDonnell 1990; McGlynn *et al.* 2002). As antecedent soil moisture increases, macropore networks self-organise into larger preferential flow systems which expand upslope during rain events (Sidle *et al.* 2001; Tsuboyama *et al.* 1994), resulting in a greater proportion of subsurface lateral flow (Kim *et al.* 2005; Lowery *et al.* 1982; Scanlon *et al.* 2000).

However in the texture contrast soils at the University of Tasmania Farm, those investigated by Brouwer and Fitzpatrick (2002b), and Smettem *et al.* (1991) macroporosity in the B2 horizons, prevented rather than contributed to the development of ponding and subsurface lateral flow.

9.4 Effect of antecedent soil moisture and preferential flow on rainfall effectiveness and infiltration efficiency

The volume of infiltrated dye tracer retained in the effective root zone (0 - 30 cm) was significantly influenced by antecedent soil moisture. However, soil moisture monitoring demonstrated antecedent soil moisture had no significant effect on rainfall effectiveness (proportion of total rainfall stored in the soil profile), despite being significantly related to the occurrence of preferential flow. In dry soil, between 30.8 % and 73.0 % of the infiltrated dye tracer was 'lost' below the effective root zone, whilst in soil at high antecedent soil moisture all but 0.3 % (site B) of the infiltrated dye tracer was retained in the effective root zone (0 - 30 cm). At high antecedent soil moisture, an average of 54 % of the total applied dye tracer was not 'recovered' due to lateral flow through the A1 horizon beyond the excavation area (Appendix 7.3).

The amount of precipitation was found to be poorly correlated (R^2 0.47) with the amount of rainfall stored in the soil profile. Rainfall effectiveness, was not significantly related to either antecedent soil moisture or the occurrence of preferential flow. This was somewhat unexpected as it had been assumed that at lower antecedent soil moisture, occurrence of preferential flow would result in decreased change in soil moisture. The poor correlation between rainfall and the change in soil moisture occurred at both high and low soil moisture content. In dry soil hydrophobicity induced runoff and development of finger flow reduced the amount of rainfall stored in the soil profile. Whilst in wet soil conditions after June 2009, additional rainfall saturated the soil profile resulting in both surface runoff and subsurface lateral flow above the B2 horizons.

Infiltration uniformity (ability to evenly wet-up the entire effective root zone, 0 - 30 cm) was not significantly affected by antecedent soil moisture, as uneven wetting patterns developed at both high and low antecedent soil moisture. The degree of spatial variation in wetting patterns in both soil water treatments indicated potential issues for the evenness of pasture and crop growth (Bauters *et al.* 2000b).

9.5 Implications for management of texture contrast soils

Although not specifically investigated in this study, results demonstrate opportunities and insights to improve agricultural management of texture contrast soils. Current management guidelines for the application of pesticides provide little information on timing of pesticide application. For example the South Australian EPA recommend that in order to reduce the chance of runoff to waterways pesticides should not be applied when soils are wet (EPA 2005). Consideration is not given to pesticide contamination of groundwater resulting from preferential flow in agricultural soils as demonstrated by numerous studies in Europe and America (Flury 1996; Gerke *et al.* 2010; Jarvis 2007; Kladivko *et al.* 2001; Köhne *et al.* 2006a; Kordel *et al.* 2008). Soil moisture monitoring and dye staining experiments demonstrated that when soils are dry, preferential flow was able to rapidly transport solutes to depth below the chemically and biologically active topsoil where degradation is greatest (Roulier and Jarvis 2003). Thus guidelines for the application of pesticides and other agrochemicals to agricultural soils need to consider the risks posed by preferential flow of contaminants to ground water. In texture contrast soils or soils with either water repellent or vertic properties, agrochemical application should be prevented when soils are dry. Soil water monitoring indicated that for texture contrast soils at the University of Tasmania Farm, pesticide application should be conducted when soils are between the threshold soil water content (70 -76 % of total soil water) and field capacity.

Water repellence is not commonly cited as a management issue in texture contrast soils, however at the University of Tasmania Farm, water repellence in a series of texture contrast soils resulted in finger flow, uneven wetting patters, runoff, decreased rainfall effectiveness, decreased infiltration efficiency and decreased irrigation uniformity. Options for improved management of water repellence include claying, use of surfactants and reduced drying as discussed by Blackwell (2000). By overcoming the effects of water repellence through the use of claying or surfactants it is expected that rainfall and irrigation will be able to infiltrate the soil more evenly resulting in increased application efficiency and uniformity. In addition, it is postulated that early irrigation with surfactants may reduce water repellence and prevent its re-establishment by leaching water repellent compounds from the A1 horizon.

9.6 Soil water modelling

Differences in parameterisation methodology resulted in considerable variation in estimated van Genuchten parameters and saturated hydraulic conductivity. Variance in parameter values was partly attributed to differences in moisture content prior to assessment, which influenced soil structure and water repellence. Saturation of soil prior to analysis using traditional laboratory drying approaches is thought to have resulted in parameter values which did not reflect field hydraulic properties. Parameter uncertainty also resulted from difficulty accounting for preferential flow in both direct and inverse parameterisation approaches. Inverse solution of infiltration data from tension infiltrometers also had difficulty obtaining local minima when the residual water content was included in the objective function. Parameter uncertainty cast doubt on the use of both direct and inverse parameterisation approaches for simulating soil water movement in texture contrast soils. This served to undermine confidence in the use of the models.

Despite the use of a range of soil parameterisation approaches, neither HYDRUS-1D nor MACRO 5.1 were able to adequately reproduce the dye tracer experiments or long term soil moisture monitoring data. At low soil moisture, poor model performance resulted from an inability to simulate hydrophobicity induced finger flow, which led to the model overestimating soil water accumulation in the A1 horizon. In wet soil, error resulted from inability to simulate development of perched watertables and lateral flow due to one-dimensional conceptualisation. Poor model performance was also attributed to the low correlation between precipitation and the change in soil moisture which was not able to be reproduced in the models.

Poor model performance in texture contrast soils raises broader issues about the ability and use of soil water models to simulate soil water availability, deep drainage and solute leaching in crop production models such as APSIM (Keating *et al.* 2003). These models typically employ the use of tipping bucket or single pore domain models to simulate water availability and movement (Probert and Verburg 1995). In texture contrast soils, APSIM has been used to simulate crop production (Asseng *et al.* 2001; Robertson *et al.* 2005), deep drainage (Robertson *et al.* 2005) and salinity risk (Asseng *et al.* 2001; Lisson *et al.* 2005; Pracilio *et al.* 2003). However, these models do not explicitly account for preferential flow (Jarvis and Larsson 2001; van Dam *et al.* 2004), and water outflow from each layer is assumed to be zero until field capacity is exceeded. Consequently leaching and deep drainage is only simulated when the lowest soil layer exceeds field capacity. This usually requires saturation of the whole soil profile (Littleboy *et al.* 1999; Ward *et al.* 1998).

At the University of Tasmania Farm preferential flow resulted in 39 % - 73 % of infiltration being lost beneath the root zone (0 - 30 cm), in which preferential flow accounted for approximately 93 % of the infiltration to 70 cm depth. Neither Hydrus-1D or MACRO 5.1 were able to adequately simulate the frequency and magnitude of infiltration below 70 cm depth, nor simulate bypass flow beneath the root zone, as demonstrated by the dye staining experiments. Consequently in texture contrast soils containing hydrophobic topsoils and vertic subsoils, the use of tipping bucket, single porosity or duel permeability models that do not explicitly account for finger flow are not supported for the prediction of deep drainage or solute leaching. Use of tipping bucket and single pore domain models may however still be appropriate for simulating processes such as crop growth when preferential flow only accounts for a minor loss of soil water beneath the root zone.

9.7 Extension of results to other texture contrast soils

It was anticipated that pedotransfer or hydropedological approaches could be employed to parameterise preferential flow models (Lin *et al.* 2005) such as MACRO 5.1 or MACRO-DB, in order to determine the frequency and magnitude of preferential flow events over many seasons. However model uncertainty resulting from poor validation at the pedon scale undermined confidence with the ability of the models to predict flow processes. This limited ability to use the models to further explore the effects of preferential flow, land use, and management practices on the occurrence of deep drainage and agrochemical mobilisation at larger scales or longer time periods.

However the extent or risk of preferential flow in other texture contrast soils or soils with similar properties may however be inferred from soil morphology and simple field tests provided the key soil properties responsible for the development of preferential flow are known. The dye staining experiments demonstrated that differences in soil morphology between sites had little influence on dye tracer distribution down the soil profile. However, the occurrence and extent of preferential flow was shown to be strongly influenced by antecedent soil moisture which influenced the degree of water repellence in the A1 horizon and shrinkage crack development in the B2 horizons. Consequently extrapolation of results and conceptual models to other texture contrast soils with water repellent topsoils and vertic clay subsoils appears feasible.

At the pedon scale, the occurrence of preferential flow may be inferred in the field from presence of shrinkage cracks or slickensides indicating the depth of seasonal shrinkage and swelling of clay subsoils, and simple filed tests for water repellence such as the WDPT and MED tests. In addition at high antecedent soil moisture, the presence of tongued or broken boundaries between the A and B horizons may be used to predict funnel flow, while the presence of structure less and non-porous A2 horizons may be used to predict lateral flow in the A1 horizon.

9.8 Prediction of environmental harm resulting from preferential flow

This thesis has not produced evidence of environmental harm resulting from the occurrence of preferential flow. However data presented in this thesis has demonstrated that in dry texture contrast soils potential exist for rapid and deep mobilisation of solutes via preferential flow to at least 1.0 meters depth following rainfall or irrigation. This constitutes a risk for shallow groundwater contamination and off site mobilisation of environmental contaminants. Preferential movement of water and solutes by macropore flow is a key process for the fate of agrochemicals such as pesticides, because it reduces the residence time of the solute in the topsoil, where chemical and biological degradation are highest (Roulier and Jarvis 2003). The dye staining experiments and soil moisture monitoring demonstrated that preferential flow resulted in the majority of rainfall and the dye tracer accumulating in dead end pores or pores with internal catchment (Bouma and Dekker 1978) between 50 cm and 70 cm depth. Jarvis (2007) calculated that the maximum allowed leaching loss for a single pesticide to exceed the EU drinking water standard was only 0.1 % of the applied amount, whereas pesticide losses due to macropore flow may range up to 5 % of the applied dose. It is postulated that in winter development of shallow groundwater (< 5 meters) within the vicinity of the University of Tasmania Farm (Dell 2005; Lisson *et al.* 2005) may intercept 'preserved' pockets of pesticide residing in dead end pores (Kordel *et al.* 2008) resulting in groundwater contamination and lateral transport of contaminants to surface waterways via groundwater flow. Ground and surface water contamination by pesticides has recently been reported in 4 out of 58 ground water bores (DPIPWE 2009) and 21 out of 55 waterways (DPIPWE 2010) in Tasmania, however the mechanism by which these contaminants were mobilised is largely unknown.

Little is known about the quantitative significance of preferential flow on contamination of water resources at the larger catchment scale (Jarvis 2007). Assessment of potential agrochemical contamination risk resulting from preferential flow at the catchment or region scale requires the use of soil water models which explicitly account for preferential flow to integrate the effects of agricultural practice, soil properties, climate and landform on the occurrence and magnitude of contaminant leaching events. This thesis and a limited number of other studies have reported the existence of preferential flow in texture contrast soils (Brouwer and Fitzpatrick 2002b; Leaney *et al.* 1993; Silberstein *et al.* 1999; Smettem *et al.* 1991; Ticehurst 2004). However few attempts have been made to conceptualise macropore flow in conceptual or analytical models of water and solute movement in texture contrast soils. Past studies of soil water movement in texture contrast soils have frequently ignored the existence of macropore flow and represented the upper surface of the B horizon as a single uniform layer, with a single value for hydraulic conductivity (Cook and Rassam 2002; Stolte *et al.* 1999; Ticehurst *et al.* 2003a; Ticehurst *et al.* 2003b).

In order to assess the risk of agrochemical mobilisation in texture contrast soils at the hillslope or catchment scale it is necessary to include preferential flow processes within the modelling routine, and account for the spatial and temporal variation in the hydraulic conductivity of the impeding soil layers as suggested by Silberstein *et al.* (1999). However as Weiler and McDonnell (2007) lament *'One of the greatest challenges in the field of hillslope hydrology is conceptualizing and parameterizing the effects of lateral preferential flow'* , or as Clothier *et al.* (2008) recently concluded, research attention is urgently required to *'link soil macroporous information and physical understanding of preferential flow processes to the larger hydrological scales both spatially and temporally'*.

10.0 Conclusion

The soil morphology and hydrology of the four texture contrast soil profiles investigated in this thesis were considerably more complex than had previously been reported in the literature. In contrast to the majority of literature on texture contrast soils, development of perched water tables and subsurface lateral flow did not simply result from the texture discontinuity between the A and B horizons, rather development of perched water tables was controlled by antecedent soil moisture which influenced subsoil hydraulic conductivity and the presence of silica bridging in the A2 horizon.

Occurrence of preferential flow was not significantly related to either rainfall intensity or rainfall magnitude, rather occurrence of preferential flow was significantly related to antecedent soil moisture content. Differences in soil chemistry, subsoil structure and the abundance of sand infills between sites resulted in few differences in the proportion of dye stained soil with depth. Occurrence of preferential flow was found to be more closely related to antecedent soil moisture than differences in soil morphology between the four sites.

Water repellence had a profound effect on the development of finger flow in the A1 horizon, and subsequent occurrence of preferential flow further down the soil profile. The relationship between soil moisture and water repellence was not straightforward. Water repellence was influenced by rainfall history such that following saturation, soil did not return to prior levels of repellence when dry. While the processes responsible for the accumulation and break down of water repellent compounds were not fully understood, data indicated that winter rainfall may have leached water repellent compounds from the soil, and that input of new compounds was required for soils to return to past levels of water repellence.

In dry soil conditions, infiltration was not able to be predicted by the Richards Equation due to the occurrence of up to five different forms of preferential flow which included: hydrophobicity induced finger flow in the A1 horizon, funnel flow along the upper surface of the B21 horizon and within the sand infills, bypass flow through shrinkage cracks in the B21 and B22 horizons, saturated backfilling of shrinkage cracks and voids in the subsoil, and macropore flow through biopores in the A1, A2 and B21 horizons. Finger flow in the A1 horizon resulted in as little as 12 % of the soil participating in flow at 10 cm depth, whilst flow through shrinkage cracks bypassed up to 99 % of the soil matrix in the B21 horizon and 94 % in the B22 horizon. Preferential flow resulted in wetting front velocities which were up to three to four orders of magnitude higher than the measured saturated hydraulic conductivity.

Results indicate that at low antecedent soil moisture, agrochemical mobilisation by preferential flow may constitute a contamination risk to shallow water tables in the region. However long term prediction of the magnitude and frequency of preferential flow events was not possible due to the inability of the soil water models to accurately predict changes in soil moisture associated with the dye staining experiments and soil moisture monitoring. Poor model performance was largely attributed to inability to simulate water repellence in dry soil conditions and lateral flow in wet soil conditions. Despite poor model performance, the risk of agrochemical mobilisation and shallow groundwater contamination at the site, and other locations containing texture contrast soils may be inferred from soil morphology including shrinkage cracks, slickensides, and simple tests for water repellence.

It is hoped that data and insights about the nature of preferential flow in these highly complex soils will provide opportunity for future model development and testing.

10.1 Future research

Many issues and opportunities for further research have been identified in this thesis. Priority areas for future research have been selected in the expectation that they will yield the greatest advancement in capacity to predict the occurrence and magnitude of preferential flow. Further research is required to:

- Improve modelling of water repellence and finger flow in soils which demonstrate a hysteretic relationship between soil moisture and water repellence.
- Improved processes for parameterising and representing changes in soil structure resulting from shrinkage and swelling of clay soils in soil water models.
- Further development and testing of *in situ* devices and procedures for inferring the occurrence of preferential flow at the pedon to landscape scale.
- Determine the processes responsible for development of water repellence and its dissipation in soils which demonstrate a hysteretic relationship between soil moisture and water repellence.
- Improve estimation of parameter values for dual permeability models using inverse solution of *in situ* tension infiltrometer data.
- Determine the extent of shallow groundwater contamination in agricultural regions containing texture contrast soils.